Fakultät für
Mathematik, Informatik
und Naturwissenschaften

Physiologically-based modeling of bile acid metabolism in mice and human

Von der Fakultät für Mathematik, Informatik und Naturwissenschaften
der RWTH Aachen University zur Erlangung des akademischen Grades
eines Doktors der Naturwissenschaften genehmigte Dissertation

vorgelegt von

Bastian Kister, Master of Science

aus

Schweinfurt, Deutschland

Berichter:	Univ.-Prof. Dr.-Ing. Lars Mathias Blank Univ.-Prof. Dr. rer. nat. Lars Küpfer
Tag der mündlichen Prüfung:	17.05.2024

Diese Dissertation ist auf den Internetseiten der Universitätsbibliothek verfügbar.

Eidesstattliche Erklärung

Hiermit erkläre ich, Bastian Kister, dass diese Dissertation und die darin dargelegten Inhalte die eigenen sind und selbstständig, als Ergebnis der eigenen originären Forschung, generiert wurden.

Hiermit erkläre ich an Eides statt:

1. Diese Arbeit wurde vollständig oder größtenteils in der Phase als Doktorand dieser Fakultät und Universität angefertigt;

2. Sofern irgendein Bestandteil dieser Dissertation zuvor für einen akademischen Abschluss oder eine andere Qualifikation an dieser oder einer anderen Institution verwendet wurde, wurde dies klar angezeigt;

3. Wenn immer andere eigene- oder Veröffentlichungen Dritter herangezogen wurden, wurden diese klar benannt;

4. Wenn aus anderen eigenen- oder Veröffentlichungen Dritter zitiert wurde, wurde stets die Quelle hierfür angegeben. Diese Dissertation ist vollständig meine eigene Arbeit, mit der Ausnahme solcher Zitate;

5. Alle wesentlichen Quellen von Unterstützung wurden benannt;

6. Wenn immer ein Teil dieser Dissertation auf der Zusammenarbeit mit anderen basiert, wurde von mir klar gekennzeichnet, was von anderen und was von mir selbst erarbeitet wurde;

7. Ein Teil oder Teile dieser Arbeit wurden zuvor veröffentlicht und zwar in:

   - Kister, B., Viehof, A., Rolle-Kampczyk, U., Schwentker, A., Treichel, N.S., Jennings, S., Wirtz, T.H., Blank, L.M., Hornef, M.W., von Bergen, M., Clavel, T., Kuepfer, L., 2023. A physiologically based model of bile acid metabolism in mice. iScience. Volume 26. Issue 10. 107922.

Köln, der 08.11.2023

Bastian Kister

Funding

The presented work was performed in the scope of the collaborative research center 'Gut-Liver axis' and its funding was provided from the German Research Foundation (DFG) – Project-ID 403224013 – "SFB 1382".

Acknowledgements

I am deeply grateful to the following individuals and organizations for their invaluable contributions to the completion of this thesis:

My sincere appreciation goes to Lars Kuepfer for serving as my supervisor. His guidance, expertise, and unwavering support were instrumental in shaping this thesis. Giving me the freedom to shape this project and pursue my interests in it but also being constantly available were highly appreciated.

I would like to extend my gratitude to Lars Blank, for his encouragement, discussions and for providing the opportunity to work on this project.

Priyata Kalra deserves special recognition for her invaluable insights, mentorship, and encouragement throughout this journey. Her guidance has been pivotal to my growth and helped my through various rough patches.

I want to acknowledge Zita Soons for her collaborative spirit and discussions that enriched the content and quality of this thesis.

I extend my deepest appreciation to Vanessa Baier for her invaluable assistance and guidance during the initial stages of this work and her support during my transition into PhD life. Her insights were instrumental in laying the foundation for this project.

I want to acknowledge Annika Schneider for her role as a confidante and someone I could turn to when needing to vent or seek understanding. Her support in this capacity was invaluable.

The iAMB and the Institute of Systems Medicine deserve special recognition for creating an enabling research environment and offering valuable resources that significantly contributed to the success of this project. Although I could only experience the beginning of the new ISMFOI, I am curious to see how the group will develop.

To my dear friends Ibrahim "Ibris" Hawwari, Jan Steck, and Robin Wetschera, your unwavering friendship, encouragement and support were a constant source of motivation and inspiration throughout this journey. I could truly rely on your support - scientifically, professionally and personally.

To my family, especially my mother, who supported me unwaveringly even when understanding was lacking. You sustained me during challenging times, and I am profoundly grateful for your unwavering support and encouragement.

To all those mentioned above, as well as anyone else who played a part, whether directly or indirectly, in the realization of this thesis, I offer my heartfelt thanks. Your contributions have been indispensable, and I am truly appreciative of your assistance.

Thank you.

Contents

Funding v

Acknowledgements vii

List of abbreviations xiii

Abstract xxix

Zusammenfassung xxxi

1 General introduction 1

2 Background 9

2.1 Bile acids 11

2.1.1 Biochemistry 11

2.1.2 Bile acid metabolism 16

2.1.3 Enterohepatic circulation 24

2.1.4 Bile acids in homeostasis and pathophysiological conditions 31

2.1.5 Species differences in BA metabolism 44

2.2 Computational modelling 48
2.2.1 PBPK modelling 55
2.2.2 Published models of BA metabolism 57

3 A physiologically-based model of bile acid metabolism in mice 61

3.1 Model development and data 64
3.2 6BA Model 73
3.3 Murine Conjugation Model 83
3.4 Discussion of physiologically-based models of murine BA metabolism 93

4 A physiologically-based model of bile acid metabolism in humans. 99

4.1 Model development and data 101
4.2 5BA Model 110
4.3 Human Conjugation Model 118
4.4 Discussion of physiologically-based models of human BA metabolism 126

5 General conclusion and future work 131

6 Material and Methods 137

A A physiologically-based model of bile acid metabolism in mice 147

B A physiologically-based model of bile acid metabolism in human 173

References **227**

Curriculum vitae **273**

Abbreviations

ASBT	Apical sodium-dependent bile acid transporter
BA	Bile acids
BAAT	Bile acid aminotransferase
BAD	Bile acid diarrhea
BAM	Bile acid malabsorbtion
BMI	Body Mass index
BSEP	Bile salt export pump
BSH	Bile salt hydrolase
C4	7α-hydroxy-4-cholesten-3-one
CA	Cholic acid
CDCA	Chenodeoxycholic acid
CMC	Critical micellar concentration
CYP7A1	7α-hydroxylase
DCA	Deoxycholic acid
EHC	Enterohepatic circulation
FXR	Farnesoid X receptor
GF	Germ-free
G-UDCA	Glycoursodeoxycholic acid
G-LCA	Glycolithocholic acid
G-DCA	Glycodeoxycholic acid
G-CDCA	Glycochenodeoxycholic acid
G-CA	Glycocholic acid
G-BA	Glyco-conjugated bile acid
HDCA	Hyodeoxyhcolic acid

HPLC	High-performance liquid chromatography
IBD	Inflammatory bowel disease
ICP	Intrahepatic cholestasis of pregnancy
IQR	Interquartile Range
LCA	Lithocholic acid
LTX	Liver transplantation
LXR	Liver-X-receptor
MCAs	Muricholic acid
MDCA	Murideoxycholic acid
MRP3/4	Multidrug resistance-associated protein 3/4
NADPH	Nicotinamide adenine dinucleotide phosphate
NTCP	Sodium-taurocholate cotransporting polypeptide
OATPs	Organic-anion-transporting polypeptides
OCA	Obeticholic acid
OMM	Oligo-Mouse-Microbiota
OSTα/β	Organic solute transporter alpha/beta
PBPK	Physiologically-based pharmacokinetic model
SHP	Small heterodimer partner
SPF	Specific pathogen free
SULTS	Sulfotransferases
TIPS	Transjugular intrahepatic portosystemic shunt
T-MCA	Tauromuricholic acid
T-UDCA	Tauroursodeoxycholic acid
T-LCA	Taurolithocholic acid
T-DCA	Taurodeoxycholic acid
T-CDCA	Taurochenodeoxycholic acid
T-CA	Taurocholic acid
T-BA	Tauro-conjugated bile acid
tBA	Total bile acids
tCA	Total cholic acids
tCDCA	Total chenodeoxycholic acids

tDCA	Total deoxycholic acids
tLCA	Total lithocholic acids
tMCAs	Total muricholic acids
tUDCA	Total ursodeoxycholic acids
uBA	Unconjugated/free bile acid
UDCA	Ursodeoxycholic acid

List of Figures

2.1 Structure of BA species 12

2.2 Overview of BA metabolism 17

2.3 Synthesis of primary BAs in the liver 18

2.4 Synthesis of secondary BAs 23

2.5 Enterohepatic circulation of BA 25

2.6 Overview of BA regulation 32

2.7 Overview of BA mediated signalling through FXR and TGR5 39

2.8 Illustration of the iterative model development process in systems biology 52

2.9 Illustration of PBPK modeling 56

2.10 Illustration of applications of PBPK modeling 57

3.1 Schematic overview of the physiologically-based bile acid model in mice 64

3.2 Measured bile acid levels in SPF mice 66

3.3 Physiological differences between male and female SPF mice 67

3.4 Sex-related differences in intestinal BA metabolism in SPF mice 69

3.5 Schematic overview of the 6BA model in mice 73

3.6 6BA model fit to data from SPF mice 75

3.7 6BA model validation to data from GF mice 77

3.8 6BA model predictions of changes in GF mice 78

3.9 6BA model predictions of BA pool sizes at the whole body level 79

3.10 6BA model predictions of BA pool distribution 80

3.11 6BA model predictions of BA malabsorption 81

3.12 6BA model predictions of impaired intestinal barrier function 82

3.13 Schematic overview of the conjugation model in mice 83

3.14 Murine conjugation model fit to data from SPF mice 85

3.15 Murine conjugation model validation to data from GF mice . 87

3.16 Murine conjugation model predictions of changes in GF mice 88

3.17 Murine conjugation model predictions of BA pool sizes . . . 89

3.18 Murine conjugation model predictions of BA pool distribution 90

3.19 Murine conjugation model predictions of BA malabsorption and loss of intestinal barrier function 91

3.20 Murine conjugation model predictions of impaired intestinal barrier function 92

4.1 Schematic overview of the physiologically-based bile acid model in human 102

4.2 Comparison of bile acid levels in venous blood plasma, bile and feces between healthy subjects and liver diseased patients 109

4.3 Schematic overview of the 5BA model in human 110

4.4 5BA model fit to literature data 111

4.5 5BA model validation to literature data 113

4.6 Population simulation of the 5BA model 114

4.7 Scan of parameters with high sensitivity in the 5BA model for extrapolation to liver diseased patients 115

4.8 Schematic overview of the conjugation model in human . . . 118

4.9 Human conjugation model fit to literature data 119

4.10 Human conjugation model validation to literature data . . . 121

4.11 Population simulation of the human conjugation model . . . 122

4.12 Scan of parameters with high sensitivity in the human conjugation model for extrapolation to liver diseased patients . 124

A.1 Measured bile acid levels in GF mice 149

A.2 Sex-related differences in intestinal BA transporter expression in GF mice 150

A.3 Physiological differences between male and female GF mice 150

A.4 Assessment of sensitivity coefficients in male and female 6BA mouse model 151

A.5 6BA model predictions of intracellular BA pool sizes at the whole body level 152

A.6 6BA model predictions of BA pool composition in various organs 152

A.7 6BA model predictions of BA pool distribution and composition along the EHC and gut axis 153

A.8 Assessment of sensitivity coefficients in male and female murine conjugation model 154

A.9 Murine conjugation model predictions of intracellular BA pool sizes at the whole body level 155

A.10 Murine conjugation model predictions of BA pool composition in various organs 155

B.1 Data of postprandial response in venous blood from literature 175

B.2 Overview of total bile acid levels in patients undergoing liver transplantation 176

B.3 Overview of total bile acid levels in patients undergoing transjugular intrahepatic portosystemic shunt 177

B.4 Comparison of bile acid levels in venous blood plasma and feces between liver transplant and TIPS patients before intervention 177

B.5 Bile acid levels in venous blood plasma, bile and feces in patients with liver disease 178

B.6 Scan of functional liver volume in the 5BA model 179

B.7 Scan of relative NTCP activity in the 5BA model 180

B.8 Scan of relative BSEP activity in the 5BA model 181

B.9 Scan of relative ASBT activity in the 5BA model 182

B.10 Scan of relative OSTα/β activity in the 5BA model 183

B.11 Scan of relative microbial activity in the 5BA model 184

B.12 Scan of changes in intestinal pH in the 5BA model 185

B.13 Scan of relative blood plasma protein concentration in the 5BA model 186

B.14 Scan of hepatic parameters with high sensitivity in the human conjugation model 187

B.15 Scan of intestinal parameters with high sensitivity in the human conjugation model 188

B.16 Scan of blood-related parameters with high sensitivity in the human conjugation model 188

B.17 Scan of functional liver volume in the human conjugation model 189

B.18 Scan of relative NTCP activity in the human conjugation model 190

B.19 Scan of relative BSEP activity in the human conjugation model 191

B.20 Scan of relative ASBT activity in the human conjugation model 192

B.21 Scan of relative OSTα/β activity in the human conjugation model 193

B.22 Scan of relative BSH activity in the human conjugation model 194

B.23 Scan of relative BAAT activity in the human conjugation model 195

B.24 Scan of changes in intestinal pH in the human conjugation model 196

B.25 Scan of relative blood plasma protein concentration in the human conjugation model 197

B.26 Scan of hepatic parameters with high sensitivity in the human conjugation model 198

B.27 Scan of intestinal parameters with high sensitivity in the human conjugation model 199

B.28 Scan of blood-related parameters with high sensitivity in the human conjugation model 199

List of Tables

2.1 Critical micellar concentration of bile acids 15

2.2 Bile acid transporters 26

2.3 Bile acid receptive receptors 36

3.1 Physicochemical properties of BAs used for the murine 6BA model 70

3.2 Physicochemical properties of BAs used for the murine conjugation model 71

4.1 Overview of the literature data set 103

4.2 Physicochemical properties of BAs used for the human 5BA model 105

4.3 Physicochemical properties of BAs used for the human conjugation model 106

4.4 Changes of BAs level in unobserved organs for parameter scans within the 5BA model 117

4.5 Changes of BAs level in unobserved organs for parameter scans within the human conjugation model 125

A.1 Fitted parameter values of enzymatic reactions in the 6BA model 156

A.2 Fitted parameter values of hepatic transport reactions in the 6BA model 156

A.3 Fitted parameter values of intestinal transport reactions in the 6BA model 157

A.4 Sensitivity analysis of fitted 6BA model parameters on BA concentration in liver 158

A.5 Sensitivity analysis of fitted 6BA model parameters on BA concentration in venous blood plasma 158

A.6 Sensitivity analysis of fitted 6BA model parameters on BA concentration in kidney 159

A.7 Sensitivity analysis of fitted 6BA model parameters on BA concentration in SI content 160

A.8 Sensitivity analysis of fitted 6BA model parameters on BA concentration in SI tissue 161

A.9 Sensitivity analysis of fitted 6BA model parameters on BA concentration in cecal content 162

A.10 Sensitivity analysis of fitted 6BA model parameters on BA concentration in cecal tissue 163

A.11 Sensitivity analysis of fitted 6BA model parameters on BA concentration in LI content 164

A.12 Sensitivity analysis of fitted 6BA model parameters on BA concentration in LI tissue 165

A.13 Fitted parameter values of enzymatic reactions in the murine conjugation model 165

A.14 Fitted parameter values of transport reactions in the murine conjugation model 166

A.15 Sensitivity analysis of fitted murine conjugation model parameters on BA concentration in liver 167

A.16 Sensitivity analysis of fitted murine conjugation model parameters on BA concentration in venous blood plasma . . . 167

A.17 Sensitivity analysis of fitted murine conjugation model parameters on BA concentration in kidney 168

A.18 Sensitivity analysis of fitted murine conjugation model parameters on BA concentration in SI content 168

A.19 Sensitivity analysis of fitted murine conjugation model parameters on BA concentration in SI tissue 169

A.20 Sensitivity analysis of fitted murine conjugation model parameters on BA concentration in cecal content 170

A.21 Sensitivity analysis of fitted murine conjugation model parameters on BA concentration in cecal tissue 170

A.22 Sensitivity analysis of fitted murine conjugation model parameters on BA concentration in LI content 171

A.23 Sensitivity analysis of fitted murine conjugation model parameters on BA concentration in LI tissue 171

B.1 Literature data of bile acid concentration in venous blood plasma used for model development 200

B.2 Literature data of bile acid concentration in portal blood plasma used for model development 201

B.3 Literature data of bile acid pool size in liver used for model development 201

B.4 Literature data of synthesis and excretion rates used for model development 201

B.5 Literature data of fecal composition used for model development 202

B.6 Literature data of bile composition used for model development 202

B.7 Literature data of intestinal bile flows used for model development . . . 203

B.8 Literature data of postprandial responses in small intestine used for model development . . . 203

B.9 Fitted parameter values of enzymatic reactions and postprandial responses in the 5BA model . . . 204

B.10 Fitted parameter values of hepatic transport reactions in the 5BA model . . . 205

B.11 Fitted parameter values of intestinal transport reactions in the 5BA model . . . 205

B.12 Sensitivity analysis of fitted 5BA model parameters on BA concentration in liver . . . 206

B.13 Sensitivity analysis of fitted 5BA model parameters on BA concentration in PV . . . 208

B.14 Sensitivity analysis of fitted 5BA model parameters on BA concentration in VB . . . 209

B.15 Sensitivity analysis of fitted 5BA model parameters on BA composition in feces . . . 212

B.16 Sensitivity analysis of fitted 5BA model parameters on BA composition in bile . . . 214

B.17 Fitted parameter values of enzymatic reactions and postprandial responses in the human conjugation model . . . 215

B.18 Fitted parameter values of transport reactions in the human conjugation model . . . 215

B.19 Sensitivity analysis of fitted human conjugation BA model parameters on BA concentration in liver . . . 216

B.20 Sensitivity analysis of fitted human conjugation model parameters on BA composition in PV . . . 218

B.21 Sensitivity analysis of fitted human conjugation BA model parameters on BA concentration in VB 219

B.22 Sensitivity analysis of fitted human conjugation model parameters on BA composition in feces 220

B.23 Sensitivity analysis of fitted human conjugation model parameters on BA composition in bile 226

Abstract

Bile acid (BA) metabolism represents a multifaceted system involving a diverse array of primary and secondary, conjugated and unconjugated BAs that engage in constant enterohepatic circulation (EHC). Disruptions in both BA composition and dynamics have been correlated with various ailments. Nonetheless, a comprehensive understanding of the intricate interplay between altered BA metabolism and associated diseases remains elusive. A range of animal models have been harnessed to explore BA metabolism's implications in human disease. Among these models, mice take a prominent role; however, disparities between this preclinical model and humans regarding BA composition, recycling mechanisms, gut physiology, and energy homeostasis exist. Given the inherent intricacy of BA metabolism and the necessity for robust cross-species extrapolation strategies, computational modeling serves as a tool to unravel the mechanistic foundations of the complex network governing BA metabolism. This work endeavors to construct physiologically-based models of BA metabolism in both murine and human contexts. These models recapitulate the synthesis, hepatic and microbial transformations, systemic distribution, excretion, and EHC of BAs at the whole-body level. The murine models were applied in assessments of sex-related and species-specific differences in BA metabolism, as well as the effects of pathophysiological scenarios like BA malabsorption and compromised intestinal barrier function. Conversely, the human models reproduced inter-individual variations in BA levels reported in literature, but also proposing conceivable mechanisms explaining elevated BA levels observed in patients with liver-related disorders. The models developed in this thesis constitute a robust framework for conducting model-assisted inquiries into BA metabolism within prospective studies. Their potential contributions align with the principles of the '3Rs' (Reduction, Refinement, and Replacement) of animal testing and hold potential to advance patient care by enhancing our understanding and prediction of BA-related dynamics in disease.

Zusammenfassung

Der Gallensäure-Stoffwechsel (GS) umfasst ein facettenreiches System, das eine vielfältige Mischung aus primären und sekundären, konjugierten und nichtkonjugierten GS umfasst, die in ständigem enterohepatischem Kreislauf (EHK) zirkulieren. Störungen sowohl in der Zusammensetzung als auch in der Dynamik der GS wurden mit verschiedenen Krankheiten in Verbindung gebracht. Dennoch bleibt ein tieferes Verständnis der komplexen Wechselwirkungen zwischen verändertem GS-Stoffwechsel und assoziierten Krankheiten schwer greifbar. Eine Vielzahl von Tiermodellen wurde genutzt, um die Auswirkungen des GS-Stoffwechsels auf menschliche Krankheiten zu erforschen. Unter diesen Modellen haben Mäuse eine wichtige Stellung. Dennoch bestehen Unterschiede zwischen Mäusen und Menschen, einschließlich der Zusammensetzung der GS, der Recyclingmechanismen, der Darmphysiologie und des Energiegleichgewichts. Angesichts der inhärenten Komplexität des GS-Stoffwechsels und der Notwendigkeit robuster Strategien zur extrapolierenden Untersuchung zwischen Spezies erweist sich die computerbasierte Modellierung als Werkzeug, um die mechanistischen Grundlagen des komplexen physiologischen Netzwerks, das den GS-Stoffwechsel steuert, zu entschlüsseln. Diese Arbeit zielt darauf ab, physiologisch basierte Modelle des GS-Stoffwechsels sowohl im Maus- als auch im humanen Kontext zu entwickeln. Diese Modelle rekapitulieren die Synthese, die hepatischen und mikrobiellen Transformationen, die systemweite Verteilung, die Ausscheidung und den EHK von GS für den gesamten Körper. Die Mausmodelle wurden zur Untersuchung geschlechts- und artenspezifischer Unterschiede im GS-Stoffwechsel sowie der Auswirkungen pathophysiologischer Szenarien, wie GS-Malabsorption und funktioneller Beeinträchtigung der Darmbarriere, eingesetzt. Im Gegensatz dazu reproduzierten die humanen Modelle interindividuelle Variationen der GS-Spiegel und schlugen gleichzeitig denkbare Mechanismen vor, die die erhöhten GS-Werte bei Patienten mit Leber-Krankheiten erklären könnten. Die in dieser Arbeit entwickelten Modelle stellen einen robusten Rahmen für modellgestützte Untersuchungen des GS-Stoffwechsels in prospektiven Studien dar. Ihr potenzieller Beitrag steht im Einklang mit den Grundsätzen der "3Rs" (Reduction, Refinement and Replacement) von Tierversuchen und birgt das Potenzial, die Patientenversorgung durch ein besseres Verständnis und eine Vorhersage der GS-bedingten Dynamik in Krankheiten zu verbessern.

Chapter 1

General introduction

Contributions:
B. Kister wrote this chapter. I. Hawwari, L.M. Blank and L. Kuepfer reviewed the chapter.

Bile acids (BAs), a group of molecules synthesized in the liver from cholesterol, hold a pivotal position in various essential physiological processes. Their multifaceted functions have sparked considerable interest within the scientific community, encompassing not only their contribution to digesting and absorbing dietary fats but also their role as signaling molecules that govern metabolic pathways and gene expression. The intricate interactions between BAs and diverse physiological systems emphasize their significance in upholding overall well-being and have spurred researchers to delve deeper into their intricate behaviors. However, the inherent complexity of BA metabolism make studies challenging and necessitate sophisticated approaches. These intricacies stem from the diverse functions they perform in maintaining physiological homeostasis and their involvement in various diseases. Understanding these complexities and their functional interplay is crucial for unraveling the full impact of BAs on health and disease.

Diverse functions and regulation. Bile acids are more than lipid-digesting agents; they act as signaling molecules and are involved in various metabolic pathways and gene expression. They interact with both nuclear and cell surface receptors, such as farnesoid X receptor (FXR) [1; 2; 3] and pregnane X receptor (PXR) [4], and influence the synthesis of fibroblast growth factors (FGFs) [5; 6], which in turn regulate energy balance, glucose metabolism [7], and lipid homeostasis [8]. The interplay of these pathways is complex and involves intricate feedback mechanisms.

Bile acid pool composition. The BA pool is not a homogeneous entity; it consists of a wide range of primary and secondary BA species, along with their glycine- and taurine-conjugated and sulfated forms. These different BA species exhibit distinct physicochemical properties, like solubility, hydrophobicity, and receptor-binding affinities [9] but also signalling properties [10; 11]. The composition of the BA pool varies among species [12], individuals [13; 14; 15], and physiological conditions, adding layers of complexity to their metabolism.

Enterohepatic circulation. Bile acids undergo a continuous recycling process known as the enterohepatic circulation (EHC). This involves their secretion into bile, storage in the gallbladder, release into the small intestine upon food consumption, reabsorption from the intestine, and subsequent return to the liver via the portal vein. The EHC plays a pivotal role in BA homeostasis and requires coordination between the liver, gallbladder, intestine, and systemic circulation.

Gut microbiota interaction. The gut microbiota significantly influences BA metabolism. Microbes can metabolize primary BAs to generate secondary BAs [16; 17]. These microbial modifications include deconjugation, dehydrogenation, dehydroxylation, and epimerization. Conversely, BAs can shape the composition of the gut microbiota [18; 19], creating a bidirectional relationship that further complicates their role in health and disease.

Pathophysiological implications. Bile acid dysregulation is implicated in various diseases, including metabolic disorders (e.g., obesity, diabetes), liver diseases (e.g., non-alcoholic fatty liver disease, cholestasis) [20; 21; 22; 23; 24; 25], inflammatory bowel diseases [26; 27], and even certain cancers [28]. The intricate cross-talk between BAs, immune responses, and cellular signaling pathways suggests a role in disease pathogenesis.

Inter-individual variability. Due to a multitude of factors, such as genetic differences, variations in enzymatic activity, transporter expression, and microbial composition, there is significant inter-individual variability in BA metabolism. This variability contributes to differences in response to dietary intake, medications, and disease susceptibility [13; 14; 15].

Temporal dynamics. Bile acid levels and composition can exhibit temporal variations influenced by circadian rhythms, meal timing, and fasting periods [29; 30; 31; 32]. These temporal dynamics introduce additional layers of complexity when attempting to model and predict BA behavior.

In essence, the complexities of BA metabolism stem from the interplay of diverse functions, intricate regulatory pathways, variations in BA pool composition, microbiota interactions, disease implications, inter-individual variability, temporal dynamics, and therapeutic considerations.

Computational modeling, physiologically-based (pharmacokinetic; PBPK) approaches in particular, has emerged as a valuable tool to study BA metabolism and its impact on various aspects of human health and disease. These models leverage mathematical and computational techniques to simulate the behavior of biological systems, offering a unique vantage point to study processes that are challenging to investigate solely through traditional experimental methods. The interest in PBPK modeling of BAs stems from several compelling reasons:

Mechanistic insight. PBPK models are based on a mechanistic understanding of the underlying physiological processes. This enables a detailed and comprehensive representation of the entire lifecycle of BAs, including their synthesis, hepatic and microbial transformations, circulation, distribution, and excretion. Such mechanistic insight allow for the exploration of the complexities of BA metabolism with a high degree of precision.

Integration of diverse data. Bile acid metabolism involves a plethora of factors, including genetics, enzymatic reactions, transporters, gut microbiota, and dietary influences. Computational models provide a platform to integrate diverse data types and knowledge from different disciplines, facilitating a more holistic understanding of the intricate factors that influence BA behavior.

Prediction and hypothesis generation. Computational models allow researchers to predict how changes in specific parameters or components might impact BA metabolism. These predictions can guide experimental design, aid in hypothesis generation, and identify key factors driving complex behaviors.

Cross-species extrapolation. Bile acids vary significantly between species like mice and humans in terms of composition and recycling mechanisms. PBPK models are adaptable and can be parameterized for different species, facilitating cross-species extrapolation. This is crucial for understanding the relevance of findings in animal studies to human physiology.

Reduction of animal experiments. By simulating various scenarios and conditions, PBPK models can reduce the need for extensive animal experiments, aligning with ethical considerations and the ″3R″ principles of reduction, refinement, and replacement in animal testing. By using computational models, researchers can minimize the use of animals in experiments while still obtaining valuable insights.

Clinical relevance. PBPK models can be tailored to clinical scenarios, making them highly relevant for studying BAs in the context of human diseases. By incorporating patient-specific data, these models can simulate BA behavior in individuals with specific health conditions, aiding in diagnosis and treatment planning.

Personalized medicine and therapeutic insights. Bile acid-based therapies are being explored for various diseases. PBPK models can assist in optimizing strategies for therapeutic intervention by simulating how different treatments might modulate BA metabolism in specific patient populations.

Disease modeling. PBPK modeling allows for the investigation of how alterations in BA metabolism are associated with various diseases. Pathological conditions can be simulated to gain insights into the mechanisms underlying these diseases.

In summary, physiologically-based modeling offers a powerful and versatile approach to study BA metabolism, providing mechanistic insights, enabling cross-species extrapolation, and offering clinical relevance. It reduces the reliance on animal testing, aids in hypothesis generation, and allows for the exploration of various scenarios, making it an invaluable tool in understanding the complexities of BA metabolism and its implications for health and disease.

Scope of this thesis This work is an endeavor to develop physiologically-based computational models that elucidate the intricacies of BA metabolism at the whole-body level, for both mice and humans. These models aim to address the multifaceted nature of the BA pool with a sufficient level of intricacy, encompassing processes such as synthesis, hepatic and microbial conversions, (re-)circulation, and excretion. The murine model's potential applications align with the principles of the "3Rs" of animal testing, while also offering a platform for further inquiries into interactions with the microbiome. On the other hand, the human model seeks to analyze BA measurements within a patient cohort affected by liver disease.

The outlined structure was followed:

1. General Introduction: Overview and motivation
2. Background: Introduction to current knowledge of BA metabolism and details about the applied methodology
3. Results for both mouse and human models: Model development followed by model predictions
4. General conclusion and outlook
5. Material and methods for the results discussed before
6. Appendices containing additional and supportive information

The subsequent research chapters are first underpinned by an introduction and background section, where the scientific foundation of this work is presented. This segment delves into the existing knowledge of BA metabolism, expounding upon their physicochemical properties, synthesis, metabolism, circulation, regulation, and implications in signaling and disease. Furthermore, this section illustrates the basics of model development, elucidating various modeling approaches, with a specific emphasis on PBPK models. These sophisticated tools facilitate the simulation of drug/molecule fate within the body. This introductory section extends to encompass instances of published PBPK models that describe BA metabolism. Chapters 3 and 4 present the mechanistic models of BA metabolism developed as part of this thesis. Each chapter commences by outlining the general development process, fundamental considerations for model construction, and the dataset used for calibration and validation. Subsequently, these chapters focus sequentially on two distinct model variants, one encapsulating different BA species and the other accounting for their conjugation status. These sections delve first into the specifics of each model variant - including more detailed information of their structure, in-depth discussions on model calibration and validation, and the execution of predictions that underscore the model's applicative potential. In this context, chapter 3 delves into the murine models' ability at predicting BA levels and composition throughout the body, as well as its insights into pathophysiological scenarios like bile acid malabsorption (BAM) and compromised gut barrier function. A portion of Chapter 3's findings were published as an original article in iScience [33]. Chapter 4, in turn, showcases the human models' proficiency in recapitulating inter-individual variations during postprandial responses through population simulations. Moreover, it was used to propose plausible mechanisms behind markedly elevated BA levels in patients afflicted with liver disease. In conclusion, the final chapter provides a concise summary and outlook that encapsulates the research chapters while situating the study within the current scientific context. Preceded by the material and methods section, as well as the bibliography referenced in this work, supplementary information pertinent to the research chapters is compiled in the appendices.

Chapter 2

Background

Contributions:
B. Kister prepared the figures and wrote this chapter. J. Steck, I. Hawwari, L.M. Blank and L. Kuepfer reviewed the chapter.

2.1 Bile acids

The importance of bile to a healthy metabolism has been recognized since the early days of medicine, even during the Hippocratic era. In Greek, Roman, and medieval medicine, yellow bile associated with the gallbladder was identified as one of the four main "humours" that should be balanced for good health. However, very little of the ancient humourism theory has stood the test of time, as modern medicine has progressed significantly. Although some descriptions of yellow bile from ancient times can be related to modern medicine and the greek terms are still in use today, most of the ancient practices and theories have been rendered obsolete, e.g. the association of excess of yellow bile and fiery personality traits (choleric). Nevertheless, it wasn't until the latter half of the 20th century, with advancements in technology, that a deeper understanding of bile metabolism and composition was achieved [34]. Despite the progress made in the past 70 years, the topic remains a subject of ongoing scientific discussion. Modern medicine may have moved away from the ancient concept of humourism, but the complexity of BA function, structure, and metabolism, as well as the enzymes and genes involved, is still not fully understood. Bile acids have been recognized as multifunctional metabolites that serve as endogenous detergents in the intestines, a major route of cholesterol excretion, modulate the intestinal bacterial community, and regulate central metabolic genes through various cell signalling cascades. Understanding the various effects of BAs on energy metabolism and homeostasis has become increasingly complex, making it challenging to fully characterize and quantify their role in metabolic health and disease.

2.1.1 Biochemistry

In biomedical literature, the term "bile acids" or "bile salts" typically refers to the "modern" BAs [35], which have 24 carbon atoms and are abbreviated as C24 BAs. In contrast, "primitive" BAs, found in primitive (e.g. coelacanth and sharks) and less primitive (e.g. reptiles and amphibians) vertebrates, have 25-27 carbon atoms (C25, C26, C27 BAs) in their BA pool.

Bile acids have a distinctive molecular structure with an approximate length of 20 Å and an average radius of about 3.5 Å [36]. They are derived from a saturated tetra-cyclic hydrocarbon perhydrocyclopentanophenanthrene system known as the steroid nucleus, which consists of three six-member rings (A, B, and C) and a five-member ring (D) (Figure 2.1).

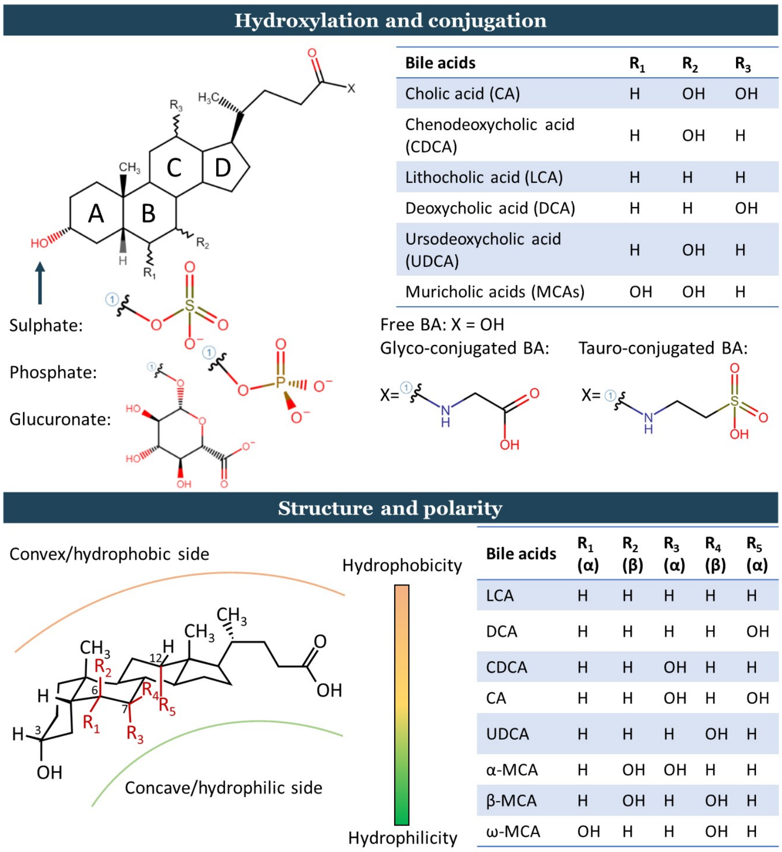
Hydroxylation and conjugation
A
B
C
D
Sulphate:
Phosphate:
Glucuronate:
Free BA: X = OH
Glyco-conjugated BA:
Tauro-conjugated BA:
Structure and polarity
Convex/hydrophobic side
Concave/hydrophilic side
Hydrophobicity
Hydrophilicity

Bile acids	R_1	R_2	R_3
Cholic acid (CA)	H	OH	OH
Chenodeoxycholic acid (CDCA)	H	OH	H
Lithocholic acid (LCA)	H	H	H
Deoxycholic acid (DCA)	H	H	OH
Ursodeoxycholic acid (UDCA)	H	OH	H
Muricholic acids (MCAs)	OH	OH	H

Bile acids	R_1 (α)	R_2 (β)	R_3 (α)	R_4 (β)	R_5 (α)
LCA	H	H	H	H	H
DCA	H	H	H	H	OH
CDCA	H	H	OH	H	H
CA	H	H	OH	H	OH
UDCA	H	H	H	OH	H
α-MCA	H	OH	OH	H	H
β-MCA	H	OH	H	OH	H
ω-MCA	OH	H	H	OH	H

Figure 2.1: Structure of BA species. Overview of different BA species, their structure and resulting polarity. The upper panel shows sites for and configuration of hydroxylation and conjugation with varies moieties and resulting BA nomenclature of BA species. The lower panel displays the 3D structure of BAs and the relationship between BA hydroxylation and the molecule's hydrophobicity. Adapted from Thomas et al. [37].

The molecular nucleus has a curved or flat structure, depending on a cis- or trans-fused configuration between the A and B rings. In mammals, the nucleus is almost always 5α (A/B junction in cis configuration), while in lower vertebrates, some BAs, known as allo-BAs, exhibit an A/B trans-fusion. There are 11 chiral carbon atoms. As far back as the 1960s, Haslewood recognized the biological importance of chemical differences in bile salts [38] and observed that the chemical nature of the bile salts of more primitive animals indicates an evolution from C27, 5α-alcohol sulfates to C24, 5β-acids [39]. Bile acids from different species differ chemically in three structural aspects: (1) side-chain structure; (2) stereochemistry of the A/B ring fusion (as mentioned above); and (3) the distribution of the number, position, and stereochemistry of hydroxyl groups in the steroid nucleus. Nearly all primary BAs and bile alcohols, which occur in less evolved forms of life, have a 7α-hydroxyl group, with the exception of ursodeoxycholic acid (UDCA). Most evolved mammalian BAs have a 5β-configuration with hydroxyl groups at 3α, 7α, and 12α, whereas C27 bile alcohol sulfates, which increase water solubility, are widespread in nature. The most common BAs in human and mice are depicted in figure 2.1. These C27 BA are the dominant bile salts of ancient mammalian species, cartilaginous fishes, and some amphibians. The West Indian manatee was the first mammal found to lack BAs, presumably because it lacks the enzymes required for oxidation of the 26-hydroxyl group to a carboxylic acid [36].

At physiological conditions, BAs exist as bile salts in ionized form due to their weak acid properties. The pKa values of unconjugated BAs (uBAs) are around 5, but conjugation with amino acids lowers pKa to less than 2 for taurine conjugates (T-BAs) and around 4 for glycine conjugates (G-BAs). Bile acid amidation enhances their physicochemical properties, including increased hydrophilicity and aqueous solubility, reduced cytotoxicity, and better resistance to precipitation during digestion under low pH or the presence of divalent cations like Ca^{2+} [40]. As such, conjugated BAs are slightly stronger acids with lower pKa values, and T-BAs are soluble even at gastric pH values [41].

The natural BAs are derivatives of 5β-cholanic acid with a cis A-B ring junction, which imparts a slight curvature to the steroid skeleton. This curvature creates two distinct hemispheres in BA molecules: a convex, hydrophobic β side with angular methyl groups at C18 and C19, and a concave, hydrophilic α side with 1-3 polar hydroxyl groups [42] (Figure 2.1). The polar groups' orientation towards one hemisphere imparts facial amphiphilicity to BAs, in contrast to conventional surfactants that have clearly separated polar head groups and long non-polar hydrocarbon chains. The exception are ursodeoxycholic acid (UDCA) and muricholic acids (MCAs), which have hydroxyl groups on both α and β sides, giving it increased hydrophilicity [43].

Bile acids, as facial amphiphiles, have specific surface-active and interfacial properties. They tend to orient at the oil-water interface with the steroid backbone parallel to the interface, allowing the hydroxyl groups to interact with water molecules. However, due to less efficient packing at the interface compared to conventional surfactants, BAs have higher surface tension values in aqueous solutions [44]. It has been demonstrated that increasing the hydrophobicity of BAs, as in the case of deoxycholic acid (DCA) obtained by removing a hydroxyl group from cholic acid (CA), leads to higher affinity for the oil-water interface and more efficient inter-facial protein displacement [45]. Hydrophobicity and cytotoxicity of BAs depends heavily on the number, position and orientation of hydroxyl groups as well as conjugation with taurine or glycine (tauro-conjugation more hydrophilic than glyco-conjugation; free species most hydrophobic) [46]. Bile acid hydrophobicity as well as cytotoxicity decrease in general with the number of hydroxyl-groups but is most strongly reduced with hydroxyl-groups oriented towards the hydrophobic, convex β side of the steroid nucleus. Bile acid hydrophobicity increases in the following order: MCAs ($\omega < \beta < \alpha$) $<$ UDCA $<$ CA $<$ chenodeoxycholic acid (CDCA) $<$ DCA $<$ lithocholic acid (LCA), with MCAs and UDCA being the most hydrophilic and LCA the most hydrophobic natural BA in mouse and human.

Bile acids are able to form supra-molecular aggregates or micelles in water due to their amphiphilic properties. Micelle formation occurs when the concentration of BAs exceeds a certain value called the critical micellar concentration (CMC). Naturally occurring BAs have CMC in the range of 2-20 mM in water, which is consistent with their aqueous solubility at body temperature. Because of their rigid molecular framework and planar polarity, BAs tend to form smaller micelles with low aggregation numbers and higher CMC values compared to conventional surfactants [47]. A list of CMC of BAs that were used here is displayed in table 2.1.

Table 2.1: Critical micellar concentration of bile acids. Adapted from Pavlovic et al. [48]

Bile acid	**OH groups**	**CMC [mM]**
CA	$3\alpha\ 7\alpha\ 12\alpha$	11-13
CDCA	$3\alpha\ 7\alpha$	4-9
DCA	$3\alpha\ 12\alpha$	3-10
UDCA	$3\alpha\ 7\beta$	7-19
T-CA	$3\alpha\ 7\alpha\ 12\alpha$	6-10
G-CA	$3\alpha\ 7\alpha\ 12\alpha$	10-12
T-CDCA	$3\alpha\ 7\alpha$	3
G-CDCA	$3\alpha\ 7\alpha$	2-6
T-DCA	$3\alpha\ 12\alpha$	2
G-DCA	$3\alpha\ 12\alpha$	2-6
T-UDCA	$3\alpha\ 7\beta$	2
G-UDCA	$3\alpha\ 7\beta$	4

The CMC of BAs are inversely proportional to their hydrophobicity, as measured by reverse phase HPLC retention factors [49; 50]. This indicates that micelle formation is driven by minimizing the hydrophobic surface. However, conjugation of BAs with glycine or taurine can result in lower CMC values, suggesting that the interplay between the hydrophobic effect and specific hydrogen bonding interactions may contribute to the micellization process [49; 50]. The stability of BA micelles depends on both the structural properties of BAs and solution conditions such as temperature, pH, and ionic strength. Generally, CMC values increase with the addition of hydroxyl groups, changing the orientation of a hydroxyl group from α- to β-side of the steroid backbone, replacing the hydroxyl group with a keto (oxo) group, and shortening the side chain of conjugated BAs [51]. The reaction of 7β-epimerization of CDCA mediated by intestinal bacteria leads to the formation of UDCA, which has a higher CMC value and reduced solubilization capacity for lipids compared to CDCA. This is due to the presence of polar groups on both hemispheres of the BA molecule [16]. The CMC of BAs decreases with increasing ionic strength because electrolyte addition reduces repulsive electrostatic interactions between charged groups. Reduction of pH to values close to the pKa of the BA also lowers CMC due to partial protonation of BA anions, which become solubilized in bile salt micelles [52].

Bile acids are able to self-assemble over a broad concentration range, which sets them apart from conventional surfactants. They have two CMC values and form spherical micelles at the first CMC. The structural transition from spherical to long rod-like micelles occurs at the second CMC value [53]. The micellization process involves two key forces: hydrophobic and hydrogen bonding interactions and follows a two-step model [54]. The first step involves the formation of primary aggregates, driven by hydrophobic interactions between hydrophobic surfaces of the monomers creating a hydrophobic cavity with polar groups pointing outwards. At higher BA concentrations, intermolecular hydrogen bonding between the hydrophilic groups of primary units creates a central hydrophilic core, which is a complementary mechanism to the formation of secondary micelles.

2.1.2 Bile acid metabolism

Perivenous (centrilobular) hepatocytes, which are located around the central vein, are responsible for producing the highest amount of BAs in the liver [55]. Cholesterol, which is hydrophobic and uncharged, is converted into organic anions, i.e. BAs, during this process. This pathway is essential for cholesterol catabolism, and the rate of BA formation plays a vital role in maintaining cholesterol homeostasis [55]. Nearly 50% of the daily turnover of cholesterol is accounted for by the synthesis of BAs [56]. Besides synthesis of BAs from cholesterol, BA undergo conjugation with amino acids, microbial transformations in the gut and further varying modifications, diversifying the BA pool tremendously. Figure 2.2 illustrates the significant steps involved in BA metabolism.

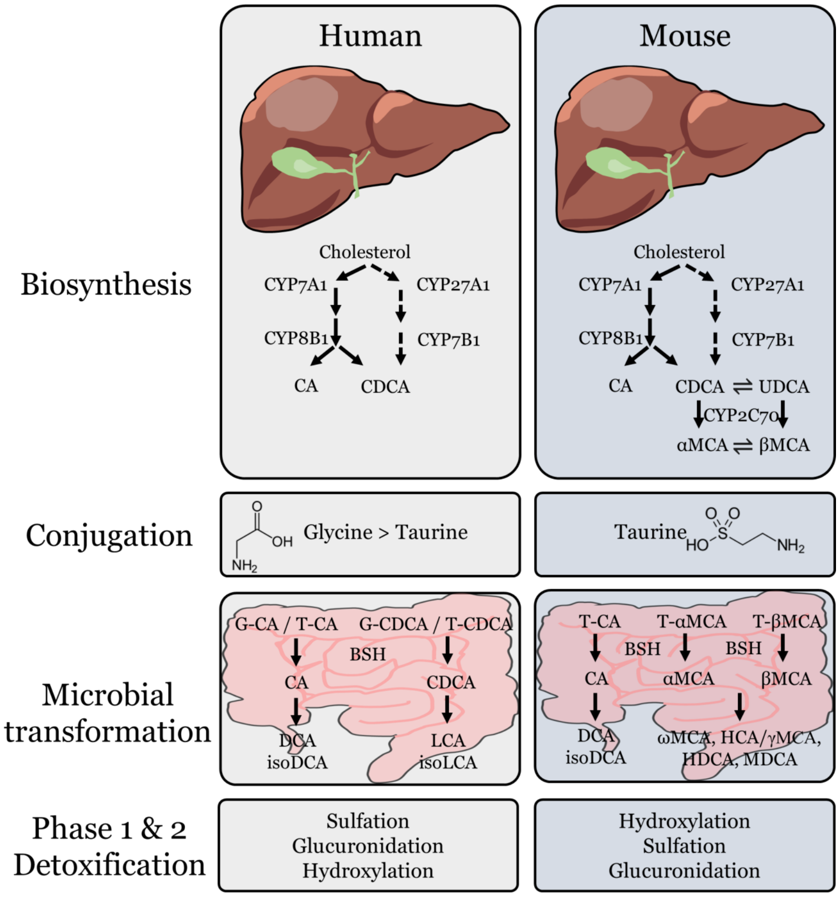
Human
Mouse
Biosynthesis
Cholesterol
CYP7A1
CYP27A1
CYP8B1
CYP7B1
CA
CDCA
CDCA ⇌ UDCA
CYP2C70
αMCA ⇌ βMCA
Conjugation
Glycine > Taurine
Taurine
Microbial transformation
G-CA / T-CA
G-CDCA / T-CDCA
BSH
CA
CDCA
DCA
isoDCA
LCA
isoLCA
T-CA
T-αMCA
T-βMCA
BSH
CA
αMCA
βMCA
DCA
isoDCA
ωMCA, HCA/γMCA,
HDCA, MDCA
Phase 1 & 2 Detoxification
Sulfation
Glucuronidation
Hydroxylation
Hydroxylation
Sulfation
Glucuronidation

Figure 2.2: Overview of BA metabolism. Schematic overview of BA metabolism detailing synthesis, conjugation, microbial transformation as well as phase 1 and 2 detoxification in human and mouse. Adapted from Li and Dawson [17]

The process of (primary) BA synthesis is complex and involves multiple enzymes in various cellular compartments, including the cytosol, endoplasmic reticulum, mitochondria, and peroxisomes (Figure 2.3). The overall pathway can be divided into two major pathways: the classic (neutral) pathway and the alternative (acidic) pathway. The classic pathway produces most of the BAs in mice and humans [57]. In this pathway, the sterol nucleus of cholesterol is modified before the oxidative cleavage of its side chain. On the other hand, the alternative pathway starts with an initial hydroxylation on the side chain of cholesterol, followed by 7α-hydroxylation of the sterol nucleus.

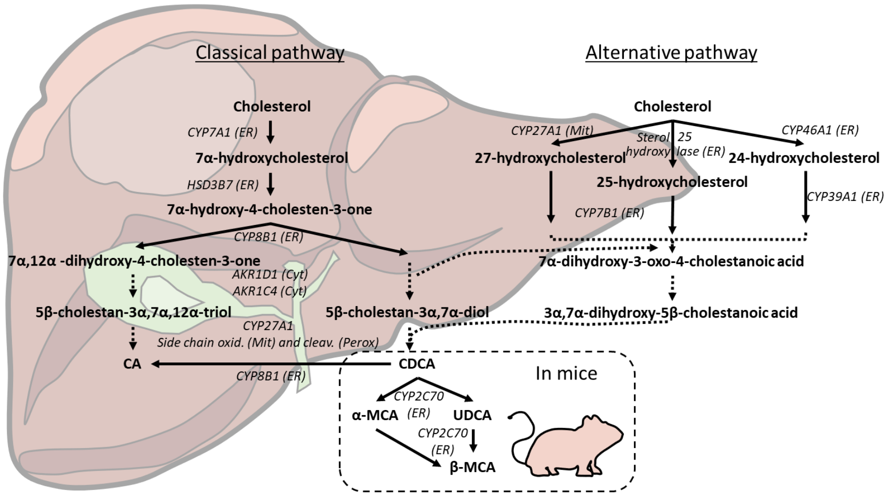
Classical pathway
Cholesterol
CYP7A1 (ER)
7α-hydroxycholesterol
HSD3B7 (ER)
7α-hydroxy-4-cholesten-3-one
CYP8B1 (ER)
7α,12α -dihydroxy-4-cholesten-3-one
AKR1D1 (Cyt)
AKR1C4 (Cyt)
5β-cholestan-3α,7α,12α-triol
5β-cholestan-3α,7α-diol
CYP27A1
Side chain oxid. (Mit) and cleav. (Perox)
CA
CDCA
CYP8B1 (ER)
Alternative pathway
Cholesterol
CYP27A1 (Mit)
Sterol 25 hydroxylase (ER)
CYP46A1 (ER)
27-hydroxycholesterol
25-hydroxycholesterol
24-hydroxycholesterol
CYP39A1 (ER)
CYP7B1 (ER)
7α-dihydroxy-3-oxo-4-cholestanoic acid
3α,7α-dihydroxy-5β-cholestanoic acid
In mice
CYP2C70 (ER)
α-MCA
UDCA
CYP2C70 (ER)
β-MCA

Figure 2.3: Synthesis of primary BAs in the liver. Overview of the reactions and enzymes involved in synthesis of primary BAs through the classical and alternative pathway. If not otherwise stated, reactions occur both in human and murine liver. Dotted arrows depict multi-step processes. Used abbreviations: ER: endoplasmic reticulum; Mit: mitochondria; Cyt: cytosol; Perox: peroxisomes.

The classic pathway

Bile acid synthesis occurs mainly in the liver [58] predominately driven via the classic or "neutral" pathway. In this pathway, modifications to the steroid nucleus occur before side-chain oxidation by CYP27A1; wherefore, most intermediaries do not have a carboxyl-side group until later in the pathway.

Cholesterol 7α-hydroxylase (CYP7A1) is the microsomal enzyme responsible for hydroxylating cholesterol at the C7 position, which is the first and rate-limiting step of the pathway. The resulting 7α-hydroxycholesterol is converted to 7α-hydroxy-4-cholesten-3-one (C4) by HSD3B7, a microsomal hydroxysteroid dehydrogenase. HSD3B7 also catalyzes the epimerization of the 3β-hydroxyl group of cholesterol to the 3α-hydroxyl of BAs [59].

C4 is the precursor for the synthesis of two primary BAs: CA and CDCA, and its concentration in serum is used as a biomarker for the rate of BA synthesis. Microsomal sterol 12α-hydroxylase (CYP8B1) metabolizes C4 and converts it to CA, or if its action is absent, C4 is converted to CDCA. Thus, the activity of CYP8B1 determines the ratio of CA to CDCA.

The hydroxylation of C4 at the C12 position by CYP8B1 produces 7α,12α-dihydroxy-4-cholesten-3-one, which undergoes NADPH-dependent reductions at the C5 and C3 positions by aldo-keto reductase 1D1 (AKR1D1) and 1C4 (AKR1C4), respectively. Reduction of the C3 double bond by AKR1C4 produces 3α,7α,12α-cholesten-5β-triol.

The intermediaries then have their side chains oxidized by CYP27A1 in mitochondria (-OH $\rightarrow$ -COOH) to form 3α,7α,12α-trihydroxycholestanoic acid or 3α,7α-dihydroxycholestanoic acid without CYP8B1 action, depending on its presence or absence. These intermediaries are activated to form BA-CoA thioesters by peroxisomal long-chain acyl-CoA synthase (BACS), and then enter peroxisomes via an ATP-binding cassette (ABC) D3 transporter for β-oxidation reactions to cleave a propionyl-CoA to form cholyl-CoA and chenodeoxycholyl-CoA, respectively. Bile acid-acyl-CoAs are then conjugated to the amino acids taurine or glycine by BA-CoA: amino acid N-acyltransferase (BAAT) to form conjugated BAs, which are secreted into bile. Fan et al. [60] have shown that human CYP8B1 can directly convert CDCA to CA by catalyzing 12α-hydroxylation using a fission yeast-based expression system. However, the relevance of this observation *in vivo* needs to be further examined.

The alternative pathway

The "acidic" pathway, also known as the alternative pathway of BA synthesis, differs from the classical or "neutral" pathway in that it involves cholesterol side-chain oxidation upstream of the pathway before modifications to the steroid nucleus. C27 BAs and oxysterols produced in various cells are transported to the liver to produce C24 BAs in hepatocytes. The majority of 24-hydroxycholesterol in the liver originates from the brain [58], while 27-hydroxycholesterol is the most abundant oxysterol in mouse and human plasma [61; 62]. Sterol 27-hydroxylase synthesizes 27-hydroxycholesterol from cholesterol in multiple tissues, including the liver.

The first step of the acidic pathway is catalyzed by mitochondrial/microsomal C24, C25, and C27 sterol hydroxylases that hydroxylate cholesterol to form 24-, 25-, and 27-hydroxycholesterol, respectively. These are then quickly hydroxylated at 7α-position by microsomal oxysterol 7-

hydroxylase (CYP7B1) [63]. Sterol 24-hydroxylase (CYP46A1) hydroxylates cholesterol to form 24-hydroxycholesterol in the membranes of the smooth endoplasmic reticulum of neurons in the mammalian central nervous system [64]. In studies of CYP46A1 and CYP27A1 knockout mice, no alterations in BA synthesis could be observed. Moreover, cholesterol 7α-hydroxylase deficient mice show BA pool sizes half of wildtype mice as these cannot convert cholesterol directly into BA [65; 66]. Based on observations in a human subject with cholesterol 7α-hydroxylase deficiency [67], it is estimated that the alternative pathway in humans contributes only 5%-10% to the overall BA pool, whereas in mice estimates are around 50%. Interestingly, female mice have little or no CYP7B1 but do not have decreased BA levels [68].

The alternative pathway's products feed into the downstream reactions shared by the classic pathway. The alternative pathway for oxysterol synthesis is present in numerous tissues, with side-chain oxidation followed by 7α-hydroxylation of the sterol nucleus by CYP7B1 in most tissues. Notably, CYP7A1 and CYP7B1 both add a 7-hydroxyl group to their respective substrates, but CYP7A1 is a highly specific cholesterol 7α-hydroxylase in the classic pathway, while CYP7B1 is an oxysterol 7α-hydroxylase in the alternative pathway. CYP7B1 prefers 25-hydroxycholesterol and 27-hydroxycholesterol as substrates, whereas CYP39A1 sterol 7α-hydroxylase is selective for 24-hydroxycholesterol [58].

Synthesis of MCAs

CYP2C70 is responsible for converting CDCA (3α,7α) into β-MCA (3α,6β,7α) through 6β-hydroxylation in mice. In addition, UDCA (3α,7β) which is a primary BA in mice, is produced from CDCA through epimerisation by CYP2C70.

The synthesis of β-MCA (3α,6β,7β) occurs through two pathways: the epimerization of the hydroxyl-group on C7 (from 7α to 7β) of α-MCA and the 6β-hydroxylation of UDCA [69; 70; 71]. CYP2C70 is responsible for both reactions [71]. Previous studies have reported that CYP2C70 converts CDCA to α-MCA and UDCA to β-MCA. Knockout mice models lacking *Cyp2c* gene cluster were shown to have complete absence of both α-MCA and β-MCA in the liver. The analysis of individual recombinant *Cyp2c* genes expressed in HepG2 cells revealed that CYP2C70 produces α-MCA from CDCA and β-MCA from UDCA [69]. These findings were further validated by the generation of *Cyp2a12* and *Cyp2c70* single and double knockout mice by Honda et al. [70]. They also demonstrated that murine Cyp2A12 converts DCA, a secondary BA, to primary BAs as evidenced by the accumulation of DCA in *Cyp2A12*-null mice. However, the accumulation of UDCA was found to be much lower than CDCA in *Cyp2C70* knockout mice, suggesting that most β-MCA is synthesized from CDCA via α-MCA. Therefore, epimerization of α-MCA to produce β-MCA appears to be the predominant pathway rather than producing β-MCA directly from UDCA [70; 72]. Inactivation of liver-specific CYP2C70 function resulted in mice with a human-like BA composition, including a decrease in FXR antagonist β-MCA and an increase in FXR agonist CDCA, leading to increased BA concentrations and even hepatotoxicity [73].

Conjugation

Bile acid synthesis involves eventually the addition of an amino acid, typically glycine or taurine, to the C24 via an amide linkage. Conjugated BAs show decreased cytotoxicity and are more soluble than their unconjugated counterparts. Newly synthesized BAs as well as those recycled to the liver via enterohepatic circulation are activated by reacting with coenzyme A, forming a BA-coenzyme A thioester (BACO-SCoA). This reaction is catalyzed by BACS (SLC27A5), and the BACO-SCoA then reacts with either taurine or glycine to form conjugated BAs, which is catalyzed by a cytosolic BA-CoA–amino acid N-acyltransferase (BAAT). This reaction is very efficient. The two steps, shown briefly, proceed as follows:

$$\mathrm{BA + CoA + ATP \xrightarrow{BACS} BA{-}CoA + AMP + PPi}$$

$$\mathrm{BA{-}CoA + Taurine/Glycine \xrightarrow{BAAT} G{-}BA/T{-}BA + CoASH}$$

Bile acid side chains in mammals are usually conjugated with either taurine or glycine, resulting in notable species-specific differences in conjugation patterns. For instance, rabbits and guinea pigs primarily produce glycine conjugates, while sheep, dogs, and mice mostly form taurine conjugates [17]. In mice, the BAAT enzyme is specific for taurine, explaining the prevalence of taurine-conjugated BAs in mice [74]. On the other hand, both glycine and taurine conjugates are formed in humans and rats. Interestingly, some primates like chimpanzees, baboons, and rhesus monkeys also exhibit a preference for taurine conjugation, whereas humans tend to produce 70-75% glycine conjugates and 25-30% taurine conjugates

[75; 76]. This difference may be attributed to the species-specific affinity of the BAAT enzyme for either taurine or glycine.

Under physiological conditions, BA sulfation constitutes a minor process, but during cholestasis, slowing or stalling of bile flow through the biliary system, it plays a significant role in eliminating BAs through bile and urine. The process of sulfation involves the transfer of a sulfonate group (SO_3^-) from a universal donor molecule called 3′-phosphoadenosine 5′-phosphosulfate (PAPS) to an acceptor molecule, such as a hydroxyl, amino, or carboxylic acid group of the substrate, and is catalyzed by sulfotransferases (SULTs). The resulting conjugates are negatively charged and highly water-soluble, which enhances their clearance. Although ″sulfonation″ is the more accurate chemical term, ″sulfation″ is used for historical reasons [77].

The pathway for the elimination of BA-sulfates is via urine or feces. BA-sulfates may be exported from the liver into bile and subsequently excreted in feces. This clearance is facilitated by the fact that BA-sulfates are not efficiently absorbed from the intestine. Bile acid sulfates may also be shuttled into the sinusoidal blood by multidrug resistance-associated protein (MRP) 3 and MRP4 for renal excretion [77]. In cholestasis, bile flow decreases and sulfated BAs are excreted in larger amounts into the sinusoidal blood for renal excretion, indicating a cellular adaptive response [78; 79].

Cytosolic SULTs catalyze BA sulfation, and over half of LCA present in human bile is in sulfated form [80]. Previous studies have reported conflicting results regarding the proportion of BA-sulfate species in humans, but it is now understood that in humans, the primary site for sulfation is the 3α-OH, whereas in mice, it is the 7α-OH. This results in the formation of BA-3-sulfate and BA-7-sulfate species in humans and mice, respectively [81; 82]. SULT2A1 is responsible for BA-3-sulfation in humans [83], while SULT2A1 and 2A8 catalyze BA-7-sulfation in mice [84]. Bile acid-7-sulfates are more resistant to hydrolysis and metabolism by the intestinal microbiome than BAs sulfated at the C3 position which in turn prevents their absorption from the intestine [85].

Gut microbiome and bile acids

Bile acids undergo microbial transformation primarily in the distal part of the small intestine and the large intestine [16; 17]. This process generates secondary BA through various reaction pathways, including deconjugation, dehydrogenation, dehydroxylation, and epimerization. Bile salt hydrolase (BSH) catalyzes the deconjugation of BA, removing the amino acid (taurine or glycine) and producing unconjugated BA (uBA). Hydroxysteroid dehydrogenases are bacterial enzymes that epimerize and oxidize/reduce the 3-, 7-, and 12-OH groups of BAs. The 7-dehydroxylation of primary BA by BA 7-dehydroxylating bacteria is particularly important in generating 7-dehydroxylated secondary BAs (e.g., DCA and LCA). The 7-dehydroxylated BA, especially DCA and LCA, constitute the majority of secondary BA [86] and DCA and LCA predominate in the feces. In mice, ω-MCA is the major β-MCA metabolite produced by gut microbiota [87]. Unconjugated α-, β-, and ω-MCAs can be subjected to bacterial 7α or 7β-dehydroxylation to yield HDCA or MDCA; however, this appears to be a minor pathway compared with 7α-dehydroxylation of CA in the intestine of rats [17]. In humans, CYP3A4 further metabolizes LCA into more hydrophilic hyocholic acid (HCA) and UDCA in the intestine, which are less toxic. Overall dehydrogenation, epimerization and oxidation reactions can produce over 20 metabolites around C-3, C-7, and C-12 [16] and are illustrated in figure 2.4.

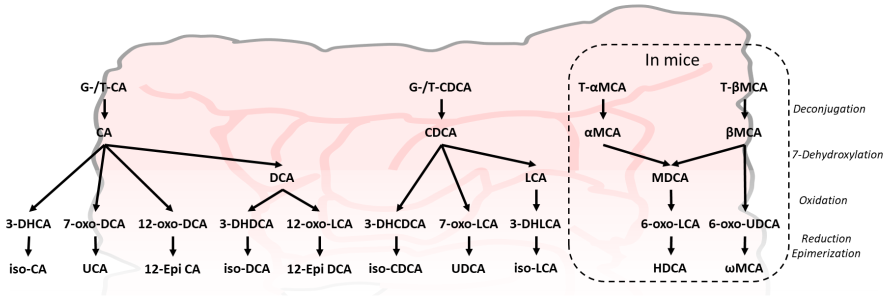
In mice
G-/T-CA
CA
DCA
G-/T-CDCA
CDCA
LCA
T-αMCA
T-βMCA
αMCA
βMCA
MDCA
Deconjugation
7-Dehydroxylation
Oxidation
Reduction
Epimerization
3-DHCA
7-oxo-DCA
12-oxo-DCA
3-DHDCA
12-oxo-LCA
3-DHCDCA
7-oxo-LCA
3-DHLCA
6-oxo-LCA
6-oxo-UDCA
iso-CA
UCA
12-Epi CA
iso-DCA
12-Epi DCA
iso-CDCA
UDCA
iso-LCA
HDCA
ωMCA

Figure 2.4: Synthesis of secondary BAs. Overview of microbial reactions in the gut yielding secondary BAs. If not otherwise stated, reactions occur both in human and murine intestine.

Recirculated bile acids in the liver

Bile acids that are recirculated via EHC and transported to the liver are taken up by hepatocytes through the sodium-taurocholate cotransporting polypeptide (NTCP) and organic-anion-transporting polypeptides (OATPs), as described in a later section of this chapter, thus completing the enterohepatic circulatory cycle. Within hepatocytes, the deconjugated BAs are subject to modification through reconjugation with glycine or taurine. The extent of modification, particularly at position 7 for rehydroxylation, differs among species. In humans, DCA does not undergo 7-rehydroxylation, whereas in mice and rats, it is converted to CA through 7-rehydroxylation, which is mediated by CYP2A12 in mice [70]. Bile acids with a 3β-OH group are epimerized to 3α-OH BAs. The degree of reduction of oxo groups to α- and/or β-OH groups varies depending on the species [16].

2.1.3 Enterohepatic circulation

The enterohepatic circulation acts as a recycling pathway for BA between the liver and the intestine. This intricate process involves multiple essential steps:

(i) Bile salt export pump (BSEP) mediated BA efflux from liver into bile canaliculi

(ii) Reabsorption of BA from the intestinal lumen into enterocytes by active uptake through the apical sodium-dependent bile acid transporter (ASBT) or passive diffusion.

(iii) Excretion from enterocytes into portal blood by the organic solute transporter (OST) α/β heterodimer.

(iv) Uptake from blood into hepatocytes by NTCP and OATPs.

(v) This cycle of events repeats continuously, maintaining the balance of BA pool, normal bile flow, and regulating BA and cholesterol levels.

Figure 2.5 visually illustrates the enterohepatic circulation pathway and table 2.2 highlights the main BA transporters involved. This intricate recycling mechanism is vital for the maintenance of a healthy BA pool, normal bile flow, and the overall regulation of bile acid and cholesterol homeostasis.

In humans, this constant recycling of BA is very efficient. During each cycle of the enterohepatic circulation, approximately 95% of bile acids are recycled from the gut back to the liver, while the remaining 5% is eliminated through feces. The lost 5% is replenished by the liver through the synthesis of new BA from cholesterol. Overall the human BA pool undergoes recycling around 4 to 12 times per day [88; 89]. On the other hand, efficiency of EHC and recycling times of BA in mice are largely unknown.

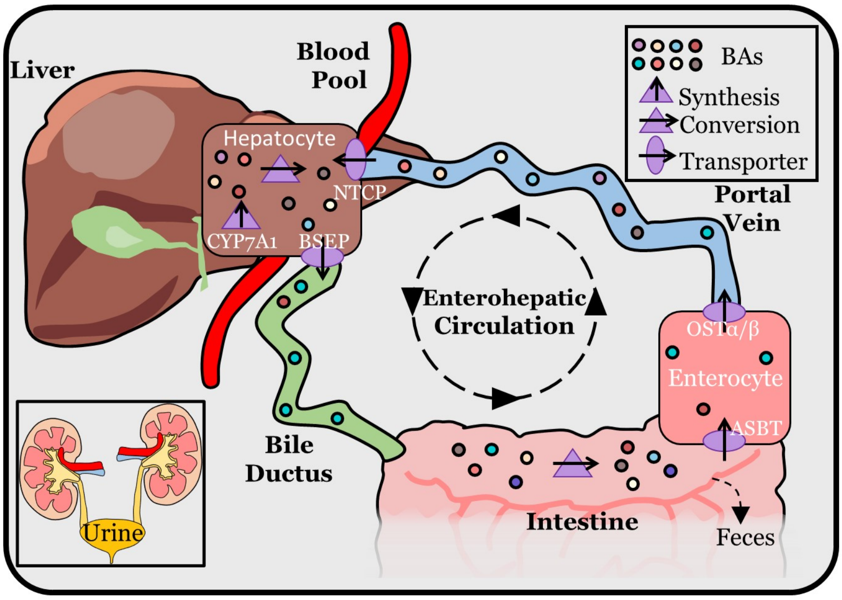
Liver
Blood Pool
BAs
Synthesis
Conversion
Transporter
Hepatocyte
NTCP
CYP7A1
BSEP
Portal Vein
Enterohepatic Circulation
OSTα/β
Enterocyte
ASBT
Bile Ductus
Urine
Intestine
Feces

Figure 2.5: Enterohepatic circulation of BA. Schematic overview illustrating the enterohepatic circulation (EHC) of bile acids. Depicted is BA synthesis by CYP7A1, hepatic and microbial transformation, active transport processes via BSEP, ASBT, OST-α/β and NTCP, as well as fecal and renal excretion.

Table 2.2: Bile acid transporters. Names, localization and function of major bile acid transporters

Abbreviation (human gene)	**Name**	**Localization**	**Substrates**
NTCP (*SLC10A1*)	Sodium-taurocholate co-transporter	Hepatocytes; basolateral membrane	Mainly conjugated bile salts
OATPs (*SLCO1B1* and *SLCO1B3*)	Organic-anion-transporting polypeptides	Hepatocytes; basolateral membrane	Bile salts, organic anions, amphipathic organic solutes
OSTα/β	Organic solute transporter alpha/beta	Enterocytes; basolateral membrane. Hepatocytes; basolateral (induced in cholestasis). Cholangiocytes	Bile salts
BSEP (*ABCB11*)	Bile salt export pump	Canalicular membrane	Bile salts
MRP3 (*ABCC3*)	Multidrug-resistance-associated protein 3	Hepatocytes; basolateral membrane. Cholangiocytes	Bilirubin and bile acid glucuronides
MRP4 (*ABCC4*)	Multidrug-resistance-associated protein 4	Hepatocytes; basolateral membrane (induced in cholestasis)	Cyclic nucleotides and sulfated bile acid
ASBT (*SLC10A2*)	Apical sodium-dependent bile acid transporter	Mainly terminal ileal enterocytes; apical brush border membrane	Mostly conjugated bile salts

Bile acid efflux from liver into bile canaliculi

Bile acids are transported by the bile salt export pump (BSEP, gene symbol *ABCB11* in humans, *Abcb11* in mice) from hepatocytes into bile canaliculi. Although BESP transports both conjugated and unconjugated BA, it has a much higher affinity to conjugated BA [90]. From there, they are transported through bile ductules, bile ducts, and eventually reach the duodenum either directly (in animals without a gallbladder, e.g., rats, horses, deer, whales) or via the gallbladder (in animals with a gallbladder, such as mice, humans), depending on the species. Interestingly, even in species with a gallbladder, a significant portion of bile bypasses storage in the gallbladder and flows directly into the duodenum. Upon food intake, a hormonal response is triggered. Cholecystokinin is synthesized and secreted by enteroendocrine cells in the duodenum and stimulates gallbladder contraction releasing its content into the duodenal lumen.

A study conducted by Strautnieks et al. [91] revealed that mutations in the BSEP gene are responsible for the development of progressive familial intrahepatic cholestasis type 2 (PFIC2) in humans. This finding strongly suggests that BSEP serves as the primary mechanism for exporting conjugated BA from the liver into bile. When BSEP function is compromised due to these mutations, hepatocytes experience an accumulation and overload of BA, leading to the manifestation of PFIC2 as well as the less severe benign recurrent intrahepatic cholestasis type 2 (BRIC2) [92]. While PFIC2 can progress to cirrhosis and necessitates liver transplantation, BRIC2 is characterized by recurring episodes of cholestasis.

Further investigations conducted by Kagawa et al. [93] shed light on the phenotypic differences between PFIC2 and BRIC2, establishing a correlation with the stability of the BSEP protein. In PFIC2, BSEP mutations result in the rapid degradation of the BSEP protein, leading to impaired secretion of BA. Both conditions, PFIC2 and BRIC2, are marked by liver injury that can potentially progress to cirrhosis, hepatic failure, hepatocellular carcinoma, and even mortality. The severity of the disease is closely associated with the extent of functional impairment in BSEP. Furthermore, the compromised function of BSEP also makes women more susceptible to intrahepatic cholestasis of pregnancy (ICP) [94].

Reabsorption of BA from the intestinal lumen into enterocytes

Reabsorption of BA from the intestinal lumen can be distinguished into active transport mediated by ASBT and passive diffusion into the enterocytes. ASBT, a member of the SLC10 family of solute carrier proteins, facilitates the active uptake of BA into enterocytes and relies for its functionality on sodium cotransport. ASBT (gene: *SLC10A2* in human or *Slc10a2* in rodents) is expressed on the apical membrane of enterocytes and is most abundant in the terminal ileum. Contrary to traditional believes that active BA absorption is exclusive to the small intestine, it is more likely that small amounts of BA are indeed actively reabsorbed in the colon as well. Expression of ASBT, albeit at lower levels than in the ileum, were reported in the colon of mice [95; 96] and human [97].

The mechanism and significance of BA transport in the proximal intestine, compared to ileal absorption, are not as well-defined. In mice, bile acids are primarily taurine-conjugated and hydrophilic, which restricts their diffusion and requires a carrier to facilitate their transport across the enterocyte apical brush border membrane. This was confirmed through the study of ASBT null mice, where the absorption of bile acids in the intestines was greatly reduced. An important finding was that feeding ASBT null mice a diet containing cholestyramine did not lead to a further increase in fecal bile acid excretion [98]. These findings support the conclusion that non-ASBT mechanisms contribute minimally to bile acid absorption in the mouse intestines. The presence of a bile acid binding resin like cholestyramine would reduce alternative passive or active mechanisms for bile acid absorption.

Irrespective of how BA are taken up, as weak acids BA have the tendency to become ionized within the neutral pH of the cytosolic compartment. This ionization process can potentially result in the retention of BA within the cell, emphasizing the need for efflux carriers.

Excretion from enterocytes into portal blood by OSTα/β

Subsequent to reabsorption from the intestinal lumen, BA are further transported within the enterocyte from the apical to basolateral side. Three intracellular lipid binding proteins are expressed in the small intestine: the liver fatty acid binding protein (LFABP; gene *Fabp1*), the intestinal fatty acid binding protein (IFABP; gene *Fabp2*), and the (IBABP; gene *Fabp6*) [99]. While IBABP has the ability to bind both fatty acids and

BA, it exhibits a higher affinity for the latter and thus plays an important role in facilitating the apical-basolateral transport of BA.

The transfer of BA from enterocytes to the portal circulation relies on a heterodimeric complex composed of OSTα and OSTβ (gene: *SLC51A* and *SLC51B* in humans; *Slc51a* and *Slc51b* in rodents). Interestingly, the OSTα/β heterodimer acts as an efficient transporter, whereas the homodimer does not exhibit this function [100]. The heterodimer was shown to specifically transport substances such as taurocholate, estrone sulfate, digoxin, and prostaglandin E2. Notably, this transport process occurs independently of sodium. Seward et al. identified potential human and mouse OST homologs by analyzing data from genome sequencing of both species and hypothetical proteins available in databases [101].

Within the small intestine, the basolateral membrane of enterocytes expresses the OSTα/β heterodimer, playing a pivotal role in the efficient efflux of BA from enterocytes into the portal circulation. This function is vital for the maintenance of enterohepatic circulation [102; 103].

In addition to the OSTα/β heterodimer, MRP3 (gene: *Abcc3*) has been proposed as a possible carrier for basolateral bile acid transport in the ileum, supported by indirect evidence such as its localization on the basolateral membrane and its demonstrated ability to transport BA *in vitro*. However, studies utilizing MRP3-null mice did not reveal any apparent disruptions in intestinal bile acid absorption [104].

Sinusoidal uptake into hepatocytes

Bile acids enter hepatocytes through the basolateral (sinusoidal) membrane using two transporters: NTCP and OATP1B2. NTCP relies on sodium ions for transport, while OATP1B2 functions independently of sodium. However, the uptake of BA by hepatocytes in the enterohepatic circulation is not completely efficient. Bile acids that are not immediately taken up by hepatocytes escape into the systemic circulation. These BA are then brought back to the liver through the hepatic arterial blood and/or hepatic portal blood, where they can be eventually absorbed by hepatocytes. Therefore, the systemic blood contains BA that were initially not absorbed by the liver.

NTCP (gene *SLC10A1* in humans; *Slc10a1* in rodents) serves as the primary transporter responsible for the uptake of conjugated BA from the serum into hepatocytes across the hepatic sinusoidal membrane. Co-transporting BA and Na^+ in the same direction, NTCP acts as a symporter relying on the presence of sodium ions. While glycine- and taurine-conjugated BA are the transporters preferred substrates, it can also transport unconjugated BA, although their affinity as substrates is moderate to weak [105].

The initial characterizations of OATPs (*SLCO* gene in humans; *Slco* in rodents, e.g., *SLCO1B1, Slco1b2*) involved the cloning of rat OATP1A1, previously known as OATP1. This transporter operates independently of sodium ions and was demonstrated to have the ability to transport BA *in vitro* [106]. When considering the orthologous relationships within the OATP1A/1B gene family between humans and rodents, the picture becomes more complex. For example, humans possess only one OATP1A isoform, namely OATP1A2, while rats and mice exhibit the presence of several OATP1A forms (OATP1A1, OATP1A4, OATP1A5, and OATP1A6). In humans, there are two OATP1B isoforms, OATP1B1 and OATP1B3, whereas rats and mice have a singular OATP1B2 [107]. In mice, OATP1A1, OATP1A4, and OATP1B2 are predominantly expressed in the liver, OATP1A5 is primarily expressed in gonads, and OATP1A6 shows significant expression in the kidneys [108].

Cholehepatic shunt

In addition to the recycling of BA between the liver and intestine through the enterohepatic circulation, there exists another pathway called the cholehepatic shunt. This shunt enables a shorter recycling path for BA between hepatocytes and cholangiocytes. Facing the bile flow, the apical membrane of cholangiocytes are exposed to high BA concentrations. Specific transporters are located on their apical and basolateral membranes that facilitate the uptake and efflux of bile acids. In humans, the uptake transporters ASBT and OATP1A2 are expressed apically and Ostα/β and MRP3 facilitate BA efflux on the basolateral side [109].

By utilizing these transporters, cholangiocytes transport bile acids and recycle them back to the hepatocytes through the peribiliary plexus. This recycling process prevents the harmful accumulation of bile acids in cholangiocytes, thereby protecting them from toxic effects.

The cholehepatic shunt also plays a vital role in promoting bile flow. Within the bile ducts, unconjugated bile acids undergo protonation, resulting in protonated bile acids and bicarbonate ions. The protonated bile acids, being more soluble in lipids, are absorbed by the epithelial cells of the bile ducts and subsequently returned to the hepatocytes. These bile acids are then resecreted into the bile, leading to an increase in bile flow (choleresis). This process also stimulates the production and secretion of fluid rich in bicarbonate [110].

An example of a bile acid that enhances bile flow is norUDCA, which is secreted in an unconjugated form [34]. The cholehepatic shunt and the mechanisms involved in bile acid recycling and protonation contribute to the efficient regulation of bile acid levels and the prevention of their detrimental effects on cholangiocytes.

2.1.4 Bile acids in homeostasis and pathophysiological conditions

Regulation of BA metabolism

The regulation of cholesterol and BA metabolism involves a dual mechanism consisting of feed-forward activation by oxysterols and feedback repression by BAs. The liver-X-receptor (LXR) serves as the nuclear receptor responsible for the feed-forward activation triggered by oxysterols. On the other hand, FXR, originally believed to be the receptor for farnesol but later discovered to be a receptor for BA, functions as the nuclear receptor involved in the feedback repression. Despite its revised role, the name FXR continues to be used for this receptor. A schematic overview of regulation through LXR and FXR are illustrated in figure 2.6.

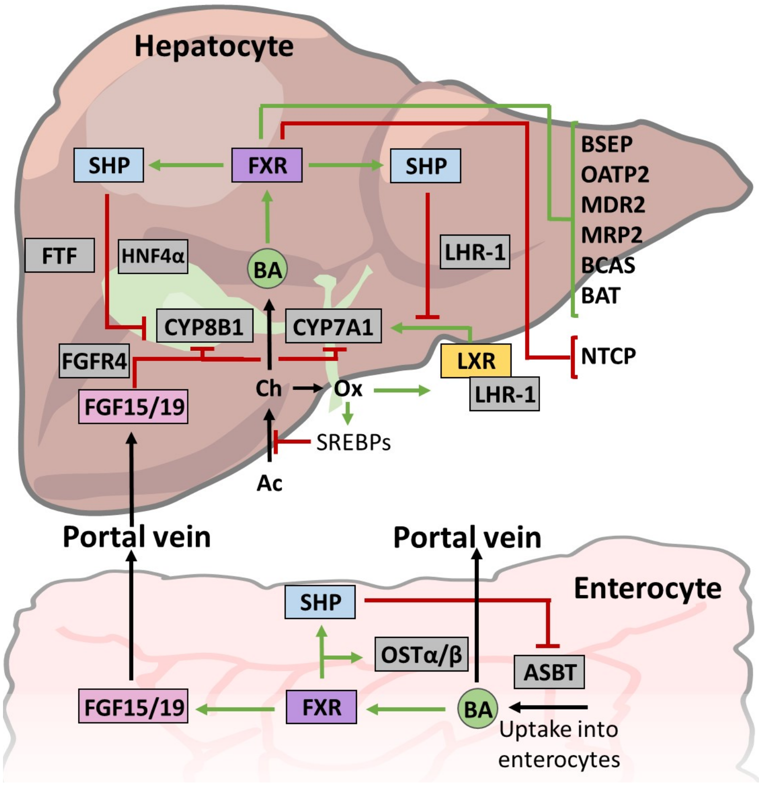
Hepatocyte
SHP
FXR
SHP
BSEP
OATP2
MDR2
MRP2
BCAS
BAT
FTF
HNF4α
BA
LHR-1
CYP8B1
CYP7A1
LXR
NTCP
FGFR4
Ch
Ox
LHR-1
FGF15/19
SREBPs
Ac
Portal vein
Portal vein
Enterocyte
SHP
OSTα/β
ASBT
FGF15/19
FXR
BA
Uptake into enterocytes

Figure 2.6: Overview of BA regulation. Schematic overview of FXR and LXR mediated regulation of BA homeostasis. Green arrows indicate positive regulation, red arrows show inhibitory action, black arrows show mass flow, conversion or transport. Used abbreviations: cholesterol (Ch), oxysterols (Ox), acetyl-CoA (Ac).

LXR Oxysterols serve as natural ligands for LXRs and are espically increased when cholesterol levels are elevated. In rodents, this activation specifically targets LXRα, working alongside the liver receptor homolog 1 (LRH-1), to induce *Cyp7a1* transcription. This process, in turn, stimulates the synthesis of BA and the excretion of cholesterol. Among the LXR family members, LXRα and LXRβ, LXRα exhibits higher expression levels in both murine and human liver and demonstrates a stronger binding affinity to the LXR response element (LXRE) [111]. Consequently, the LXRE present in the promoter region of the mouse *Cyp7a1* gene is predominantly activated by LXRα.

However, it is important to note that in contrast to findings in rats and mice, treatment with LXRα agonists in primary human hepatocytes leads to the suppression of CYP7A1 expression [112]. This repression can be attributed, at least in part, to the direct induction of the small heterodimer partner, a gene that exerts a repressive effect on CYP7A1 through liver receptor homolog 1 (LRH-1) [113]. These contrasting observations underscore the presence of species-specific molecular strategies in regulating cholesterol homeostasis, underscoring the importance of employing relevant experimental models for the development of pharmaceuticals intended for human use.

Apart from its role in controlling BA synthesis, LXR also plays a significant role in regulating BA catabolism. Recent studies have demonstrated that ligand-activated LXRα upregulates the expression of the human UGT1A3 gene by binding to an LXRE-like sequence in the promoter [114]. UGT1A3 is among the highly active enzymes responsible for the glucuronide conjugation of BA, enabling their conversion into metabolites excreted in urine. Based on these findings, it has been postulated that the activation of LXRα may facilitate the elimination of cholesterol through the excretion of urinary BA glucuronides.

FXR With increasing BA pool sizes, a feedback mechanism is initiated from the intestine to inhibit hepatic de novo BA synthesis. This feedback loop relies on FXR, which operates in two systems and their communication: one in the liver and the other in the intestine. While BA were in general shown to act as specific ligands for FXR [1; 2; 3], different BAs and salts show varying binding affinities. Studies of binding affinities to human FXR showed overall higher affinity for more hydrophobic BA (from high to low: LCA $>$ CDCA $>$ T-CDCA $>$ G-CDCA $>>$ DCA $>$ UDCA $>>$ CA $>$ T-CA $>$ G-CA)[11]. FXR can be activated by both free and conjugated BAs. On the other hand, T-βMCA, a highly hydrophilic BA, acts as a strong antagonist to FXR [10].

Within the intestine, BA regulation functions through the FXR-FGF15/19 pathway. Upon activation by BA, intestinal FXR stimulates the expression of FGF15/19 in the enterocytes. FGF19 serves as the human counterpart of FGF15 in mice. Interestingly, FGF15 and FGF19 exhibit a mere 53% amino acid identity, highlighting their evolutionary divergence [115]. Subsequently, FGF15/19 is released into the portal blood and travels to the liver, where it binds to its specific hepatocyte membrane receptor complex, known as the FGF receptor 4/β-klotho (FGFR4/β-KL). Binding of FGF15/19 to FGFR4/β-KL triggers downstream signaling pathways, orchestrating postprandial responses that include the suppression of BA synthesis by reducing *Cyp7a1* and *Cyp8b1* gene expression [116].

This downregulation is achieved in part by FGFR4-mediated activation of the extracellular signal-regulated kinase 1/2 (ERK1/2) signaling pathway, and to a lesser degree, the c-Jun N-terminal kinase 1/2 (JNK1/2) pathway In essence, the interplay between ileal FGF15/19 and hepatic FGFR4/β-KL establishes an endocrine axis that actively regulates BA synthesis in the liver, thereby ensuring the maintenance of BA homeostasis [5; 6].

Within the liver, BAs activate the transcription factor FXR, a negative regulator of *Cyp7a1*, *Cyp8b1*, *Cyp27a1*, and *Cyp7b1* expression [117] and triggers the expression of SHP. As SHP lacks the DNA-binding domain, increased SHP protein levels hinder LRH-1 activity by forming a nonfunctional heterodimeric complex, ultimately leading to targeted repression of both *Cyp7a1* and *Cyp8b1* gene expression [116]. For instance, when SHP interacts with LRH-1 and/or LXRα, the resulting complex acts as an inhibitor, suppressing the transcription of the *Cyp7a1* gene [113; 118]. The repression of *Cyp8b1* transcription by SHP involves the participation of two factors: the fetoprotein transcription factor (FTF) and the hepatocyte nuclear factor 4α (HNF-4α), with FTF likely playing a more prominent role. When SHP binds to FTF and/or HNF-4α, it forms an inhibitory complex that suppresses the transcription of *Cyp8b1* [119; 120]. A recent study also demonstrated that the activation of FXR leads to the expression of various transcriptional repressors, including the musculoaponeurotic fibrosarcoma oncogene homolog G (MAFG). MAFG directly represses the expression of the *Cyp8b1* gene by binding to specific regions called MAFG response elements (MAREs) within the promoter of the *Cyp8b1* gene. This mechanism further contributes to the downregulation of *Cyp8b1* gene activity [121].

FXR plays further a role in regulating the expression of various BA transporters and enzymes involved in BA metabolism. These include BSEP, NTCP, ASBT, OSTα/β, as well as BA conjugation enzymes such as BACS and BAAT. Among these targets, the expressions of BSEP, OSTα/β heterodimer, BACS, and BAAT are induced by FXR activation, while NTCP and ASBT expressions are repressed. Besides FXR mediated regulation, BA transporters are regulated as well through other means.

Regulation of bile acid transporters The expression of NTCP is regulated by various factors, including substrates, cytokines, liver injury, and hormones [122; 123]. In different forms of cholestatic liver disease associated with inflammation, ethinylestradiol and pregnancy, obstruction, as well as exposure to drugs or toxins, NTCP transcription is decreased. This reduction in NTCP gene expression is part of a coordinated response aimed at minimizing liver injury [122]. Although the specific molecular mechanisms and transcription factors involved may vary, a common theme among these regulatory pathways is the decreased expression of the sinusoidal uptake transporter. This adaptive response aims to limit the entry of BA into hepatocytes. Under physiological conditions, the short-term adjustment of NTCP activity to match the BA load and Na^+-dependent uptake is predominantly regulated by posttranscriptional mechanisms [124].

Transcription of BSEP mRNA was shown to be increased when BA concentration in hepatocytes is elevated. This can occur after a dietary challenge with BA [125] or in certain cholestatic conditions [126; 127; 128]. Vitamin A, specifically 9-cis retinoic acid, has been identified as a potential regulator of BSEP. FXR forms a heterodimer with RXR, and *in vitro* studies suggest that activation of RXR by 9-cis retinoic acid inhibits the FXR-induced transcription of human BSEP [129]. Besides transcriptional regulation, there is substantial evidence indicating posttranscriptional regulation of BSEP protein localization to the canalicular membrane [92]. This short-term regulation allows hepatocytes to quickly adjust BA secretion in response to changes in BA flux and to pathophysiological conditions like cholestasis [124].

The precise regulation of ASBT expression along the longitudinal axis of the intestine is not yet as well understood; however, recent studies have highlighted the crucial role of the transcription factor GATA4 in this process. Interestingly, when GATA4 is specifically deactivated in the intestine of mice, there is a significant increase in ASBT expression in the proximal intestine [130; 131]. Apart from BA, cholesterol also appears to have a negative regulatory effect on ASBT mRNA expression. *In vitro* studies using Caco-2 cells have demonstrated that sterols, such as 25-hydroxycholesterol, downregulate both ASBT mRNA expression and promoter activity [132]. This suggests that cholesterol plays a role in modulating ASBT expression, adding another layer of complexity to the regulatory mechanisms governing BA absorption in the intestine.

The coordinated expression of both OSTα and OSTβ subunits is crucial for their proper function [103; 133]. Consequently, the genes encoding these subunits appear to be regulated in a coordinated manner. The promoters of OSTα and OSTβ contain functional responsive elements for both LRH-1 and FXR, providing a mechanism for both positive and negative regulation by BA [134]. While the positive regulation by BA is dominant, this dynamic push-pull regulation allows the cell to finely adjust the expression of OSTα/β to match the BA flux. The predominant positive regulation ensures efficient export of BA, thereby preventing cellular injury caused by intracellular accumulation. In addition to regulation by FXR, OSTα and OSTβ expression may also be induced by LXR through an inverted repeat-1 element shared with FXR [135]. This suggests a potential cross-talk between the LXR and FXR pathways in regulating OSTα and OSTβ expression.

Bile acid mediated signalling and control

Bile acids themselves are not merely passive molecules but play a role in a complex network of signalling pathways within the body. Bile acids communicate with various receptors, including nuclear receptors and cell surface receptors, to regulate an array of physiological processes. These receptors receive and transmit signals from BAs, orchestrating responses that influence lipid metabolism, inflammation, and even cell growth and survival. Table 2.3 summarizes various receptors targeted by BAs.

Nuclear receptors Besides acting as ligands for FXR, it has become evident that additional nuclear receptors respond to BA: pregnane X receptor/steroid and xenobiotic-sensing receptor (PXR/SXR; NR1I2) [4], constitutive androstane receptor (CAR; NR1I3) [136; 137; 138] and the vitamin D3 receptor (VDR; NR1I1) [139]. These receptors exhibit a preference for secondary BA, often require elevated BA levels for stimulation and activate the expression of genes involved in the later steps of BA catabolism. This suggests that these receptors play a role in mitigating potential harmful concentration of cytotoxic and hydrophobic secondary BA in liver and intestine. In deed, both VDR and PXR were shown to induce

Table 2.3: Bile acid sensitive receptors. List of cell surface and nuclear receptors that are responsive to BAs.

Receptors	
Cell surface	**Nuclear**
TGR5	FXR
S1PR2	VDR
FPR	PXR/SXR
mAChR	CAR
Integrins	

CYP-mediated detoxification and inhibit BA synthesis when LCA concentration are high [4; 139; 140]. While CAR can regulate BA clearance and bilirubin detoxification in interacting with PXR [141; 142; 143; 144; 145], it is unclear if BA interact directly with CAR. Recent studies showed functionalities of LCA-VDR axis beyond regulation BA detoxification including influencing adaptive and innate immunity [146; 147; 148] and modulating the gut microbiota [149].

Cell surface receptors In addition to nuclear receptors, BA are known to interact with a number of cell surface receptors. Most of these function as GPCRs and include G-protein-coupled BA receptor (TGR5 or GPBAR1), sphingosine 1-phosphate receptor 2 (S1PR2), formyl-peptide receptors (FPRs), and muscarinic acetylcholine receptors (mAChRs). TGR5 belongs to the rhodopsin-like subfamily of GPCRs and is recognized as the prototype receptor for BAs within this subclass [37]. Exhibiting the signal amplification characteristic of GPCRs, TGR5 is expressed to a minimal to moderate extent in nearly all tissues and cell types, except for the gallbladder epithelium, where its expression is abundant [150]. Both conjugated and unconjugated BA can activate TGR5. Typically, more hydrophobic BA species act as stronger agonist and taurine-conjugation of BA results in increased TGR5 stimulation compared to glycine-conjugates or unconjuagted BA [151]. Upon activation, TGR5 interacts with Gαs proteins, triggering the activation of adenylate cyclase and resulting in a transient increase in cAMP [151]. This, in turn, initiates various downstream signalling pathways, including PKA [152; 153; 154] and the exchange protein directly activated by cAMP (EPAC) [152; 153]. Furthermore, TGR5 activation was shown to induce MAPK signaling, primarily through ERK1/2 [155; 156; 157], proto-oncogene protein-tyrosine kinase (SRC) [158], and the mechanistic target of rapamycin (mTOR) [159; 160].

Signalling through S1PR2 is mainly activated by sphingolipids, but T-CA and other conjugated BA were also reported to be suitable ligands [161]. Inhibition of S1PR2 has been shown to reduce portal vein pressure and liver injury, indicating a pathological role for S1PR2 in cholestasis [162; 163]. FPRs are expressed in neutrophils and monocytes [164] but are believed to mainly play a role in pathological conditions. Elevated CDCA [165] and DCA [166] levels can inhibit binding of an FPR agonist that also serves as a potent chemoattractant in monocytes, suggesting an anti-inflammatory effect of BA through FPRs. Lastly, mAChRs were shown to interact with conjugated secondary BA and increase cancer cell growth via EGFR signalling [167; 168] and are in general involved in nitric oxide-induced vascular relaxation of the aorta [169] and contribute to the pathology of cholestasis-induced cardiac arrhythmia [170; 171].

Apart from GPCRs, other cell surface receptors are known to use BA as ligands. For instance, binding of T-UDCA to the $\beta1$ subunit of the $\alpha5\beta1$-integrin pathway results in anti-apoptotic effects in hepatocytes [172; 173]. T-UDCA is further involved in other processes including osteoblast differentiation from mesenchymal stem cells, which occurs through a similar integrin-mediated pathway [174].

Microbiome Additionally, BA are believed to play a part in regulating bacterial growth in the small intestine [18]. Due to their amphiphatic nature, BA have been found to possess inhibitory properties against certain bacterial strains suppressing their growth. This inhibitory effect of BA have been observed in species such as *Bacteroides, Clostridia, Lactobacillus, Bifidobacteria, Escherichia coli, Enterococcus fecalis*, as well as 7α-dehydroxylating bacteria like *Clostridium scindens, Clostridium hylemonae*, and *Clostridium hiranonis* [19]. Bile acids enact their inhibitory effect by disrupting bacterial cell membranes, damaging DNA, modifying protein conformation, and chelating iron and calcium. Consequently, bacteria present in the intestinal tract, such as *Lactobacillus, Bifidobacterium*, and *Bacillus*, have mechanisms to repair damage caused by BA. Counteracting adverse effects, bacteria that are exposed to BA for extended periods of time overexpress BA efflux transporters as well as enzymes that modulate metabolism globally [19]. In general, unconjugated BA exhibit stronger antibacterial properties, and gram-positive bacteria tend to be more susceptible to the effects of BA [19].

FXR and TGR5 as regulators of intermediary metabolism Upon food intake, BA are released from the gallbladder and result in postprandial oscillations of BA levels throughout the body. By doing so, BA can act as a surrogate for the presence of nutrients. Consequently, enterocytes and various intestinal cell types, such as enteric neurons, smooth muscle cells, and enteroendocrine cells, can detect BA levels to derive information about nutrient availability and induce physiological responses. In this context, BA induced FXR and TGR5 signalling play a significant role in regulating the absorption and availability of nutrients, fluids, and ions throughout the gastrointestinal tract. A number of processes are affected by FXR and TGR5 signalling such as fluid transportation, hormone secretion, transport protein expression, intestinal motility, and secretory reactions and are illustrated in figure 2.7.

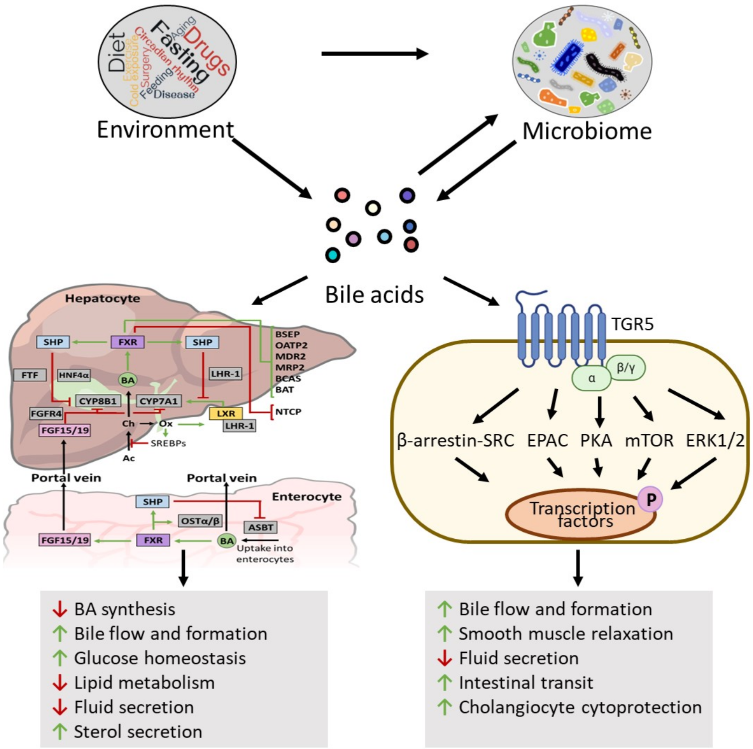
Diet
Fasting
Drugs
Aging
Circadian rhythm
Surgery
Feeding
Disease
Environment
Microbiome
Bile acids
Hepatocyte
SHP
FXR
SHP
FTF
HNF4α
BA
LHR-1
CYP8B1
CYP7A1
FGFR4
FGF15/19
LXR
LHR-1
Ch
Ox
SREBPs
Ac
BSEP
OATP2
MDR2
MRP2
BCAS
BAT
NTCP
Portal vein
Portal vein
Enterocyte
SHP
OSTα/β
ASBT
FGF15/19
FXR
BA
Uptake into enterocytes
TGR5
α
β/γ
β-arrestin-SRC
EPAC
PKA
mTOR
ERK1/2
Transcription factors
P
↓ BA synthesis
↑ Bile flow and formation
↑ Glucose homeostasis
↓ Lipid metabolism
↓ Fluid secretion
↑ Sterol secretion
↑ Bile flow and formation
↑ Smooth muscle relaxation
↓ Fluid secretion
↑ Intestinal transit
↑ Cholangiocyte cytoprotection

Figure 2.7: Overview of BA mediated signalling through FXR and TGR5. Schematic overview of BA mediated signalling through FXR and TGR5. Physiological and environmental factors, as well as disease or disease intervention can influence gut microbiome and BA pool size/composition which in turn control TGR5 and FXR signaling. Green arrows indicate increased processes, red arrows show inhibition of processes.

FXR, especially, functions as an important regulator of intermediary metabolism. This nuclear receptor is known to promote and repress the expression of multiple genes associated with glucose, lipid, and amino acid metabolism within the liver. While several studies have identified the significance of FXR integrating various nutritional and environmental cues, its full complexity is not yet understood.

Lipid metabolism BA signalling through FXR modulates lipid metabolism by three main pathways. Signalling through the FXR-SHP axis represses key regulators of hepatic *de novo* lipogenesis (sterol regulatory binding protein-1c,SREBP-1c) [8] and of microsomal triglyceride transfer protein (MTP) and ApoB expression (HNF4α), which are important for very low-density lipoprotein (VLDL) secretion [175]. Thirdly, FXR interferes with ChREBP binding to the promoter of the liver pyruvate kinase (LPK) [176]. Additionally, FXR influences several apolipoproteins known to affect lipoprotein lipase activity [177; 178] and reverse cholesterol transport [81; 179; 180], thereby contributing to the beneficial modulation of lipid metabolism. On the other hand, the exact mechanism by which FXR signaling regulates hepatic fat accumulation is still not fully understood. While a comparative study using liver- and intestine-specific *Fxr*$^{-/-}$ mice suggests that the liver is the primary site where BA-mediated protection against lipid accumulation occurs [181], other studies demonstrate that FGF15/19 alone is sufficient to inhibit SREBP-1c and hepatic lipogenesis [182; 183]. However, a study by Jiang et al. [184] indicates that intestinal FXR activation promotes SREBP-1c levels and lipid buildup in the liver through ceramide-dependent mechanisms. Further research is needed to determine which tissues dominate the control of hepatic fat accumulation, including the contribution from the immune system.

Glucose metabolism Activation of hepatic FXR works in concert with insulin via SHP by reducing the transcription of enzymes involved in gluconeogenesis, namely phosphoenolpyruvate carboxykinase (PEPCK) and glucose 6-phosphatase (G6Pase). This inhibition is partially achieved through the repression of nuclear receptors FOXO1 and HNF4α [185; 186; 187; 188]. On the other hand, intestinal FXR signalling and feedback through FGF15/19 strongly downregulates glucose production in the liver by opposing cAMP response element-binding protein (CREB) action, a key gluconeogenic regulator [7]. This intestinal axis also lowers glycogen synthase kinase 3 (GSK3) activity in the liver, supporting hepatic glycogen synthesis following the decline of insulin signaling [189]. Additionally, FXR directly influences glucose balance in the pancreas, where its activation stimulates insulin secretion in response to glucose in isolated pancreatic β-cells [190]. These findings underscore the complementary effects of hepatic and intestinal FXR activation, redirecting glucose metabolites from glycolysis towards glycogen synthesis.

Amino acid metabolism Continuous stimulation of FXR was shown to induce gene expression associated with amino acid catabolism and ammonium detoxification [191; 192]. Studies in FXR KO mice demonstrated that the expression of the rate-limiting enzyme in the urea cycle, carbamoyl phosphate synthetase I, as well as other enzymes responsible for amino acid degradation were reduced [191; 192]. Via signalling through the FXR-FGF15/19 axis, intestinal activation of FXR stimulates de novo protein synthesis [189].

Bile acids in disease

Given the broad role of BA receptors in coordinating bile homeostasis and biliary physiology, it is not surprising that impaired signaling is associated with the development of various diseases, affecting metabolic regulation to immune modulation and even cancer progression. Among these disease and pathological conditions associated with dysregulation of BA are primary sclerosing cholangitis (PSC), primary biliary cholangitis (previously known as primary biliary cirrhosis), nonalcoholic fatty liver (NAFL), and nonalcoholic steatohepatitis (NASH) as well as obesity and insulin resistance. Here, a short introduction of the relationship between BA and BA-mediated signalling and diseased states are given for inflammation, cholestasis, cancer as well as for conditions in non-EHC organs.

Bile acids and inflammation Initially, BAs were primarily classified as proinflammatory agents due to their detergent properties and ability to disrupt cellular membranes. This classification was reinforced by observations that elevated BA levels due to bile duct obstruction or liver disease resulted in hepatic inflammation [193; 194], and systemic accumulation of BAs could cause damage to extrahepatic tissues, the kidney in particular [195]. Contrary to their proinflammatory role, BAs were shown to possess strong anti-inflammatory properties. This was first demonstrated in patients with jaundice as well as elevated systemic BA levels experienced significant relief from rheumatic symptoms [196]. Moreover, emerging evidence suggests that the activation of BA receptors exerts anti-inflammatory effects in various inflammatory diseases. These include experimental autoimmune encephalomyelitis [197; 198], atherosclerosis [154; 188; 199; 200; 201; 202; 203], and hepatic inflammation [204; 205; 206; 207; 208; 209; 210].

Cholestasis The etiology of cholestasis can vary significantly, including impaired bile secretion across the hepatocytes' canalicular membrane (intrahepatic cholestasis) or impaired bile flow due to bile duct disorders such as primary biliary cholangitis (PBC) and primary sclerosing cholangitis (PSC) [23; 24; 25]. Immune system related genes have been found to play a significant role in cholangitis-related conditions, as indicated by genome-wide association studies conducted in PBC and PSC patients [211]. Genetic variation in the *TGR5* gene has been been identified in PSC patients [212], and specific single-nucleotide polymorphisms in *FXR* have been linked with increased risk of ICP [213] and progressive familial intrahepatic cholestasis [214]. In general, substantial evidence supports the beneficial role of FXR agonism in various preclinical cholestasis models [215; 216] underscoring the importance of intact FXR signaling in mitigating pathological BA overload. Activation of FXR mediated signaling was shown to increase bile flow, inhibit BA synthesis, and enhances phospholipid secretion, thereby reducing toxic BA levels in liver [217; 218; 219].

Extrahepatic diseases While BA signaling has been established as beneficial for cardiometabolic homeostasis [154; 159; 203; 220], increased levels of BA can have cardiotoxic effects, leading to progressive cardiomyopathy [221]. Highlighting the potential detrimental actions of BA in disease, conjugated BAs, particularly T-CA, have been found to induce arrhythmic contractions in human atria [222]. Although cardiac expression of BA-responsive receptors is evident, their exact contribution to human cardiac disease remains incompletely understood. In cardiomyocytes, stimulation of FXR induces apoptosis whereas inhibition of the nuclear receptor appears to be protective against cardiac insults induced by ischemia [223]. Further research is necessary to fully elucidate the underlying mechanisms involved. While less extensively studied, concerns regarding cardiovascular implications have also been raised for TGR5. TGR5 has been suggested to mediate cardiac hypertrophy in a mouse model of liver injury [224], and reflex tachycardia, resulting from reduced vascular tone and blood pressure, has been observed in dogs [225]. However, other studies attribute a cardioprotective role to TGR5 [154; 226]. In order to determine the precise impact of TGR5, as well as other noncanonical BA receptors such as muscarinic receptors, on cardiovascular risk, dedicated studies and clinical trials are needed.

Another example of extrahepatic diseases influenced by BAs is pruritus. While itching in general can serve as a protective reflex to eliminate skin irritants as well as pathogens, chronic pruritus is linked to pathological conditions and significantly affects quality of life. Peripheral neurons located in the dorsal root ganglia express TGR5 and its stimulation leads to the release of neuropeptide transmitters associated with itch sensation. This was demonstrated in vivo, as treatment with DCA induced spontaneous scratching in mice with intact *Tgr5* gene, while *Tgr5*-deficient mice did not exhibit the same response [227]. However, the mechanism underlying pruritus may be more intricate than simply stimulating TGR5 [228; 229].

Cancer The association between increased levels of BAs and a higher incidence of cancer in various digestive organs has been well-established. As early as 1940, experiments involving subcutaneous injection of DCA in rodents demonstrated its carcinogenic properties [230], leading to the prevailing belief that BAs, particularly hydrophobic species, act as promoters of tumor development. Since then, extensive research has revealed several pathways through which BAs contribute to cancer formation, including the induction of oxidative stress, DNA damage, genomic instability, apoptosis, and interactions with the gut microbiota (as discussed in detail by Jia et al. [28]).

These mechanisms can also arise as a result of external factors such as dietary choices, lifestyle factors, and exposure to environmental toxins. The impact of these mechanisms is most prominent in the hepato-gastrointestinal tract, with a particular focus on the liver, biliary tract, and colon (as extensively reviewed [28; 231; 232; 233]). Key underlying processes involve the heightened generation of reactive oxygen and nitrogen species within cells [234] and the dysregulation of genes involved in tumor suppression and promotion [235]. The oncogenic potential of BAs is influenced by their hydrophobicity, as evidenced by experiments demonstrating the hepatotoxicity of different BA concentrations in the liver: UDCA < CA < CDCA < DCA < LCA [236]. Accordingly, spontaneous liver cancer can be often seeen in Fxr-/- mice due to their constant elevated BA levels [237]. Moreover, reduction of the BA pool in these mice through the use of cholestyramine, a BA sequestrant, significantly inhibits tumor lesions [237]. While intestine-restricted FXR agonists are generally regarded as having beneficial therapeutic effects, it is important to acknowledge that sustained elevation of circulating FGF19 has been associated with liver cancer [238].

More recently, a direct correlation between BAs and cancer progression has been demonstrated. Specifically, T-βMCA has been found to initiate colorectal cancer by inducing DNA damage, while also actively promoting the proliferation of cancer stem cells [233]. On the other hand, there is also evidence suggesting oncoprotective properties of BAs. While most studies focus on the direct impact of BA on cancer cells [239; 240; 241], a recent study has shown that the gut microbiome can utilize BAs to modulate immunity against liver cancer by enabling the recruitment of natural killer T cells, resulting in selective suppression of tumors in the liver [193].

2.1.5 Species differences in BA metabolism

Mice are commonly used as animal models to investigate human metabolism due to their homogeneous genetics, accessibility to mutant, germ-free and/or transgenic models, comparable physiology, and relatively low cost. Furthermore, the use of mouse models has been vital in several groundbreaking studies that have identified the role of gut microbiota in various diseases. Despite the clear advantages of mouse models, there are concerns that may affect translatability, such as gross anatomy, compositional differences of the gut microbiota between humans and mice, and environmental factors that may complicate studies.

The BA composition is a strong indicator of the metabolic differences between mice and humans [12], that could play a significant role in poor predictions using preclinical models. Among other species, the highest sulfation of BAs was observed in humans and chimpanzees, whereas glycine amidation is predominant in humans, minipigs, hamsters, and rabbits. In contrast, taurine amidation is predominant in mice, rats, and dogs. Bile acid profiles primarily consist of tri-hydroxyl BAs in hamsters, rats, dogs, and mice, di-hydroxyl BAs in humans, rabbits, and minipigs, and mono-hydroxyl BAs in chimpanzees. The profiles mostly comprise of hydrophilic and less toxic BAs in mice, rats, pigs, and hamsters, while they consist mostly of hydrophobic and more toxic BAs in humans, rabbits, and chimpanzees. As a result, the hydrophobicity index, a measure of the relative hydrophobicity, or how soluble a molecule is in water, is lowest in minipigs and mice, while it is highest in rabbits, monkeys, and humans. Glucuronidation and glutathione conjugation are low in all species and across all BAs. The total concentration of BAs in urine is up to 10 times higher and more hydrophilic than in plasma in most species, primarily because of the presence of more tri-hydroxyl, amidated, sulfated, and primary BAs in urine compared to plasma. In general, the BA profiles of chimpanzees and monkeys are most similar to those of humans, whereas those of minipigs, rats, and mice are most dissimilar to humans [12].

Bile acids have been shown to regulate various processes including lipid and carbohydrate metabolism, inflammation, fibrosis, and carcinogenesis through their interaction with nuclear and transmembrane G protein-coupled receptors [242]. Therefore, the BA composition is an important factor in creating relevant mouse models of human diseases [243; 244]. While there are differences in BA metabolism between humans and mice [17], the characteristic phenotype associated with the BA composition in mice is determined by two reactions. Firstly, CDCA, which is an end product in the human liver, is further metabolized to MCAs by CDCA 6β-hydroxylase in the liver of mice and rats. Secondly, CDCA is a cytotoxic BA [245; 246] and is the most potent physiological activator of FXR mediated signalling [1; 2]. In contrast, MCAs are cytoprotective [246] and have antagonistic effects on FXR [10], changing the murine BA pool to a more hydrophilic, cytoprotective and FXR antagonistic state.

Besides differences in BA composition, there are several other relevant differences between mice and human that complicate extrapolation from studies of murine BA metabolism to a clinically relevant context.

Gut differences

The characteristics of the intestinal tract differ considerably between mice and humans. While mice are exclusive herbivores, humans can consume a variety of foods, and their intestinal tract reflects this versatility. Although there are many anatomical, histological, and physiological similarities between the two species, there are also distinct differences that need to be taken into account during experimental design and interpretation [247].

For instance, mice have a non-glandular forestomach that covers two-thirds of their stomach, which is absent in humans. This forestomach has no secretory activity and is used for food storage [248]. The remaining third is the glandular stomach, which is similar to that of humans, however, food processing differs vastly. The gastric emptying rate of mice is different from humans, as their foraging and feeding patterns are mostly nocturnal and almost continuously, while humans consume most of their food during the daytime when the stomach is empty. In human gastric emptying occurs linearly with a half time of 30 min (emptying rate of 1.64% per min) whereas in mice an exponential decay with a constant of 77 ± 17 min and a half time of 34 min can be observed [247].

Mice and humans have vastly different small intestine lengths, with the former measuring at approximately 33 cm and the latter at around 700 cm. When considering the length of the small intestine per kg of body weight, mice have 1500 cm per kg while humans have 10 cm per kg. The small intestine is divided into three parts - the duodenum, jejunum, and ileum. The duodenum is the closest region to the stomach, where bile and pancreatic secretions enter the intestinal lumen. The jejunum and ileum follow the duodenum, with the outer mucosa layer of the small intestine displaying notable differences between mice and humans. In humans, the mucosal layer contains circular folds, known as plicae circularis, to increase the surface area. This allows for a niche for mucus-associated bacteria, which is not present in mice and could be an important difference in microbial composition. Additionally, the villi shape and structure in the small intestine varies significantly between mice and humans, with the human jejunum featuring taller, frond-like villi and the ileum displaying thinner, sparser villi. Conversely, the duodenal villi in both mice and humans have a leaf-like structure, but in mice, they change to a more cylindrical shape in the jejunum and ileum [247].

The length of the large intestine differs significantly between mice and humans, with mice having a relatively shorter large intestine of up to 14 cm, while in humans, it can reach up to 105 cm and can be divided into the cecum and colon. The cecum of mice, which is about 3-4 cm long, plays a significant role as a microbial fermentation vessel, while in humans, it is relatively smaller at 6 cm and of minor importance. When expressed relative to body weight, the length of the large intestine is 700 cm per kg in mice and 1.5 cm per kg in humans. Similarly, the cecum is 175 cm per kg in mice and 0.086 cm per kg in humans. This demonstrates that, in relation to body weight, the large intestine is much larger in mice than in humans. Although both humans and mice have a cecal appendix, it is not a prominent separate section in mice, as it is in humans. Additionally, the human colon has pouches called haustra, whereas the mouse colon appears smooth. In the mouse, the proximal colon has a mucosa with transverse folds, the colonic mucosa is flat halfway, and in the distal colonic mucosa, there are longitudinal folds, while in humans, the colonic mucosa has transverse folds throughout the colon.

The overall intestinal transit time also differs between mice and humans, with mice having a much faster transit time than humans. In humans, the transit time after a meal can range from 14 to 76 hours, depending on dietary and population factors. The type of diet has a significant impact on the transit time, and the consumption of resistant starch can increase the transit time by almost 20 hours compared to fully digestible starch [249]. In contrast, the total transit time in mice is only between 6 and 7 hours, which is up to ten times faster than in humans. This is consistent with the total metabolic rate of mice, which is approximately seven times higher than that of humans when corrected for body weight [247].

Mice have lower intestinal pH values, oxygen tension levels, and a different glycan profile in the mucus than humans. These differences in intestinal characteristics are likely responsible, at least in part, for observed differences in microbial composition and in turn introduce inter-species variation in BA metabolism between mice and humans. [250; 251; 252].

Energy and eating

Small animals, due to their high metabolic rate, require a greater amount of food per unit of body weight compared to larger animals. It has been estimated that an average adult mouse has a metabolic rate about seven times higher than that of an average adult human [253]. To meet their high energy demands, mice need to consume food constantly, particularly during their active time at night. This exposes their intestinal tissue to different microbes and metabolites throughout the day, which can affect the hosts circadian rhythm. Small animals need a shorter retention time for their food, especially when the food is not easily digestible, to maintain their high energy demands. The generation interval of gut microbiota, whether human or murine, should be 0.69 times the retention time to maintain the same population size and avoid depletion [253]. Coprophagy, the ingestion of feces, is a behavior that mice practice to maximize the nutritional value of their diet. This allows them to absorb certain nutrients, such as vitamin K, some B vitamins, and fatty acids produced by microbiota in the cecum but also bile acids, which would otherwise be lost through defecation [254]. Coprophagy is known to affect the intestinal microbiota within litters and can be prevented by using cages equipped with grids, but it remains a crucial difference between human and mouse digestive systems [255].

2.2 Computational modelling

In recent years, computational modeling has emerged as a powerful tool that revolutionizes our understanding of complex biological systems and their relation to human health. By leveraging mathematical and computational techniques, it is possible to simulate and analyze intricate biological processes that are often difficult to observe directly but are fundamental to diseases, drug responses and personalized medicine.

Computational modeling in biology and biomedicine involves the construction of mathematical representations, or models, that capture the essential features of biological systems. These models can range from simple equations to highly sophisticated simulations, depending on the complexity of the system under investigation. The models are built based on existing biological knowledge, experimental and clinical data, and theoretical principles.

One of the key advantages of computational modeling is its ability to integrate diverse data from various sources. By combining experimental and clinical data with theoretical concepts, computational models provide a framework for studying the behavior and dynamics of biological systems and apply them to a clinically relevant context. This interdisciplinary and integrative approach allows to gain insights into the underlying mechanisms and predict how biological systems may respond under different conditions such as in disease mechanisms, drug administration, and individualized patient responses to treatments.

However, computational modeling comes with its own set of challenges and limitations that researchers need to be aware of. Some of the key problems and limitations of computational modeling in biology include:

- Complexity and Incompleteness: Biological systems are usually incredibly complex, with numerous interacting components and pathways. Capturing the entirety of this complexity in a computational model can be challenging and often results in simplifications and assumptions. While these simplifications are necessary, they can lead to potential biases and inaccuracies in model predictions. Additionally, many biological processes and mechanisms are not fully understood or characterized, leading to incomplete models that may not accurately represent the real-world system.

- Data Availability and Quality: Computational models rely heavily on experimental data for parameterization, validation, and calibration. However, obtaining comprehensive and high-quality data can be difficult in biology due to experimental limitations and the sheer scale of biological processes. Inaccurate or incomplete data can lead to unreliable model predictions.

- Parameter Uncertainty: Many biological processes involve parameters that are challenging to measure precisely. The uncertainty associated with these parameters can significantly impact model outcomes. Parameter sensitivity analysis and uncertainty quantification techniques are often used to address this issue, but inherent uncertainty remains. Parameters may be structural non-identifiable, which manifest in functionally related model parameters or practical non-identifiable which might be caused by limited amount and quality of experimental data. However, it is usually difficult to discern if the uncertainty arise due to the model structure or the data.

- Scale and Granularity: Biological systems span multiple scales *in vivo*, from molecular interactions to cellular processes to whole-organism behavior. Determining the appropriate level of granularity for a computational model is crucial, as increasing complexity can lead to computational challenges and data requirements that may be difficult to manage.

- Model Validation and Testing: Validating computational models against experimental data is critical for their reliability and relevance. However, validation can be complex and resource-intensive, especially for large-scale systems. Additionally, overfitting to specific datasets can limit the model's ability to generalize to new scenarios.

- Lack of Standardization: Unlike some fields in engineering or physics, biology lacks standardized models and model-building practices. This lack of standardization can make it challenging to compare and integrate different models or reproduce and validate existing ones.

- Model Interpretability: Some computational models, especially those based on machine learning and deep learning algorithms, can be difficult to interpret. Understanding the underlying biological mechanisms and causality from these black-box models might be challenging, limiting their application in certain contexts.

Despite these challenges, computational modeling plays a crucial role in studying diverse biological phenomena, including genetic networks, cellular processes, physiological systems, and even ecosystems. For example, computational models can simulate and integrate the interactions between genes and proteins within a cell, shedding light on how diseases develop and progress. They can also be used to investigate the effects of drug treatments, aiding in the design and optimization of new therapeutics. Moreover, they can predict the efficacy and potential side effects of drugs on specific patient populations and predict the outcomes of different therapeutic interventions, facilitating personalized medicine and treatment selection.

Furthermore, computational modeling enables hypothesis testing and exploration of complex biological systems that are challenging to study experimentally. It enables researchers to perform 'virtual experiments' or simulations, exploring a wide range of scenarios and parameter settings that may be difficult, costly or ethically unfeasible to investigate in a laboratory or clinical setting. Computational modeling may aid in the exploration of the complex interplay between genetic, environmental, and lifestyle factors in disease development and progression. By simulating disease processes at the molecular, cellular, and organ levels, these models provide insights into the underlying mechanisms of a process or disease.

In summary, computational modeling is a vital tool in modern biology and biomedicine, enabling researchers to bridge the gap between experimental observations, clinical data and theoretical and mechanistic understanding. It provides a means to simulate, analyze, and predict the behavior of complex biological systems, offering valuable insights into fundamental biological processes, disease mechanisms, and potential therapeutic strategies. By integrating diverse biomedical data and refining models through iterative validation, computational modeling contributes to advancing our knowledge of diseases, improving drug discovery, and ultimately guiding personalized treatment strategies. As computational techniques continue to advance, computational modeling in biology will undoubtedly contribute to transformative discoveries and advancements in the life sciences and improving patient outcomes.

Model development

The development of such computational models is an iterative process that involves a series of steps for refinement of the model and its usefulness and is illustrated in figure 2.8. This iterative approach allows to gradually enhance the model's representation of the biological system under investigation, incorporating new data, refining assumptions, and validating predictions.

After initial model construction, experimental data is incorporated into the model to refine and calibrate its parameters. This step involves comparing the model's predictions with available data and adjusting the model's parameters to improve its fit to the observed experimental results. Calibration may involve the use of optimization algorithms or statistical methods to find parameter values that minimize the differences between model predictions and experimental data.

Once the model is calibrated, it is necessary to validate its predictions against independent datasets or experiments not used in the calibration process. Model validation helps to assess the model's ability to generalize and make accurate predictions beyond the data used for calibration. It provides confidence in the model's predictive capabilities and ensures its reliability for further analyses.

Through model validation and analysis, areas of improvement and limitations of the model can be analysed. These insights lead to refinements in the model structure, parameter values, or assumptions. The model is then iteratively updated and recalibrated based on new data or knowledge, enhancing its accuracy and robustness.

Once the model has undergone several iterations and validation, it can be applied to address specific research questions or make predictions about the behavior of the biological system. The model can be used to explore scenarios, design experiments, optimize interventions, or guide decision-making processes. The predictions generated by the model can be further tested and validated through experimental or clinical studies, contributing to a iterative cycle of model refinement and improvement.

The iterative process of model development is an ongoing and dynamic cycle, as new experimental data, technological advancements, and scientific insights emerge. This iterative approach allows for a continuous refinement of models, ensuring that they capture the complexity of biological systems and provide valuable insights into their behavior and regulation. Ultimately, it leads to more accurate and reliable models that advance our understanding of biology and contribute to scientific and medical advancements.

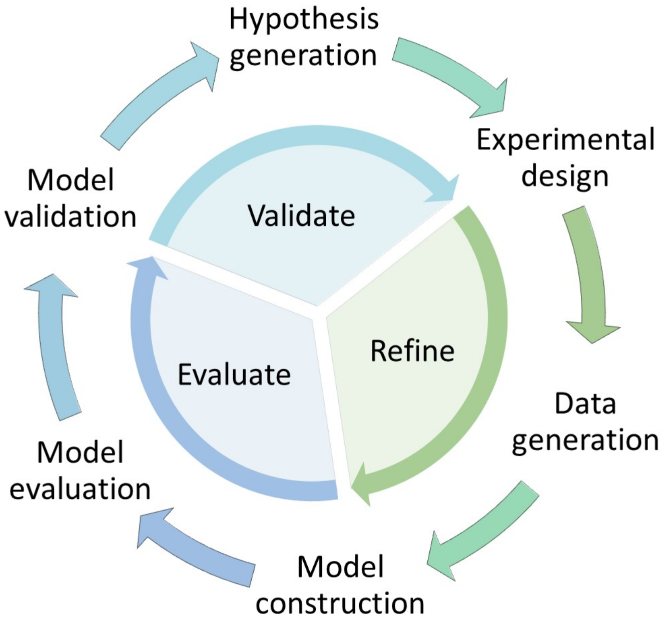
Hypothesis generation
Experimental design
Data generation
Model construction
Model evaluation
Model validation
Validate
Refine
Evaluate

Figure 2.8: Illustration of the iterative model development process in systems biology. The typical process for development of any computational model with adequate level of complexity necessitates a gradual and iterative refinement of the model. Starting from a hypothesis or question, experiments are designed that can generate data needed for model development. Once an initial model is built, it is evaluated and tested against unseen data. By doing so, shortcomings of the model can be identified but also new questions and hypothesis can be generated. For this, new data needs to be generated that can be fed again into the model for further refinement, starting the iteration process anew.

Computational models in systems biology

Systems biology is an interdisciplinary field that seeks to understand biological systems as a whole, considering the interactions and behaviors of their individual components. It integrates concepts and techniques from biology, mathematics, physics, and computer science to study the complexity and dynamics of biological processes at various levels, from molecular interactions to cellular networks and entire organisms. Various types of computational models are employed in biology, each tailored to address specific research questions and capture different aspects of biological processes. These models can range between simple and complex, deterministic and stochastic as well as data-driven and mechanistic. Each type of computational model brings its own strengths and limitations to biological and biomedical research. The choice of model depends on the research question, the level of detail required, and the available data. Often, multiple types of models are integrated to provide a more comprehensive understanding of biological systems. Here, some of the commonly used computational models in biology are explained briefly.

Agent-Based models: Agent-based models (ABMs) simulate the behavior of individual entities, known as agents, and their interactions within a system. Each agent follows a set of predefined rules, and their collective behavior gives rise to emergent properties of the system. ABMs are useful for studying complex systems where individual-level interactions are crucial, such as cellular processes, immune responses, and social behavior in organisms.

Cellular Automata models: Cellular automata (CA) models are discrete models that divide space into a grid of cells, each having a specific state. The state of each cell evolves over time based on a set of rules and the states of its neighboring cells. CA models are well-suited for studying spatially distributed processes, such as tissue growth, pattern formation, and ecological systems.

Network models: Network models represent biological systems as interconnected networks, where nodes represent components (e.g., genes, proteins, or individuals) and edges represent interactions between them. Network models are used to study genetic regulatory networks, protein-protein interaction networks, ecological food webs, and social networks.

They provide insights into the structure, dynamics, and robustness of complex biological systems.

Machine Learning models: Machine learning techniques, such as neural networks, decision trees, and support vector machines, are increasingly used in biology and biomedicine. These models learn patterns and relationships from large datasets and can be applied to tasks like gene expression analysis, protein structure prediction, drug discovery, and medical diagnosis. Machine learning models can uncover hidden patterns and make predictions based on complex data.

Systems of differential equations: Systems of differential equations describe how variables change over time based on their current values and the rates of change. These models are particularly useful for studying dynamic processes, such as biochemical pathways, gene regulatory networks, and physiological systems. They can capture and analyze the complex, nonlinear relationships that are inherent in biological systems. Nonlinear dynamics allows for the representation of intricate phenomena such as feedback loops, oscillations, bistability, bifurcations and chaos, which are prevalent in biological systems.

Biological systems are often represented as systems of ordinary differential equations (ODEs), where the state of the system evolves over time based on a set of mathematical equations or rules, based on known mechanisms or derived empirically, that describe the interactions between its components. These components can vary from gene numbers, protein levels, metabolite concentration to cell counts, and even to higher-level entities such as tissue or organ mass. Such an ODE model then describes the change of a state variable **x** over time:

$$\frac{dx}{dt} = f(x, p, u) \quad x(t = 0) = x_0$$

Here, x_0 represents the initial value of the state variable x, p denotes model parameters and u describes the model input. Using a non-linear function f with p and u, the change of state variable x over time can be described. In biology, f is often modelled as mass action or Michaelis-Menten kinetics.

2.2.1 PBPK modelling

Physiologically-based pharmacokinetic modeling is a computational approach used in pharmacology and toxicology to simulate the absorption, distribution, metabolism, and excretion (ADME) of drugs and chemicals in the human body. It combines physiological principles with mathematical equations to provide a detailed understanding of how substances are processed within the body.

The main objective of PBPK modeling is to predict the concentration profiles of substances in different tissues and organs over time. Unlike simpler models, PBPK models take into account the anatomical and physiological characteristics of specific tissues, as well as the interplay of various processes involved in drug disposition.

PBPK models consist of a series of interconnected compartments that represent different tissues and organs. Each compartment is characterized by its specific blood flow, tissue volume, and physiological properties. Mathematical equations, often based on principles of mass balance and diffusion, govern the movement of substances between compartments. The model incorporates specific parameters for absorption, distribution, metabolism, and excretion processes, which can be derived from experimental data or estimated from known physiological parameters. A schematic representation of PBPK is shown in figure 2.9.

PBPK modeling has diverse applications in biomedical and pharmaceutical research (Figure 2.10). They can be used to optimize dosing regimens, predict drug-drug interactions, and guide formulation strategies. PBPK modeling also plays a crucial role in assessing the safety of chemicals, evaluating exposure levels, and estimating potential risks to human health in occupational or environmental settings. By considering factors such as body weight, age, sex, organ size, blood flow rates, and enzyme activity, PBPK models can provide personalized predictions but also extrapolate findings to special populations such as infants, pregnant people or elderly as well as to other species.

Additionally, PBPK modeling can aid in understanding and interpreting experimental data. By integrating *in vitro* data, preclinical studies, and clinical observations, PBPK models provide a mechanistic framework for interpreting complex pharmacokinetic data and gaining insights into the underlying processes governing drug and chemical disposition.

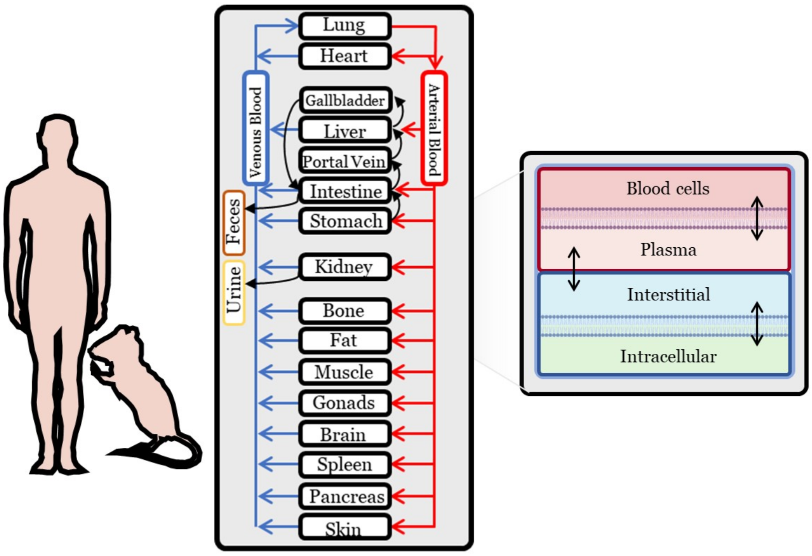
Lung
Heart
Gallbladder
Liver
Portal Vein
Intestine
Stomach
Kidney
Bone
Fat
Muscle
Gonads
Brain
Spleen
Pancreas
Skin
Venous Blood
Arterial Blood
Feces
Urine
Blood cells
Plasma
Interstitial
Intracellular

Figure 2.9: Illustration of PBPK modeling. PBPK models can be built for various organism by using species specific physiological properties. In a PBPK model, all major organs are represented as compartments that are interconnected by the systemic blood flow and parameterized in a species-specific manner. Excretion via feces and urine are included as a means of removing compounds from the system. Depending on the desired complexity, each organ can additionally include subcompartments representing the vascular space, such as blood cells and plasma, the interstitium as well as the cells. Transport between these subcompartments occurs via passive diffusion or active transport if applicable. Figure was adapted from [256].

As computational tools and data availability continue to advance, PBPK modeling is becoming an indispensable tool in the field of pharmacology and toxicology. Its ability to incorporate physiological complexity, individual-specific parameters, and experimental data enables researchers and regulators to make informed decisions regarding drug safety, optimize dosing strategies, and assess the potential risks associated with exposure to chemicals.

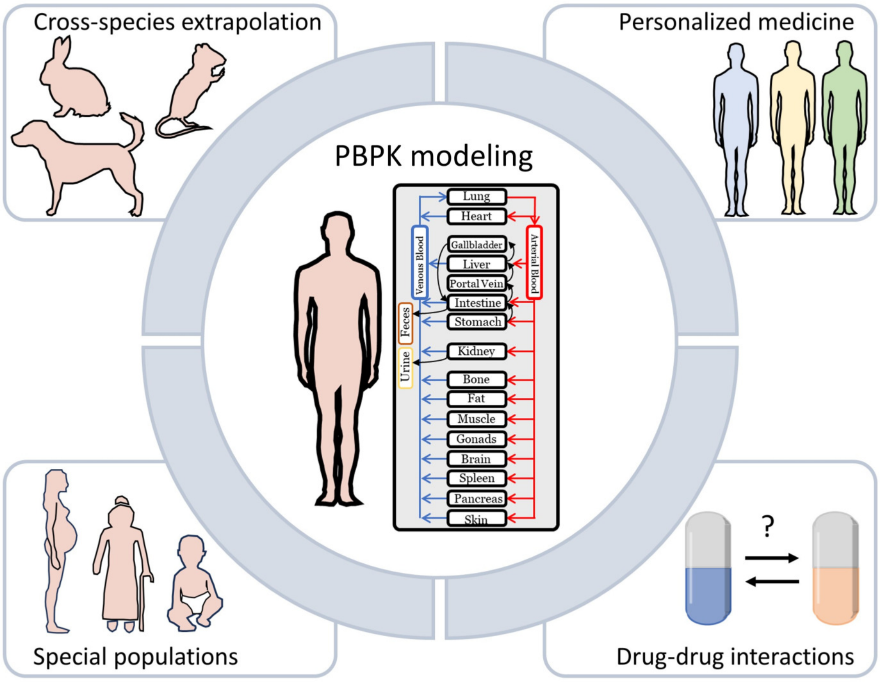
Cross-species extrapolation
Personalized medicine
PBPK modeling
Lung
Heart
Gallbladder
Liver
Portal Vein
Intestine
Stomach
Kidney
Bone
Fat
Muscle
Gonads
Brain
Spleen
Pancreas
Skin
Venous Blood
Arterial Blood
Feces
Urine
?
Special populations
Drug-drug interactions

Figure 2.10: Illustration of applications of PBPK modeling. PBPK modeling can be used for various applications, including extrapolation to other species, prediction of drug-drug interactions (DDI), adaptation to special populations such as infants, elderly or pregnant people as well as personalization to individuals. Figure was adapted from [257].

2.2.2 Published models of BA metabolism

Given the intricate and interconnected network of mechanisms that regulate BA metabolism, there is a clear imperative to quantitatively characterize the composition, distribution and dynamics of the BA pool. This characterization stands as a crucial step toward unraveling the complexities inherent in diseases associated with BAs, where imbalances or dysregulation can be symptomatic for underlying diseases or can even have far-reaching consequences for health.

In this pursuit, physiologically-based/PBPK modeling emerges as a robust analytical tool, adept at untangling the heterogeneous physiological and biological information that arises from a multitude of experimental conditions. Building on this foundation, a variety of physiologically-based models have been developed, each with the aim of encapsulating the intricate metabolism and EHC of BAs. Of note, all models described below were developed within the human context. A brief overview of these published models is illustrated here:

- **Hofmann et al. [258; 259] and Molino et al. [260]** In these studies, multicompartmental pharmacokinetic models were developed on physiological principles and parameterized with experimental data. Three individual models were developed describing either CA [258], CDCA [260] or DCA [259] in their glyco-, tauro- and unconjugated forms. The nine compartments that were modeled were liver, gallbladder, bile ducts, jejunum, ileum, colon, portal blood, sinusoidal blood and general circulation. No subcompartments were considered. All reactions were modeled using zero order kinetics as constant flows. Postprandial responses were included by providing two different parameter values for the fasting and digestive state.
- **Edwards et al. [261]** Based on the model published by Molino et al. [260], an analouges model was developed for obeticholic acid (OCA). This semisynthetic BA, is a selective and potent FXR agonist in development for the treatment of chronic nonviral liver diseases.
- **Zuo et al. [262]** The model developed by Zuo et al. was based on the models developed by Hofmann et al. [258; 259]. This model was developed to describe the metabolism and disposition of UDCA and its conjugates in healthy subjects based on pharmacokinetic (PK) data from published studies in order to study the distribution of oral UDCA.
- **Voronova et al. [263]** Extending the model by Hofmann et al. and Molino et al., the here published model simultaneously follows CA, CDCA and DCA as well as their conjugated and unconjugated forms. Voronova et al. further included regulation through the FXR-FGF19 axis.
- **Guiastrennec et al. [264]** In this study, a non-linear mixed-effects model with a simplified description of the EHC was developed to study the effects of meal composition on the distribution of tBAs.
- **Sips et al. [265]** This model outlines the metabolism and conversion of BAs in a cycle of 18 connected compartments that represent the EHC. The range of BAs encompassed in this model includes CA, CDCA, DCA, LCA, UDCA, and a collection of ”other” BAs, along with their various conjugated, unconjugated, and sulfated forms. Notably, this modeling approach places a particular emphasis on the

intestinal transit, which is modeled in a temporally and spatially heterogeneous way. In response to the ingestion of a meal, this model incorporates a transient acceleration in the speed of intestinal transit. This surge in transit speed propels the contents of the intestines forward, accounting for the changes that occur during the digestive process.

- **de Bruijin et al. [266; 267]** This model follows G-CA, G-CDCA, G-DCA as well uBAs in gall bladder, upper and lower intestine, colon, blood, rapidly perfused tissue, slowly perfused tissue,adipose tissue and extra-and intracellular water in liver. While the model incorporates active transport via BSEP, ASBT and NTCP, active transport by MRP3/4 and OSTα/β was not modeled. Most parameters of transport processes could be derived experimentally.
- **Woodhead et al. [268]** This study aimed to develop a submodel of BA homeostasis within DILISym, a mechanistic model of DILI (Simulations Plus). This model was constructed for rats and humans following tBA, CDCA and LCA as BA that are specifically implicated in hepatotoxicity. The model incorporates bile acid synthesis, uptake, recirculation, and efflux.
- **Baier et al. [269]** A whole body physiologically-based BA model that follows the levels of G-CDCA as an exemplary BA. This model was developed using the Open Systems Pharmacology Suite and is used as a basis for the work presented here.

Chapter 3

A physiologically-based model of bile acid metabolism in mice

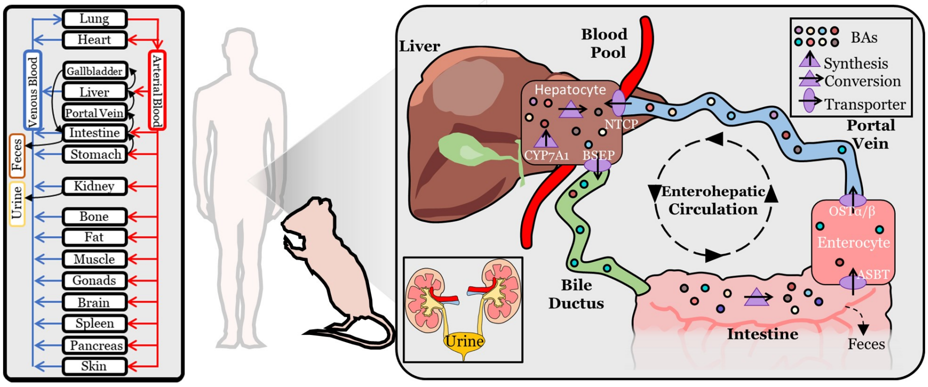
Lung
Heart
Gallbladder
Liver
Portal Vein
Intestine
Stomach
Kidney
Bone
Fat
Muscle
Gonads
Brain
Spleen
Pancreas
Skin
Venous Blood
Arterial Blood
Feces
Urine
Liver
Blood Pool
BAs
Synthesis
Conversion
Transporter
Hepatocyte
NTCP
CYP7A1
BSEP
Portal Vein
Enterohepatic Circulation
OSTα/β
Enterocyte
ASBT
Bile Ductus
Urine
Intestine
Feces

Partially published as:
Kister, B., Viehof, A., Rolle-Kampczyk, U., Schwentker, A., Treichel, N.S., Jennings, S., Wirtz, T.H., Blank, L.M., Hornef, M.W., von Bergen, M., Clavel, T., Kuepfer, L., 2023. A physiologically based model of bile acid metabolism in mice. iScience. Volume 26. Issue 10. 107922.
[Reprinted (adapted) with permission from Elsevier. Open access CC-BY © The Authors 2023]

Contributions:

B. Kister developed the model, performed the simulations, analyzed the data, created the figures, and wrote the chapter. A. Viehof collected samples from the mouse models. U. Rolle-Kampcyzyk performed the bile acid measurements. A. Schwentker measured the transporter expression. N. Treichel sequenced the cecal microbiome. L.M. Blank and L. Kuepfer discussed the data and reviewed the chapter.

Bile acid metabolism plays a vital role in maintaining the overall homeostasis of the liver and gastrointestinal system. Bile acids are not only essential for the digestion and absorption of dietary fats but also serve as signaling molecules involved in various physiological processes. Understanding the intricate dynamics of BA metabolism is crucial for elucidating its impact on health and disease. The development of a computational model of murine BA metabolism involves the integration of diverse data sources, ranging from experimental measurements, including BA measurements, transporter expression and microbiome characterization, to prior physiological knowledge of the organism. Physiologically-based pharmacokinetic modeling serves as a plausible approach for capturing the intricate interplay between various compartments, including the liver, gut, bloodstream, and other relevant tissues. By incorporating physiological parameters, organ volumes, tissue composition, and transport kinetics, PBPK models can provide a detailed representation of the murine system.

The computational models presented in this chapter elucidate the sex-related differences and kinetics influencing murine BA metabolism. By considering the specificities of male and female mice, the models capture variations in BA levels, transporters' expression, microbiota composition, and other key factors. Through the integration of physicochemical properties, distribution models, and available experimental data, the models can provide insights into the mechanisms of BA metabolism and can facilitate the exploration of novel therapeutic interventions.

This chapter illustrates at first the general development of the computational models of murine BA metabolism, the data generated for this and their implication on necessary model simplifications. In the following sections, model variants are examined in more detail describing model calibration, validation and predictions derived from the final models. Finally, results of this chapter are discussed critically summarizing the capabilities and limitations of the here presented models

3.1 Model development and data

The computational models for murine BA metabolism are based on physiological principles and encompasses various processes such as synthesis, hepatic and microbial transformations, (re-)circulation, and excretion of BAs. A diagram illustrating the overview of the mouse models (6BA and murine conjugation model; described below) can be found in figure 3.1. To develop these models, a PBPK modeling approach was used, as described by Küpfer et al. [257], where the circulating molecules were represented by BA metabolites. The PBPK models provides a comprehensive representation of mouse physiology, incorporating detailed information on organ volumes, tissue composition, organ surface areas, and blood perfusion rates, based on prior knowledge [270; 271]. Importantly, the mechanistic structure of the PBPK models allows for extrapolation to new scenarios and conditions [270; 272].

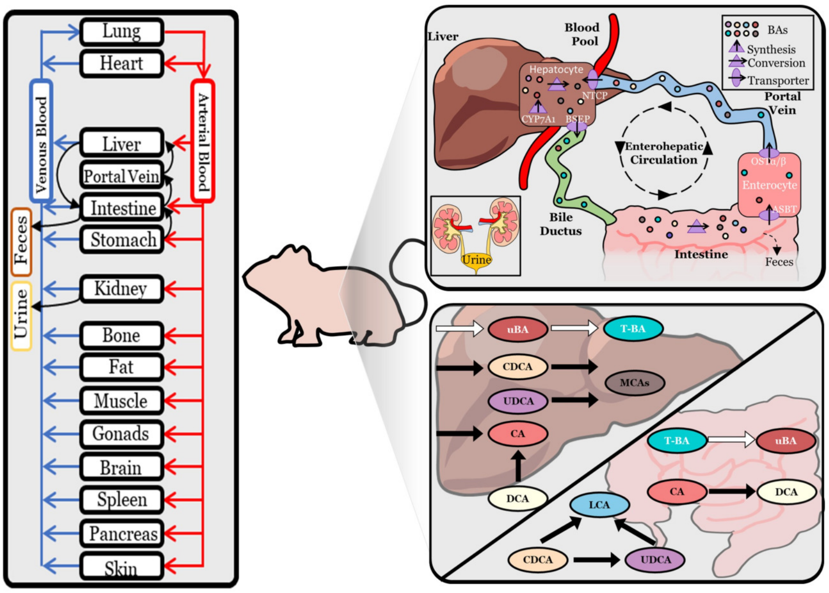
Lung
Heart
Venous Blood
Arterial Blood
Liver
Portal Vein
Intestine
Stomach
Feces
Kidney
Urine
Bone
Fat
Muscle
Gonads
Brain
Spleen
Pancreas
Skin
Liver
Blood Pool
Hepatocyte
NTCP
CYP7A1
BSEP
BAs
Synthesis
Conversion
Transporter
Portal Vein
Enterohepatic Circulation
OSTα/β
Enterocyte
ASBT
Bile Ductus
Intestine
Feces
Urine
uBA
T-BA
CDCA
MCAs
UDCA
CA
DCA
T-BA
uBA
CA
DCA
LCA
CDCA
UDCA

Figure 3.1: Continued on the next page.

Figure 3.1: Physiologically-based bile acid model. Schematic overview of a PBPK model of BA biosynthesis via CYP7A1, hepatic and microbial transformation, active transport processes via BSEP, ASBT, OST-α/β and NTCP, as well as fecal and renal excretion. In the computational model, excretion to the gallbladder is neglected and BAs are directly secreted into the duodenum. Reactions of BAs are located either in the intracellular space of the liver or in the intestinal lumen. Reactions colored in white are present in the murine conjugation model, those in black are considered in the 6BA model.

To obtain precise physiological and kinetic parameters for BA metabolism in mice, a comprehensive set of experimental data was gathered. This dataset included measurements of BA levels and composition in various tissues of specific pathogen-free (SPF) mice, as illustrated in figure 3.2. Additionally, physiological parameters were assessed, as depicted in figure 3.3, along with the quantification of transporter gene expression in different segments of the gut. Moreover, the diversity and composition of the cecal microbiome were analyzed, as shown in figure 3.4. Upon conducting an initial examination of BA levels, it was observed that female mice generally exhibited higher BA concentration compared to their male littermates, which aligns with previously published studies [273]. The data consistently revealed increased total BA concentrations in female mice across various tissues, including venous blood serum, liver, bile, and intestinal tissues (Figure 3.2A-E, I, K, L). Furthermore, BA levels in the gut lumen were higher in the small intestine (Figure 3.2F, H), while the large intestine's content did not present a clear pattern (Figure 3.2J, M). Notably, only the ileal tissue exhibited higher BA concentrations in male mice compared to female mice (Figure 3.2G).

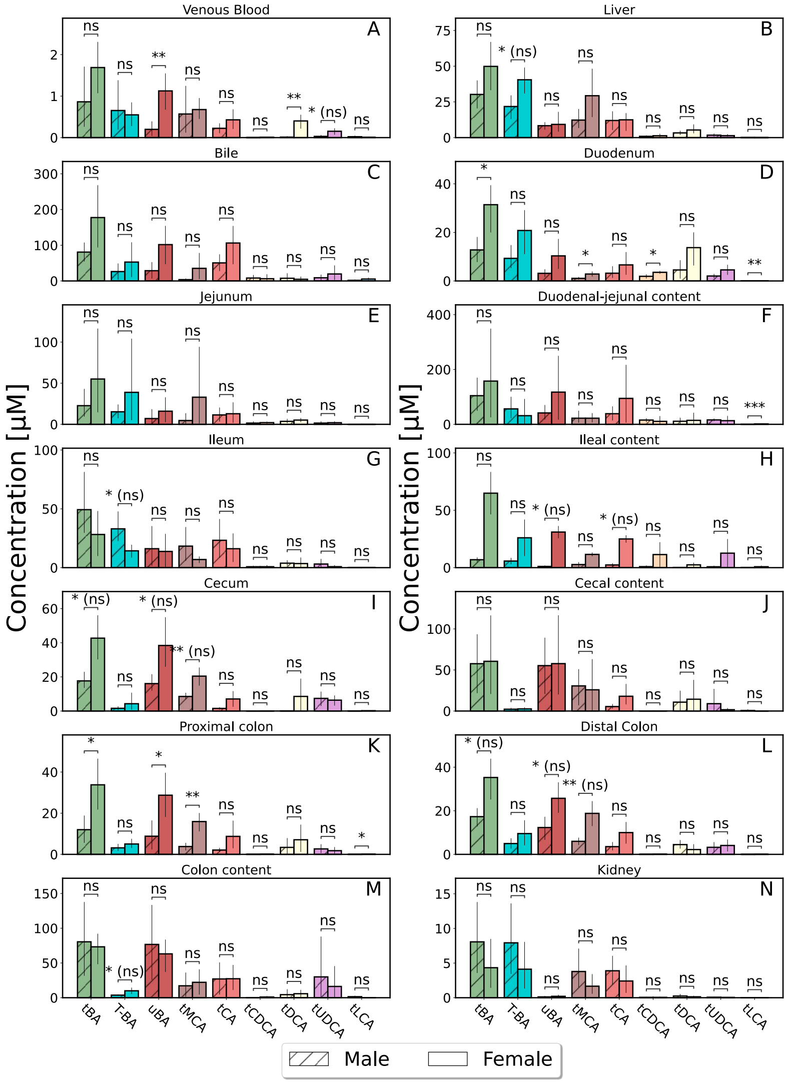

Figure 3.2: Bile acid levels in SPF mice. Concentration of total BAs (tBA), tauro-conjugated BAs (T-BA), unconjugated BA (uBA), total cholic acid (tCA), total muricholic acids (tMCA), total chenodeoxycholic acid (tCDCA), total deoxycholic acid (tDCA), total ursodeoxycholic acid (tUDCA) and total lithocholic acid (tLCA) in various organs and samples from male (striped bars) and female SPF mice (open bars). Statistical differences were assessed by independent t-test. Statistical significance is marked with asterisks and (ns) indicates non-significance after correction for multiple testing using Benjamini-Hochberg correction.

To accommodate the variations in BA metabolism related to sex, distinct computational models were developed for male and female SPF mice. By employing physiologically-based modeling, detailed information regarding the organism's physiology, as assessed in figure 3.3, could be incorporated. Notably, male mice in this study exhibited an approximate 30% higher body weight (Figure 3.3A). Conversely, female mice displayed smaller liver and kidney sizes in proportion to their body weight (Figure 3.3C). Interestingly, irrespective of sex, the length of the intestine remained relatively consistent; therefore, female mice possessed a comparatively longer intestine in relation to their body weight (Figure 3.3B).

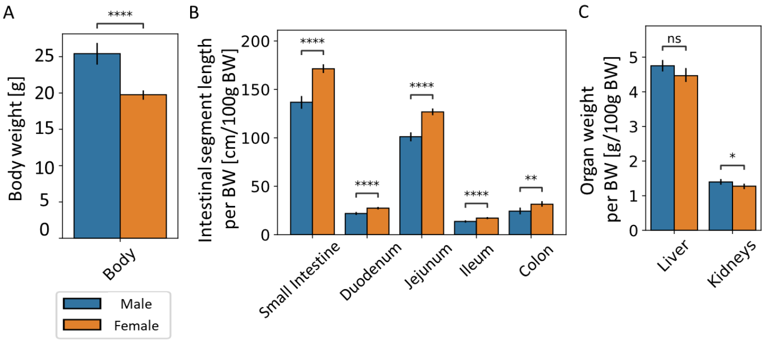

Figure 3.3: Physiological differences between male and female mice. Assessment of sex-related differences in body weight (A), length of intestinal segments (B) as well as weight of the liver and the kidneys (C) in SPF mice (male (blue bars), female (orange bars)). Significant differences were tested by two-way, independent t-test and significance was marked with asterisks.

The models incorporate four essential transport processes: (1) BSEP facilitates the excretion of BAs from the liver into the duodenum. (2) BAs are taken up from the gut lumen by ASBT (3) Enterocytes excrete BAs to the portal blood using OSTα/β. (4) Hepatocytes absorb BAs from portal blood via NTCP. Expression levels of the transporters (ASBT, OSTα/β) along the gut axis did not exhibit significant differences between male and female mice overall. However, there were substantial variations observed among different gut segments, as illustrated in figure 3.4A.

In order to investigate potential variances in the microbiota between male and female mice, the microbial diversity and composition within the cecum was assessed. Initially, the within-sample taxonomic diversity was analyzed by determining the α-diversity. The measurements of species richness and Shannon effective counts revealed no significant differences associated with sex, as demonstrated in figure 3.4B. Subsequently, the similarities in microbial community structure, referred to as β-diversity, using generalized UniFrac distances [274; 275] were evaluated. Notably, there was no notable separation of mice based on sex, indicating a high overall similarity among all samples (see figure 3.4C).

On the other hand, composition of the cecal microbiome between male and female mice showed noteworthy differences. Specifically, the *Lactobacillaceae* family showed higher abundance in female mice, while an unidentified genus within the *Muribaculacea* family was more prevalent in male mice (Figure 3.4D). It is worth noting that certain *Lactobacilla* species have the capability to metabolize BAs [276]. However, the difference in relative abundance between male and female mice, while only statistically significant without p-value adjustment, was relatively minor. Additionally, no available information connects the other significantly abundant genus to BA metabolism. In conclusion, these findings indicate that there are no substantial disparities in the expression of intestinal transporters or the diversity and composition of the microbiota between male and female mice.

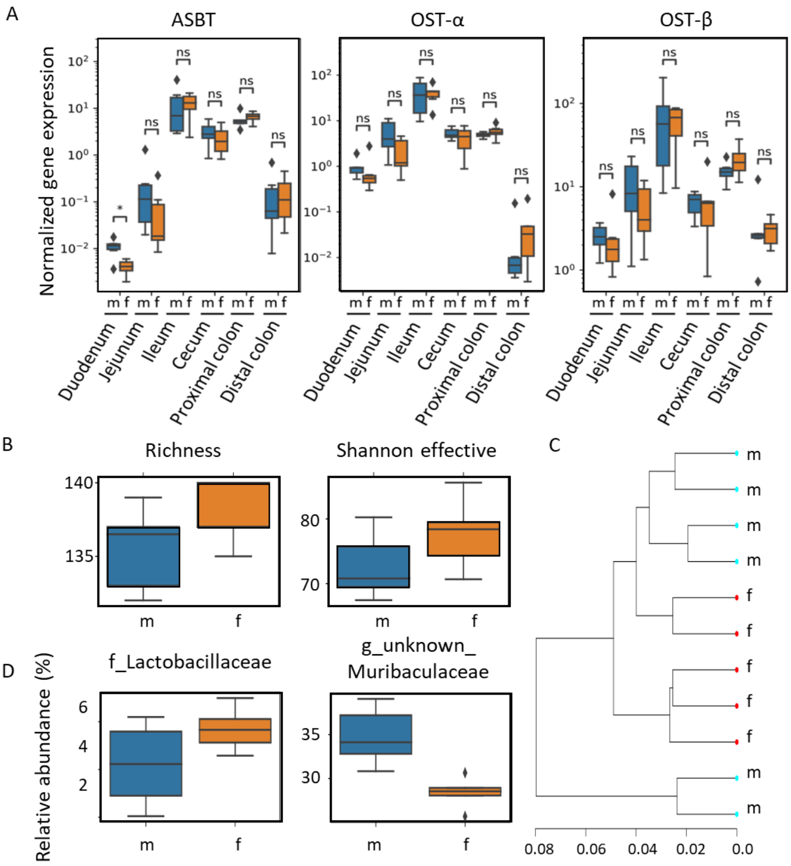

Figure 3.4: Sex-related differences in intestinal BA metabolism. Assessment of sex-related differences in the intestine relevant to BA metabolism: A) Expression of the BA transporters ASBT, OST-α and OST-β (from left to right) along the gut axis in male and female SPF mice measured by qPCR. Statistical significance was assessed by Mann-Whitney U-test and statistical significance is marked with asterisks (male (blue bars), female (orange bars)). B) Analysis of the cecal microbiome in male and female SPF mice by assessing observed species richness and effective Shannon index as indices of α-diversity, and C) β-diversity by hierarchical clustering of samples. D) The relative abundance of the family of *Lactobacillaceae* and an unknown genus of the *Muribaculaceae*, which significantly differed between male and female mice. Statistical significance was determined using Kruskal-Wallis and Wilcoxon rank sum test (α = 0.05).

In addition to considering the organism's physiology, physicochemical properties such as molecular weight, solubility, lipophilicity (logP), and plasma-protein binding (fraction unbound) constitute another crucial aspect of PBPK models [257]. These properties enable the determination of organ-plasma partitioning and passive transport through the application of suitable distribution models. For the PBPK models of BA metabolism, the physicochemical properties of tauro-conjugated forms (Table 3.1) or of MCAs (Table 3.2) were utilized to inform the compound properties within the PBPK model for small molecules.

Table 3.1: Physicochemical properties of bile acids used. Overview of physicochemical properties and their source that were used to inform compound specific parameters in the PBPK model. For the total BA (total CA: tCA, total CDCA: tCDCA, total UDCA: tUDCA, total DCA: tDCA, total LCA: tLCA, total MCAs: tMCA) the corresponding physicochemical values of the tauro-conjugated form (T-BA) were taken.

BA species	Property	Value	Source
tCA	MW [g/mol]	515.7	PubChem Identifier: CID 6675
tCA	Solubility [g/l]	0.077	ALOGPS (HMDB [277])
tCA	logP	0	Heuman et al. [278]
tCA	pKa (acidic)	-0.88	ChemAxon (HMDB [277])
tCA	pKa (basic)	-0.053	ChemAxon (HMDB [277])
tCA	FU	0.359	Predicted [279]
tCDCA	MW [g/mol]	499.7	PubChem Identifier: CID 387316
tCDCA	Solubility [g/l]	0.00748	ALOGPS (HMDB [277])
tCDCA	logP	0.46	Heuman et al. [278]
tCDCA	pKa (acidic)	-0.99	ChemAxon (HMDB [277])
tCDCA	pKa (basic)	0.18	ChemAxon (HMDB [277])
tCDCA	FU	0.0776	Predicted [279]
tUDCA	MW [g/mol]	499.7	PubChem Identifier: CID 9848818
tUDCA	Solubility [g/l]	0.0075	ALOGPS (HMDB [277])
tUDCA	logP	-0.94	Heuman et al. [278]
tUDCA	pKa (acidic)	-0.99	ChemAxon (HMDB [277])
tUDCA	pKa (basic)	0.18	ChemAxon (HMDB [277])
tUDCA	FU	0.0776	Predicted [279]
tDCA	MW [g/mol]	499.7	PubChem Identifier: CID 2733768
tDCA	Solubility [g/l]	0.0078	ALOGPS (HMDB [277])
tDCA	logP	0.59	Heuman et al. [278]

Continuation of table 3.1

BA species	Property	Value	Source
tDCA	pKa (acidic)	-0.75	ChemAxon (HMDB [277])
tDCA	pKa (basic)	-0.2	ChemAxon (HMDB [277])
tDCA	FU	0.0768	Predicted [279]
tLCA	MW [g/mol]	483.7	PubChem Identifier: CID 439763
tLCA	Solubility [g/l]	0.00028	ALOGPS (HMDB [277])
tLCA	logP	1	Heuman et al. [278]
tLCA	pKa (acidic)	-0.63	ChemAxon (HMDB [277])
tLCA	pKa (basic)	-1.1	ChemAxon (HMDB [277])
tLCA	FU	0.0618	Predicted [279]
tMCA	MW [g/mol]	515.7	PubChem Identifier: CID 168408
tMCA	Solubility [g/l]	0.075	ALOGPS (HMDB [277])
tMCA	logP	-0.81	Heuman et al. [278]
tMCA	pKa (acidic)	-0.98	ChemAxon (HMDB [277])
tMCA	pkA (basic)	0.084	ChemAxon (HMDB [277])
tMCA	FU	0.365	Predicted [279]

Table 3.2: Physicochemical properties of bile acids used. Overview of physicochemical properties and their source that were used to inform compound specific parameters in the PBPK model. For the tauro-conjugated BA and unconjugated BA the corresponding physicochemical values of MCAs were taken (tauro-conjugated BA: T-BA, unconjugated BA: uBA).

BA species	Property	Value	Source
T-BA	MW [g/mol]	515.7	PubChem Identifier: CID 168408
T-BA	Solubility [g/l]	0.075	ALOGPS (HMDB [277])
T-BA	logP	-0.81	Heuman et al. [278]
T-BA	pKa (acidic)	-0.98	ChemAxon (HMDB [277])
T-BA	pkA (basic)	0.084	ChemAxon (HMDB [277])
T-BA	FU	0.365	Predicted [279]
uBA	MW [g/mol]	408.6	PubChem Identifier: CID 119473
uBA	Solubility [g/l]	0.069	ALOGPS (HMDB [277])
uBA	logP	-0.69	Heuman et al. [278]
uBA	pKa (acidic)	4.6	ChemAxon (HMDB [277])
uBA	pKa (basic)	-2.7	ChemAxon (HMDB [277])
uBA	FU	0.0885	Predicted [279]

In mice, the most abundant BA species are CA, ($\alpha/\beta/\omega$-)MCA, CDCA, DCA, UDCA and LCA followed by traces of a plethora of secondary BA. Each of these BA species can occur among others as free BAs, taurine conjugated bile salts or 3′-sulfated BAs, resulting in a highly complex BA pool. Given the here used modeling software, it was computationally not feasible for a single model to capture the full complexity of the BA pool. Therefore, two model variants were developed independently that cover different important aspects of the BA pool. One variant follows the total levels of the six most abundant BA species CA, MCAs (simplified $\alpha/\beta/\omega$-MCAs), CDCA, DCA, UDCA and LCA is referred to as ″6BA model″. The other variant describes the conjugation status of BAs and follows tauro-conjugated BA or free/unconjugated BA and is called ″murine/mouse conjugation model″.

For either model variant, *de novo* synthesis of BAs were modeled as a constant formation rate within the intracellular space of the liver. To estimate the magnitude of this synthesis rate, the excretion rates of BAs in feces [98; 280; 281] and urine [282] were taken into account. Both excretion processes were accounted for using passive transport or active clearance mechanisms, respectively. Further hepatic and microbial transformations were included dependent on the model variant and are shown in figure 3.1.

3.2 6BA Model - describing the six most abundant bile acids

The 6BA model incorporates subsequent to synthesis of CA and CDCA, the formation of MCAs from CDCA or UDCA, as well as hepatic hydroxylation of DCA. Microbial metabolism of BAs was modeled as net enzymatic reactions, with the relative abundance of the corresponding enzymes along the gut correlated to the activity of BSH [283]. The included reactions encompassed dehydroxylation of CA to DCA, and CDCA and UDCA to LCA, as well as epimerization of CDCA to UDCA. A schematic overview of the 6BA model is illustrated in figure 3.5.

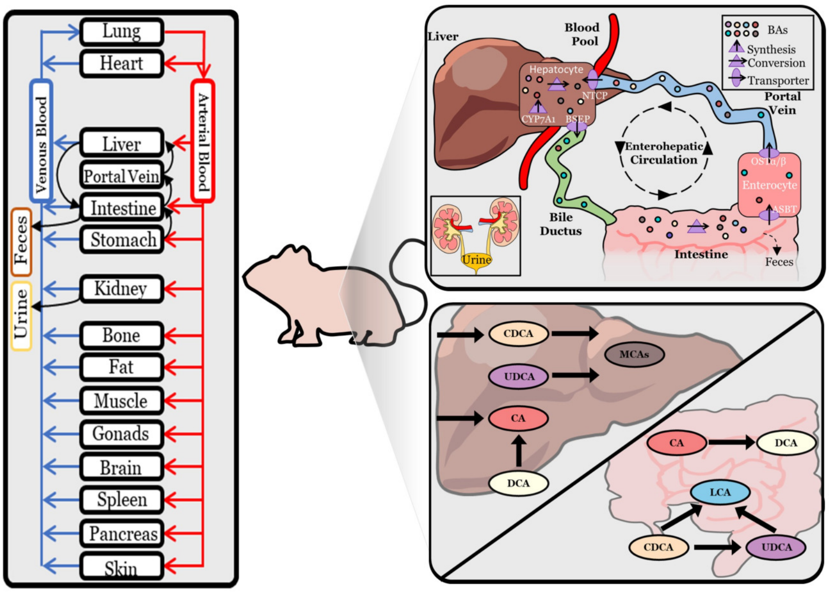
Lung
Heart
Venous Blood
Arterial Blood
Liver
Portal Vein
Intestine
Stomach
Feces
Kidney
Urine
Bone
Fat
Muscle
Gonads
Brain
Spleen
Pancreas
Skin
Liver
Blood Pool
Hepatocyte
NTCP
CYP7A1
BSEP
BAs
Synthesis
Conversion
Transporter
Portal Vein
Enterohepatic Circulation
OSTα/β
Enterocyte
ASBT
Bile Ductus
Intestine
Feces
Urine
CDCA
MCAs
UDCA
CA
DCA
CA
DCA
LCA
CDCA
UDCA

Figure 3.5: Physiologically-based bile acid model - 6BA. Schematic overview of a PBPK model of bile acid biosynthesis via CYP7A1, hepatic and microbial transformation, active transport processes via BSEP, ASBT, OST-α/β and NTCP, as well as fecal and renal excretion. In the computational model, excretion to the gallbladder is neglected and BAs are directly secreted into the duodenum. Reactions of BAs are located either in the intracellular space of the liver or in the intestinal lumen.

Model calibration to data from SPF mice

In a first step, the 6BA model was calibrated to BA measurements in SPF mice. During parameter estimation, sex-related differences were only considered in active hepatic processes. Testing different combination of differential parameters showed that the downregulation of BA synthesis and the transporter sodium/taurocholate cotransporting polypeptide (NTCP) in male mice was both necessary and sufficient to adequately accounted for the observed sex differences in BA composition and levels SPF mice (data not shown). These findings align with previous research indicating an upregulation of BA synthesis enzymes (*Cyp7a1, Cyp27a1*) [284] and elevated expression of the basolateral uptake transporter NTCP in female mice [285]. This remarkable concordance with prior findings provides initial evidence of the computational model's predictive capabilities and instills confidence for further analyses.

After parameter estimation, utilizing the fitted parameters presented in supplementary tables A.1-A.3, the final computational model effectively captured the BA levels in various organs of both male and female SPF mice (Figure 3.6A-B). Up to 60% of the predictions fell within one standard deviation (SD), while 92% were within a two-fold SD range. Only 12 out of 156 data points deviated by more than two SDs (Figure 3.6C-D). Despite the complexity of the modeled system and the considerable variation observed in the measured data, particularly within the intestine, the model demonstrated a strong agreement between the experimental data and simulated results.

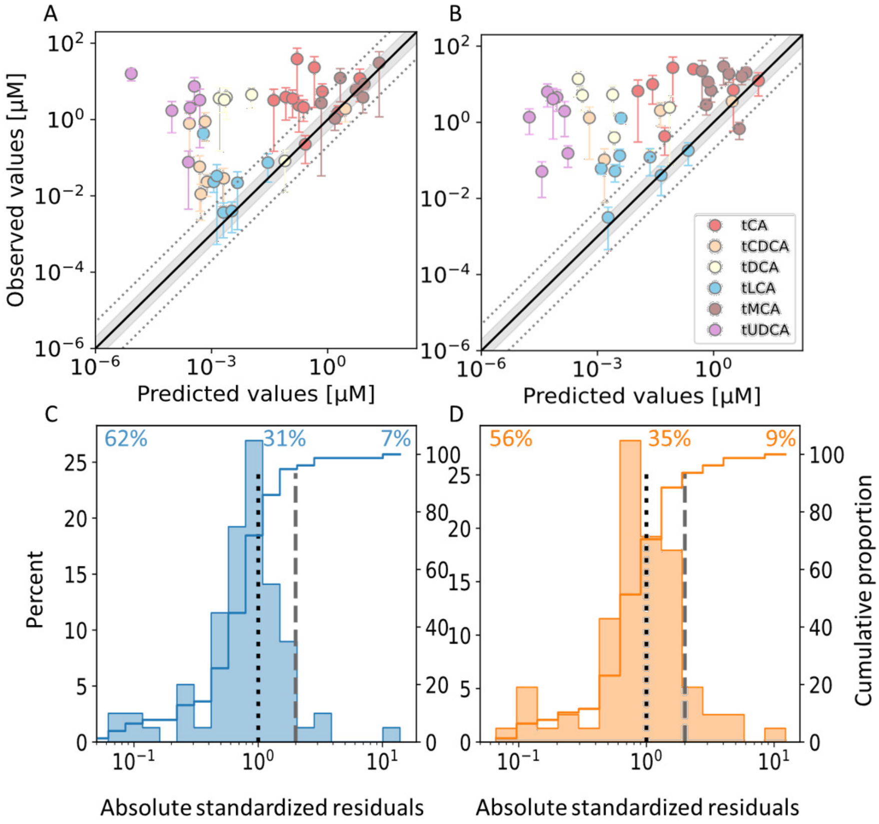

Figure 3.6: Model fit to data from SPF mice. Model simulations of bile acid concentration in male (A) and female mice (B) against corresponding data points used for fitting. Only data points with a coefficient of variation below 1 are shown. Unity is represented by a solid black line, a two- and five-fold range between predicted and observed values is indicated as a gray area or with dotted lines, respectively. Error bars show the SD. Distribution of the absolute standardized residuals between model simulations and data of male (C) and female (D) mice (histogram) and the corresponding cumulative function (line). The dotted and dashed lines indicate differences between model simulation and measured data of one SD and two SD, respectively. Cumulative proportions of predictions that are within one SD (top left, residuals left of dotted line), between one and two SD (top middle, residuals between dotted and dashed line) and above two SD (top right, residuals right of dashed line) of measured data are stated at the top of the panel.

In order to evaluate the behavior of the model, a sensitivity analysis was conducted to determine the impact of the fitted parameters on various experimentally measured BA concentrations (Supplementary Tables A.4-A.12). Changes in BA synthesis exhibited an influence on all assessed BA levels. The activity of the BSEP showed the strongest effects on BA concentrations in the liver and intestinal content. Parameters related to ASBT primarily influenced the concentrations of all BA species in the intestine, with ASBT parameters for secondary BAs affecting the concentration of corresponding secondary BAs beyond the gut. The transport processes mediated by OSTα/β had the most significant control over BA levels in intestinal tissues, although their coefficients remained below the chosen threshold (data not shown). Concentrations of BAs in venous blood plasma and the kidney exhibited sensitivity to both BA uptake from portal blood through NTCP and excretion via urine. Overall, the sensitivity coefficients of all model parameters demonstrated a high correlation between the two models. Some differential sensitivities were observed; however, these corresponding parameters lacked physiological relevance (Supplementary Figure A.4).

Model qualification to germ-free mice

The physiologically-based computational model of murine BA metabolism, due to its mechanistic structure, offers the possibility of considering new scenarios. To validate the model, BA levels in germ-free (GF) mice were simulated. As a first approach, any microbial activity in the SPF model was disabled by setting the corresponding rates to zero. The resulting predictions reasonably reproduced the BA concentrations observed in male and female GF mice (Figure 3.7A and Supplemental Figure A.1). Approximately 59% of the predicted concentrations were recapitulated within one standard deviation, while 80% were within a two-fold variation. Fifteen predicted BA levels deviated more significantly from the measured values (Figure 3.7B).

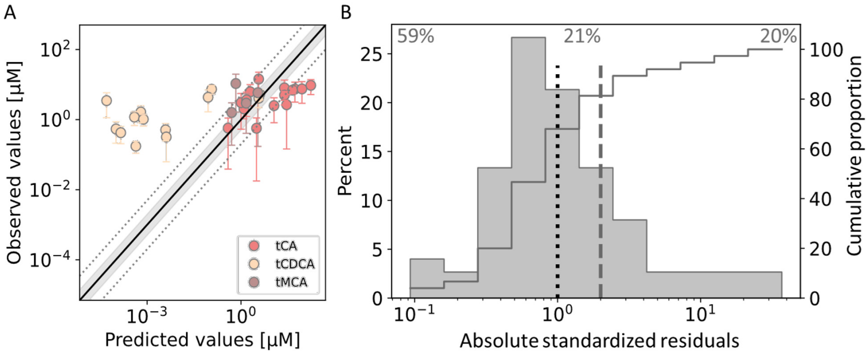

Figure 3.7: Model prediction of germ-free mice. Model predictions of concentration of bile acids in both male and female, germ-free mice against corresponding data points used for fitting (A). Only data points with a coefficient of variation below 1 are shown. Unity is shown as a solid black line shows unity, a two- and five-fold range between predicted and observed values is indicated as a gray area or with dotted lines, respectively. Error bars represent the standard deviation. B) Distribution of the absolute standardized residuals model predictions (histogram) and the corresponding cumulative function (line). The dotted and dashed lines indicate differences between model simulation and measured data of one SD and two SDs, respectively. Cumulative proportions of predictions that are within one SD (top left, residuals left of dotted line), between one and two SDs (top middle, residuals between dotted and dashed line) and above two SDs (top right, residuals right of dashed line) of measured data are stated at the top of the panel.

Subsequently, additional information concerning the physiology and expression of intestinal transporters were included (Supplementary Figure A.2 and A.3) assessing whether this would enhance the agreement between model simulations and experimentally measured BA concentrations. Surprisingly, the inclusion of this information led to a slight deterioration in the model predictions. Fewer predictions fell within one standard deviation, although 80% still remained within two standard deviations (Figure 3.8A). These findings suggest the existence of additional disparities in BA metabolism between SPF and GF mice. Previous studies [10; 286; 287] have indeed demonstrated elevated expression levels of the synthesizing enzymes CYP7A1, CYP27A1, and CYP7B1 in GF mice. However, improving model predictions by solely increasing BA synthesis required considering differential regulation of other hepatic enzymes and processes. Specifically, enhancing the expression of BSEP, reducing the expression of NTCP and the production of muricholic acid (MCA) from chenodeoxycholic acid (CDCA) yielded only marginal improvements in predictions (Figure 3.8B). The most accurate predictions of BA levels in GF mice were achieved by incorporating reduced BA synthesis alongside differential regulation of hepatic processes. With this combined approach, approximately 57% of the predicted concentrations fell within one standard deviation, more than 80% fell within two standard deviations, and only 12% exhibited poor agreement with the measured data (Figure 3.8C).

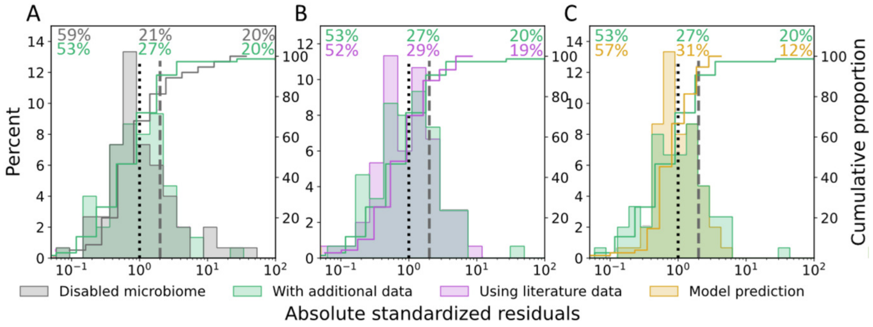

Figure 3.8: Model prediction of changes in germ-free mice. Comparison of different model variants for describing BA metabolism in germ-free mice by comparing the distribution of the absolute standardized residuals (histograms) and their corresponding cumulative function (lines). The dotted and dashed lines indicate differences between model simulation and measured data of one SD and two SDs, respectively. Cumulative proportions of predictions that lie within one SD (top left, residuals left of dotted line), between one and two SDs (top middle, residuals between dotted and dashed line) and above two SDs (top right, residuals right of dashed line) of measured data are stated at the top of the panel. A) Comparison of a simple extrapolation of the base model by disabling any microbial reaction (grey) against a model variant with additional information about physiology and intestinal transporter expression (green). The latter was also tested against model variants that introduce further expressional changes in the liver (B) according to literature (pink) or (C) as suggested by the model itself (yellow).

Model analyses

After calibration and validation, the developed computational model successfully captured BA metabolism in both male and female mice, demonstrating good agreement with experimental data. Consequently, the models can be applied to comprehensively characterize the distribution and pool sizes of BAs throughout the body (Figure 3.9 and 3.10). The model simulations revealed that BA levels were highest in the small intestine (SI) tissue, liver, and intestinal lumen. Significant amounts of BAs were also predicted in muscle, fat, and skin, with levels comparable to those observed in organs involved in the EHC (Figure 3.9A, Supplementary Figure A.5). The BA pool was estimated to be recycled within the EHC approximately 4.8 times per day in females and 4.1 times per day in males.

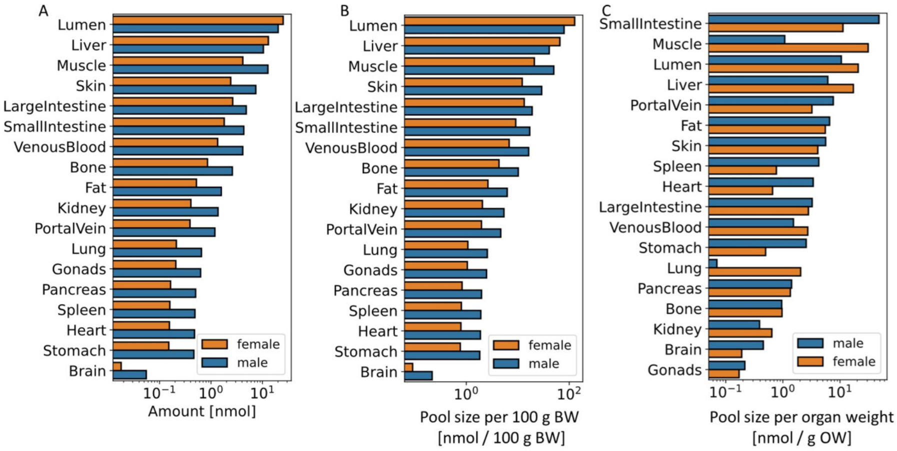

Figure 3.9: 6BA model prediction of BA pool sizes. Simulated bile acid pool sizes as total levels (A), per 100g organ weight (B) and per organ weight (C) in different organs in male and female mice. See also supplementary figure A.5.

In addition to pool sizes, the model enabled the simulation of BA composition at a sub-organ level. For instance, the liver predominantly contained CA, while other organs were primarily composed of MCAs (Supplementary Figure A.6). Furthermore, the model was utilized to simulate BA pools along the EHC and the gut axis (Figure 3.10C, Supplementary Figure A.7). The model indicated a relative accumulation of BAs in the liver and intestinal lumen, consistent with previous findings in other rodents where 70-95% of BAs are located in the lumen [29; 30]. Along the gut axis, BAs exhibited pronounced accumulation in the cecum, leading to higher levels throughout the large intestine. This observation aligns with reduced transporter expression (Figure 3.4A) and a slower intestinal transit rate in the cecum compared to the ileum (data not shown).

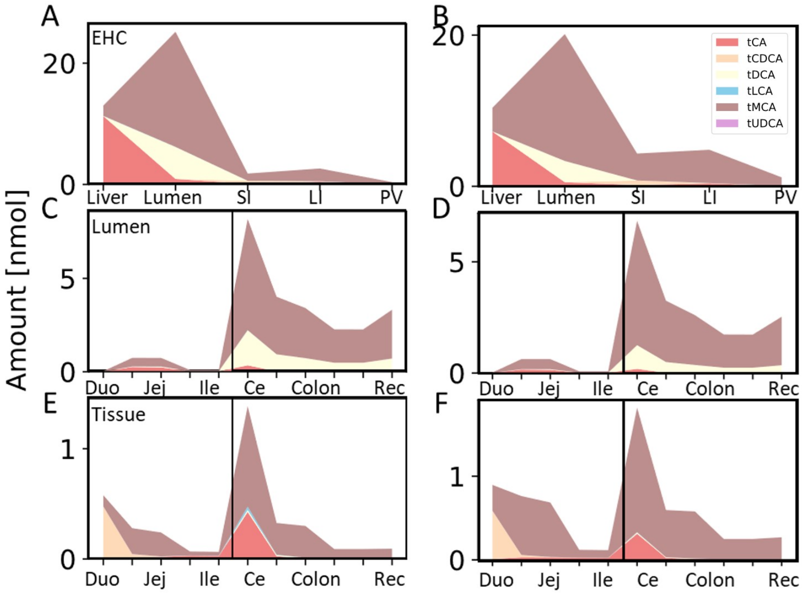

Figure 3.10: 6BA model prediction of BA pool distribution. Simulated bile acid pools along the EHC and gut axis in female (left column: A, C and E) and male (right column: B, D, F) mice. For EHC axis (A, B), BA level and composition are shown in liver, the intestinal lumen, small and large intestinal tissue (SI and LI) as well as portal blood plasma (PV). Along the gut axis (lumen C, D; tissue E, F), duodenum (Duo), jejunum (Jej), ileum (Ile), cecum (Ce), proximal and distal colon (Colon) and rectum (Rec) are shown and the separation of SI and LI are indicated by a vertical black line. See also supplementary figure A.7.

In addition to functional analyses of BA metabolism, the computational model also allows for extrapolation to other physiological scenarios. Exemplifying this, the impact of pathophysiological alterations on BA metabolism were predicted for BAM (Figure 3.11) and impaired intestinal barrier function (Figure 3.12 on BA levels.

For BAM, different possible explanations have been proposed [288]. Here, impaired reabsorption in the terminal ileum (Figure 3.11A and D), increased BA synthesis (Figure 3.11B and E) as well as reduced activity of ASBT (Figure 3.11C and F) were considered. The defective uptake of BAs by the ileal mucosa had relatively minor effects on BA pool sizes, except for observed increases in both tissue and lumen concentrations within the LI. On the other hand, increased BA synthesis resulted in elevated BA levels overall, with the most significant effects observed in the lumen of the SI, LI, and liver. Predictions for the disruption of intestinal barrier function suggested depletion of BA pools within the gut lumen. However, there was an accumulation of BAs in the liver, venous blood plasma, and portal blood plasma, reaching 14-fold and 10-fold increases, respectively. While a similar trend was observed in male mice, the accumulation of BAs was less pronounced compared to female mice, displaying a four-fold and three-fold difference, respectively. Impairment in ASBT function, showed overall minor effects except for a reduction of BA level in gut tissue and portal blood by up to 100-fold.

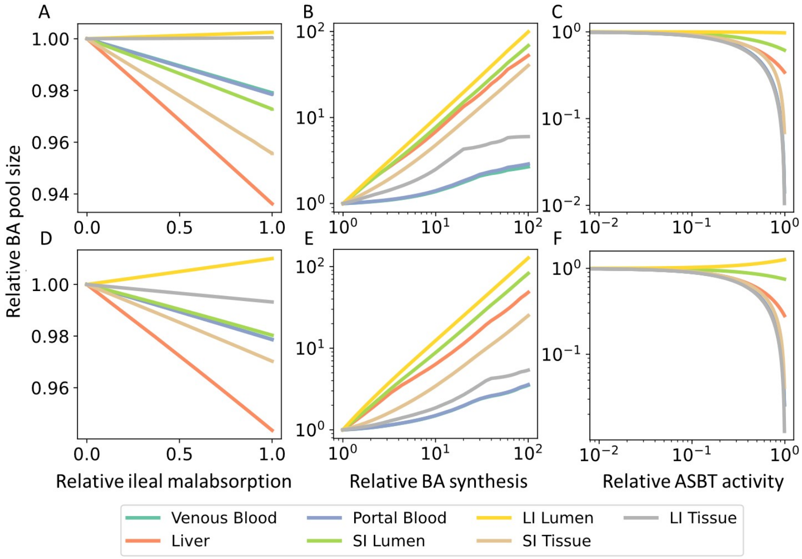

Figure 3.11: 6BA model prediction of BA pool sizes in BA malabsorption. Predicted changes in bile acid pool sizes in different organs in female (upper row) and male (lower row) mice for decreasing BA absorption in the terminal ileum (A, D), for increasing BA synthesis (B, E) as well as decreasing ASBT activity (C, F).

For impaired intestinal barrier function, changes in paracellular (Figure 3.12A and D), transcellular (Figure 3.12B and E) and total (Figure 3.12C and F). All disruptions of the intestinal barrier function depleted BA pools within the gut lumen, whereas in liver as well as venous and portal blood plasma BAs accumulated strongly. For paracellular permeability, hepatic and blood BA level increased by 14- and 10-fold, respectively, whereas for transcellular and total permeability BA concentration could rise 100-fold. In general, while the same trend was present in male mice, the accumulation of BAs was not as pronounced as in female mice.

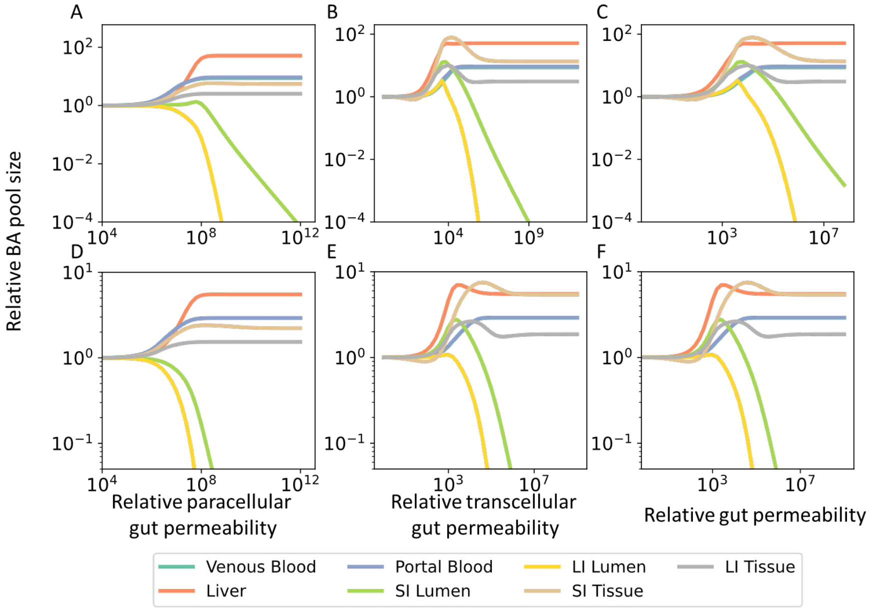

Figure 3.12: 6BA model prediction of BA pool sizes in impaired intestinal barrier function. Predicted changes in bile acid pool sizes in different organs in female (A, B, C) and male (D, E, F) mice in increasing paracellular (A,D), transcellular (B,E) or total (C,F) intestinal permeability.

3.3 Murine Conjugation Model - describing the conjugation status of bile acids

The mouse conjugation model incorporates subsequent to synthesis of uBA, conjugation with taurine to form T-BA. Microbial deconjugation by BSH activity was modeled as net enzymatic reactions. Activity along the gut was derived from a study by Tannock et al. [283]. A schematic overview of the murine conjugation model is illustrated in figure 3.13.

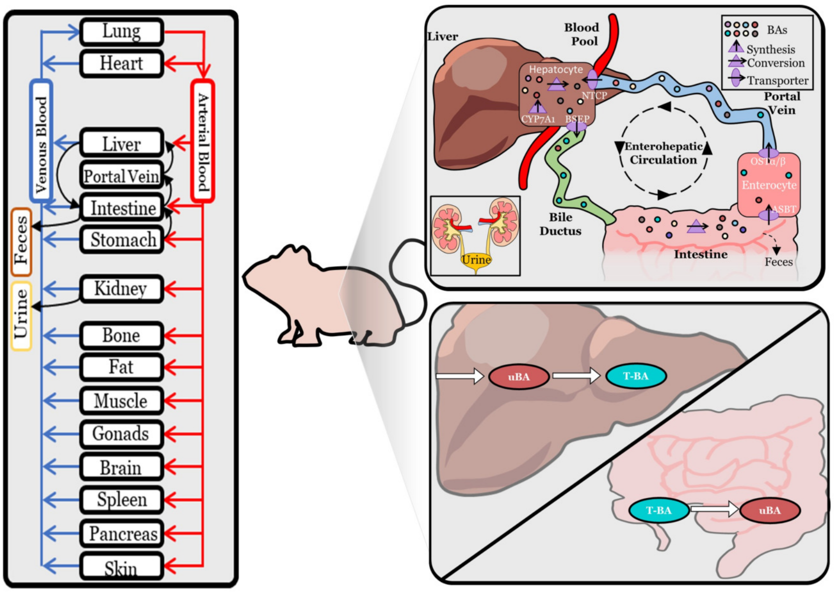
Lung
Heart
Liver
Portal Vein
Intestine
Stomach
Kidney
Bone
Fat
Muscle
Gonads
Brain
Spleen
Pancreas
Skin
Venous Blood
Arterial Blood
Feces
Urine
Liver
Blood Pool
Hepatocyte
NTCP
CYP7A1
BSEP
BAs
Synthesis
Conversion
Transporter
Portal Vein
Enterohepatic Circulation
OSTα/β
Enterocyte
ASBT
Bile Ductus
Intestine
Feces
Urine
uBA
T-BA
T-BA
uBA

Figure 3.13: Physiologically-based bile acid model - murine conjugation model. Schematic overview of a PBPK model of bile acid biosynthesis via CYP7A1, hepatic and microbial transformation, active transport processes via BSEP, ASBT, OST-α/β and NTCP, as well as fecal and renal excretion. In the computational model, excretion to the gallbladder is neglected and BAs are directly secreted into the duodenum. Reactions of BAs are located either in the intracellular space of the liver or in the intestinal lumen.

Model calibration to data from SPF mice

The first step in model development involved calibrating the conjugation model to BA measurements in SPF mice. During parameter estimation, only active hepatic processes were considered in relation to sex-related differences. Various combinations of differential parameters were tested, revealing that the downregulation of BA synthesis in male mice was both necessary and sufficient to account for the observed sex differences in BA composition and levels in SPF mice (data not shown).

After conducting parameter estimation and utilizing the fitted parameters as presented in supplementary tables A.13- A.14, the final computational model proved highly effective in accurately representing the BA levels in various organs of both male and female SPF mice (Figure 3.14A-B). Remarkably, up to 63% of the predictions (with breakdowns of 58% for males and 69% for females) fell within one SD of the experimental data, while 30% (with divisions of 42% for males and 19% for females) lay within a two-fold SD range. Only a small portion, 6% of the data (with no instances for males and 12% for females), deviated by more than two SDs (Figure 3.14C-D). Despite the intricate nature of the modeled system and the considerable variability observed in the measured data, particularly within the intestine, the model exhibited a robust agreement between the experimental data and the simulated results.

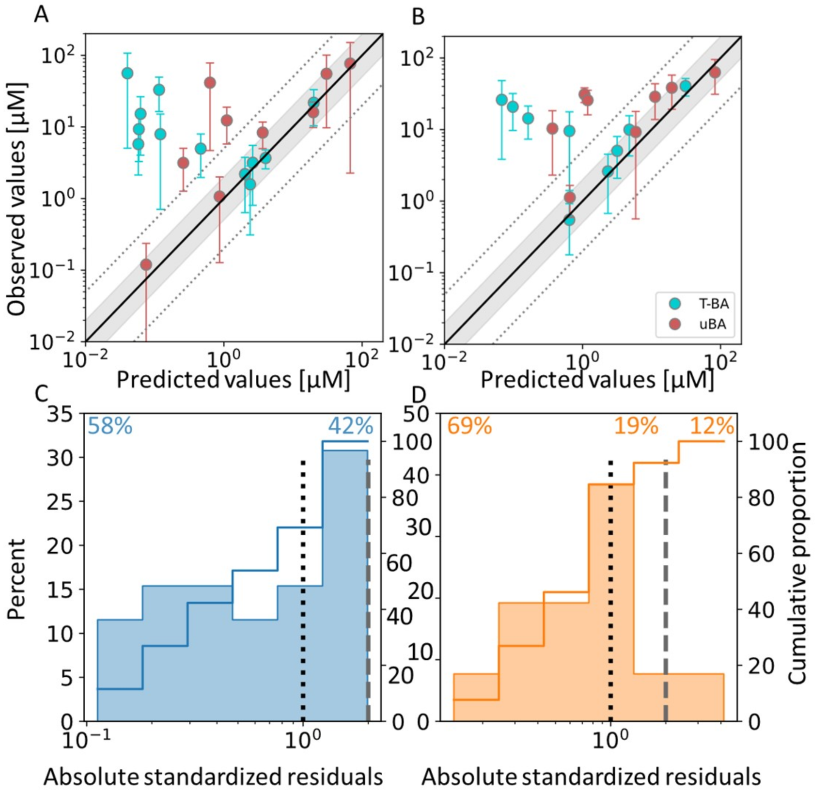

Figure 3.14: Murine conjugation model fit to data from SPF mice. Model simulations of bile acid concentration in male (A) and female mice (B) against corresponding data points used for fitting. Only data points with a coefficient of variation below 1 are shown. Unity is represented by a solid black line, a two- and five-fold range between predicted and observed values is indicated as a gray area or with dotted lines, respectively. Error bars show the SD. Distribution of the absolute standardized residuals between model simulations and data of male (C) and female (D) mice (histogram) and the corresponding cumulative function (line). The dotted and dashed lines indicate differences between model simulation and measured data of one SD and two SD, respectively. Cumulative proportions of predictions that are within one SD (top left, residuals left of dotted line), between one and two SD (top middle, residuals between dotted and dashed line) and above two SD (top right, residuals right of dashed line) of measured data are stated at the top of the panel.

To assess the model's behavior, a sensitivity analysis was performed to gauge the impact of fitted parameters on experimentally measured concentrations of various BA species (see Supplementary Tables A.15 to A.23). The activity of the hepatic export transporter BSEP showed significant effects on BA levels throughout the body. Moreover, BAAT activity strongly influenced conjugated BA levels in all evaluated organs. Parameters related to ASBT and OSTα/β primarily affected the concentrations of BA species in intestinal tissue, while BSEP activity had a substantial impact on gut content. In venous blood plasma and the kidney, sensitivity to both BA uptake from portal blood through NTCP and excretion via urine was observed. Notably, the sensitivity coefficients of all model parameters displayed a high correlation between the two models (refer to Supplementary Figure A.8).

Model qualification to germ-free mice

Thanks to its mechanistic structure, the physiologically-based computational model of murine BA metabolism offers the potential to explore novel scenarios. To validate the model, simulations were conducted on germ-free (GF) mice to assess BA levels. In the first step, all microbial activity in the SPF model was deactivated by setting the corresponding rates to zero. The resulting predictions demonstrated reasonable agreement with the observed BA concentrations in both male and female GF mice (see Figure 3.15 and Supplemental Figure A.1). Notably, around 40% of the predicted concentrations fell within one standard deviation of the measured values, while approximately 65% showed a two-fold variation. However, a third of the predicted BA levels displayed more significant deviations from the measured values (see Figure 3.15B).

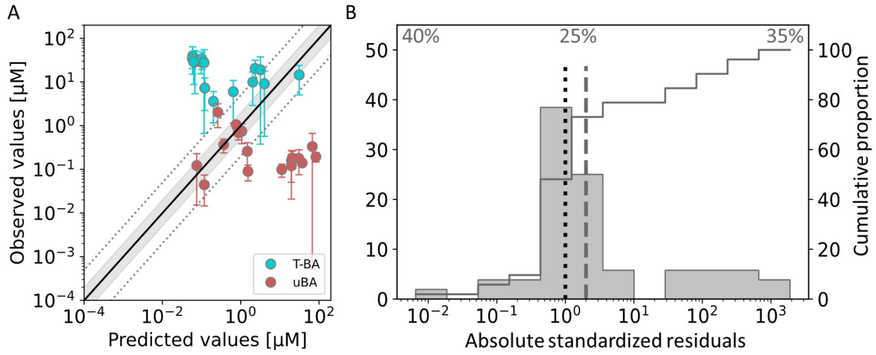

Figure 3.15: Murine conjugation model prediction of germ-free mice. A) Model predictions of concentration of bile acids in both male and female, germ-free mice against corresponding data points used for fitting. Only data points with a coefficient of variation below 1 are shown. Unity is shown as a solid black line shows unity, a two- and five-fold range between predicted and observed values is indicated as a gray area or with dotted lines, respectively. Error bars represent the standard deviation. B) Distribution of the absolute standardized residuals model predictions (histogram) and the corresponding cumulative function (line). The dotted and dashed lines indicate differences between model simulation and measured data of one SD and two SDs, respectively. Cumulative proportions of predictions that are within one SD (top left, residuals left of dotted line), between one and two SDs (top middle, residuals between dotted and dashed line) and above two SDs (top right, residuals right of dashed line) of measured data are stated at the top of the panel.

Afterward, additional information on the physiology and expression of intestinal transporters was integrated (see Supplementary Figure A.2 and A.3), aiming to improve the agreement between model simulations and experimentally measured BA concentrations. Similar to the findings in the 6BA model, this inclusion resulted in a deterioration of the model predictions. Only less than half of the predictions could be explained within two standard deviations (see Figure 3.16A).

Parallel to the results of the 6BA model, increased BA synthesis in female mice [10; 286; 287] was not sufficient to improve model predictions but also necessitated considering the differential regulation of other hepatic enzymes and processes. Specifically, reducing the expression of BSEP and NTCP while increasing BA conjugation resulted in only marginal improvements in predictions (see Figure 3.16B). The most accurate predictions of BA levels in GF mice were achieved by combining reduced BA synthesis with the differential regulation of hepatic processes. With this approach, approximately 50% of the predicted concentrations fell within one standard deviation, more than 77% were within two standard deviations, and only 23% showed poor agreement with the measured data (see Figure 3.16C).

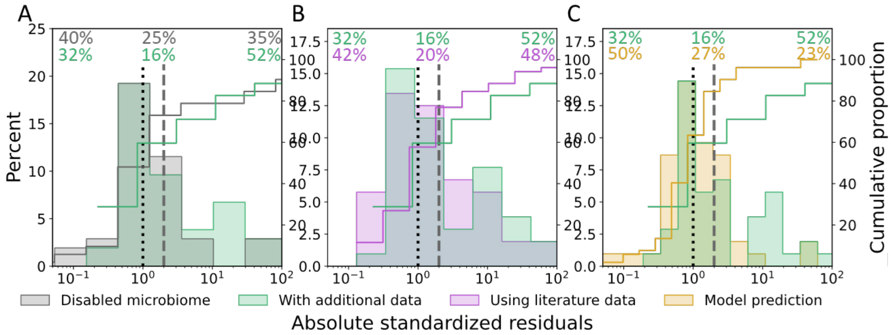

Figure 3.16: Murine conjugation model prediction of changes in germ-free mice. Comparison of different model variants for describing BA metabolism in germ-free mice by comparing the distribution of the absolute standardized residuals (histograms) and their corresponding cumulative function (lines). The dotted and dashed lines indicate differences between model simulation and measured data of one SD and two SDs, respectively. Cumulative proportions of predictions that lie within one SD (top left, residuals left of dotted line), between one and two SDs (top middle, residuals between dotted and dashed line) and above two SDs (top right, residuals right of dashed line) of measured data are stated at the top of the panel. A) Comparison of a simple extrapolation of the base model by disabling any microbial reaction (grey) against a model variant with additional information about physiology and intestinal transporter expression (green). The latter was also tested against model variants that introduce further expressional changes in the liver (B) according to literature (pink) or (C) as suggested by the model itself (yellow).

Model analyses

Following calibration and validation, the computational model successfully captured the BA level in both male and female mice, demonstrating excellent agreement with experimental data. As a result, these models can now be employed to comprehensively characterize the distribution and pool sizes of BAs throughout the body (see Figure 3.17 and Figure 3.18). The simulations revealed that BA levels were highest in the intestinal lumen, liver as well as small and large intestinal tissue. Additionally, substantial amounts of BAs were predicted in muscle and skin, comparable to the levels observed in organs involved in the enterohepatic circulation (EHC) (Figure 3.17A, Supplementary Figure A.9). Based on the model, it was estimated that the BA pool is recycled within the EHC approximately 2.7 times per day in females and 2.6 times per day in males.

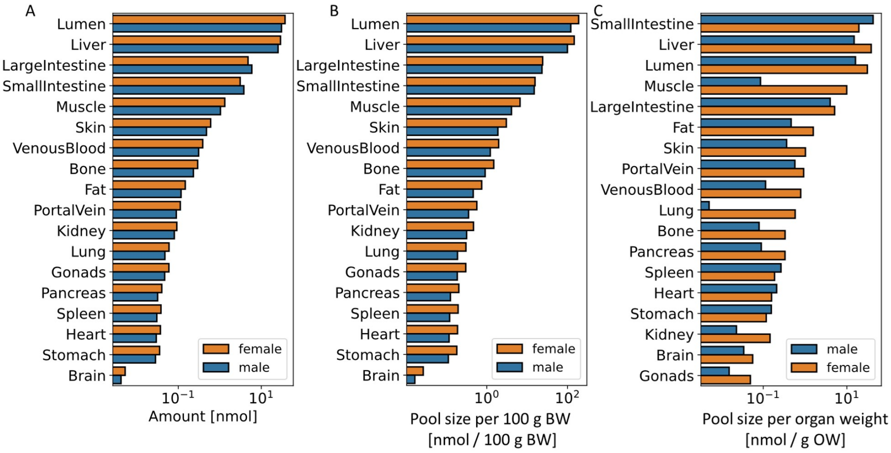

Figure 3.17: Murine conjugation model based BA pool sizes. Simulated bile acid pool sizes per organ weight in different organs in male and female mice (A) and model-based bile acid composition in liver, portal blood plasma and skin in female mice (B) as well as simulated bile acid pools along the EHC and gut axis (C). For the EHC axis, BA level and composition are shown in liver, the intestinal lumen, small and large intestinal tissue (SI and LI) as well as portal blood plasma (PV). Along the gut axis, duodenum (Duo), jejunum (Jej), ileum (Ile), cecum (Ce), proximal and distal colon (Colon) and rectum (Rec) are shown and the transition of SI and LI are indicated by a vertical black line. See also Supplementary Figure A.9.

Moreover, the model allowed for the simulation of BA composition at a more detailed sub-organ level. Notably, in liver, portal blood and skin, unconjugated BA were more abundant than conjugated BA; however, EHC organs showed overall higher proportions of conjugated BA than unconjugated BA. (Supplementary Figure A.10). Furthermore, the model was employed to simulate the distribution of BA pools along the EHC (Figure 3.18A,B) and the gut axis (Figure 3.18C-F). The results indicated a relative accumulation of BAs in the liver and intestinal lumen, which is consistent with previous findings in other rodents where 70-95% of BAs are localized in the lumen [29; 30]. Along the gut axis, there was a pronounced accumulation of BAs in the cecum, leading to higher levels throughout the large intestine. This observation aligns with reduced

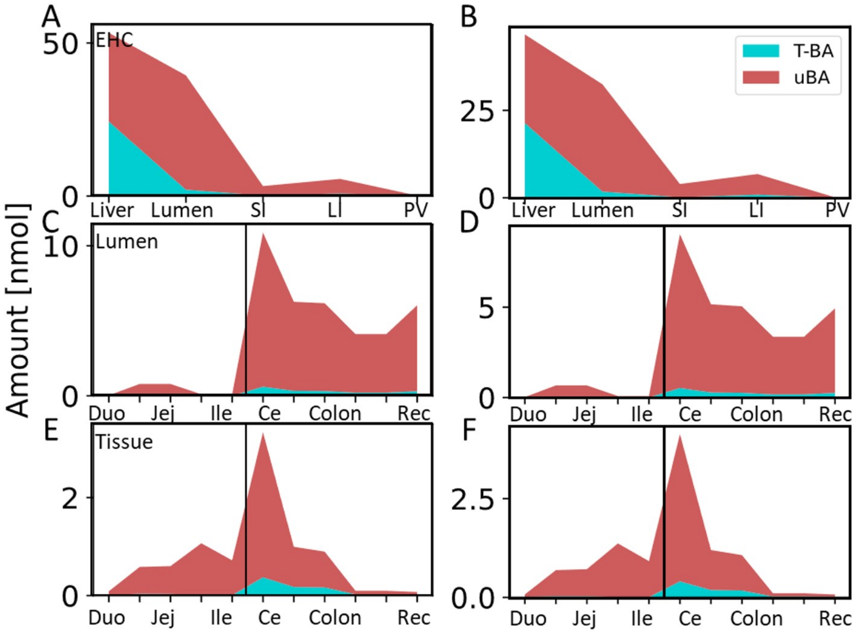

Figure 3.18: Murine conjugation model based BA pool distribution. Simulated bile acid pools along the EHC and gut axis in female (left column: A, C and E) and male (right column: B, D, F) mice. For EHC axis (A, B), BA level and composition are shown in liver, the intestinal lumen, small and large intestinal tissue (SI and LI) as well as portal blood plasma (PV). Along the gut axis (lumen C, D; tissue E, F), duodenum (Duo), jejunum (Jej), ileum (Ile), cecum (Ce), proximal and distal colon (Colon) and rectum (Rec) are shown and the separation of SI and LI are indicated by a vertical black line.

transporter expression (Figure 3.4A) and a slower intestinal transit rate in the cecum compared to the ileum (data not shown).

In a next step, the murine conjugation model was applied for the same extrapolation to pathophysiological alterations as the 6BA model, namely BAM (Figure 3.19) and impaired intestinal barrier function (Figure 3.20). Regarding BAM, the model considered impaired reabsorption in the terminal ileum (Figure 3.19A and D), increased BA synthesis (Figure 3.19B and E), as well as reduced activity of ASBT (Figure 3.19C and F). The defective uptake of BAs by the ileal mucosa had relatively minor effects on BA pool sizes, except for observed increases in both tissue and lumen concentrations within the large intestine (LI). On the other hand, increased BA synthesis resulted in elevated BA levels overall, with the most significant effects observed in the lumen of the SI and LI, and liver. Impairment in ASBT function, showed overall minor effects except for a 10-fold reduction of BA level in gut tissue.

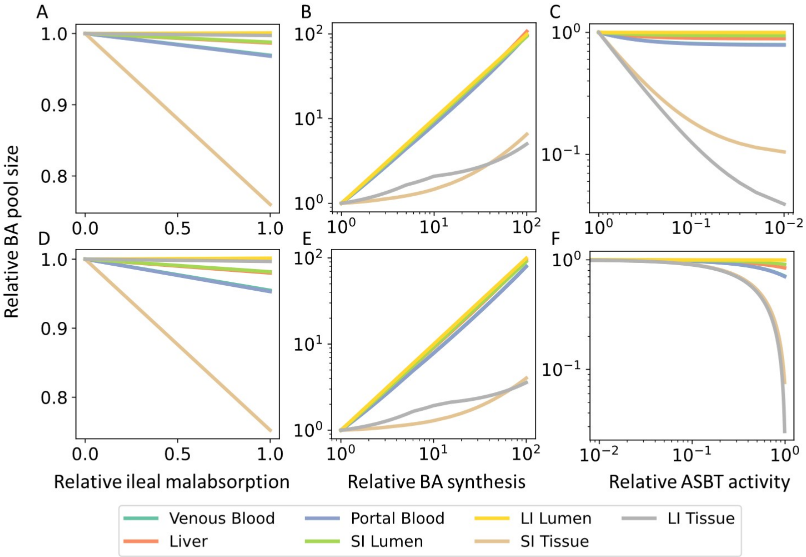

Figure 3.19: Murine conjugation model prediction of BA pool sizes in BA malabsorption and loss of intestinal barrier function. Predicted changes in bile acid pool sizes in different organs in female (upper row) and male (lower row) mice for decreasing BA absorption in the terminal ileum (A, D), for increasing BA synthesis (B, E) as well as increasing paracellular permeability along the whole gut (C, F).

Regarding impaired intestinal barrier function, alterations in paracellular permeability (Figure 3.20A and D), transcellular permeability (Figure 3.20B and E), and total permeability (Figure 3.20C and F) and their effects on BA level were simulated. All disruptions of the intestinal barrier function led to depletion of BA pools within the gut lumen, while BAs accumulated significantly in the liver, venous blood plasma, and portal blood plasma. Specifically, for paracellular permeability, hepatic and blood BA levels increased by 14- and 10-fold, respectively, whereas for transcellular and total permeability, BA concentrations could rise up to 100-fold. Although a similar trend was observed in male mice, the accumulation of BAs was not as pronounced as in female mice.

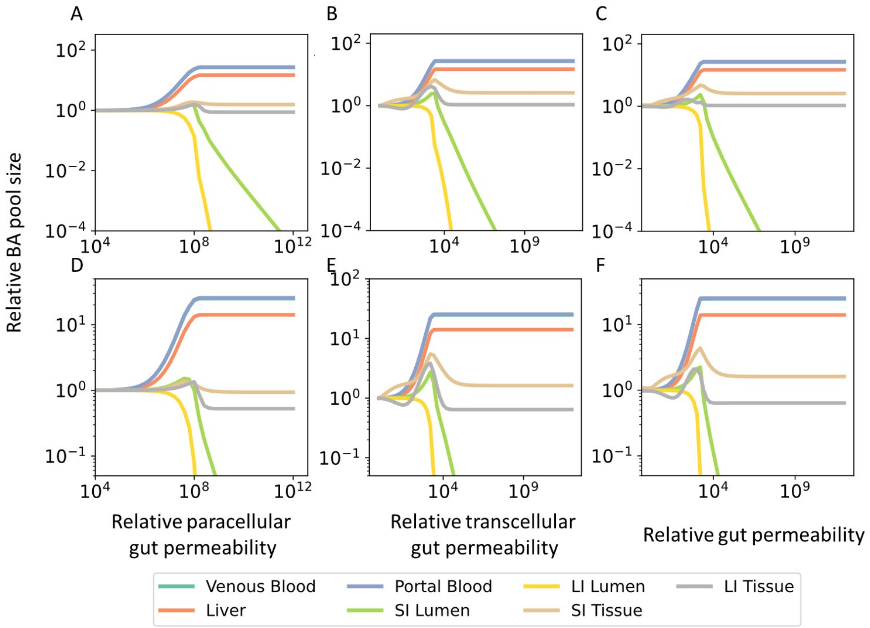

Figure 3.20: Model prediction of BA pool sizes in impaired intestinal barrier function. Predicted changes in bile acid pool sizes in different organs in female (A, B, C) and male (D, E, F) mice in increasing paracellular (A,D), transcellular (B,E) or total (C,F) intestinal permeability.

3.4 Discussion of physiologically-based models of murine bile acid metabolism

In this work, physiologically-based models of BA metabolism in mice were developed. Due to technical limitations, it was necessary to reduce model complexity by considering only partial aspects of the complex BA pool and developing specialized model variants. In this context, one model variant describes BA levels of the six most abundant BAs, i.e. MCA, CA, CDCA, DCA, LCA and UDCA, (6BA model) whereas the other captures conjugation status of BA by distinguishing between (tauro-)conjugated and unconjugated BA (murine conjugation model).

The models encompass various aspects such as systemic circulation, synthesis, hepatic and microbial conversions, and excretion of the modeled BAs. Additionally, the models specifically account for sex differences in BA concentration and composition, which have been previously documented in the literature and were also evident in the experimental data specifically generated for this work. To ensure the models' accuracy, they were established and validated carefully using a comprehensive dataset collected from both male and female SPF mice. This dataset incorporates diverse information, including BA concentrations in different organs, expression of transporters along the gut segments, physiological parameters, and microbial composition in the cecum. Notably, it was required for both models that female SPF mice exhibit an upregulation of BA synthesis. However, while this differential regulation of the synthesizing step was sufficient for the murine conjugation model, the 6BA model also required upregulation of NTCP in female mice. This aligns with previous findings from other studies [284; 285] showing increased expression of enzymes related to BA synthesis and the transporter NTCP. Importantly, this observation was an independent outcome of model development process and was not considered as prior knowledge when building the models.

Moreover, the final models developed for SPF mice were shown to be able to predict BA measurements in germ-free mice by specifically excluding microbial processes. Both models recapitulated the BA levels in GF mice reasonably well; however, the 6BA model showed overall better agreement with the data than the murine conjugation model. Aiming to further refine the models, additional information regarding physiological parameters and intestinal transporter expression were incorporated resulting in worse predictions of either variant. Considering upregulation of BA synthesis in GF mice, as reported in the literature [10; 286; 287], was also insufficient on its own to improve predictions but required additional expressional changes in the liver. Both variants agreed on the downregulation of the uptake transporter NTCP, but disagreed on regulation of BSEP. On the other hand, unrestricted predictions propose the possibility of downregulation of BA synthesis in GF mice. This discrepancy warrants further investigation to determine whether it results from potential model inaccuracies, inherent strain differences or more complex interactions between BA species and their conjugation status. Overall, these results serves as a strong indication of the overall quality of the model, instilling confidence in its applicability for further analyses and predictions.

The ability of the models to handle extrapolation to previously unseen scenarios and contextualization of existing knowledge in a systemic manner is evident. For instance, it can be effectively applied to predict outcomes in disease contexts or extrapolate findings across different species. Numerous diseases have been linked to changes in BA composition and dynamics. Inflammatory bowel disease, ulcerative colitis, Crohn's disease, liver cirrhosis, liver cancer, irritable bowel syndrome, short bowel syndrome, and obesity have all been associated with alterations in BA composition [20; 21; 22]. Moreover, impairments in the EHC of BA have been linked to cholestatic drug-induced liver injury, chronic liver disease, cholesterol gallstone disease, malabsorption, dyslipidemia, and atherosclerosis [289; 290; 291; 292; 293; 294].

In this work, both models were employed to predict the effects of BA malabsorption as a potential cause for idiopathic BA diarrhea (BAD), as proposed in [288], and the impairment of intestinal barrier function observed in celiac disease [295; 296; 297; 298], IBD [26; 27], and metabolic-associated fatty liver disease (MAFLD) [299; 300; 301] on BA metabolism. Consistent with other studies, both models demonstrated that an increase in BA synthesis [292; 302; 303] and overflow of reabsorption resulted in a significant accumulation of BAs in the large intestinal lumen. In contrast, malabsorption in the terminal ileum, without any obvious gastrointestinal disease, as well as reduced functionality of the transporter ASBT were insufficient to induce BAD [304].

To assess 'leaky gut' conditions, the intestinal permeability was altered equally in all gut segments. Impairment of gut barrier function can affect transport across epithelial cell (transcellular permeability) or through the spaces between those cells (paracellular permeability) or a combination of both. Testing these different mechanisms, both model variants suggested similar behaviour of BA pool sizes:

- Depletion of BA in the gut lumen
- Relative accumulation within the liver
- Increasing transcellular permeability with stronger effect on BA level

However, this assessment of impaired gut barrier function is limited due to a lack of data and the default model structure within the OSP suite. Without providing additional information, PBPK model developed with the OSP suite consider by default only transcellular permeability that is derived from a molecule's molecular weight and lipophilicity; thus, it was necessary to use the calculated transcellular permeability for the paracellular one as well. Furthermore, there was no information available for the relative increase of permeability in 'leaky gut' conditions, especially in relation to BAs. This introduces a systemic bias to the analysis and it is unclear if the results are with physiological relevance. These concerns can only be addressed by experimental measurements if the model is to be applied for predictions concerning impaired gut barrier function. Future computational analyses could explore regional differences in permeability, as demonstrated by Thomson et al. [305]. In summary, these predictions were made possible due to the detailed model of the gastrointestinal tract contained within the fundamental model structure of OSP suite models [306; 307]. The results highlight how the these models can shed light on the intricate interactions between pathophysiological alterations, including physiological or expressional changes, microbial dysbiosis, and drug administration, within the context of BA metabolism.

To investigate the connection between BA metabolism and their role in human disease, various animal models have been utilized, including lamprey, skate, zebrafish, rat, mouse, hamster, rabbit, prairie dog, and monkey [308; 309; 310]. Among the small animal models, hamsters display the closest similarity to humans concerning BA metabolism [311; 312; 313]; however, mice remain the most commonly used animal model to investigate human metabolism [314; 315]. A notable difference between humans and mice lies in their BA composition [12; 17]. The murine BA pool is significantly influenced by MCAs, leading to increased hydrophilicity, reduced cytotoxicity, and a shift towards a more antagonistic FXR-signaling regime [12]. Additionally, there are relevant differences in gastrointestinal tract physiology [247; 248; 250; 251; 252], energy homeostasis [253], and nutrient and BA recycling through coprophagy [254; 255]. Consequently, extrapolating from mouse studies to humans concerning BA signaling or BA-related diseases is challenging. As an initial assessment of species differences between mice and humans, both mouse models were used to estimate the recycling times of the BA pool per day. In humans, the complete

BA pool is recycled four to twelve times a day [89]. This number is often assumed and cited even for other species although it has never been assessed. Although the model variants disagree on the exact number (6BA: 4-5 times, conjugation: 2-3 times), the models' predictions suggest that the murine BA pool is recycled less often than the human one. This provides an initial assessment of species differences between mice and humans.

To address concerns of cross-species differences, a recent study utilized mouse models with a more human-like BA composition [316]. These "humanized" mice have single or double knock-out (KO) in *Cyp2a12* and *Cyp2c70*, resulting in much more hydrophobic BA pools [70; 73]. This alteration occurs because hepatic DCA cannot be rehydroxylated to CA (*Cyp2a12*), and MCAs cannot be synthesized (*Cyp2c70*). Within the framework of the 6BA model, it is possible to recapitulate these gene KO and to simulate BA levels in 'humanized' mice. Initial model predictions for *Cyp2a12* KO mice revealed a substantial accumulation of DCA, while *Cyp2c70* KO mice showed an absence of MCAs and an increase in hepatobiliary CDCA. In mice with double KO, DCA, CDCA, and LCA were strongly increased (data not shown). These initial findings align well with the reported BA composition in these mice [70]. This demonstrates that the developed computational model in this study has the potential to support cross-species extrapolation due to the mechanistic structure of the underlying PBPK model [270]).

Lastly, the models' utility extends to optimizing experimental designs for mouse studies aimed at understanding the complex behavior of BAs in health and disease. This application is particularly significant in the context of adhering to the "3R" principles proposed by Russel and Burch in 1959 [317], which emphasize Reduction, Refinement, and Replacement of animal testing. Within this context, this work demonstrated the models' ability to predict BA levels and composition throughout the body, even in experimentally challenging-to-access organs such as the liver or portal blood, under both physiological and pathophysiological conditions. Importantly, all these predictions were made without necessitating any further animal sacrifice. The models presented here can serve as a valuable platform for conducting model-assisted investigations of BA metabolism in prospective studies, thereby promoting the reduction and refinement of animal experiments in line with the "3R" principles.

In this study, two distinct model variants were formulated in response to technical constraints. This approach allowed for the examination of different aspects of the BA pool. The murine conjugation model specifically accounts for the increased solubility and polarity observed when BAs are conjugated with taurine. Consequently, it provides a more precise representation of passive diffusion since conjugated BAs exhibit high polarity and necessitate active transporters for passage, whereas unconjugated BAs can traverse cell membranes more easily and are more readily reabsorbed by the intestine. Additionally, this model benefits from a higher level of confidence in microbial activity data, as it directly incorporates measurements of BSH activity. Conversely, the 6BA Model offers a more accurate depiction of the diversity within the BA pool. It distinguishes not only between primary and secondary BAs but also between MCAs (and UDCA) and the remaining BAs. This differentiation is particularly significant for future model iterations aiming to incorporate FXR-mediated signaling. However, there are noteworthy qualitative considerations. Both variants adequately explained the datasets for SPF and GF mice. While the murine conjugation model demonstrated superior performance in recapitulating the SPF data, the 6BA Model exhibited greater accuracy in predicting BA level in GF mice. For the remaining predictions, the two models yielded similar results. Notably, during the development of the 6BA Model, achieving alignment with the data necessitated not only a reduction in BA synthesis but also an additional upregulation of NTCP in female mice, a phenomenon supported by existing literature [285]. Conversely, the murine conjugation model only required a reduction in BA synthesis to match the data. If this represents an actual model inaccuracy or an artifact from developing two model variants only partially explaining the BA pool is unclear.

Limitation of the models

In future analyses, the physiologically-based models may undergo structural revisions to address some of its limitations. The current version of the computational models include only the most abundant BA species but disregard sulfation and the distinction of $\alpha/\beta/\omega$-MCA. Consequently, the models cannot fully capture the complexity of the BA pool, potentially introducing a systemic bias in the predictions due to variations in kinetics among different BA species [9]. Another simplification relates to the dynamic behavior of BA circulation. In the computational models, all BAs are directly secreted into the duodenum, omitting the gallbladder. As a result, postprandial responses and the impact of coprophagy on BA recycling [254; 255] were neglected, as these effects are challenging to describe in mice. Consequently, the models cannot account for circadian rhythm effects as observed in other rodents [29; 30; 31; 32]. Additionally, the microbiota was only assessed in the cecum, which functions as a large microbial fermentation vessel in mice [247]. However, variations in microbial composition in other gut segments might contribute to the observed sex differences. Previous studies have shown that similar microbial communities may be enriched for different functions [318]. Besides compositional variation, there might be differences in microbial density between male and female mice, which were not assessed in this study. Despite these limitations, the models successfully recapitulated BA composition and levels at the whole-body level and accurately accounted for sex-related differences in BA metabolism.

Chapter 4

A physiologically-based model of bile acid metabolism in humans.

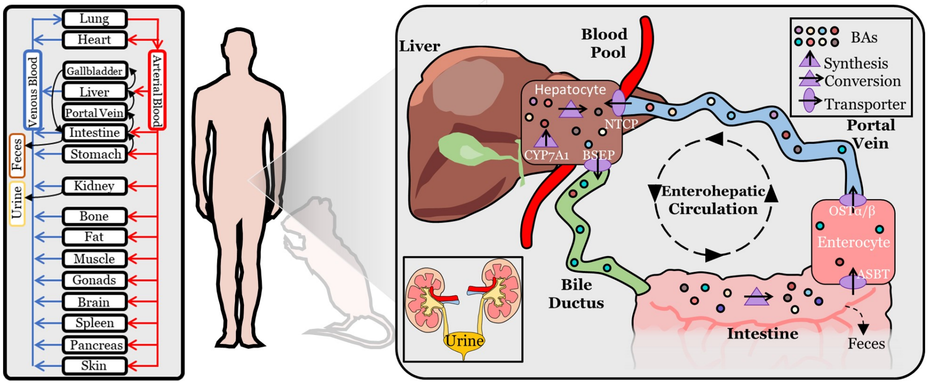
Lung
Heart
Venous Blood
Arterial Blood
Gallbladder
Liver
Portal Vein
Intestine
Stomach
Feces
Urine
Kidney
Bone
Fat
Muscle
Gonads
Brain
Spleen
Pancreas
Skin
Liver
Blood Pool
BAs
Synthesis
Conversion
Transporter
Hepatocyte
NTCP
CYP7A1
BSEP
Portal Vein
Enterohepatic Circulation
OSTα/β
Enterocyte
ASBT
Bile Ductus
Urine
Intestine
Feces

Contributions:

B. Kister developed the model, performed the simulations, compiled the literature data, analyzed the data, created the figures, and wrote the chapter. T. Wirtz provided the patient data. T. Wirtz and L. Kuepfer discussed the data. L.M. Blank and L. Kuepfer reviewed the chapter.

Bile acid metabolism holds a fundamental role in upholding the overall homeostasis of both the liver and the gastrointestinal system. Beyond their function in processing and emulsifying dietary fats, BAs also function as signaling molecules that participate in a multitude of physiological processes. Unraveling the dynamics of BA metabolism stands as a pivotal endeavor for comprehending its implications on both health and disease.

The creation of a computational framework to model human BA metabolism entails the integration of a broad spectrum of data sources, spanning from measurements of BAs levels and flows to existing physiological characteristics, such as body weight and blood flows. The utilization of PBPK modeling stands out as a promising strategy for capturing the intricate interplay among various compartments like the liver, gastrointestinal tract, bloodstream, and other pertinent tissues. By integrating physiological parameters, e.g. organ sizes or tissue composition, as well as transport kinetics, PBPK models can represent the human system/body.

This chapter illustrates at first the general development of the computational models of human BA metabolism, the data collected from literature and provided by clinical partners and necessary preparatory steps for this and their implication on simplifications necessary. In the following sections, model variants are examined in more detail describing model calibration, validation and predictions derived from the final models. Finally, results of this chapter are discussed critically summarizing the capabilities and limitations of the here presented models.

4.1 Model development and data

The computational models of human BA metabolism are constructed on a physiologically detailed representation of the organism, encompassing a range of processes including synthesis, hepatic and microbial transformations, systemic and enterohepatic circulation, and the elimination of BAs from the system. An diagram outlining the overall structure of the human model can be seen in figure 4.1. For the creation of this model, a methodology rooted in PBPK modeling was employed [257]. Within this framework, the metabolites of BAs represented the molecules circulating in the system. The PBPK model offers a comprehensive depiction of human physiology by incorporating detailed information regarding organ volumes, tissue composition, organ surface areas, and blood perfusion rates. These details are established based on prior knowledge [270; 271]. An essential feature of the mechanistic structure of the PBPK model is its capability to extend its applicability to novel situations and conditions [270; 272].

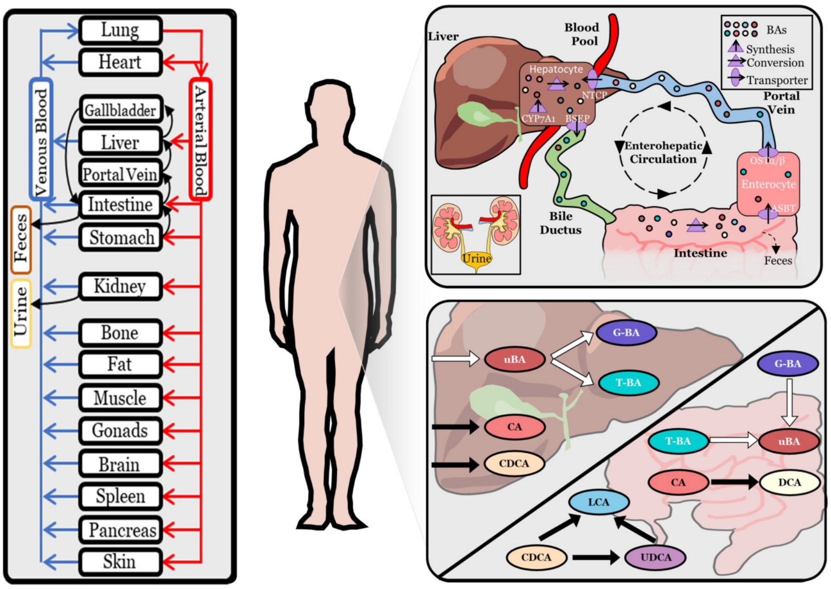
Lung
Heart
Gallbladder
Liver
Portal Vein
Intestine
Stomach
Kidney
Bone
Fat
Muscle
Gonads
Brain
Spleen
Pancreas
Skin
Venous Blood
Arterial Blood
Feces
Urine
Liver
Blood Pool
BAs
Synthesis
Conversion
Transporter
Hepatocyte
NTCP
CYP7A1
BSEP
Portal Vein
Enterohepatic Circulation
OSTα/β
Enterocyte
ASBT
Bile Ductus
Intestine
Feces
Urine
G-BA
uBA
T-BA
CA
CDCA
G-BA
T-BA
uBA
CA
DCA
LCA
CDCA
UDCA

Figure 4.1: Physiologically-based bile acid model. Schematic overview of a PBPK model of BA biosynthesis via CYP7A1, hepatic and microbial transformation, active transport processes via BSEP, ASBT, OST-α/β and NTCP, as well as fecal and renal excretion. Reactions of BAs are located either in the intracellular space of the liver or in the intestinal lumen. Reactions colored in white are present in the human conjugation model, those in black are considered in the 5BA model.

In order to inform the kinetic parameters of a computational model of BA metabolism in human, an extensive dataset is needed. To this end, an exhaustive literature research was conducted and reported BA measurements from 39 studies were collected (Table 4.1. This dataset included various baseline measurements in venous and portal blood, liver, feces and bile, but also postprandial responses in blood as well as synthesis, excretion and flow rates. Addressing variability between measurements from different studies, effect sizes were synthesized using a meta-analysis approach applying a Bayesian mixed-effect model with weakly informative priors [319; 320; 321]. Postprandial responses were each normalized to the initial fasting time point and scaled to the synthesized basal BA concentration in venous blood (Supplementary Figure B.1). Resulting values that were used for model establishment are summarized in supplementary tables B.1-B.8.

Table 4.1: Overview of the literature data set. Shown are the number of studies that could be found reporting bile acid measurements in specific organs or for processes. See also supplementary tables B.1-B.8.

Organ	Number of studies
Systemic circulation	18
Portal blood	4
Liver	4
Synthesis rate	5
Renal excretion	4
Feces	2
Bile	1
Intestinal bile flow	2
Single meal studies	5
Multiple meal studies	2

Based on the literature dataset and subsequent meta-analysis, it is possible to provide a more detailed characterization of the 'healthy' reference state for BA metabolism:

- **Systemic circulation** The baseline BA levels in systemic circulation were found to be approximately 2.83 μM, with CDCA being the most abundant BA species. Conjugated BAs accounted for about 61% of the total, with glycine-conjugates making up approximately 87% of this fraction. Following food intake, single-meal studies reported an increase of up to 4.3-fold, while multiple-meal studies showed increases of up to 6.3-fold (Supplementary Table B.1).

- **Liver and portal blood** Concentrations in portal blood were reported for CA, CDCA, and DCA, with primary BAs being nearly twice as abundant as secondary BAs. CA and CDCA together comprised about 42% of the total BA pool, approximately 61 μM. Unfortunately, information on the conjugation status of BAs in these organs could not be obtained (Supplementary Tables B.2 and B.3). In all three organs (systemic circulation, portal blood, and liver), DCA was the most abundant secondary BA, while LCA and UDCA were equally abundant.

- **Biliary composition** Biliary composition of BAs exhibited high variability, but CAs, CDCAs, and DCAs each comprised approximately

30% of the BA pool in bile. Glycine-conjugated BAs were more abundant than T-BAs, and uBAs, as well as LCAs and UDCAs, together accounted for less than 3% (Supplementary Table B.6).

- **Intestinal BA flow** Basal intestinal BA flow through the SI was highest in the duodenum, at 7.44 μmol/min, and decreased along the gut axis (jejunum: 5.29 μmol/min; ileum: 2.66 μmol/min). In contrast, the most significant postprandial increase was observed in the ileum and diminished towards the duodenum (ileum: 40-fold; jejunum: 22-fold; duodenum: 9-fold). See also supplementary tables B.7 and B.8.

It is important to note that while this dataset serves as a comprehensive foundation for model development, there are both qualitative and quantitative differences among the various BA data points characterizing this 'healthy' reference state. The BA levels, especially in systemic circulation, have a strong statistical basis and encompass all relevant BA species. However, data from other organs are based on fewer studies and individuals and only partially cover the BA pool. Additionally, there is limited information regarding the conjugation status of BAs outside of systemic circulation.

The models encompass four fundamental transportation mechanisms: (1) BSEP enables the removal of BAs from the liver to either bile or the duodenum. (2) ASBT is responsible for the uptake of BAs from the intestinal lumen. (3) Enterocytes release BAs into the portal bloodstream using OSTα/β. (4) NTCP facilitates the absorption of BAs from the portal bloodstream into hepatocytes. Unfortunately, no data on expression of ASBT and OSTα/β along the gut segments was available. Thus, it was assumed that ASBT is equally expressed in the small intestine, with no expression in the large intestine whereas OSTα/β is expressed in both at a constant level but more strongly in the large intestine. Additionally, in humans it is possible to observe postprandial responses in BA level and several studies measuring BA concentration after a meal are available. Therefore, postprandial dynamics and food intake was included in the models with varying number of meals per day and different times between meals. For model establishment, three meals per day with 4 h breaks between meals (0h-4h-8h) were considered. This is possible as the here used modeling software provides a function that triggers gallbladder emptying into the duodenal lumen upon food intake. Parameters defining the kinetics of the process had to be adjusted to the experimental data but was restricted within physiological reasonable ranges.

Apart from accounting for the organism's physiological aspects, crucial elements of PBPK models also encompass physicochemical attributes like molecular weight, solubility, lipophilicity, and the binding to plasma proteins [257]. These characteristics play a pivotal role in determining the distribution between organs and plasma, as well as passive transport, achieved through appropriate distribution models. In the context of PBPK models related to BA metabolism, the physicochemical properties of glyco-conjugated forms (Table 4.2) or of CDCA (Table 4.3) were employed to establish the compound attributes within the PBPK model designed for small molecules.

Table 4.2: Physicochemical properties of bile acids used. Overview of physicochemical properties and their source that were used to inform compound specific parameters in the PBPK model. For the total BA (total CA: tCA, total CDCA: tCDCA, total UDCA: tUDCA, total DCA: tDCA, total LCA: tLCA) the corresponding physicochemical values of the glyco-conjugated form (G-BA) were taken.

BA species	Property	Value	Source
tCA	MW [g/mol]	465.6	PubChem Identifier: CID 6675
tCA	Solubility [g/l]	0.025	ALOGPS (HMDB [277]
tCA	logP	0.07	Heuman et al. [278]
tCA	pKa (acidic)	3.77	ChemAxon (HMDB [277])
tCA	pKa (basic)	-0.17	ChemAxon (HMDB [277])
tCA	FU	0.3247	Predicted [279]
tCDCA	MW [g/mol]	449.6	PubChem Identifier: CID 387316
tCDCA	Solubility [g/l]	0.0079	ALOGPS (HMDB [277])
tCDCA	logP	0.51	Heuman et al. [278]
tCDCA	pKa (acidic)	3.77	ChemAxon (HMDB [277])
tCDCA	pKa (basic)	-0.29	ChemAxon (HMDB [277])
tCDCA	FU	0.0966	Predicted [279]
tUDCA	MW [g/mol]	449.6	PubChem Identifier: CID
tUDCA	Solubility [g/l]	0.00135	ALOGPS (HMDB [277])
tUDCA	logP	-0.89	Heuman et al. [278]
tUDCA	pKa (acidic)	3.77	ChemAxon (HMDB [277])
tUDCA	pKa (basic)	-0.49	ChemAxon (HMDB [277])
tUDCA	FU	0.0966	Predicted [279]

Continuation of table 4.2

BA species	Property	Value	Source
tDCA	MW [g/mol]	449.6	PubChem Identifier: CID 2733768
tDCA	Solubility [g/l]	0.072	ALOGPS (HMDB [277])
tDCA	logP	0.65	Heuman et al. [278]
tDCA	pKa (acidic)	3.29	ChemAxon (HMDB [277])
tDCA	pKa (basic)	-0.61	ChemAxon (HMDB [277])
tDCA	FU	0.0965	Predicted [279]
tLCA	MW [g/mol]	433.6	PubChem Identifier: CID 439763
tLCA	Solubility [g/l]	0.0015	ALOGPS (HMDB [277])
tLCA	logP	1.05	Heuman et al. [278]
tLCA	pKa (acidic)	3.77	ChemAxon (HMDB [277])
tLCA	pKa (basic)	-1.1	ChemAxon (HMDB [277])
tLCA	FU	0.0682	Predicted [279]

Table 4.3: Physicochemical properties of bile acids used. Overview of physicochemical properties and their source that were used to inform compound specific parameters in the PBPK model. For the conjugated and unconjugated BAs the corresponding physicochemical values of CDCA were taken (glyco-conjugated BA: G-BA, tauro-conjugated BA: T-BA, unconjugated BA: uBA)

BA species	Property	Value	Source
G-BA	MW [g/mol]	449.6	PubChem Identifier: CID 387316
G-BA	Solubility [g/l]	0.0079	ALOGPS (HMDB [277])
G-BA	logP	0.51	Heuman et al. [278]
G-BA	pKa (acidic)	3.77	ChemAxon (HMDB [277])
G-BA	pKa (basic)	-0.29	ChemAxon (HMDB [277])
G-BA	FU	0.0966	Predicted [279]
T-BA	MW [g/mol]	499.7	PubChem Identifier: CID 168408
T-BA	Solubility [g/l]	0.00748	ALOGPS (HMDB [277])
T-BA	logP	0.46	Heuman et al. [278]
T-BA	pkA (acidic)	-0.99	ChemAxon (HMDB [277])
T-BA	pkA (basic)	0.18	ChemAxon (HMDB [277])
T-BA	FU	0.0776	Predicted [279]

Continuation of table 4.3

BA species	Property	Value	Source
uBA	MW	392.6	PubChem Identifier: CID 119473
uBA	Solubility [g/l]	0.02	ALOGPS (HMDB [277])
uBA	logP	0.59	Heuman et al. [278]
uBA	pKa (acidic)	4.6	ChemAxon (HMDB [277])
uBA	pKa (basic)	-0.54	ChemAxon (HMDB [277])
uBA	FU	0.0608	Predicted [279]

Within the human system, the dominant BA species comprise CA, CDCA, DCA, UDCA, and LCA, with additional small quantities of various secondary BAs. These BA species can manifest in diverse forms, including unconjugated BAs, bile salts conjugated with taurine or glycine, and 3′-sulfated BAs, collectively creating a complex BA pool. Due to the constraints imposed by the utilized modeling software, creating a singular model to encompass the entire intricacy of the BA pool proved computationally unfeasible. Consequently, two distinct model variations were separately developed, each addressing specific significant aspects of the BA pool. The first variant focuses on the cumulative levels of the five most abundant BA species – CA, CDCA, DCA, UDCA, and LCA – and is termed the ″5BA model.″ The second variant characterizes the conjugation patterns of BAs, encompassing glyco- and tauro-conjugated BAs as well as free/unconjugated BAs, and is named the ″human conjugation model.″

For each of the model variations, BA synthesis was modeled as a constant formation rate within the liver′s intracellular compartment. The magnitude of this synthesis rate and the rate of renal excretion were guided by data available in literature (Supplementary Table B.4). While the rate of fecal excretion was not explicitly provided, the model ensured a state of equilibrium over an extended period. As a result, the collective rates of excretion were balanced against the summation of all synthesis rates. These excretion processes were modeled by either passive transport or active clearance, depending on the specific process. To achieve system stability, the models necessitated simulation spanning several hundred hours and numerous meal events. Additionally, the models integrated further transformations within the liver and by microorganisms, dependent on the chosen model variant, as depicted in figure 4.1. The overall microbial activity was correlated to the approximated bacterial density as proposed by Gorkiewicz et al. [322].

In a next step, the established models were to be applied to analyze BA levels in patients treated with liver transplantation (LTX) or transjugular intrahepatic portosystemic shunt (TIPS). Both patient cohorts were collected at the University Hospital RWTH Aachen including samples of blood, bile and feces up to 6 months post surgical intervention. Bile acid levels were measured at the University of Gothenburg and were provided by Theresa Wirtz. Initial analysis of the available data showed for LTX patients a curative effect after surgical intervention by reducing average BA levels over time (Supplementary Figure B.2). Stratification of patients with and without complications showed that this reduction over time was stronger for patients with any complication event; however, due to the number of patients without complications and the high variability, no significant difference could be observed. For patients undergoing TIPS treatment, no curative effect could be observed on tBA level (Supplementary Figure B.3). To increase the number of data points per time point, time points were pooled to describe BA levels before intervention, within one week, within one month and up to six months post intervention. In order to recapitulate these various time points post intervention, it was necessary in a first step to extrapolate the models to the diseased state. Comparing BA levels of LTX and TIPS patients pre-intervention showed no significant differences between the cohorts (Supplementary Figure B.4); wherefore, BA levels of both were pooled to represent concentration in a liver disease state (Supplementary Figure B.5).

Comparisons between healthy reference levels derived from literature and the measurements within both cohorts showed strongly elevated BA concentration in blood plasma of patients with liver disease (Figure 4.2). Average tBA were elevated 26-fold, with primary BA being increased by up to 39-fold (tCA: 39, tCDCA: 30), whereas secondary BA showed overall similar level (tDCA: 2.8, tLCA: 1.1). In contrast, tUDCA were by 73-folds higher in liver disease patients as this BA is often administered to prevent or delay liver damage. Conjugated BA were much more strongly elevated than uBA (Conj-BA: 41, uBA: 2.9) and tauro-conjugates were more severely altered than glyco-conjugates (T-BA: 106, G-BA: 31).

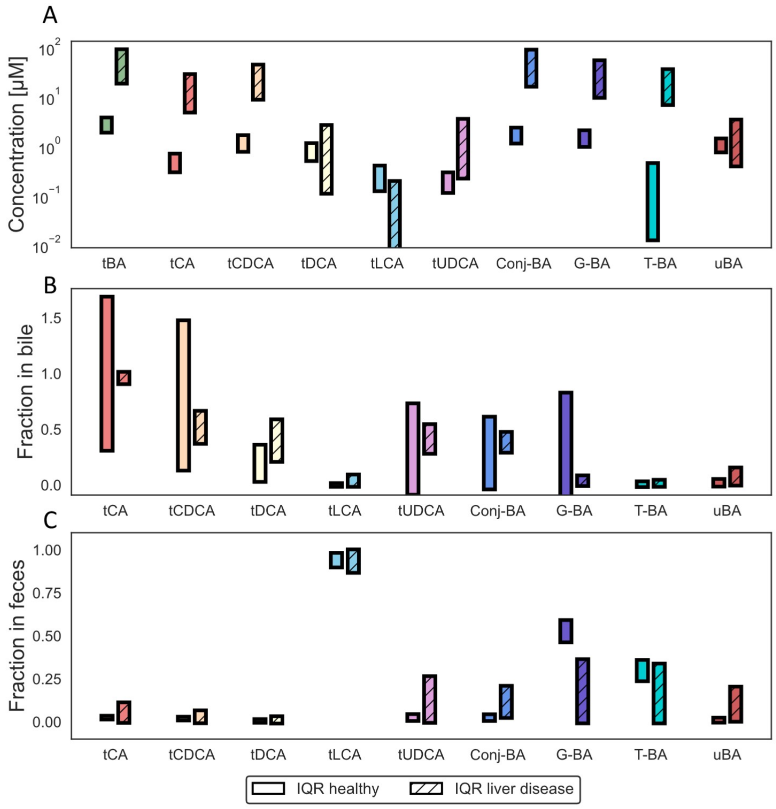

Figure 4.2: Comparison of bile acid levels in venous blood plasma, bile and feces between healthy subjects and liver diseased patients. Comparison of BA levels in venous blood plasma (A) and BA composition in bile (B) and feces (C) between healthy reference subjects (clear bars) and liver diseased patients (striped bars). Shown are the interquartile ranges (IQR) of the provided patient data and calculated IQR from literature data.

4.2 5BA Model - describing the five most abundant bile acids

Within the 5BA model, BA metabolism is initiated by synthesis of CA and CDCA as a constant flow within hepatocytes. Microbial metabolism of BAs within the gut lumen was modeled as net enzymatic reactions, with the relative abundance of the corresponding enzymes along the gut correlated to the approximated bacterial density [322]. The included reactions encompassed dehydroxylation of CA to DCA, and CDCA and UDCA to LCA, as well as epimerization of CDCA to UDCA. A schematic overview of the 5BA model is illustrated in figure 4.3.

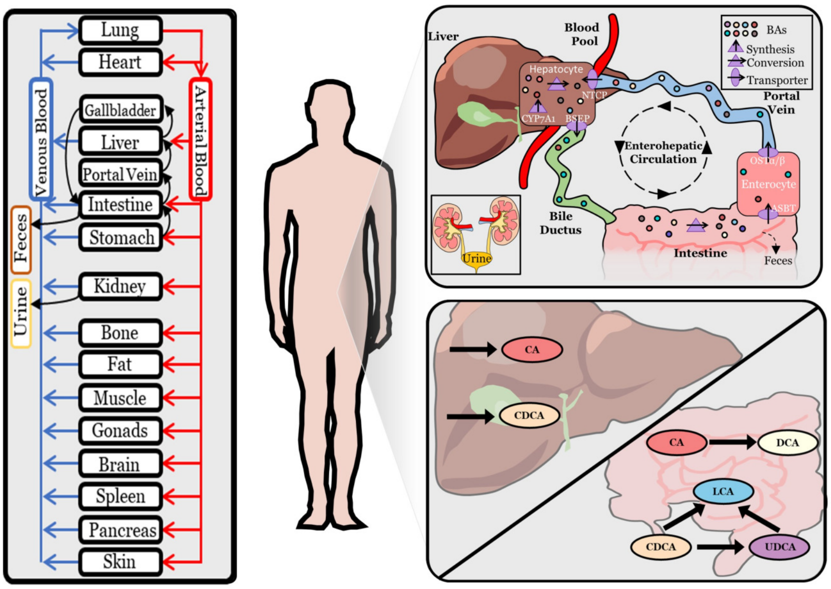
Lung
Heart
Gallbladder
Liver
Portal Vein
Intestine
Stomach
Kidney
Bone
Fat
Muscle
Gonads
Brain
Spleen
Pancreas
Skin
Venous Blood
Arterial Blood
Feces
Urine
Liver
Blood Pool
BAs
Synthesis
Conversion
Transporter
Hepatocyte
NTCP
CYP7A1
BSEP
Portal Vein
Enterohepatic Circulation
OSTα/β
Enterocyte
ASBT
Bile Ductus
Intestine
Feces
Urine
CA
CDCA
CA
DCA
LCA
CDCA
UDCA

Figure 4.3: Physiologically-based bile acid model - 5BA model. Schematic overview of a PBPK model of bile acid biosynthesis via CYP7A1, hepatic and microbial transformation, active transport processes via BSEP, ASBT, OST-α/β and NTCP, as well as fecal and renal excretion. Reactions of BAs are located either in the intracellular space of the liver or in the intestinal lumen.

Model calibration and validation to literature data

In a first step, the 5BA model was calibrated to BA measurements collected from literature. By doing so, the model was able to recapitulate the BA levels reasonably well (Figure 4.4). A list of final model parameters are summarized in Supplementary Tables B.9-B.11.

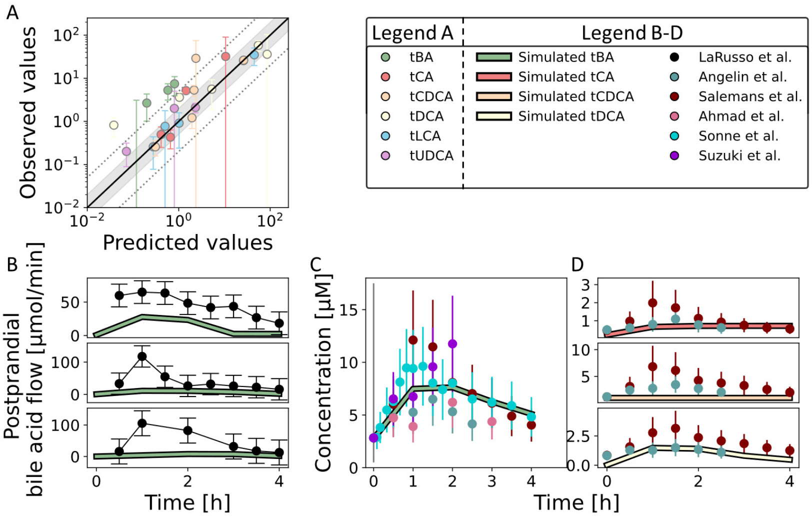

Figure 4.4: 5BA model fit to literature data. Model simulations of bile acid concentration in human against corresponding data points used for fitting. Shown are concentration in a fasting state against data points synthesized by meta-analysis of various studies published in literature (A), postprandial total BA flows in the small intestine (B; from top to bottom: duodenum, jejunum, ileum), as well as postprandial responses of tBA (C) as well as tCA, tCDCA and tDCA (D, from top to bottom) in venous blood plasma. Error bars show the SD. In panel A, the black line represents unity, the gray area the two-fold range and the dashed lines the five-fold range.

All but one of the baseline measurements in the fasting state (Figure 4.4A) were predicted within a five-fold range considering the variation within the data. On the other hand, postprandial flow of tBAs within the small intestinal lumen was consistently underpredicted by the model but the dynamics followed overall the same trend (Figure 4.4B). This was accepted as sufficient because the corresponding data was collected only from one individual with no replicates in the 1970s [323] raising concerns regarding reliability. In contrast, the dynamics of gallbladder emptying and postprandial BA levels in blood plasma (Figure 4.4C-D) were captured very well. The magnitude and dynamics of the postprandial responses were predicted with good accuracy for tBA, tCA and tDCA; however, for tCDCA the response was overall underpredicted.

Despite the intricacies inherent in the modeled system and the considerable scarcity of data, particularly in regions beyond the bloodstream, the model displayed a robust concurrence between the experimental data and the outcomes generated through simulation.

In order to evaluate the behavior of the model, a sensitivity analysis was conducted to determine the impact of the fitted parameters on various BA concentrations that were derived from literature (Supplementary Tables B.12-B.16). All assessed BA levels, especially of secondary BA, were sensitive to changes in intestinal pH. Changes in BA synthesis, BSEP activity and plasma protein concentration had strong effects on BA concentration in venous and portal blood plasma as well as in the liver. Variation of the functional liver volume affected mostly BA in liver and venous blood plasma, the latter also displaying sensitivity towards NTCP activity. Fecal BA composition was most strongly influenced by parameters related to microbial activity, ASBT transporter activity and intestinal transit time.

The accuracy and reliability of any computational model rely upon its ability to replicate real-world observations and experimental data. In this context, the 5BA model was tested against literature data that was withheld from model calibration including postprandial and fasting tBA flow in the duodenum [324; 325] and postprandial responses in blood plasma for multiple meal studies [326; 327]. The comparison of simulated outcomes and actual, before unseen measurements are displayed in figure 4.5. Similar to the observations made during model calibration, predictions of duodenal tBA flow were too low (Figure 4.5A). Recapitulating postprandial responses after a second and third meal (Figure 4.5B) yielded BA levels that were slightly underpredicted, whereas responses after six meals in 1.5 days were too high (Figure 4.5C). This was expected since both of these studies reported BA levels that were either too high or too low and considered not compatible with the remaining studies used in this work (Supplementary Figure B.1). While the absolute values of either studies cannot be explained while also considering the data used for calibration, the general trend was captured very well.

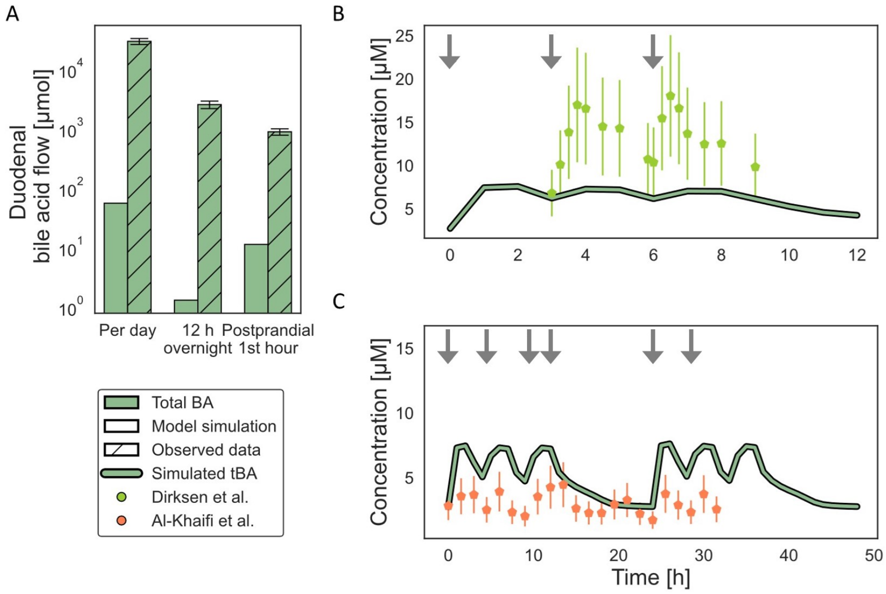

Figure 4.5: 5BA model validation to literature data. Model predictions of duodenal tBA flow (A) and postprandial tBA concentration in venous blood plasma (B and C) in human against corresponding data points from literature. For postprandial responses, the model was simulated with 3 meals per day with 3 h between meals (0-3-6) to recapitulate the data from Dirksen et al. ([326], B) or with 4 meals per day at 0-4.5-9.5-12 h for data from Al-Khaifi et al. ([327], C) Error bars show the SD and arrows indicate a meal event.

For a more comprehensive approach to model validation, a population simulation involving a virtual cohort of 1,000 healthy individuals was executed within PK-Sim. The work by Baier et al. [269] already demonstrated the need for population simulations to adequately address the variability observed in the data. This cohort exhibited diverse anthropometric attributes, spanning ages from 20 to 60 years and encompassing an equal sex distribution (50% females). The individuals' body mass index (BMI) ranged from 19 to 25 kg/m^2. Within the context of this simulation, reference concentrations for all relevant transporters, enzymes, and gallbladder emptying kinetics were varied within a 10% range.

In this context, a special emphasis was put on postprandial responses of BAs (in blood) as most data was available that also showed the strong variability in BA levels. Its results are illustrated in figure 4.6. Similar to previous results, population level tBA flows in the SI were underpredicted (Figure 4.6A). In contrast, variation in tBA levels in blood plasma after a meal were captured very well for a single meal (Figure 4.6B, C) and for multiple meals (Figure 4.6D, E). Despite contending with the intricacies inherent in the modeled system, the limited availability of data, and the challenge of reconciling conflicting data points, the model exhibited a commendable level of agreement between the experimental data and the outcomes generated through simulation.

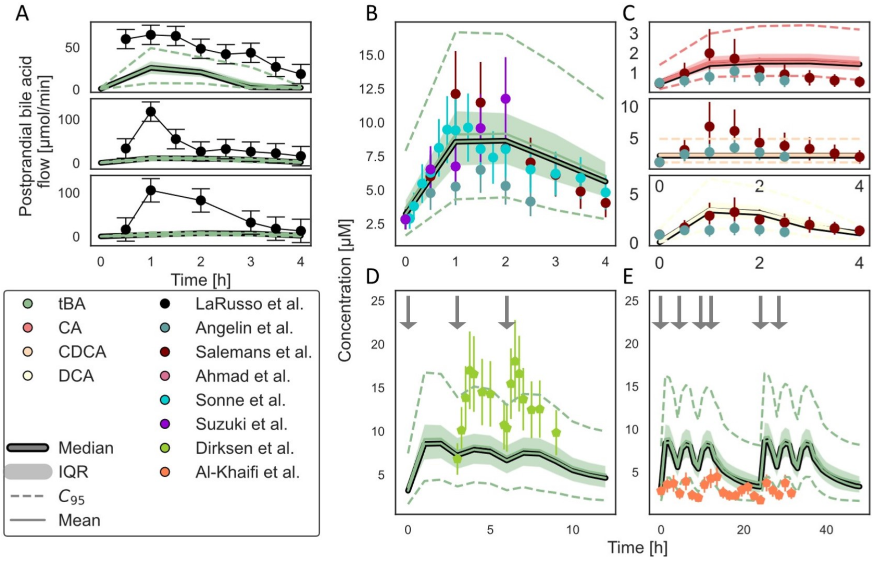

Figure 4.6: Population simulation of the 5BA model for the prediction of postprandial responses. Model simulation of postprandial total BA flows in the small intestine (A; from top to bottom: duodenum, jejunum, ileum), as well as postprandial responses of tBA (B, D and E) as well as tCA, tCDCA and tDCA (C, from top to bottom) in venous blood plasma in a virtual population of 1,000 individuals. Shown are the median (thick line), mean (thin line), IQR (area) as well as the 2.5 and 97.5 percentile (dashed lines) of the population simulations. Error bars show the SD and arrows indicate a meal event.

Parameter scan for pathophysiological conditions

Following calibration and validation, the constructed computational model adeptly captured the dynamics of BA metabolism in healthy individuals across both fasting and postprandial scenarios, displaying concordance with empirical data. As a result of this, the model's mechanistic structure renders it suitable for extrapolation to novel scenarios such as diseased states. In this particular context, the model served as a tool for analyzing BA measurements in patients with liver disease. The initial step aimed to detect potential modifications within the established model that could account for the notably elevated BA levels observed within this specific patient group.

The outcomes of the sensitivity analysis highlighted that the concentration of BAs in venous blood plasma (Supplementary Table B.14), as well as their composition in bile (Supplementary Table B.16) and feces (Supplementary Table B.15), were primarily influenced by factors including plasma protein concentration, functional liver volume, intestinal pH, microbial activity, and the expression levels of the transporters NTCP, BSEP, ASBT, and OSTα/β. By varying these parameters within a physiologically reasonable range (Supplementary Figure B.6-B.13), the analysis revealed that only the reduction in plasma protein levels, the functional liver volume, and NTCP expression could induce the necessary elevation in BA concentration (Figure 4.7). This result was consistent for all assessed BA species (Supplementary Figures B.6, B.13 and B.7).

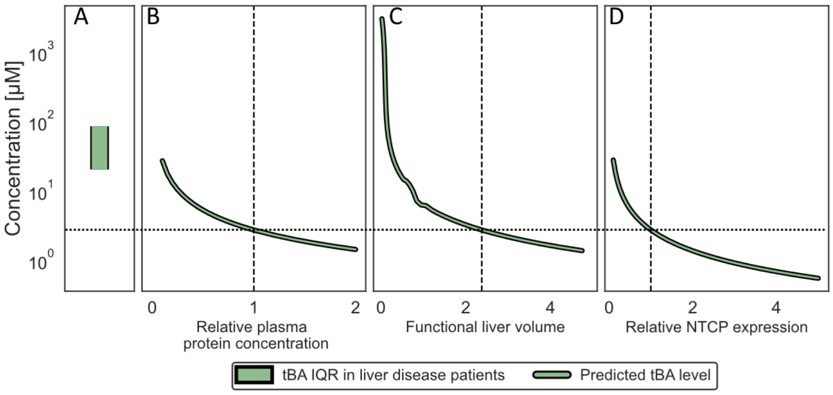

Figure 4.7: Parameter scan for extrapolation of the 5BA model to liver diseased patients. Continued on the next page.

Figure 4.7: Parameter scan for extrapolation of the 5BA model to liver diseased patients. Parameters identified by sensitivity analysis and filtered for strong effect on bile acid level in venous blood plasma were scanned to see if the model can recapitulate the high bile acid levels in blood observed in liver diseased patients (A, shown is IQR of total bile acid concentration). Only variation of plasma protein concentration (B), functional liver volume (C) and relative NTCP expression (D) could alter the model predictions enough to reflect the strongly elevated bile acid levels. For reference, vertical dashed lines indicate the parameter value in the healthy reference model and horizontal dotted line shows blood bile acid level in the healthy reference model. See also supplemental figures B.6-B.13.

It is noteworthy that while diminished plasma protein concentration and reduced functional liver volume are anticipated outcomes in liver diseased patients, the downregulation of NTCP expression is not a topic widely discussed within the existing literature.

To further demonstrate the capabilities of the model established here, the prediction of BA concentrations was extended to organs that were not sampled within the patient cohort (Supplementary Figures B.14-B.16). Specifically, these organs include the portal blood, liver, SI and LI tissue, as well as gut content. This predictive assessment was conducted using the same parameter scan methodology detailed earlier.

These organs typically present challenges for routine clinical assessment due to ethical and practical considerations, while measurements in blood typically encounter fewer obstacles. However, whether variations in blood BA levels accurately reflect those occurring within internal organs remains unclear. To address this uncertainty, the predictions of BA concentrations in these organs were compared to their corresponding predictions in (venous) blood plasma for a range of parameter values (Table 4.4).

Table 4.4: Changes of BAs level in unobserved organs for parameter scans within the 5BA model. Changes in bile acid levels in unobserved organs, namely portal blood, liver, small and large intestinal tissue and gut content, for varying parameters identified by sensitivity analysis were compared to the same changes in venous blood plasma. Similar trend in fold changes are denoted with $\sim$, and if additionally $|\log_2 FC_{organ}/FC_{blood}| < 2$ as =, and divergent responses to parameter variation with $\neq$. See also supplemental figures B.14-B.16.

Parameter	Portal blood	Liver	SI Tissue	LI Tissue	Gut content
Plasma protein concentration	=	=	$\neq$	=	$\neq$
Functional liver volume	$\sim$	$\sim$	$\neq$	$\sim$	$\neq$
NTCP expression	=	$\neq$	$\neq$	$\neq$	$\neq$
BSEP expression	=	$\neq$	$\sim$	=	$\neq$
ASBT expression	=	$\neq$	$\sim$	=	$\neq$
OSTα/β expression	=	$\neq$	$\neq$	$\neq$	$\sim$
Intestinal pH	=	$\sim$	$\sim$	$\sim$	$\sim$
Microbial activity	=	=	=	=	=

The alterations observed in the gut content exhibited the greatest dissimilarity compared to those detected in the bloodstream. Notably, the variations within the portal blood closely mirrored the changes observed in the systemic blood (gut content < SI tissue < liver < LI tissue < portal blood). Modifications in microbial activity and intestinal pH had a congruent impact on BA levels across the body, although the latter's effect was comparatively milder. Conversely, fluctuations in OSTα/β expression generally yielded distinct BA changes within the internal organs, apart from the intestinal lumen. Notably, variations in both BSEP and ASBT expression led to differential behavior within the liver and gut content. The parameters identified as potential contributors to liver disease, namely NTCP expression, functional liver volume, and plasma protein concentration, predominantly influenced BA changes in divergent ways. Notably, only the latter exhibited significant alignment in terms of BA changes across the portal blood, liver, and LI tissue.

In conclusion, the variation in microbial activity generated the most comparable responses, whereas shifts in NTCP and OSTα/β expression elicited the most dissimilar effects on BA levels in systemic blood compared to those within internal organs (NTCP < functional liver volume, and OSTα/β < BSEP, and ASBT < plasma protein concentration, and intestinal pH < microbial activity).

4.3 Human Conjugation Model - describing the conjugation status of bile acids

Within the (human) conjugation model, BA metabolism is initiated by synthesis of uBA as a constant flow within hepatocytes. Subsequent to synthesis, uBA are conjugated with either glycine or taurine by BSH to form G-BA or T-BA, respectively. Microbial metabolism of BAs within the gut lumen was modeled as net enzymatic reactions, with the relative abundance of the corresponding enzymes along the gut correlated to the approximated bacterial density [322]. The included reactions encompassed deconjugation of both T-BAs and G-BAs to unconjugated BAs. A schematic overview of the conjugation model is illustrated in figure 4.8.

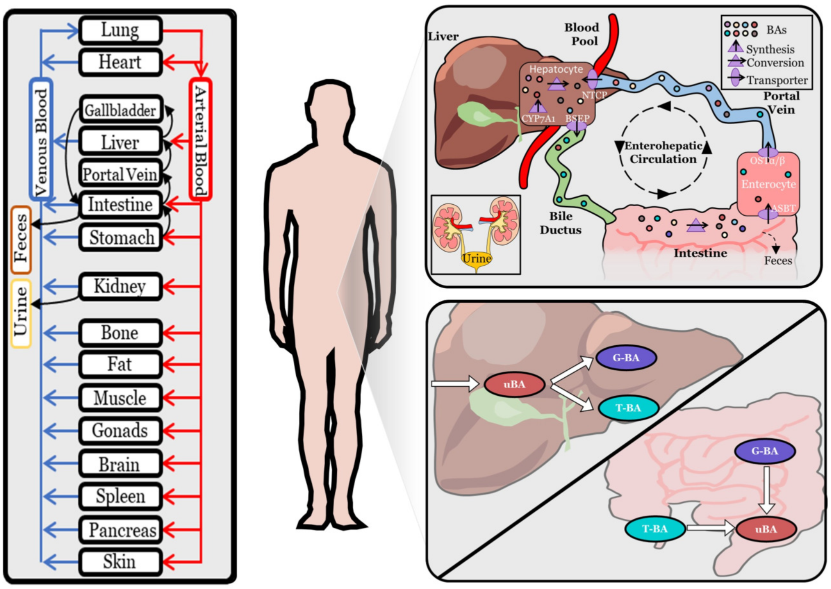
Lung
Heart
Gallbladder
Liver
Portal Vein
Intestine
Stomach
Kidney
Bone
Fat
Muscle
Gonads
Brain
Spleen
Pancreas
Skin
Venous Blood
Arterial Blood
Feces
Urine
Liver
Blood Pool
Hepatocyte
NTCP
CYP7A1
BSEP
BAs
Synthesis
Conversion
Transporter
Portal Vein
Enterohepatic Circulation
OSTα/β
Enterocyte
ASBT
Bile Ductus
Intestine
Feces
Urine
uBA
G-BA
T-BA
G-BA
T-BA
uBA

Figure 4.8: Physiologically-based bile acid model - human conjugation model. Schematic overview of a PBPK model of bile acid biosynthesis via CYP7A1, hepatic and microbial transformation, active transport processes via BSEP, ASBT, OST-α/β and NTCP, as well as fecal and renal excretion. Reactions of BAs are located either in the intracellular space of the liver or in the intestinal lumen.

Model calibration and validation to literature data

As an initial step, the (human) conjugation model underwent calibration using BA measurements obtained from relevant literature sources. This calibration process effectively allowed the model to reasonably replicate the observed BA levels, as indicated by the convergence of simulated and actual data (Figure 4.9). The parameters that underpinned the finalized model configuration are summarized in supplementary tables B.17-B.18.

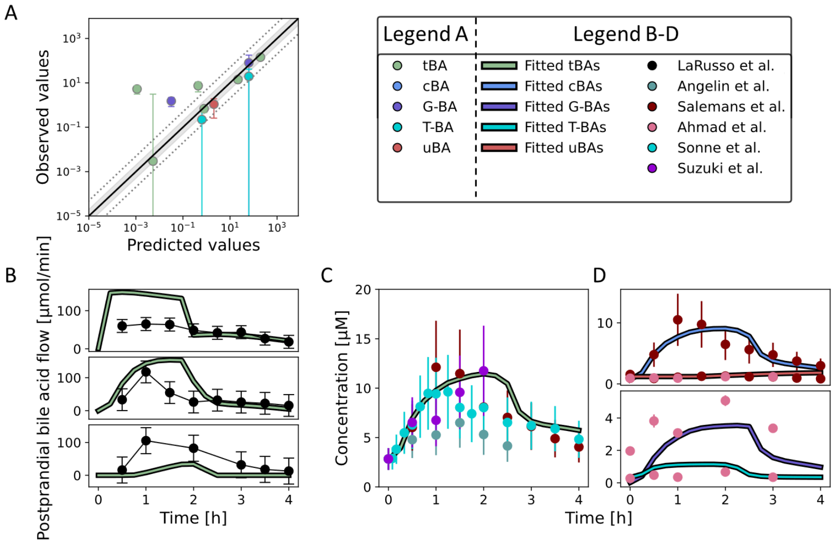

Figure 4.9: Human conjugation model fit to literature data. Model simulations of bile acid concentration in human against corresponding data points used for fitting. Shown are concentration in a fasting state against data points synthesized by meta-analysis of various studies published in literature (A), postprandial total BA flows in the small intestine (B; from top to bottom: duodenum, jejunum, ileum), as well as postprandial responses of tBA (C) as well as conjugated and unconjugated BA and glyco- and tauro-conjugated BA (D, from top to bottom) in venous blood plasma. Error bars show the SD. In panel A, the black line represents unity, the gray area the two-fold range and the dashed lines the five-fold range.

Regarding the baseline measurements during fasting conditions (Figure 4.9A), all but two instances fell within a five-fold range when accounting for the inherent variability within the dataset. Conversely, during the postprandial state, the model exhibited an initial overprediction of the flow of tBAs within the duodenal lumen; however, it aptly captured the dynamics at later time points (Figure 4.9B, upper panel). The model's predictions for tBA flow within the jejunum (Figure 4.9B, middle panel) and ileum (Figure 4.9B, lower panel) showcased reasonable accuracy. This was considered acceptable, given that the corresponding data originated from a solitary individual without replicates in the 1970s [323], which inherently raises concerns regarding its reliability. In contrast, the model remarkably captured the dynamics of gallbladder emptying and the postprandial BA levels in blood plasma (Figure 4.9C-D). The magnitude and patterns of the postprandial responses were accurately predicted for all the various BA species. In light of the complexities within the modeled system and the limitations stemming from insufficient data, particularly concerning regions beyond the bloodstream, the model exhibited a robust alignment between the experimental data and the simulation results.

In order to evaluate the behavior of the model, a sensitivity analysis was conducted to determine the impact of the fitted parameters on various BA concentrations that were derived from literature (Supplementary Tables B.19-B.23). All assessed BA levels were sensitive to changes in intestinal pH. Modifications in BA synthesis, BSEP activity, and plasma protein concentration wielded significant impacts on the concentration of BAs in both venous and portal blood plasma, as well as within the liver. The levels of BAs within the liver exhibited pronounced susceptibility to changes in the expression of BSEP, ASBT, and OSTα/β, along with variations in the functional volumes of the liver and the SI. On the other hand, fluctuations in NTCP expression, plasma protein concentration, and the volumes of the liver and SI exerted strong influences on the BA concentrations within the bloodstream. When considering fecal BA composition, it became evident that parameters tied to the activity of the transporters ASBT, OSTα/β, and BSEP, in conjunction with enzymatic reactions involving BAAT (uBAs), BSH (cBAs), and BA synthesis, as well as changes in the rate of intestinal transit, and the volumes of the SI and LI, played pivotal roles in shaping the composition of fecal BAs.

The fidelity and dependability of any computational model rest upon its capability to faithfully replicate real-world observations and empirical data. In this context, the conjugation model underwent testing against literature data that had been withheld from the model calibration process. This encompassed assessments of postprandial and fasting tBA flow within the duodenum [324; 325], as well as postprandial responses in blood plasma from multiple meal studies [326; 327]. The comparison between the outcomes generated by simulation and the actual measurements is showcased in figure 4.10.

In contrast to the findings from model calibration, predictions pertaining to duodenal tBA flow were notably lower than the observed values (Figure 4.10A). When simulating postprandial responses after a second and third meal (Figure 4.10B), the resulting BA levels were slightly underestimated and exhibited a time delay. Conversely, responses following six meals within a span of 1.5 days were overestimated (Figure 4.10C). These disparities were anticipated, given that both of these studies reported BA levels that were not aligned with the remaining studies employed in this work (Supplementary Figure B.1). Although the absolute values of these studies are in disagreement with the calibration data, the general trends were closely captured by the model.

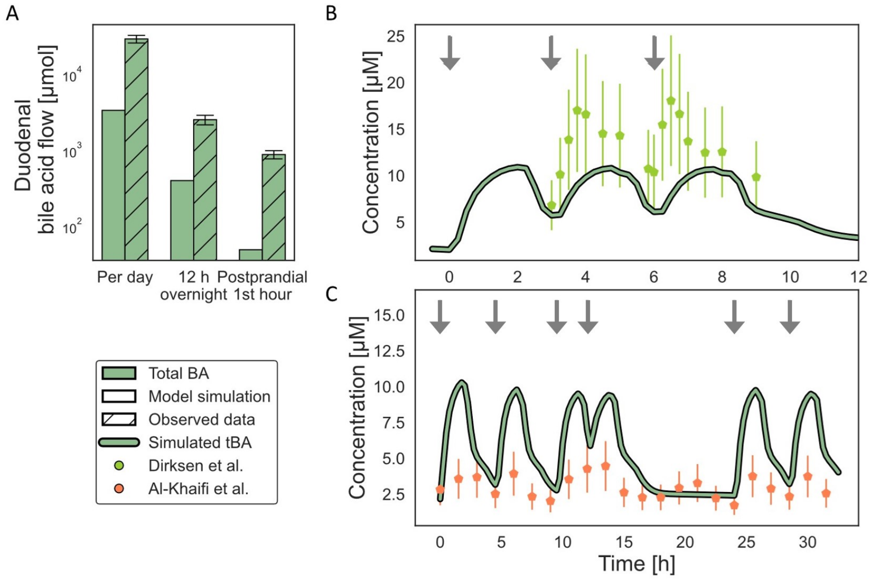

Figure 4.10: Human conjugation model validation to literature data. Model predictions of duodenal tBA flow (A) and postprandial tBA concentration in venous blood plasma (B and C) in human against corresponding data points from literature. For postprandial responses, the model was simulated with 3 meals per day with 3 h between meals (0-3-6) to recapitulate the data from Dirksen et al. ([326], B) or with 4 meals per day at 0-4.5-9.5-12 h for data from Al-Khaifi et al. ([327], C). Error bars show the SD and arrows indicate a meal event.

To achieve a more thorough model validation, a population simulation was conducted using PK-Sim, involving a virtual cohort comprising 1,000 healthy individuals. This cohort showcased a wide array of anthropometric characteristics, with ages spanning from 20 to 60 years, and an equal distribution between sexes (50% females). The individuals' BMI spanned from 19 to 25 kg/m^2. Within the framework of this simulation, reference concentrations associated with all pertinent transporters, enzymes, and gallbladder emptying kinetics were subjected to variations within a 10% range.

This analysis placed particular emphasis on the postprandial responses of BA (in blood), and the findings are visually presented in figure 4.11. Consistent with previous observations, the population-level tBA flows within the duodenum were predicted to be higher than the actual values (Figure 4.11A, upper panel). In contrast, predictions for tBA flow in the jejunum

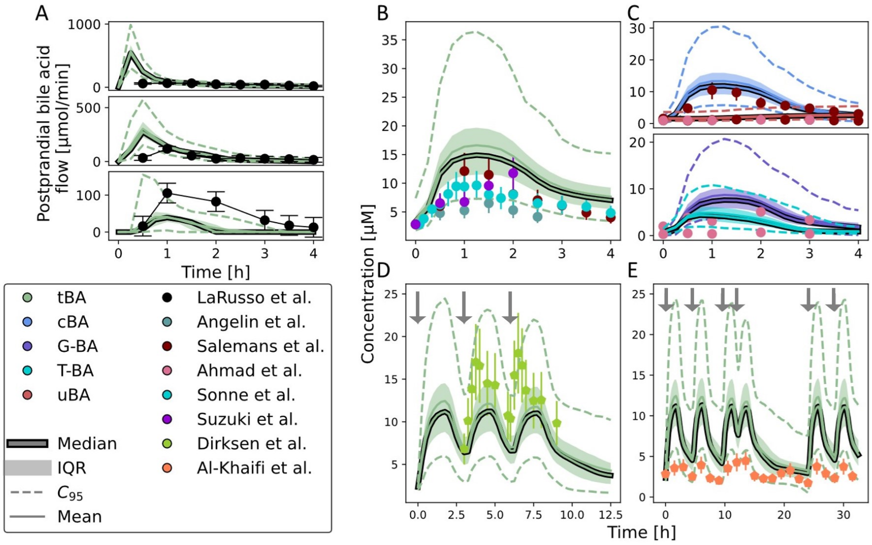

Figure 4.11: Population simulation of the human conjugation model for the prediction of postprandial responses. Model simulation of postprandial total BA flows in the small intestine (A; from top to bottom: duodenum, jejunum, ileum), as well as postprandial responses of tBA (B, D and E) as well as conjugated and unconjugated BA and glyco- and tauro-conjugated BA (C, from top to bottom) in venous blood plasma in a virtual population of 1,000 individuals. Shown are the median (thick line), mean (thin line), IQR (area) as well as the 2.5 and 97.5 percentile (dashed lines) of the population simulations. Error bars show the SD and arrows indicate a meal event.

and ileum demonstrated better alignment with the observed data (Figure 4.11A, middle and lower panel). Conversely, the model adeptly captured the variation in tBA levels within blood plasma following a meal, displaying a strong match for both single meals (Figure 4.11B, C) and multiple meals (Figure 4.11D, E). However, these predictions tended to lie toward the upper limit of the experimental data.

Despite grappling with the intricacies inherent in the modeled system, contending with limited data availability, and navigating the challenge of reconciling conflicting data points, the model exhibited an acceptable level of agreement between the experimental data and the simulation results.

Parameter scan for pathophysiological conditions

Upon successful calibration and validation, the developed computational model adeptly captured the intricate dynamics of human BA metabolism in both fasting and postprandial scenarios, consistently demonstrating alignment with empirical data. Consequently, owing to its mechanistic foundation, the model holds promise for extrapolating to novel scenarios, including diseased conditions. In this specific context, the model was applied for assessing BA measurements in individuals afflicted with liver disease. The initial phase of this assessment aimed to identify potential changes within the established model that could explain the notably elevated levels of BAs observed within this particular patient cohort.

The outcomes of the sensitivity analysis suggested potential factors influencing the concentrations of BAs in venous blood plasma (Supplementary Table B.21), as well as their compositions in bile (Supplementary Table B.23) and feces (Supplementary Table B.22). These influencing factors encompassed elements such as plasma protein concentration, functional liver volume, intestinal pH, microbial activity, and the expression levels of pivotal transporters including NTCP, BSEP, ASBT, and OSTα/β. By subjecting these parameters to controlled variations within a reasonable range (Supplementary Figure B.17-B.25), the analysis unveiled that only the reduction of plasma protein levels, functional liver volume, and NTCP expression could drive the required elevation in BA concentration (Figure 4.12), as already shown for the 5BA model. This result was consistent for all assessed BA species for variation in functional liver volume; however, lowering NTCP expression and plasma protein concentration affected mostly T-BA and uBA level.

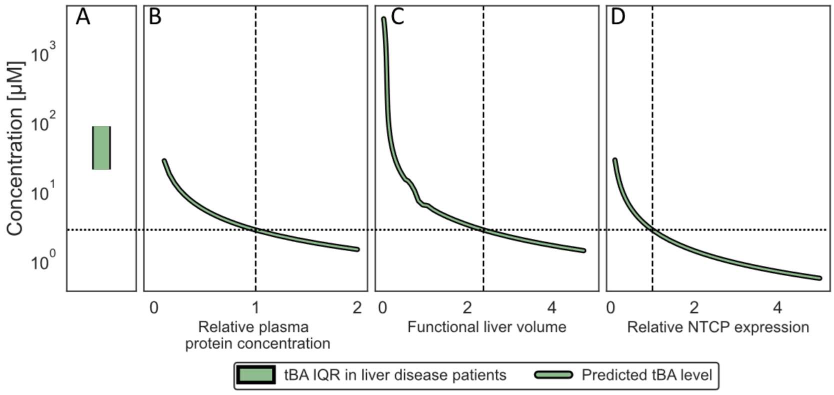

Figure 4.12: Parameter scan for extrapolation of the human conjugation model to liver diseased patients. Parameters identified by sensitivity analysis and filtered for strong effect on BA level in venous blood plasma were scanned to see if the model can recapituale the high BA levels in blood observed in liver diseased patients (A, shown is IQR of total BA level). Only variation of plasma protein concentration (B), functional liver volume (C) and relative NTCP expression (D) could alter the model predictions enough to reflect the strongly elevated BA levels. For reference, vertical dashed lines indicate the parameter value in the healthy reference model and horizontal dotted line shows blood BA level in the healthy reference model. See also supplemental figures B.17-B.25.

To further underscore the model's capabilities established in this study, the prediction of BA concentrations was expanded to encompass organs that were not sampled within the patient cohort (Supplementary Figures B.26-B.28). Specifically, these organs comprise the portal blood, liver, small intestine (SI) and large intestine (LI) tissue, along with the gut content. This predictive assessment was executed using the identical parameter scan methodology as outlined earlier.

These organs often pose challenges when considering routine clinical assessment, mainly due to ethical and practical constraints. In contrast, obtaining measurements from blood encounters fewer obstacles. Nonetheless, whether fluctuations in blood BA levels faithfully mirror those within internal organs remains a subject of uncertainty. To address this ambiguity, the model's predictions of BA concentrations within these organs were compared against the corresponding predictions in (venous) blood plasma, employing a range of parameter values (Table 4.5).

Table 4.5: Changes of BAs level in unobserved organs for parameter scans within the human conjugation model. Changes in BA levels in unobserved organs, namely portal blood, liver, small and large intestinal tissue and gut content, for varying parameters identified by sensitivity analysis were compared to the same changes in venous blood plasma. HSimilar trend in fold changes are denoted with $\sim$, and if additionally $|\log_2 FC_{organ}/FC_{blood}| < 2$ as =, and divergent responses to parameter variation with $\neq$. See also supplemental figures B.26-B.28.

Parameter	Portal blood	Liver	SI Tissue	LI Tissue	Gut content
Plasma protein concentration	$\sim$	=	$\neq$	$\sim$	$\neq$
Functional liver volume	$\sim$	$\sim$	$\neq$	$\sim$	$\neq$
NTCP expression	$\sim$	$\neq$	$\neq$	=	$\neq$
BSEP expression	=	$\neq$	$\sim$	=	$\neq$
BAAT activity	=	=	$\sim$	$\neq$	$\neq$
ASBT expression	$\sim$	$\sim$	$\sim$	$\sim$	$\neq$
OSTα/β expression	=	$\neq$	$\neq$	$\neq$	$\neq$
Intestinal pH	=	=	=	=	=
Microbial activity	=	=	=	=	=

The deviations observed in the composition of gut content stood out as the most pronounced disparities compared to the alterations detected in the bloodstream. Notably, the fluctuations observed within the portal blood closely mirrored the changes seen in the systemic blood (gut content < SI tissue < LI tissue < liver < portal blood). Adjustments in microbial activity and intestinal pH exhibited a coherent impact on BA levels throughout the body. Conversely, variations in OSTα/β expression generally gave rise to distinct BA changes within the internal organs. The parameters identified as potential contributors to liver disease – namely, NTCP expression, functional liver volume, and plasma protein concentration – primarily influenced BA alterations in divergent ways. It's worth noting that only the latter parameter exhibited noteworthy alignment in terms of BA changes across the portal blood, liver, and LI tissue.

In summary, the variations in microbial activity and intestinal pH yielded the most comparable responses, whereas shifts in NTCP and OSTα/β expression resulted in the most disparate effects on BA levels in systemic blood when compared to those within internal organs (OSTα/β < NTCP, and functional liver volume < ASBT, and plasma protein concentration < BSEP, and BAAT < microbial activity, and intestinal pH).

4.4 Discussion of physiologically-based models of human bile acid metabolism

This work focused on the construction of physiologically-based models of BA metabolism in humans. Owing to technical constraints, the complexity of the model needed to be streamlined, leading to the development of specialized model variants that capture specific facets of the intricate BA pool. In this regard, one model variant - the 5BA model - centers on quantifying BA levels for the five most predominant BAs — CA, CDCA, DCA, LCA, and UDCA — while the other variant - the human conjugation model - characterizes BA conjugation status, discerning between glyco- and tauro-conjugated as well as unconjugated BAs. These models encompass a range of fundamental processes, such as systemic circulation, synthesis, hepatic and microbial conversions, gallbladder emptying in response to meals, and excretion via feces and urine.

To ensure the precision of the models, they were established and validated carefully using a dataset compiled from 39 published studies characterizing the "healthy" reference. This comprehensive dataset encompasses a diverse array of information, ranging from various baseline measurements in venous and portal blood, liver, feces, and bile, to postprandial responses in blood and the SI, as well as synthesis, excretion, and flow rates. Despite the incorporation of numerous studies and the availability of many data points for model development, challenges arose due to data scarcity and the need to reconcile different study findings. Most studies reporting BA measurements focused on a specific type of investigation, namely postprandial responses in blood plasma within a four hour time frame post-meal. While this enhances confidence in this particular dataset, information regarding BA levels in other organs is markedly limited, and their reliability remains uncertain.

This limitation was particularly evident in data regarding postprandial BA flow within the SI, measured in either seven [324], three [325], or even a single individual [323], raising valid concerns about statistical robustness. Due to ethical constraints, sampling internal organs from healthy subjects is infeasible. Consequently, data from patients undergoing surgery for diseases not directly related to BA metabolism had to be used. Portal vein measurements were obtainable from studies in patients undergoing elective cholecystectomy [328; 329; 330; 331]. Hepatic BA levels were informed by liver studies in cancer patients who underwent laparotomy [332; 333; 334]. While this approach provided the only means of informing BA concentration outside of systemic blood circulation, the question remains whether these measurements accurately represent the "healthy" context. Furthermore, only two studies involving multiple meals were identified, and these studies could not be harmonized with the plethora of single meal studies. Dirksen et al.'s study [326] reported postprandial responses for three meals, with the first meal showing no notable increase in blood BA levels. This was attributed to a systematic measurement error, prompting the exclusion of initial time points in this study. The second and third responses exhibited more reasonable dynamics overall, albeit reported levels were notably high. Conversely, the five meal study by Al-Khaifi et al. [327] reported consistent BA levels within the study, supported by robust statistics involving 73 individuals. However, when compared to other studies, the postprandial dynamics in this case remained relatively mild. Despite these limitations, both model variants captured the literature data reasonably well.

Bile acids stand out as endogenous metabolites characterized by significant inter- and intra-individual variability [13; 14; 15]. This variability is noticeable in both fasting and postprandial states; however, the latter illustrates this particularly pronounced. To address this complexity at least in part, a meta-analysis of various studies was conducted to estimate variations between studies and within the population. Furthermore, a more in-depth exploration of the variability in BA metabolism was achieved through population simulation, a robust approach for unraveling the multifaceted behaviors of intricate biological and physiological systems. This simulation enabled the models to closely align with the distribution patterns of reported data, particularly in the context of postprandial responses in the blood stream. Collectively, these outcomes serve as compelling evidence of the models' high quality, instilling confidence in their suitability for subsequent analyses and predictions.

Due to their underlying mechanistic framework, the models exhibit the potential for extrapolation to unknown conditions, encompassing scenarios marked by disease. Within this context, both model variants were utilized to predict potential mechanisms elucidating the observed BA measurements in patients afflicted with liver disease. This patient group was combined from two cohorts distinguished by their surgical interventions — LTX and TIPS. Intriguingly, no significant distinctions could be identified in the pre-intervention time points between these cohorts. In the TIPS cohort, blood plasma and fecal samples were collected, and additional bile samples were accessible for LTX patients. However, due to the inherent structure of models within the OSP suite, fecal and bile data could solely be employed in a relative manner. When contrasting the composition of BAs in feces and bile between subjects with liver disease and "healthy" individuals, no significant distinctions emerged. Conversely, the concentration of BAs in blood exhibited a marked elevation within the patient cohort. Model predictions from either variant concurred in indicating that only reductions in plasma protein concentration, functional liver volume, and NTCP expression were able to generate the observed elevation of BA in the blood stream. This is a strong indication for the robustness of the predictions and increases confidence in the both models. Noteworthy, the downregulation of NTCP expression as a factor influencing BA levels in liver disease is not commonly discussed within existing literature - but has been recently reported in chronic liver disease in human and mice [335] - contrasting with the predictable outcomes of decreased plasma protein concentration and diminished functional liver volume — a well-anticipated consequence in liver disease. These results illustrate the models' potential to shed light upon the intricate interplay between pathophysiological alterations, inclusive of physiological or expressional changes, alongside the perturbation of microbial homeostasis, and BA metabolism.

Due to the intricate nature of the mechanisms governing BA metabolism, several computational models have been developed to encapsulate these complexities. Although numerous models for the human system have been proposed, each comes with its own limitations and none can comprehensively encompass the entire spectrum of BA metabolism complexities. The most comprehensive representation of the BA pool can be found in the work of Sips et al. [265]. This model includes a wide range of BA species, i.e. CA, CDCA, DCA, LCA, UDCA, as well as "other" BAs, including their various conjugated, unconjugated, and sulfated forms. Notably, this model focuses on modeling intestinal transit with temporal and spatial heterogeneity, allowing for more accurate predictions of the impact of diet on BA metabolism. The model by Voronova et al. [263] extends previous models by Hofmann et al. [258; 259] and Molino et al. [260], being the sole model that considers regulation through the FXR-FGF19 axis. However, it is limited to only three BA species - CA, CDCA, and DCA - along with their conjugated forms. While this model's feedback regulation enhances predictions, its narrow BA pool restricts its applicability in clinical scenarios where LCA and UDCA levels hold greater significance. More simplified BA pools are seen in the models by Guiastrennec et al. [264] and Woodhead et al. [268], tailored for specific purposes - studying meal effects on total BAs distribution and modeling of drug-induced liver injury, respectively. However, their specialized focus limits their usefulness beyond their intended applications. Another model, developed by de Bruijin et al. [266; 267], incorporates G-CA, G-CDCA, G-DCA as well uBAs, yet it overlooks tauro-conjugated forms. This model utilizes separate models for different BA species, assuming almost instantaneous conjugation and deconjugation rates. Such simplifications may introduce bias in predictions and mask nonlinear interactions between BA species. While many parameters in this study were experimentally determined, the absence of modeling active transport via OSTα/β due to lack of measurement renders the model incomplete. In general, the aforementioned models typically incorporate only a limited number of compartments, often lacking sub-compartments. These are also derived from physiological concepts rather than utilizing a comprehensive physiologically-based representation of the entire body, as done in this study. Moreover, this wholistic representation is based on pre-existing knowledge and does not require additional parametrization of physiological parameters. Notably, among these models, only the one proposed by Sips et al. [265] encompasses UDCA. This is usually sufficient under physiological circumstances; however, in cases of cholestatic liver disease, UDCA administration is a common approach [336; 337]. Likewise, LCA, a potentially toxic secondary BA associated with cholestatic conditions, is accounted for only in the works by Sips et al. [265] and Woodhead et al. [268]. Models excluding these secondary BAs might introduce biases when applied to such conditions.

In this thesis, two distinct model variations were developed due to technical limitations. This enabled an exploration of diverse facets within the BA pool. The human conjugation model can account for the heightened solubility and polarity exhibited by BAs when conjugated with glycine or taurine. Consequently, it offers a more precise representation of passive diffusion. Conjugated BAs, characterized by their high polarity, necessitate active transporters for passage, while unconjugated BAs can more readily traverse cell membranes and be reabsorbed by the intestine. Conversely, the 5BA model portrays the diversity within the BA pool more closely. It discriminates between primary and secondary BAs and encompasses clinically significant BAs, such as the cytotoxic LCA and the therapeutically-relevant UDCA. In qualitative terms, both model variants performed equally well during the development process. However, the human conjugation model recapitulated postprandial BA flow in the intestine more closely. Both variants concurred in its predictions regarding patients with liver diseases.

In summary, this work highlighted the models' capacity in predicting BA levels and their composition across the entirety of the body. This includes anatomical locations that pose practical and ethical challenges for access, such as the liver or portal blood, all within the context of both physiological and pathophysiological conditions.

Limitation of the models

In further analyses, the physiologically-based models might undergo structural refinements aimed at addressing inherent limitations. The current rendition of the computational models encompasses solely the most prevalent BA species, overlooking the inclusion of sulfated and less common secondary BAs. Consequently, the models are unable to encompass the full intricacies of the complex BA pool, which could potentially introduce a systemic bias in predictions due to differing kinetics among various BA species [9]. The most pronounced limitation lies in the scarcity of available data. Particularly within the gut, there exists only little information pertaining to BA levels and microbial density. Therefore, any predictions regarding intestinal BAs should be handled with utmost caution. Notwithstanding these constraints, the models adeptly recreated BA composition and levels across the entirety of the body, accurately capturing inter-individual variability in postprandial responses.

Chapter 5

General conclusion and future work

Contributions:

B. Kister wrote this chapter. I. Hawwari, L.M. Blank and L. Kuepfer reviewed the chapter.

Bile acids occupy an important role within a multitude of physiological processes. They have captured substantial attention in the scientific community due to their multifaceted functions, encompassing roles from facilitating the digestion and absorption of dietary fats to orchestrating signaling cascades that govern metabolic pathways and gene expression. The reach of BAs extends across a diverse spectrum of physiological and pathological contexts. They have been implicated in an array of conditions, spanning metabolic disorders, liver diseases, inflammatory bowel diseases, and more. The intricate interplay of BAs with a wide array of physiological systems underscores their importance in maintaining overall health, thereby prompting in-depth investigations into their intricate behaviors. However, studies of BAs encounter various challenges owing to the inherent intricacies of the system. Bile acid metabolism navigates through a complex network of interconnected pathways that span multiple organs, tissues, and cellular processes. This dynamic interplay is influenced by an abundance of factors, encompassing genetics, enzymatic reactions, transporters, gut microbiota, and dietary influences. Complexity is even further increased, as the BA pool consists of a mix of various different BA species, each with their distinct physico-chemical properties and metabolic behaviors.

The application of computational modeling has emerged as a valuable strategy for untangling the intricate facets of BA metabolism and its ramifications on health and disease. In alignment with this objective, this study has undertaken the development and presentation of physiologically-based models describing BA metabolism both in mice and humans. The careful construction and validation of these models against existing data, coupled with the exploration of initial predictions, underscore their potential as a framework for further investigations into BA metabolism, aiding in the generation of insights into its dynamics across species and shedding light on its implications for health and disease states.

These models encompass fundamental processes of BA metabolism such as synthesis, hepatic and microbial conversions, circulation throughout the body, enterohepatic (re-)circulation, and renal and fecal excretion. Within the human context, gallbladder emptying in response to a meal could be included as well; therefore, enabling postprandial responses in BA level. Due to technical limitations, the models' complexity were simplified, leading to specialized model variants that capture specific aspects of the intricate BA pool. One variant quantifies the levels of the predominant BAs (human: 5BA model; mouse: 6BA model), while the other characterizes conjugation status (human/murine conjugation model).

Because of the intricate complexities involved in regulating BA metabolism, various computational models have been created to represent these intricacies. While there have been numerous models proposed for the human system, each one is associated with its unique set of constraints and shortcomings. In contrast to this work, the published models were not based on preexisting knowledge; thus, physiological parameters needed to be derived *de novo*. All model parameters in this study are associated with specific physiological functions and do not merely describe processes empirically; therefore, enabling extrapolation to new scenarios. Consequently, the models introduced in this study possess the capability to describe BA levels across the whole body, making them well-suited for predicting outcomes in clinically significant contexts. Importantly, it's worth noting that all previously published models focused on describing BA metabolism within the human system. The here developed model of murine BA metabolism marks the first publicly available model dedicated to mice.

Mouse models The murine models were carefully established and validated using data from both male and female SPF mice, thereby addressing sex differences in BA concentration and composition. The models were able to predict BA levels in GF mice by excluding microbial processes. Incorporating additional physiological information resulted in varied predictions, indicating model refinement potential. Introducing further changes to the system only improved replicated BA composition and levels when these were not confined to those reported in literature. These models demonstrated the ability to predict outcomes in disease contexts and across-species. Exploring the effects of BA malabsorption and intestinal barrier impairment on BA metabolism, the models' capacity for extrapolation was illustrated, particularly for understanding BA metabolism in diseases. As a first indication of species differences, the models also estimated that the murine BA pool is recycled less frequently than in humans. In summary, the presented models robustly predicted BA levels and behaviors, providing insights into complex interactions of BA metabolism. The models' limitations can be found in focusing on prevalent BAs and the exclusion of the gallbladder. Nevertheless, the models can be applied in model-assisted investigations of BA metabolism in prospective studies and in assessments of differences across species.

Human models The human models were carefully established and validated using data from 39 studies from literature. However, challenges arose due to data scarcity and reconciling different findings. Studies mostly focused on postprandial blood measurements within a limited time frame, leading to limited knowledge of BA levels in other organs. Despite these limitations, both model variants captured literature data well. Bile acid concentration exhibit significant variability between and within individuals. A meta-analysis and population simulation were conducted to estimate variations, resulting in models aligning closely with reported data. The models' mechanistic framework allows extrapolation to unknown conditions, including disease scenarios. The models were used to predict mechanisms underlying observed BA measurements in liver disease patients, indicating potential interactions between pathophysiological alterations, expression changes, and BA metabolism. In conclusion, this study demonstrates the models' capability to predict BA levels and composition across the body, even in challenging-to-access locations. While the models have limitations, such as focusing on prevalent BAs and data scarcity, they accurately capture BA dynamics and variability, making them valuable tools for understanding complex BA metabolism.

Outlook and future work Prospective studies employing the models presented herein could potentially lead to structural refinements. Both human and murine models would gain advantages from incorporating feedback regulation, particularly emphasizing FXR signaling, which holds a pivotal role in BA homeostasis (as previously discussed). This regulatory pathway oversees the synthesis of BAs as well as the expression of transporters. Integration of this regulatory axis would yield more intricate predictions, particularly in scenarios involving cholestatic conditions. Additionally, it would facilitate predictions of therapeutic impacts when targeting components of this signaling cascade. Including this regulatory mechanism would further allow for a more comprehensive representation of the complex BA pool and the nuanced nonlinear interactions. Bile acid-mediated signaling takes place in enterocytes and hepatocytes, exerting mutual influence through the secretion of BAs and FGF15/19. Moreover, distinct BA species exert varying effects on FXR signaling; while the majority acts as activators, UDCA and MCAs inhibit FXR signaling. This complexity is particularly noteworthy in mice, given their abundance of MCAs, but also in the treatment of patients with UDCA in cholestatic liver disorders.

Subsequent investigations using the murine models could delve more deeply into the role of the intestinal microbiome in BA metabolism. This could involve more extensive measurements of bacterial density along the gut, a potential factor contributing to sex-related differences in BA metabolism. Similar to extrapolating to germ-free mice, these models could also be employed to simulate BA levels in gnotobiotic mice – a mouse model characterized by a defined microbial community, consisting of either 12 (OMM^{12}) strains [338] or 19 (OMM$^{19.1}$) strains [339]. In the OMM^{12} system, BAs cannot be metabolized, thereby precluding the production of secondary BAs. In contrast, OMM$^{19.1}$ mice possess a limited capacity for BA metabolism, attributed to *Extibacter muris* which can generate secondary BAs through 7α-dehydroxylation [340]. Comparative analyses involving germ-free, specific pathogen-free, and gnotobiotic mice could help quantify and characterize the microbiota's metabolizing role in BA metabolism. Furthermore, the integration of the models developed here with a genome-scale metabolic model of the murine microbiome could offer an even more comprehensive understanding. These sub-models would continually exchange information, potentially creating a comprehensive depiction of BA metabolism and its intricate interactions within the gut-liver and the host-microbiome axis.

The human models possess the potential for extended utilization in the comprehensive analysis of the remaining patient dataset. In this regard, an initial extrapolation of the "healthy" models into the context of liver disease was executed. These adapted "diseased" models lay the groundwork for integrating longitudinal patient measurements, thereby enabling the reconstruction of the temporal progression of BA levels post-intervention. In this manner, the models may offer insights into the relationship between BA metabolism and liver disease, potentially contributing to the identification of biomarkers indicative of emerging complications in patients.

To conclude, comprehensive whole-body physiologically-based models were constructed to elucidate BA metabolism in both mice and humans. The murine models were employed to address sex-related differences on BA levels, as well as to initiate predictions concerning species variations and the impact of pathophysiological conditions such as BA malabsorption and impaired intestinal barrier function. Conversely, the human models demonstrated applicability in replicating the reported inter-individual variability in BA levels and suggesting potential mechanisms underlying the elevated BA levels evident in patients with liver disorders. The models presented in this study offer a valuable framework for conducting model-assisted investigations into BA metabolism within prospective studies. Their potential contributions align with the principles of the '3Rs' (Reduction, Refinement, and Replacement) and hold promise for enhancing patient care through improved understanding and prediction of BA-related dynamics.

Chapter 6

Material and Methods

Partially published in:
Kister, B., Viehof, A., Rolle-Kampczyk, U., Schwentker, A., Treichel, N.S., Jennings, S., Wirtz, T.H., Blank, L.M., Hornef, M.W., von Bergen, M., Clavel, T., Kuepfer, L., 2023. A physiologically based model of bile acid metabolism in mice. iScience. Volume 26. Issue 10. 107922.
[Reprinted (adapted) with permission from Elsevier. Open access CC-BY © The Authors 2023]

Contributions:
A. Viehof collected samples from the mouse models. U. Rolle-Kampcyzyk performed the bile acid measurements. A. Schwentker measured the transporter expression. N. Treichel sequenced the cecal microbiome. B. Kister implemented all other methods and wrote this part.

Mouse housing conditions and sampling

Specimens were procured from two distinct groups of mice: germ-free (GF) and specific-pathogen free (SPF) C57BL/6N mice (50% females). These mice were euthanized for scientific purposes, following the guidelines of the German Animal Protection Law (TierSchG). The Internal Animal Care and Use Committee (IACUC) at the University Hospital of RWTH Aachen granted approval for the collection of gut content, body fluids, and organs from donor mice that had not been subjected to any experimental interventions (internal approval number: 70018A4). The GF mice were housed in isolators (NKPisotec, Flexible film isolator type 2D) under sterile conditions. To establish SPF mice with a C57BL/6N genetic background, mice were removed from the isolators and passively colonized with a complex microbiota through cohousing with SPF mice. The mice used for this study were from the initial generations of C57BL/6N SPF mice bred for research purposes. The room temperature was maintained between 21-24 °C with humidity levels ranging from 25-40%, and the mice were subjected to a 12-hour day and night cycle. All mice were provided with unrestricted access to standard chow (GF mice: γ-irradiated standard chow, V1124-927; SPF mice: autoclaved standard chow, ssniff V1124-300) and autoclaved tap water with a pH of 7. The mice were housed in single-sex cages furnished with Tek-Fresh bedding (ENVIGO). To confirm the GF status of the mice, fecal samples from GF mice were examined using microscopic observation after Gram-staining and plating on both anaerobic and aerobic agar plates. The mice were euthanized at 12 to 13 weeks of age in the afternoon and with free access to food, and various tissues and bodily fluids, including blood, urine, gut tissue and content, liver, gall bladder, and kidneys, were collected. Systemic blood was obtained from the vena cava, placed on ice for 5-10 minutes, and subsequently centrifuged at 4,500 rpm for 15 minutes to isolate serum. The small intestine was divided by length into the duodenum (proximal 16%), jejunum (middle 74%), and ileum (distal 10%). The colon was also divided into proximal (50%) and distal (50%) segments. All collected samples were promptly frozen and stored at -80°C.

Bile acid measurements

Sample preparation

To start, x milligrams of a solid matrix were combined with five times the volume of acetonitrile (ACN):water mixture (1:1, v/v) and thoroughly mixed using a TissueLyser II at 30 Hz for 10 minutes (Retsch Qiagen). Following a brief centrifugation step lasting 2 minutes at 14,000 rpm, 100 μl of the resulting supernatant were introduced to a solution consisting of 500 μl of ACN:water:methanol (3:1:2, v/v/v), and the sample was vortexed for 5 minutes. After subjecting it to sonication for 5 minutes and another round of centrifugation (14,000 rpm, 4°C, 5 minutes), 550 μl of the supernatant were carefully transferred into a new tube and evaporated until dryness was achieved. The resulting pellet was then reconstituted using 100 μl of a solution containing 50% concentration, and 10 μl of this reconstituted sample were utilized for subsequent analysis. For serum samples, 10 μl were similarly used for analysis.

LC-MS analysis

The analysis was conducted using the validated Bile Acid Kit from Biocrates Life Sciences in Innsbruck, Austria, as outlined in Pham et al.'s work [341]. In this process, 10 μl of the native samples or sample extract were pipetted onto a 96-well sandwich filter plate and prepared in accordance with the manufacturer's instructions. For quantification, seven external calibration standards, each containing all 19 BAs, were utilized alongside ten isotope-labeled internal standards. A comprehensive list of metabolites can be found on the manufacturer's website (Biocrates Life Sciences AG, Innsbruck, Austria). The LC-MS/MS analysis was performed using a Waters Acquity UPLC System coupled with a QTRAP 5500 instrument (AB Sciex, Concord, Canada). Mobile phase A (MP A) consisted of a solution containing 10 mM ammonium acetate and 0.015% formic acid, while mobile phase B (MP B) was composed of a mixture of acetonitrile, methanol, and water in a ratio of 65/30/5 (v/v/v), 10 mM ammonium acetate, and 0.015% formic acid. Data processing was carried out using the quantitation method provided by the Bile Acid Kit from Biocrates Life Sciences AG in Innsbruck, Austria.

Bile acid transporter expression

RNA extraction from homogenized tissue samples was carried out using TRIzol reagent. The tissue homogenization process utilized the FastPrep-24TM 5G equipment from MP BiomedicalsTM. The isolated RNA was subsequently transcribed into cDNA using ReverseAid (Thermo Fisher) in conjunction with RiboLock Inhibitor (Thermo Fisher). Quantitative PCR was conducted employing taqman probes (Thermo Fisher) designed for the specific gene of interest (GOI). The expression of the GOI was then normalized relative to that of a housekeeping gene.

Microbiota analysis by high-throughput sequencing

Isolation of metagenomic DNA

To isolate DNA, we followed a modified protocol based on Godon et al. [342]. Initially, frozen samples were combined with 600 μl of stool DNA stabilizer (Stratec biomedical) and allowed to thaw at room temperature. These samples were then transferred to autoclaved 2-ml screw-cap tubes containing 500 mg of 0.1 mm-diameter silica/zirconia beads. To this mixture, 250 μl of 4 M guanidine thiocyanate in 0.1 M Tris (pH 7.5) and 500 μl of 5% N-lauroyl sarcosine in 0.1 M PBS (pH 8.0) were added. Subsequently, the samples were incubated at 70°C at 700 rpm for 60 minutes. Cell disruption was performed using a FastPrep® instrument (MP Biomedicals) equipped with a 24 × 2 ml cooling adaptor filled with dry ice. This step involved three rounds of 40-second pulses at a speed of 6.5 M/s. To the disrupted samples, 15 mg of Polyvinylpyrrolidone (PVPP) was added, followed by vortexing and a 3-minute centrifugation at 15,000 x g and 4°C. Approximately 650 μl of the resulting supernatant was carefully transferred into a new 2 ml tube, which underwent a subsequent 3-minute centrifugation at 15,000 x g and 4°C. Of the supernatant obtained, 500 μl was transferred to another 2 ml tube, and 50 μg of RNase was introduced before incubating the mixture for 20 minutes at 37°C with agitation at 700 rpm. Following this step, genomic DNA (gDNA) was isolated using the NucleoSpin® gDNA Clean-up Kit from Macherey-Nagel, following the manufacturer's instructions. The elution of DNA was carried out twice using 40 μl of Elution buffer, and the concentration of DNA was determined using a NanoDrop® instrument (Thermo Scientific). The resulting samples were stored at -20°C for future use.

Illumina sequencing of 16S rRNA gene amplicons

The process of library preparation and sequencing closely followed the procedures previously outlined [343]. This entire workflow was conducted using an automation platform (Biomek400, Beckman Coulter). In summary, the V3-V4 region of the 16S rRNA genes was amplified in duplicate with 25 cycles, adhering to a two-step protocol [344] and utilizing the 341F-785R primers [345]. For purification, the AMPure XP system from Beckman Coulter was employed, after which sequencing was performed on a MiSeq system (Illumina, Inc.) in paired-end mode (PE300). In accordance with the manufacturer's guidelines, this sequencing run was carried out with pooled samples, and 25% (v/v) of the PhiX standard library was included.

Computational methods

PBPK modelling

PBPK models include a highly detailed portrayal of an organism's physiology. These models explicitly depict individual organs and establish connections between them through systemic vascular circulation. In PBPK models, it becomes feasible to simulate tissue concentrations, even when they cannot be accessed experimentally. The parameters within PBPK models are explicit representations of specific physiological functions, and they are drawn from meticulously curated collections of data, encompassing details like organ volumes, surface areas, tissue composition, and blood perfusion rates. Consequently, the identification of parameters in PBPK models is typically limited to a small subset, primarily focused on the active processes governing the distribution and elimination of compounds. PBPK models, therefore, rely heavily on substantial prior knowledge, which encompasses intricate descriptions of physiological processes, such as enterohepatic circulation and intestinal absorption.

Kinetic rate laws

Describing BA synthesis, a constant flux within the intracellular space of the liver was assumed. The following rate law was applied in mice:

$$v_{synth} = s_{GF} * s_{sex} * EM * k_{synth}$$

and in human simplified to:

$$v_{synth} = EM * k_{synth}$$

where s_{GF} and s_{sex} represent scaling factors adjusting the overall activity between SPF and GF as well as male and female mice, EM the amount of catalyzing enzyme and k_{synth} the absolute synthesis rate. For the remaining enzymatic reactions and transport processes, Michaelis-Menten kinetics were applied, following in mice:

$$v = s_{GF} * s_{sex} * EM * k_{cat} * K_{water} * C/(K_m + K_{water} * C)$$

and in humans:

$$v = EM * k_{cat} * K_{water} * C/(K_m + K_{water} * C)$$

with K_{water} describing the partition coefficient of the BA between water and the source compartment of the BA, K_m the Michaelis-Menten constant and C the BA concentration in the source compartment. k_cat represents the number of substrate BA each enzyme site converts to product per unit time, and in which the enzyme is working at maximum efficiency and is calculated as

$$k_{cat} = v_{max}/C_{ref}$$

with v_{max} being the maximum rate of reaction and C_{ref} the enzyme reference concentration of 1 μM. For renal excretion, tubular excretion with Michaelis-Menten kinetic was selected within PKSim:

$$v = fu * TS_{max} * C_{kid-pls}/(K_m + fu * C_{kid-pls})$$

with TS_{max} describes the intrinsic maximum rate for tubular secretion, *fu* the fraction unbound BA in blood plasma and $C_{kid-pls}$ the BA concentration within the plasma sub-compartment of the kidney.

Software and calculations

The PBPK model concerning bile acid metabolism was initially established within PK-Sim®, with subsequent refinements and adjustments carried out using MoBi® (Open Systems Pharmacology suite Version 11.150). Model simulations were executed utilizing the ospsuite-R package in R (version 11.0.123). Parameter fitting was conducted employing the Monte Carlo algorithm, implemented within the Open Systems Pharmacology Suite. The calculation of residuals was set to be linear, and the weights were determined based on the measured standard deviations. The majority of reactions were characterized by simple Michaelis-Menten kinetics, while a constant flux was presumed for bile acid synthesis. Plotting and statistical analyses were performed using custom Python scripts. In cases where applicable, p-value adjustments for multiple testing were implemented through the Benjamini-Hochberg correction method, facilitated by the statannotations package [346]. To evaluate impaired gut barrier function, the unperturbed paracellular permeability of bile acids was set to correspond with their transcellular permeability, which had been computed by MoBi based on their physicochemical properties.

Meta-analysis

Information from various published studies were combined using a Bayesian meta-analysis approach as described in [319; 320]. This approach relies on the functionalities of the brms package [347] for fitting of the Bayesian model and on the meta [348], metafor [349] and dmetar package [319] for the meta-analysis itself. For the Bayesian model, weakly informative priors were used.

Population simulation

For population simulation a virtual population of 1000 individuals (50% female, age 20 to 60, BMI 19 to 25) was created. For all relevant transporters and enzymes, normalized expression were drawn from a standard normal distribution with standard deviation 0.1. Fitted parameters describing gallbladder ejection half-time, ejection fraction and time for gallbladder refilling and lag time as well as EHC continuous fraction were varied by 10% around the fitted values following a normal distribution.

16S rRNA amplicon data analysis

An updated version of the workflow previously outlined by Lagkouvardos et al. [343] was employed for data analysis. The process began with the processing of raw reads utilizing the Integrated Microbial Next Generation Sequencing platform (www.imngs.org) [350], which is rooted in UPARSE [351]. In this initial step, sequences were demultiplexed and trimmed to retain only those with a quality score of at least 10 for their first base. Subsequent operations involved pairing, chimera filtering, and OTU clustering at a 97% identity threshold, all of which were carried out using USEARCH 11.0 [352]. Reads that fell below 350 nucleotides or exceeded 500 nucleotides in length, as well as paired reads with an expected error surpassing 2, were excluded from further analysis. To mitigate GC bias and non-random base composition, the remaining reads were subjected to a fifteen-nucleotide trimming on both ends. The clustering of operational taxonomic units (OTUs) maintained a 97% sequence similarity cutoff, and only those with a relative abundance exceeding 0.25% in at least one sample were retained for further analysis. The subsequent steps involved sequence alignment and taxonomic classification, which were performed using SINA 1.6.1, employing the SILVA release 138 taxonomy [353].

For the assessment of microbial richness, diversity, and community structure, the Rhea pipeline was harnessed [354] Detailed descriptions of the statistical tests applied can be found in the Rhea support information and in the corresponding scripts (https://lagkouvardos.github.io/Rhea). To normalize sequence counts, a simple division was executed based on their respective sample sizes, followed by multiplication to match the size of the smaller sample. Subsequently, alpha-diversity parameters were calculated. Beta-diversity analyses relied on the computation of unweighted and generalized UniFrac distances [274; 275].

Appendix A

A physiologically-based model of bile acid metabolism in mice

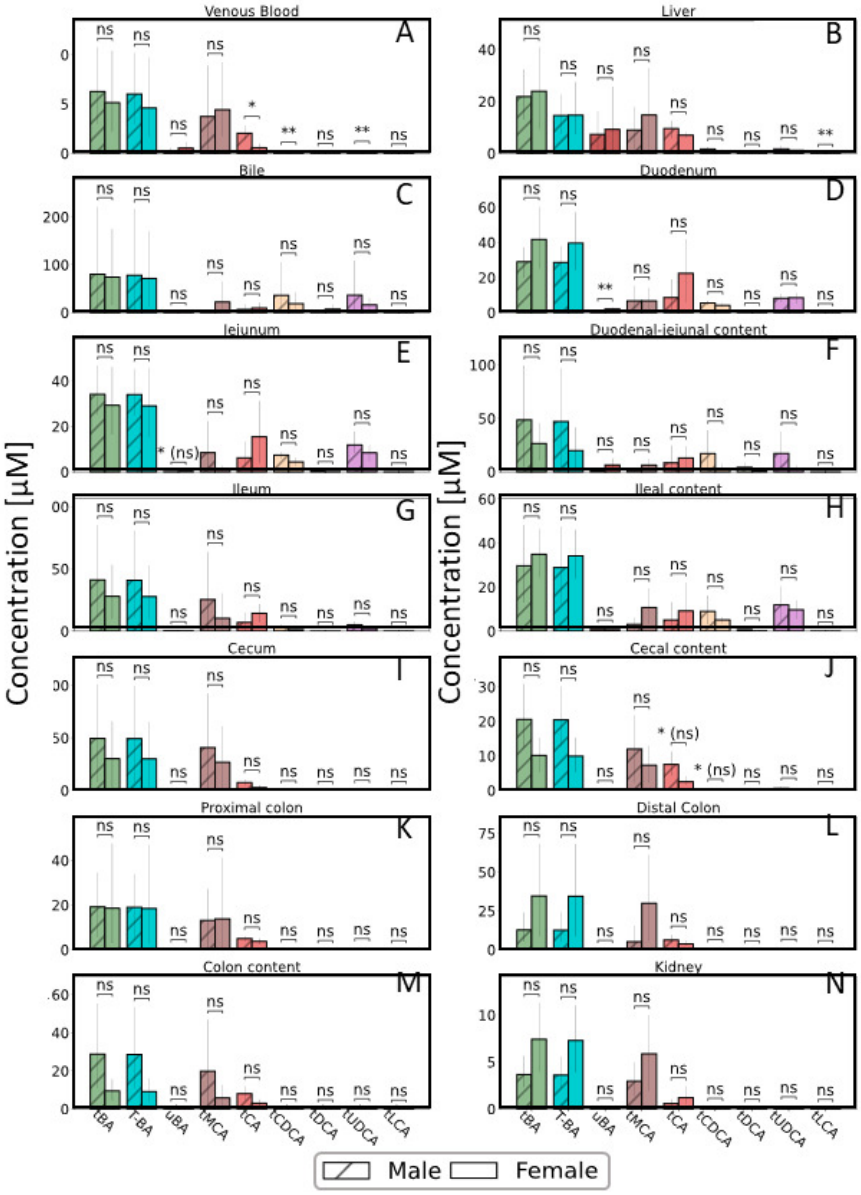

Figure A.1: Bile acid levels in GF mice. Concentration of total BAs (tBA), tauro-conjugated BAs (T-BA), unconjugated BA (uBA), total cholic acid (tCA), total muricholic acids (tMCA) and total chenodeoxycholic acid (tCDCA) in various organs in male and female GF mice (saturated coloration). Statistical differences were assessed by independent t-test. Statistical significance is marked with asterisks.

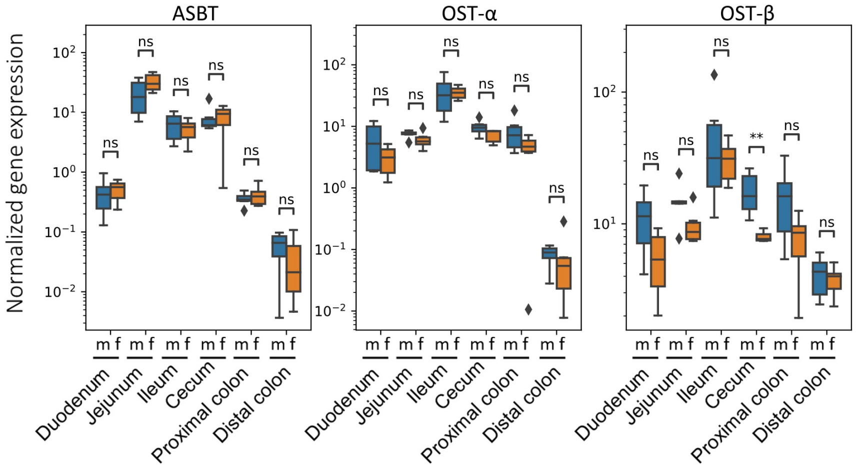

Figure A.2: Sex-related differences in intestinal BA transporter expression. Assessment of sex-related differences in the expression of the BA transporters ASBT, OST-α and OST-β (from left to right) along the gut axis in male and female GF mice measured by qPCR. Statistical significance was assessed by Mann-Whitney U-test and statistical significance is marked with asterisks.

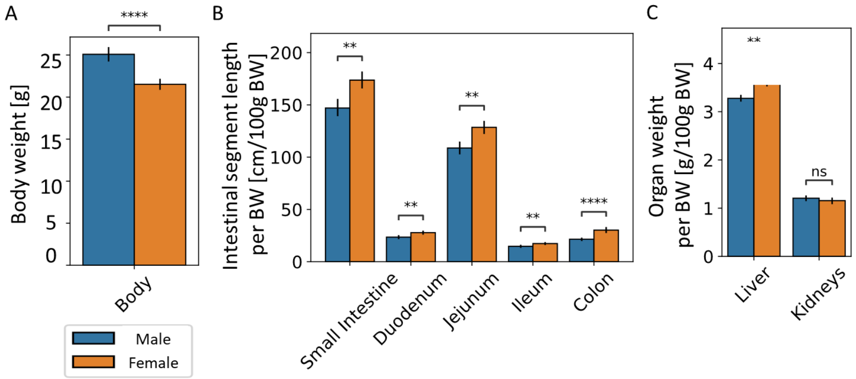

Figure A.3: Physiological differences between male and female GF mice. Assessment of sex-related differences in body weight (A), length of intestinal segments (B) as well as weight of the liver and the kidneys (C) in GF mice. Significant differences were tested by two-way, independent t-test and significance was marked with asterisks and (ns) indicates non-significance after correction for multiple testing using Benjamini-Hochberg correction.

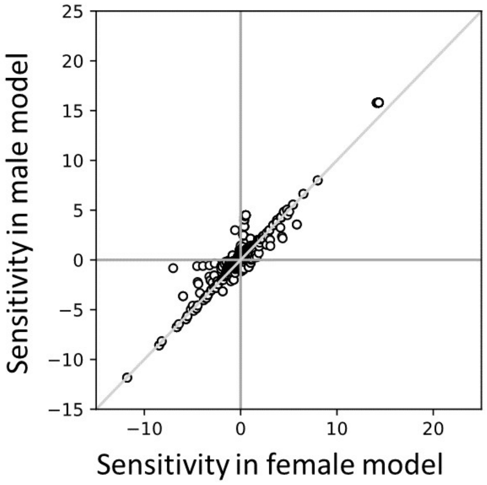

Figure A.4: Assessment of sensitivity coefficient in male and female 6BA mouse model]. Plotted are sensitivity coefficient of all parameters in the male and female 6BA model.]

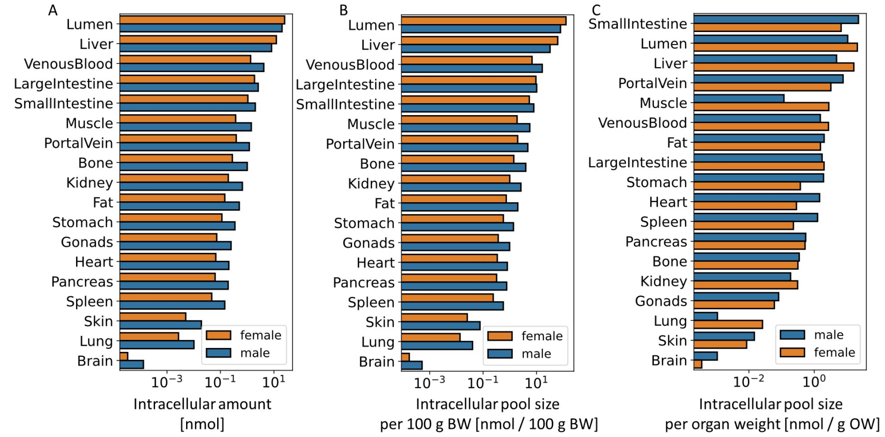

Figure A.5: Model based intracellular BA pool sizes at the whole body level. Simulated intracellular bile acid pool sizes as total levels (A), per 100g organ weight (B) and per organ weight (C) in different organs in male and female mice.

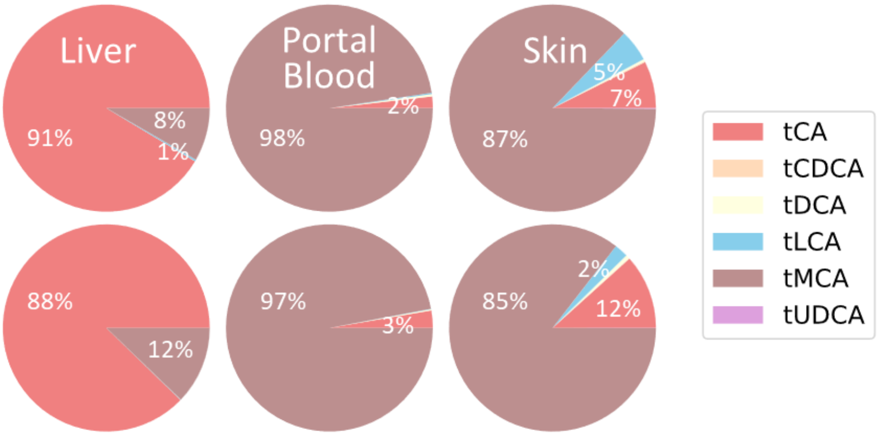

Figure A.6: Model based BA pool composition in various organs. Simulated bile acid composition in liver, portal blood plasma and skin in female mice (top row) and male mice (bottom row).

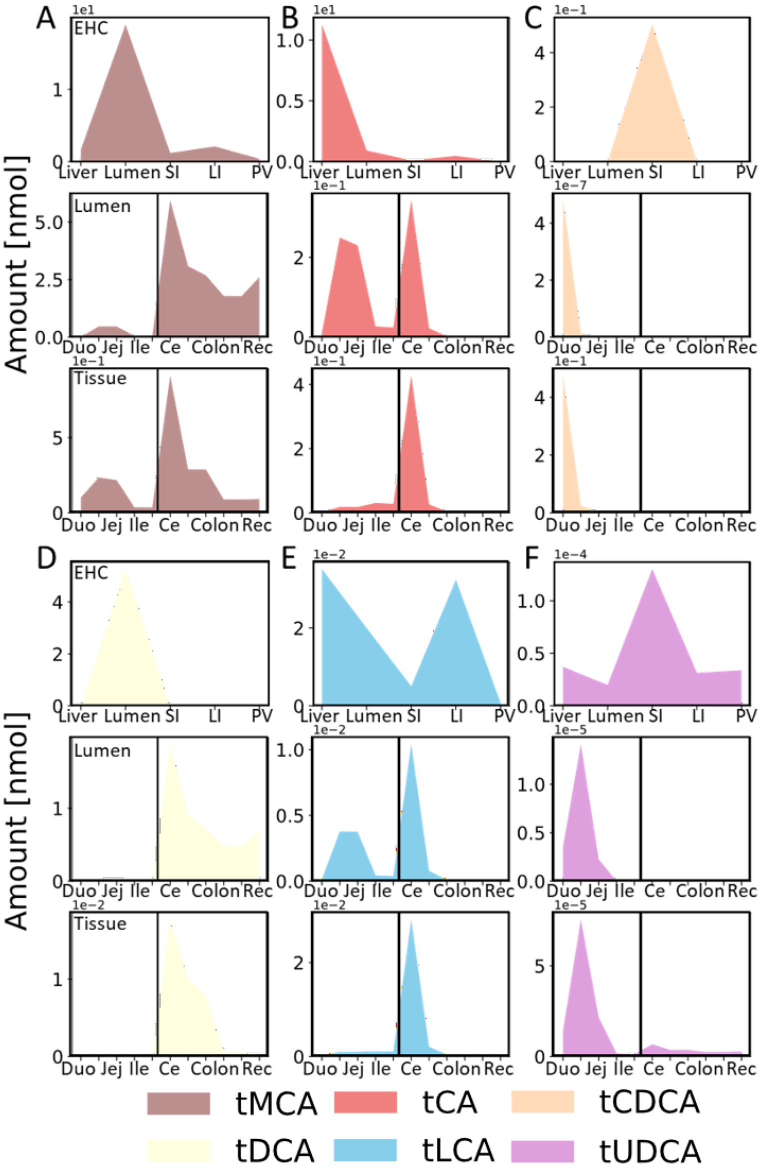

Figure A.7: Model based BA pool distribution and composition along the EHC and gut axis. Bile acid pools of total MCAs (A), total CA (B), total CDCA (C), total DCA (D), total LCA (E) and total UDCA (F) along the EHC and gut axis. For EHC axis, BA level and composition are shown in liver, the intestinal lumen, small and large intestinal tissue (SI and LI) as well as portal blood plasma (PV). Along the gut axis, duodenum (Duo), jejunum (Jej), ileum (Ile), cecum (Ce), proximal and distal colon (Colon) and rectum (Rec) are shown and the separation of SI and LI are indicated by a vertical black line.

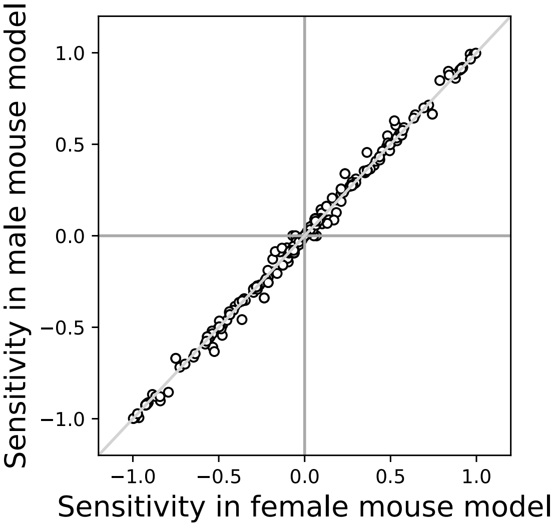

Figure A.8: Assessment of sensitivity coefficient in male and female murine conjugation model]. Plotted are sensitivity coefficient of all parameters in the male and female murine conjugation model.]

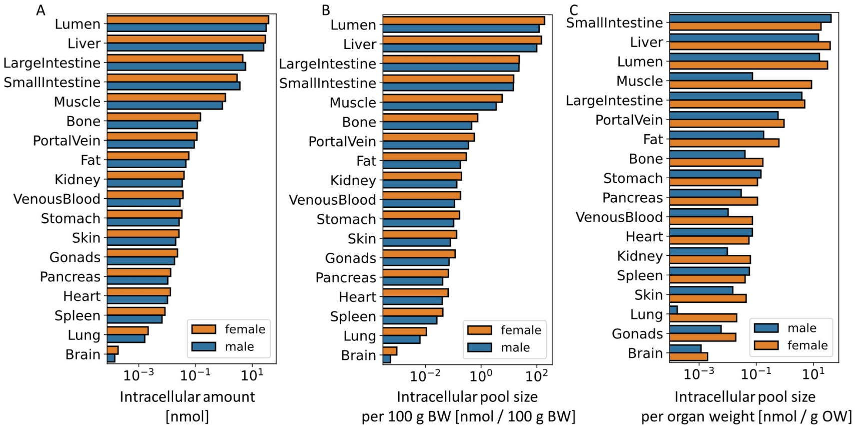

Figure A.9: Model based intracellular BA pool sizes at the whole body level. Simulated intracellular bile acid pool sizes as total levels (A), per 100g organ weight (B) and per organ weight (C) in different organs in male and female mice.

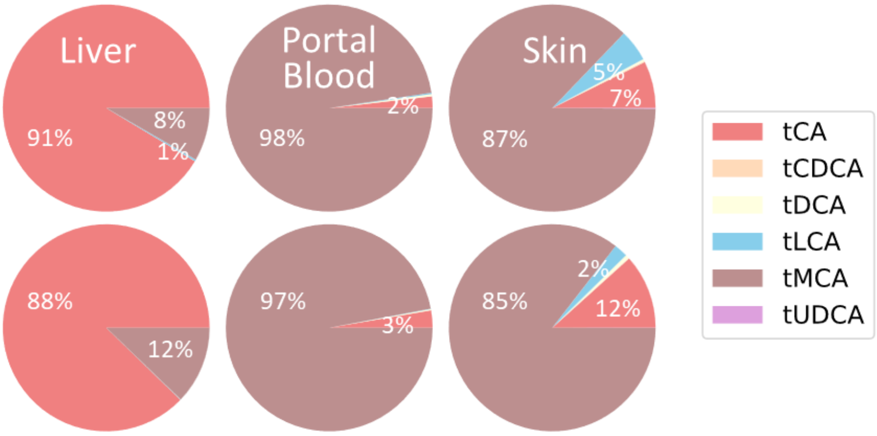

Figure A.10: Model based BA pool composition in various organs. Simulated bile acid composition in liver, portal blood plasma and skin in female mice (top row) and male mice (bottom row).

Table A.1: Fitted parameter values of enzymatic reactions in the 6BA model.

Parameter	Sex	Value	Unit
Synthesis rate (tCA)	f	2.3E-05	1/min
Synthesis rate (tCDCA)	f	9.6E-05	1/min
Synthesis rate (tCA)	m	9.0E-06	1/min
Synthesis rate (tCDCA)	m	8.1E-05	1/min
Renal Clearance (Km)	f+m	1.0E+05	μmol/l
Renal Clearance (TSmax)	f+m	9.3E+02	μmol/l/min
tCA → tDCA (Km)	f+m	4.4E+01	μmol/l
tCA → tDCA (vmax)	f+m	2.5E+00	μmol/l/min
tCDCA → tLCA (Km)	f+m	8.1E+03	μmol/l
tCDCA → tLCA (vmax)	f+m	1.5E+05	μmol/l/min
tCDCA → tMCA (Km)	f+m	5.0E+01	μmol/l
tCDCA → tMCA (vmax)	f+m	7.5E+03	μmol/l/min
tCDCA → tUDCA (Km)	f+m	3.7E+02	μmol/l
tCDCA → tUDCA (vmax)	f+m	2.9E+04	μmol/l/min
tDCA → tCA (Km)	f+m	2.5E+04	μmol/l
tDCA → tCA (vmax)	f+m	1.8E+05	μmol/l/min
tUDCA → tLCA (Km)	f+m	5.7E+04	μmol/l
tUDCA → tLCA (vmax)	f+m	3.8E+04	μmol/l/min
tUDCA → tMCA (Km)	f+m	2.7E+04	μmol/l
tUDCA → tMCA (vmax)	f+m	5.4E+03	μmol/l/min

Table A.2: Fitted parameter values of hepatic transport reactions in the 6BA model.

Parameter	Sex	Value	Unit
BSEP (tCA; Km)	f+m	1.0E+05	μmol/l
BSEP (tCDCA; Km)	f+m	1.6E+04	μmol/l
BSEP (tDCA; Km)	f+m	8.1E+04	μmol/l
BSEP (tLCA; Km)	f+m	4.9E+03	μmol/l
BSEP (tMCA; Km)	f+m	1.0E+05	μmol/l
BSEP (tUDCA; Km)	f+m	2.3E+04	μmol/l
BSEP (tCA; vmax)	f+m	1.7E+02	μmol/l/min
BSEP (tCDCA; vmax)	f+m	7.0E+02	μmol/l/min
BSEP (tDCA; vmax)	f+m	2.6E+04	μmol/l/min
BSEP (tLCA; vmax)	f+m	1.2E+02	μmol/l/min
BSEP (tMCA; vmax)	f+m	3.2E+03	μmol/l/min
BSEP (tUDCA; vmax)	f+m	9.0E+04	μmol/l/min

Continuation of table A.2

Parameter	Sex	Value	Unit
NTCP (tCA; Km)	f+m	9.5E+02	μmol/l
NTCP (tCDCA; Km)	f+m	1.2E+00	μmol/l
NTCP (tDCA; Km)	f+m	1.9E+03	μmol/l
NTCP (tLCA; Km)	f+m	3.2E+02	μmol/l
NTCP (tMCA; Km)	f+m	5.3E+02	μmol/l
NTCP (tUDCA; Km)	f+m	9.8E+04	μmol/l
NTCP (tCA; vmax)	f+m	1.7E+03	μmol/l/min
NTCP (tCDCA; vmax)	f+m	1.1E+00	μmol/l/min
NTCP (tDCA; vmax)	f+m	1.4E+05	μmol/l/min
NTCP (tLCA; vmax)	f+m	5.2E+02	μmol/l/min
NTCP (tMCA; vmax)	f+m	6.8E+00	μmol/l/min
NTCP (tUDCA; vmax)	f+m	1.1E+05	μmol/l/min
NTCP expression in male mice	m	1.0E-01	

Table A.3: Fitted parameter values of intestinal transport reactions in the 6BA model.

Parameter	Sex	Value	Unit
ASBT (tCA; Km)	f+m	5.7E+04	μmol/l
ASBT (tCDCA; Km)	f+m	1.2E+00	μmol/l
ASBT (tDCA; Km)	f+m	3.3E+04	μmol/l
ASBT (tLCA; Km)	f+m	7.3E+01	μmol/l
ASBT (tMCA; Km)	f+m	6.8E+02	μmol/l
ASBT (tUDCA; Km)	f+m	7.3E+03	μmol/l
ASBT (tCA; vmax)	f+m	2.2E+03	μmol/l/min
ASBT (tCDCA; vmax)	f+m	7.4E+03	μmol/l/min
ASBT (tDCA; vmax)	f+m	6.0E+01	μmol/l/min
ASBT (tLCA; vmax)	f+m	3.5E+00	μmol/l/min
ASBT (tMCA; vmax)	f+m	1.5E+00	μmol/l/min
ASBT (tUDCA; vmax)	f+m	2.3E+05	μmol/l/min
OSTα/β (tCA; Km)	f+m	8.9E+04	μmol/l
OSTα/β (tCDCA; Km)	f+m	2.4E+03	μmol/l
OSTα/β (tDCA; Km)	f+m	3.5E+04	μmol/l
OSTα/β (tLCA; Km)	f+m	5.1E+04	μmol/l
OSTα/β (tMCA; Km)	f+m	5.3E+04	μmol/l
OSTα/β (tUDCA; Km)	f+m	9.0E+04	μmol/l
OSTα/β (tCA; vmax)	f+m	3.7E+03	μmol/l/min

Continuation of table A.3

Parameter	Sex	Value	Unit
OSTα/β (tCDCA; vmax)	f+m	1.9E+00	μmol/l/min
OSTα/β (tDCA; vmax)	f+m	3.0E+04	μmol/l/min
OSTα/β (tLCA; vmax)	f+m	4.3E+03	μmol/l/min
OSTα/β (tMCA; vmax)	f+m	9.3E+02	μmol/l/min
OSTα/β (tUDCA; vmax)	f+m	1.4E+05	μmol/l/min

Table A.4: Sensitivity analysis of fitted 6BA model parameters on BA concentration in liver. Shown are only parameters with sensitivity coefficient above 1 or below -1.

Liver concentration [μM]	Parameter	Sensitivity coefficient female	male
tDCA	tDCA-ASBT-Vmax	1.18	1.19
tCA	CA synthesis	1.01	1.00
tUDCA	CDCA synthesis	1.00	0.49
tCDCA	CDCA synthesis	1.00	0.99
tCDCA	CDCA to MCA-Km	1.00	0.99
tCA	tCA-BSEP-Km	1.00	0.98
tDCA	CA synthesis	1.00	1.00
tCA	CA Synthesis-Sex-Scale		1.00
tMCA	CDCA synthesis	0.58	1.00
tUDCA	CDCA Synthesis-Sex-Scale		1.00
tDCA	CA Synthesis-Sex-Scale		1.00
tDCA	tDCA-ASBT-Km	-1.18	-1.20
tCDCA	CDCA to MCA-Vmax	-1.00	-1.00
tCA	tCA-BSEP-Vmax	-1.00	-0.99
tLCA	CDCA to MCA-Vmax	-0.98	-1.00
tLCA	tCDCA-BSEP-Km	-0.98	-1.00

Table A.5: Sensitivity analysis of fitted 6BA model parameters on BA concentration in venous blood plasma. Shown are only parameters with sensitivity coefficient above 1 or below -1.

VB concentration [μM]	Parameter	Sensitivity coefficient female	male
tDCA	tDCA-ASBT-Vmax	1.18	1.19
tCA	CA synthesis	1.02	1.01

Continuation of table A.5

VB concentration [μM]	Parameter	Sensitivity coefficient female	 male
tDCA	CA synthesis	1.00	1.00
tDCA	tDCA-NTCP-Km	0.99	1.00
tCDCA	tCDCA-NTCP-Km	0.99	0.93
tDCA	tDCA-ASBT-Vmax	1.18	1.19
tCA	CA synthesis	1.02	1.01
tCA	CA Synthesis-Sex-Scale		1.01
tUDCA	CDCA Synthesis-Sex-Scale		1.00
tDCA	CA synthesis	1.00	1.00
tDCA	CA Synthesis-Sex-Scale		1.00
tDCA	tDCA-NTCP-Km	0.99	1.00
tBA	BA-Renal clearance-TSmax	-0.99	-2.39
tDCA	tDCA-ASBT-Km	-1.18	-1.20
tLCA	tLCA-ASBT-Km	-1.11	-0.094
tDCA	tDCA-NTCP-Vmax	-1.00	-1.01
tCDCA	tCDCA-NTCP-Vmax	-1.00	-0.94
tDCA	tDCA-NTCP-Vmax	-1.00	-1.01
tLCA	CDCA to MCA-Vmax	-0.98	-1.00
tLCA	tCDCA-BSEP-Km	-0.98	-1.00

Table A.6: Sensitivity analysis of fitted 6BA model parameters on BA concentration in kidney. Shown are only parameters with sensitivity coefficient above 1 or below -1.

Kidney concentration [μM]	Parameter	Sensitivity coefficient female	 male
tDCA	tDCA-ASBT-Vmax	1.18	1.19
tCA	CA synthesis	1.02	1.01
tMCA	tMCA-ASBT-Vmax	1.01	1.00
tUDCA	CDCA synthesis	1.00	1.00
tUDCA	tCDCA-BSEP-Vmax	1.00	1.00
tUDCA	CDCA to MCA-Km	1.00	1.00
tDCA	CA synthesis	1.00	1.00
tCA	CA Synthesis-Sex-Scale		1.01
tUDCA	CDCA Synthesis-Sex-Scale		1.00
tDCA	CA Synthesis-Sex-Scale		1.00
tDCA	tDCA-NTCP-Km	0.99	1.00
tDCA	tDCA-ASBT-Km	-1.18	-1.20
tBA	BA-Renal clearance-TSmax	-1.00	-2.40

Continuation of table A.6

Kidney concentration [μM]	Parameter	Sensitivity coefficient female	 male
tUDCA	CDCA to MCA-Vmax	-1.00	-1.01
tUDCA	tCDCA-BSEP-Km	-1.00	-1.01
tDCA	tDCA-NTCP-Vmax	-1.00	-1.01
tCDCA	tCDCA-NTCP-Vmax	-1.00	-0.94

Table A.7: Sensitivity analysis of fitted 6BA model parameters on BA concentration in SI content. Shown are only parameters with sensitivity coefficient above 1 or below -1.

SI content concentration [μM]	Parameter	Sensitivity coefficient female	 male
Ile-CDCA	tCDCA-ASBT-Km	3.37	3.52
Ile-UDCA	tUDCA-ASBT-Km	1.80	2.01
DuoJej-LCA	tLCA-ASBT-Vmax	1.09	0.08
Ile-CA	CA synthesis	1.01	1.00
DuoJej-CA	CA synthesis	1.01	1.00
Ile-DCA	CA synthesis	1.00	1.00
DuoJej-DCA	CA synthesis	1.00	1.00
Ile-CDCA	CDCA synthesis	1.00	1.00
DuoJej-CDCA	CDCA synthesis	1.00	1.00
DuoJej-CDCA	tCDCA-BSEP-Vmax	1.00	1.00
DuoJej-CDCA	CDCA to MCA-Km	1.00	1.00
Ile-CDCA	tCDCA-BSEP-Vmax	1.00	1.00
Ile-CDCA	CDCA to MCA-Km	1.00	1.00
Ile-UDCA	CDCA synthesis	1.00	1.00
DuoJej-UDCA	CDCA synthesis	1.00	1.00
Ile-UDCA	tCDCA-BSEP-Vmax	1.00	1.00
Ile-UDCA	CDCA to MCA-Km	1.00	1.00
DuoJej-UDCA	tCDCA-BSEP-Vmax	1.00	1.00
DuoJej-UDCA	CDCA to MCA-Km	1.00	1.00
DuoJej-LCA	NTCP-Sex-Scale		1.03
Ile-LCA	NTCP-Sex-Scale		1.03
Ile-CA	CA Synthesis-Sex-Scale		1.00
DuoJej-CA	CA Synthesis-Sex-Scale		1.00
Ile-DCA	CA Synthesis-Sex-Scale		1.00
Ile-CDCA	CDCA Synthesis-Sex-Scale		1.00
DuoJej-CDCA	CDCA Synthesis-Sex-Scale		1.00
DuoJej-DCA	CA Synthesis-Sex-Scale		1.00

Continuation of table A.7

SI content concentration [μM]	Parameter	Sensitivity coefficient female	 male
Ile-UDCA	CDCA Synthesis-Sex-Scale		1.00
DuoJej-UDCA	CDCA Synthesis-Sex-Scale		1.00
Ile-CDCA	tCDCA-ASBT-Vmax	-3.41	-3.61
Ile-UDCA	tUDCA-ASBT-Vmax	-1.81	-2.04
DuoJej-LCA	tLCA-ASBT-Km	-1.09	-0.08
Ile-CDCA	CDCA to MCA-Vmax	-1.00	-1.01
DuoJej-CDCA	CDCA to MCA-Vmax	-1.00	-1.01
DuoJej-CDCA	tCDCA-BSEP-Km	-1.00	-1.01
Ile-CDCA	tCDCA-BSEP-Km	-1.00	-1.01
Ile-UDCA	CDCA to MCA-Vmax	-1.00	-1.01
DuoJej-UDCA	CDCA to MCA-Vmax	-1.00	-1.01
Ile-UDCA	tCDCA-BSEP-Km	-1.00	-1.01
DuoJej-UDCA	tCDCA-BSEP-Km	-1.00	-1.01
Ile-LCA	CDCA to MCA-Vmax	-0.98	-1.00
Ile-LCA	tCDCA-BSEP-Km	-0.98	-1.00
DuoJej-LCA	CDCA to MCA-Vmax	-0.98	-1.00
DuoJej-LCA	tCDCA-BSEP-Km	-0.98	-1.00

Table A.8: Sensitivity analysis of fitted 6BA model parameters on BA concentration in SI tissue. Shown are only parameters with sensitivity coefficient above 1 or below -1.

SI tissue concentration [μM]	Parameter	Sensitivity coefficient female	 male
Ileum-LCA	tLCA-ASBT-Vmax	1.9	0.7
Ileum-DCA	tDCA-ASBT-Vmax	1.5	1.3
Jejunum-CA	tCA-ASBT-Vmax	1.3	1.0
Ileum-CA	tCA-ASBT-Vmax	1.3	1.2
Duodenum-UDCA	tUDCA-ASBT-Vmax	1.2	0.8
Duodenum-DCA	tDCA-ASBT-Vmax	1.2	1.2
Jejunum-DCA	tDCA-ASBT-Vmax	1.2	1.2
Ileum-MCA	tMCA-ASBT-Vmax	1.0	1.0
Duodenum-CA	CA synthesis	1.0	1.0
Jejunum-CA	CA synthesis	1.0	1.0
Ileum-CA	CA synthesis	1.0	1.0
Ileum-DCA	CA synthesis	1.0	1.0
Jejunum-CDCA	CDCA synthesis	1.0	1.0
Jejunum-CDCA	CDCA to MCA-Km	1.0	1.0

Continuation of table A.8

SI tissue concentration [μM]	Parameter	Sensitivity coefficient female	male
Jejunum-CDCA	tCDCA-BSEP-Vmax	1.0	1.0
Jejunum-MCA	tMCA-ASBT-Vmax	1.0	1.0
Jejunum-DCA	CA synthesis	1.0	1.0
Duodenum-DCA	CA synthesis	1.0	1.0
Duodenum-MCA	tMCA-ASBT-Vmax	1.0	1.0
Duodenum-CA	CA Synthesis-Sex-Scale		1.0
Jejunum-CA	CA Synthesis-Sex-Scale		1.0
Ileum-CA	CA Synthesis-Sex-Scale		1.0
Jejunum-CDCA	CDCA Synthesis-Sex-Scale		1.0
Ileum-DCA	CA Synthesis-Sex-Scale		1.0
Jejunum-DCA	CA Synthesis-Sex-Scale		1.0
Duodenum-DCA	CA Synthesis-Sex-Scale		1.0
Ileum-LCA	tLCA-ASBT-Km	-1.9	-0.7
Ileum-DCA	tDCA-ASBT-Km	-1.5	-1.4
Jejunum-CA	tCA-ASBT-Km	-1.3	-1.0
Ileum-CA	tCA-ASBT-Km	-1.3	-1.2
Duodenum-UDCA	tUDCA-ASBT-Km	-1.2	-0.8
Duodenum-DCA	tDCA-ASBT-Km	-1.2	-1.2
Jejunum-DCA	tDCA-ASBT-Km	-1.2	-1.2
Jejunum-CDCA	CDCA to MCA-Vmax	-1.0	-1.0
Jejunum-CDCA	tCDCA-BSEP-Km	-1.0	-1.0
Duodenum-DCA	tDCA-NTCP-Vmax	-1.0	-1.0
Ileum-LCA	CDCA to MCA-Vmax	-1.0	-1.0
Ileum-LCA	tCDCA-BSEP-Km	-1.0	-1.0
Jejunum-LCA	CDCA to MCA-Vmax	-1.0	-1.0
Jejunum-LCA	tCDCA-BSEP-Km	-1.0	-1.0
Duodenum-LCA	CDCA to MCA-Vmax	-1.0	-1.0
Duodenum-LCA	tCDCA-BSEP-Km	-1.0	-1.0

Table A.9: Sensitivity analysis of fitted 6BA model parameters on BA concentration in cecal content. Shown are only parameters with sensitivity coefficient above 1 or below -1.

Cecal content concentration [μM]	Parameter	Sensitivity coefficient female	male
tCDCA	tCDCA-ASBT-Km	5.44	5.76
tUDCA	tUDCA-ASBT-Km	3.78	4.07
tCA	CA to DCA-Km	1.15	1.09

Continuation of table A.9

Cecal content concentration [μM]	Parameter	Sensitivity coefficient female	male
tCA	CA synthesis	1.03	1.01
tCDCA	CDCA synthesis	1.00	1.00
tCDCA	tCDCA-BSEP-Vmax	1.00	1.00
tCDCA	CDCA to MCA-Km	1.00	1.00
tUDCA	CDCA synthesis	1.00	1.00
tUDCA	tCDCA-BSEP-Vmax	1.00	1.00
tUDCA	CDCA to MCA-Km	1.00	1.00
tUDCA	UDCA to LCA-Km	1.00	0.82
tDCA	CA synthesis	1.00	1.00
tLCA	NTCP-Sex-Scale		1.03
tMCA	CDCA synthesis	0.88	1.03
tMCA	CDCA Synthesis-Sex-Scale		1.03
tCA	CA Synthesis-Sex-Scale		1.01
tCDCA	CDCA Synthesis-Sex-Scale		1.00
tUDCA	CDCA Synthesis-Sex-Scale		1.00
tDCA	CA Synthesis-Sex-Scale		1.00
tCDCA	tCDCA-ASBT-Vmax	-5.52	-6.00
tUDCA	tUDCA-ASBT-Vmax	-3.82	-4.19
tCA	CA to DCA-Vmax	-1.18	-1.12
tLCA	CDCA to MCA-Vmax	-1.00	-1.01
tMCA	tCDCA-BSEP-Km	-1.00	-1.01
tMCA	CDCA to MCA-Vmax	-1.00	-1.01
tCA	tCDCA-BSEP-Km	-1.00	-1.01
tCA	UDCA to LCA-Vmax	-1.00	-0.83
tCDCA	CDCA to MCA-Vmax	-0.99	-1.00
tCDCA	tCDCA-BSEP-Km	-0.99	-1.00

Table A.10: Sensitivity analysis of fitted 6BA model parameters on BA concentration in cecal tissue. Shown are only parameters with sensitivity coefficient above 1 or below -1.

Cecal tissue concentration [μM]	Parameter	Sensitivity coefficient female	male
tDCA	tDCA-ASBT-Vmax	1.40	1.44
tCA	CA to DCA-Km	1.15	1.08
tCA	CA synthesis	1.03	1.01
tMCA	tMCA-ASBT-Vmax	1.00	1.00
tDCA	CA synthesis	1.00	1.00

Continuation of table A.10

Cecal tissue concentration [μM]	Parameter	Sensitivity coefficient female	Sensitivity coefficient male
tCA	CA Synthesis-Sex-Scale		1.01
tDCA	CA Synthesis-Sex-Scale		1.00
tDCA	tDCA-ASBT-Km	-1.41	-1.46
tCA	CA to DCA-Vmax	-1.18	-1.10
tCDCA	tCDCA-NTCP-Vmax	-1.00	-0.94
tLCA	CDCA to MCA-Vmax	-0.98	-1.00
tLCA	tCDCA-BSEP-Km	-0.98	-1.00

Table A.11: Sensitivity analysis of fitted 6BA model parameters on BA concentration in LI content. Shown are only parameters with sensitivity coefficient above 1 or below -1.

LI content concentration [μM]	Parameter	Sensitivity coefficient female	Sensitivity coefficient male
tCDCA	tCDCA-ASBT-Km	6.51	7.00
tUDCA	tUDCA-ASBT-Km	4.81	5.19
tCA	CA to DCA-Km	1.49	1.38
tMCA	CDCA synthesis	1.10	1.43
tCA	CA synthesis	1.03	1.01
tLCA	tLCA-ASBT-Km	1.02	2.13
tUDCA	UDCA to LCA-Km	1.01	0.83
tCDCA	CDCA synthesis	1.00	1.00
tCDCA	tCDCA-BSEP-Vmax	1.00	1.00
tCDCA	CDCA to MCA-Km	1.00	1.00
tDCA	CA synthesis	1.00	1.00
tUDCA	CDCA synthesis	1.00	1.00
tUDCA	tCDCA-BSEP-Vmax	1.00	1.00
tUDCA	CDCA to MCA-Km	1.00	1.00
tMCA	CDCA Synthesis-Sex-Scale		1.43
tLCA	NTCP-Sex-Scale		1.03
tCA	CA Synthesis-Sex-Scale		1.01
tCDCA	CDCA Synthesis-Sex-Scale		1.00
tUDCA	CDCA Synthesis-Sex-Scale		1.00
tDCA	CA Synthesis-Sex-Scale		1.00
tCDCA	tCDCA-ASBT-Vmax	-6.63	-7.36
tUDCA	tUDCA-ASBT-Vmax	-4.88	-5.39
tCA	CA to DCA-Vmax	-1.53	-1.41
tLCA	tLCA-ASBT-Vmax	-1.02	-2.17

Continuation of table A.11

LI content concentration [μM]	Parameter	Sensitivity coefficient female	male
tUDCA	UDCA to LCA-Vmax	-1.01	-0.83
tCDCA	CDCA to MCA-Vmax	-1.00	-1.01
tCDCA	tCDCA-BSEP-Km	-1.00	-1.01
tUDCA	CDCA to MCA-Vmax	-1.00	-1.01
tUDCA	tCDCA-BSEP-Km	-1.00	-1.01
tLCA	CDCA to MCA-Vmax	-0.99	-1.00
tLCA	tCDCA-BSEP-Km	-0.99	-1.00

Table A.12: Sensitivity analysis of fitted 6BA model parameters on BA concentration in LI tissue. Shown are only parameters with sensitivity coefficient above 1 or below -1.

LI tissue concentration [μM]	Parameter	Sensitivity coefficient female	male
Proximal-DCA	tDCA-ASBT-Vmax	1.12	1.10
Distal-CA	CA synthesis	1.02	1.01
Proximal-MCA	tMCA-ASBT-Vmax	1.00	1.00
Proximal-DCA	CA synthesis	1.00	1.00
Proximal-CA	CA Synthesis-Sex-Scale		1.01
Distal-CA	CA Synthesis-Sex-Scale		1.01
Proximal-MCA	tMCA-ASBT-Vmax	1.00	1.00
Distal-DCA	CA Synthesis-Sex-Scale		1.00
Proximal-DCA	CA Synthesis-Sex-Scale		1.00
Proximal-DCA	tDCA-ASBT-Km	-1.12	-1.11
Proximal-CDCA	tCDCA-NTCP-Vmax	-1.00	-0.94
Proximal-LCA	CDCA to MCA-Vmax	-0.98	-1.00
Proximal-LCA	tCDCA-BSEP-Km	-0.98	-1.00

Table A.13: Fitted parameter values of enzymatic reactions in the murine conjugation model.

Parameter	Sex	Value	Unit
Parameter	Sex	Value	Unit
Synthesis rate (uBA)	1.39E-04	f	μmol/min
Synthesis rate (uBA)	1.14E-04	m	μmol/min
Renal Clearance (Km)	9.68E+04	f+m	μmol/l

Continuation of table A.13

Parameter	Sex	Value	Unit
Renal Clearance (TSmax)	3.41E+03	f+m	μmol/l/min
BAAT (Km)	8.22E+03	f+m	μmol/l
BAAT (vmax)	1.97E+01	f+m	μmol/l/min
BSH (Km)	9.99E+04	f+m	μmol/l
BSH (vmax)	1.00E+00	f+m	μmol/l/min

Table A.14: Fitted parameter values of transport reactions in the murine conjugation model.

Parameter	Sex	Value	Unit
ASBT (T-BA; Km)	f+m	2.33E+03	μmol/l
ASBT (uBA; Km)	f+m	7.11E+02	μmol/l
ASBT (T-BA; vmax)	f+m	1.00E+00	μmol/l/min
ASBT (uBA; vmax)	f+m	8.05E+00	μmol/l/min
	f+m		
BSEP (T-BA; Km)	f+m	9.99E+04	μmol/l
BSEP (uBA; Km)	f+m	2.55E+03	μmol/l
BSEP (T-BA; vmax)	f+m	1.26E+01	μmol/l/min
BSEP (uBA; vmax)	f+m	7.05E+01	μmol/l/min
	f+m		
NTCP (T-BA; Km)	f+m	5.86E+04	μmol/l
NTCP (uBA; Km)	f+m	1.08E+04	μmol/l
NTCP (T-BA; vmax)	f+m	3.35E+03	μmol/l/min
NTCP (uBA; vmax)	f+m	1.07E+04	μmol/l/min
NTCP expression in male mice	f+m	1.00E+00	
	f+m		
OSTα/β (T-BA; Km)	f+m	9.43E+04	μmol/l
OSTα/β (uBA; Km)	f+m	1.00E+05	μmol/l
OSTα/β (T-BA; vmax)	f+m	9.12E+01	μmol/l/min
OSTα/β (uBA; vmax)	f+m	2.28E+02	μmol/l/min

Table A.15: Sensitivity analysis of fitted murine conjugation model parameters on BA concentration in liver. Shown are only parameters with sensitivity coefficient above 0.5 or below -0.5.

Liver concentration [μM]	Parameter	Sensitivity coefficient	
		female	male
T-BA	uBA-BAAT Vmax	0.919609862	0.919472571
T-BA	uBA BSEP Km	0.912810122	0.913221725
uBA	uBA BSEP Km	0.912215743	0.91182683
T-BA	T-BA BSEP Km	0.635415636	0.642836723
T-BA	T-BA BSEP Vmax	-0.637277851	-0.644624627
uBA	uBA BSEP Vmax	-0.920326323	-0.919161699
T-BA	uBA BSEP Vmax	-0.920913501	-0.920555714
T-BA	uBA-BAAT Km	-0.925181209	-0.925284133

Table A.16: Sensitivity analysis of fitted murine conjugation model parameters on BA concentration in venous blood plasma. Shown are only parameters with sensitivity coefficient above 0.5 or below -0.5.

VB concentration [μM]	Parameter	Sensitivity coefficient	
		female	male
uBA	uBA NTCP Km	0.965485112	0.96558581
T-BA	uBA-BAAT Vmax	0.918876881	0.91868531
T-BA	uBA BSEP Km	0.912082105	0.912439818
uBA	uBA BSEP Km	0.743643648	0.664566457
T-BA	T-BA BSEP Km	0.56495344	0.550169731
T-BA	T-BA Renal Clearances Km	0.557338173	0.561979077
T-BA	T-BA Renal Clearances TSmax	-0.557972828	-0.56266015
T-BA	T-BA BSEP Vmax	-0.566607809	-0.551697884
uBA	uBA BSEP Vmax	-0.750255739	-0.669912242
T-BA	uBA BSEP Vmax	-0.920168483	-0.919756047
T-BA	uBA-BAAT Km	-0.92443272	-0.924480647
uBA	uBA NTCP Vmax	-0.972722698	-0.972823839

Table A.17: Sensitivity analysis of fitted murine conjugation model parameters on BA concentration in kidney. Shown are only parameters with sensitivity coefficient above 0.5 or below -0.5.

Kidney concentration [μM]	Parameter	Sensitivity coefficient	
		female	male
uBA	uBA NTCP Km	0.96548498	0.96558579
T-BA	uBA-BAAT Vmax	0.91887657	0.91868551
T-BA	uBA BSEP Km	0.91208236	0.91243983
uBA	uBA BSEP Km	0.74364386	0.66456654
T-BA	T-BA Renal Clearances Km	0.57087593	0.57551654
T-BA	T-BA BSEP Km	0.56495346	0.55016956
T-BA	T-BA BSEP Vmax	-0.56660772	-0.551698
T-BA	T-BA Renal Clearances TSmax	-0.57152612	-0.57621399
uBA	uBA BSEP Vmax	-0.75025557	-0.66991217
T-BA	uBA BSEP Vmax	-0.92016856	-0.91975621
T-BA	uBA-BAAT Km	-0.92443281	-0.92448088
uBA	uBA NTCP Vmax	-0.97272251	-0.97282404

Table A.18: Sensitivity analysis of fitted murine conjugation model parameters on BA concentration in small intestinal content. Shown are only parameters with sensitivity coefficient above 0.5 or below -0.5.

SI content concentration [μM]	Parameter	Sensitivity coefficient	
		female	male
Ile T-BA	uBA-BAAT Vmax	0.91891807	0.91902871
DuoJej T-BA	uBA-BAAT Vmax	0.91891744	0.91902843
Ile T-BA	uBA BSEP Km	0.91212336	0.9127811
DuoJej T-BA	uBA BSEP Km	0.91212297	0.9127808
DuoJej T-BA	uBA BSEP Vmax	-0.92020995	-0.92010448
Ile T-BA	uBA BSEP Vmax	-0.92021027	-0.92010492
DuoJej T-BA	uBA-BAAT Km	-0.9244743	-0.92483096
Ile T-BA	uBA-BAAT Km	-0.92447501	-0.92483128

Table A.19: Sensitivity analysis of fitted murine conjugation model parameters on BA concentration in small intestinal tissue. Shown are only parameters with sensitivity coefficient above 0.5 or below -0.5.

SI tissue concentration [μM]	Parameter	Sensitivity coefficient	
		female	male
Ileum uBA	uBA ASBT Vmax	0.99671057	0.99807526
Duodenum T-BA	uBA-BAAT Vmax	0.91887945	0.9186988
Jejunum T-BA	uBA-BAAT Vmax	0.91887429	0.91871117
Ileum T-BA	uBA-BAAT Vmax	0.91880422	0.91876793
Duodenum T-BA	uBA BSEP Km	0.91207367	0.91244197
Jejunum T-BA	uBA BSEP Km	0.91206906	0.9124549
Ileum T-BA	uBA BSEP Km	0.9120036	0.91251598
Jejunum uBA	uBA ASBT Vmax	0.84126341	0.87801384
Jejunum uBA	uBA OSTβ Km	0.57772836	0.5911611
Duodenum T-BA	T-BA Renal Clearances Km	0.54879041	0.55194549
Duodenum T-BA	T-BA BSEP Km	0.53721522	0.51897586
Jejunum T-BA	T-BA Renal Clearances Km	0.53594216	0.5346275
Ileum T-BA	T-BA ASBT Vmax	0.52243226	0.62857942
Ileum T-BA	T-BA ASBT Km	-0.52568274	-0.63285092
Jejunum T-BA	T-BA Renal Clearances TSmax	-0.53655052	-0.53527379
Duodenum T-BA	T-BA BSEP Vmax	-0.53878415	-0.52041348
Duodenum T-BA	T-BA Renal Clearances TSmax	-0.54941306	-0.55261217
Jejunum uBA	uBA OSTβ Vmax	-0.57873136	-0.59222135
Jejunum uBA	uBA ASBT Km	-0.84212791	-0.87891573
Ileum T-BA	uBA BSEP Vmax	-0.92008768	-0.91983386
Jejunum T-BA	uBA BSEP Vmax	-0.92015502	-0.91977114
Duodenum T-BA	uBA BSEP Vmax	-0.92015959	-0.91975801
Ileum T-BA	uBA-BAAT Km	-0.92435884	-0.92456485
Jejunum T-BA	uBA-BAAT Km	-0.92443033	-0.9245068
Duodenum T-BA	uBA-BAAT Km	-0.92443552	-0.92449436
Ileum uBA	uBA ASBT Km	-0.9971321	-0.99849745

Table A.20: Sensitivity analysis of fitted murine conjugation model parameters on BA concentration in cecal content. Shown are only parameters with sensitivity coefficient above 0.5 or below -0.5.

Cecal content concentration [μM]	Parameter	Sensitivity coefficient	
		female	male
T-BA	uBA-BAAT Vmax	0.919087556	0.91921555
T-BA	uBA BSEP Km	0.912291782	0.912966678
T-BA	uBA BSEP Vmax	-0.920382679	-0.920294761
T-BA	uBA-BAAT Km	-0.924648057	-0.925022125

Table A.21: Sensitivity analysis of fitted murine conjugation model parameters on BA concentration in cecal tissue. Shown are only parameters with sensitivity coefficient above 0.5 or below -0.5.

Cecal tissue concentration [μM]	Parameter	Sensitivity coefficient	
		female	male
uBA	uBA ASBT Vmax	0.99302578	0.99591704
T-BA	T-BA ASBT Vmax	0.96337591	0.99231732
T-BA	uBA-BAAT Vmax	0.91332632	0.91408734
T-BA	uBA BSEP Km	0.90657367	0.90787403
uBA	uBA OSTα Km	0.50517871	0.50749406
uBA	uBA OSTα Vmax	-0.50534596	-0.50766965
T-BA	uBA BSEP Vmax	-0.91452991	-0.91508598
T-BA	uBA-BAAT Km	-0.9187672	-0.91978606
T-BA	T-BA ASBT Km	-0.96441579	-0.99440753
uBA	uBA ASBT Km	-0.99574797	-0.99864705

Table A.22: Sensitivity analysis of fitted murine conjugation model parameters on BA concentration in LI content. Shown are only parameters with sensitivity coefficient above 0.5 or below -0.5.

LI content concentration [μM]	Parameter	Sensitivity coefficient	
		female	male
T-BA	uBA-BAAT Vmax	0.92031984	0.92053167
T-BA	uBA BSEP Km	0.91351417	0.91427338
T-BA	uBA BSEP Vmax	-0.92163393	-0.92163115
T-BA	uBA-BAAT Km	-0.92590535	-0.92636554

Table A.23: Sensitivity analysis of fitted murine conjugation model parameters on BA concentration in LI tissue. Shown are only parameters with sensitivity coefficient above 0.5 or below -0.5.

LI tissue concentration [μM]	Parameter	Sensitivity coefficient	
		female	male
Proximal uBA	uBA ASBT Vmax	0.98510713	0.99174305
Distal T-BA	uBA-BAAT Vmax	0.91443827	0.91469705
Proximal T-BA	uBA-BAAT Vmax	0.90917498	0.91076732
Distal T-BA	uBA BSEP Km	0.90767594	0.90847816
Proximal T-BA	uBA BSEP Km	0.90245418	0.90457744
Proximal T-BA	T-BA ASBT Vmax	0.87278586	0.8824621
Distal uBA	uBA ASBT Vmax	0.83684662	0.89899864
Distal uBA	uBA OSTβ Km	0.78684859	0.84860091
Proximal uBA	uBA OSTβ Km	0.69376589	0.69898941
Proximal T-BA	T-BA OSTβ Km	0.6439478	0.66130051
Distal T-BA	T-BA OSTβ Km	0.53034578	0.60405653
Distal T-BA	T-BA OSTβ Vmax	-0.5345481	-0.60884332
Proximal T-BA	T-BA OSTβ Vmax	-0.6462328	-0.66362974
Proximal uBA	uBA OSTβ Vmax	-0.69623925	-0.70148561
Distal uBA	uBA OSTβ Vmax	-0.79285086	-0.85513183
Distal uBA	uBA ASBT Km	-0.84009697	-0.90249969
Proximal T-BA	T-BA ASBT Km	-0.86726104	-0.87845909
Proximal T-BA	uBA BSEP Vmax	-0.91031379	-0.91171512
Proximal T-BA	uBA-BAAT Km	-0.91453056	-0.91639673
Distal T-BA	uBA BSEP Vmax	-0.91565839	-0.91570411
Distal T-BA	uBA-BAAT Km	-0.9199024	-0.92040857
Proximal uBA	uBA ASBT Km	-0.9878937	-0.99454896

Appendix B

A physiologically-based model of bile acid metabolism in human

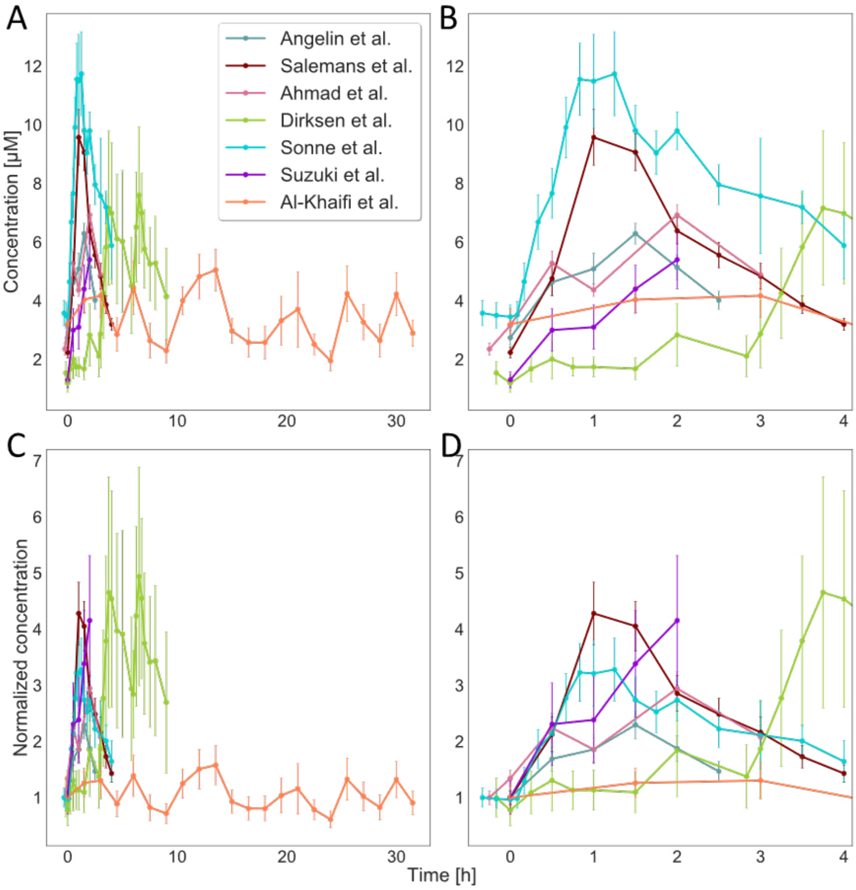

Figure B.1: Data of postprandial responses in venous blood. Postprandial responses in venous blood plasma used for model development. Displayed are the profiles as taken from literature (A), only for the first meal response (B) and corresponding profiles normalized to the initial time point (C and D). Errors bars represent the SD. Data was taken from [326; 327; 355; 356; 357; 358; 359]

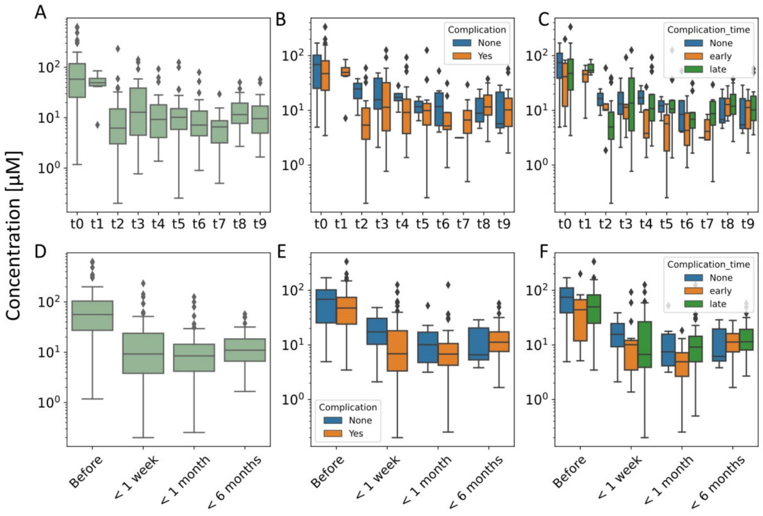

Figure B.2: Overview of total bile acid levels in patients undergoing liver transplantation. Boxplots showing the levels of total BA in patients undergoing liver transplantation (LTX) over time with all provided time points (A-C) and with simplifying the number of time points (D-F). BA levels are further stratified if patients showed any form of complication (B,E) and when complications occurred (C, F). Time points used: t0: before LTX; t1: day of LTX; t2: post operation day (POD) 1; t3: POD3; t4: POD7; t5: POD14; t6: POD21; t7: POD28; t8: 3 months; t9: 6 months.

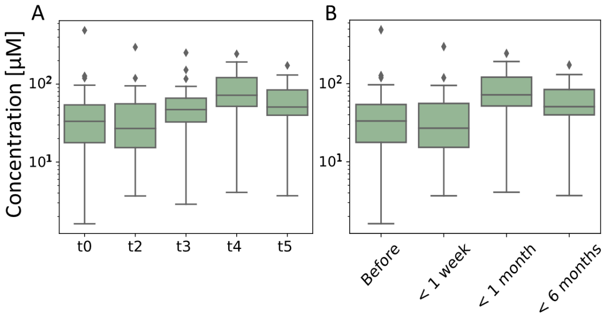

Figure B.3: Overview of total bile acid levels in patients undergoing transjugular intrahepatic portosystemic shunt. Boxplots showing the levels of total BA in patients undergoing transjugular intrahepatic portosystemic shunt (TIPS) over time with all provided time points (A) and with simplifying the number of time points (B). Time points used: t0: before TIPS; t1: day of TIPS; t2: post operation day (POD) 1; t3: POD5; t4: POD28; t5: 3 months.

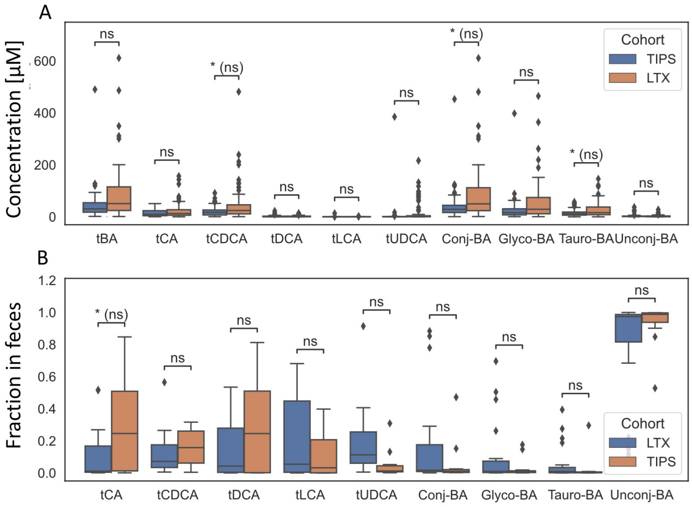

Figure B.4: Comparison of bile acid levels in venous blood plasma and feces between liver transplant and TIPS patients before intervention. Boxplots of BA levels in venous blood plasma (A) and composition in feces (B) within liver transplant patients and TIPS patients before surgical intervention. Statistical differences were assessed by independent t-test. Statistical significance is marked with asterisks and (ns) indicates non-significance after correction for multiple testing using Benjamini-Hochberg correction.

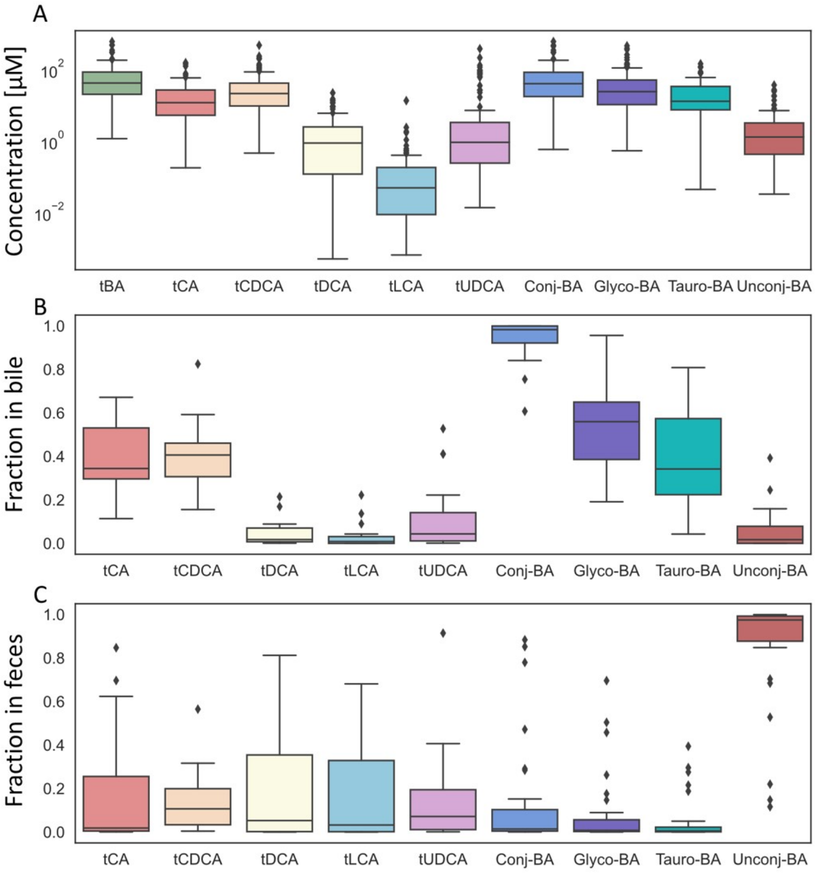

Figure B.5: Bile acid levels in venous blood plasma, bile and feces in patients with liver disease. Boxplots of BA levels in venous blood plasma (A) and composition in bile (B) and in feces (C) of patients with liver disease before surgical intervention.

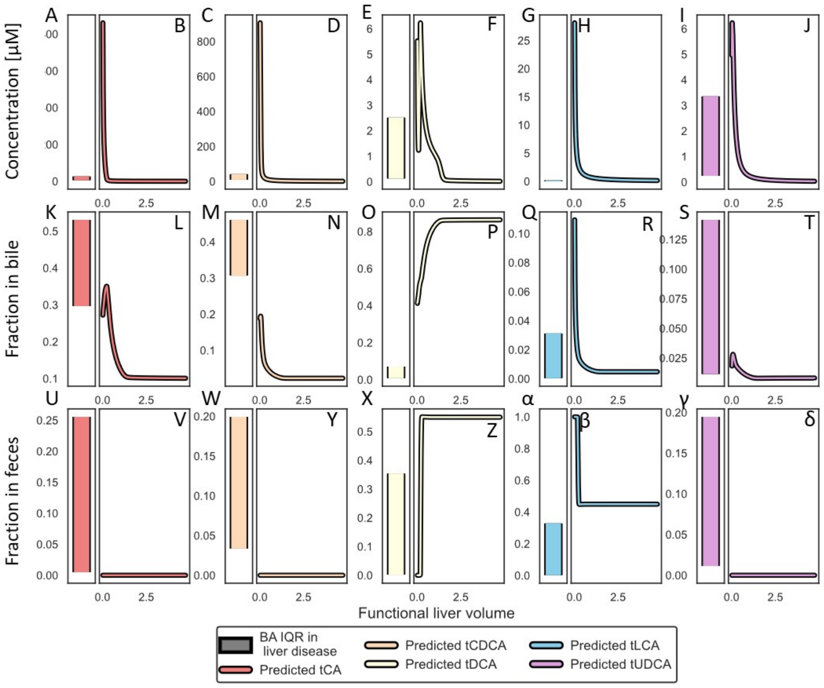

Figure B.6: Parameter scan of functional liver volume. Parameter scan of the functional liver volume to recapitulate BA levels observed in liver disease patients in blood plasma (first row), bile (second row) and feces (last row). Measurements in patients (blood: A, C, E, G, I; bile: K, M, O, Q, S; feces: U, W, X α, γ) are shown for reference against model predictions (blood: B, D, F, H, J; bile: L, N, P, R, T; feces: V, Y, Z β, δ). In each compartment tCA, tCDCA, tDCA, tLCA and tUDCA are shown from left to right.

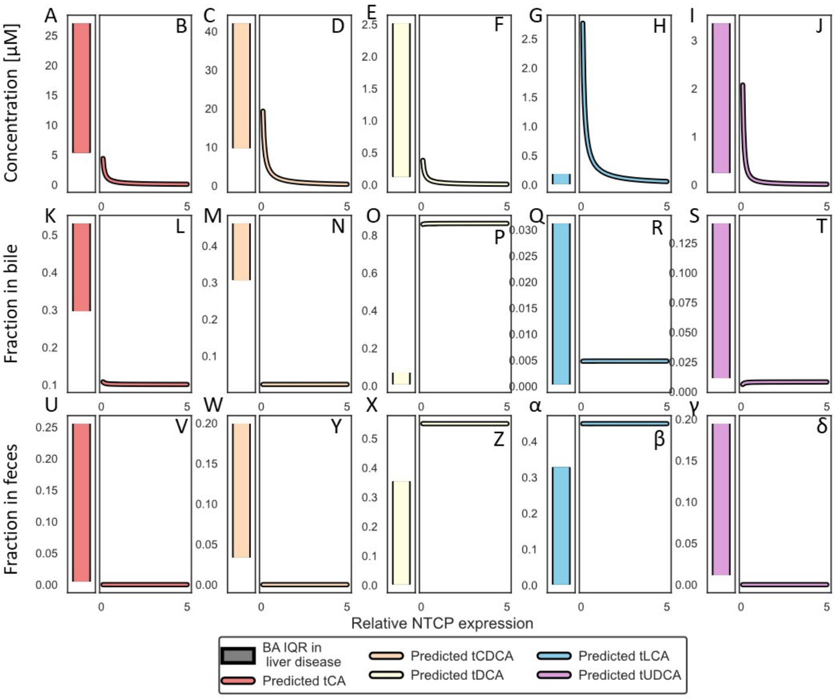

Figure B.7: Parameter scan of relative ASBT activity. Parameter scan of the relative NTCP activity to recapitulate BA levels observed in liver disease patients in blood plasma (first row), bile (second row) and feces (last row). Measurements in patients (blood: A, C, E, G, I; bile: K, M, O, Q, S; feces: U, W, X α, γ) are shown for reference against model predictions (blood: B, D, F, H, J; bile: L, N, P, R, T; feces: V, Y, Z β, δ). In each compartment tCA, tCDCA, tDCA, tLCA and tUDCA are shown from left to right.

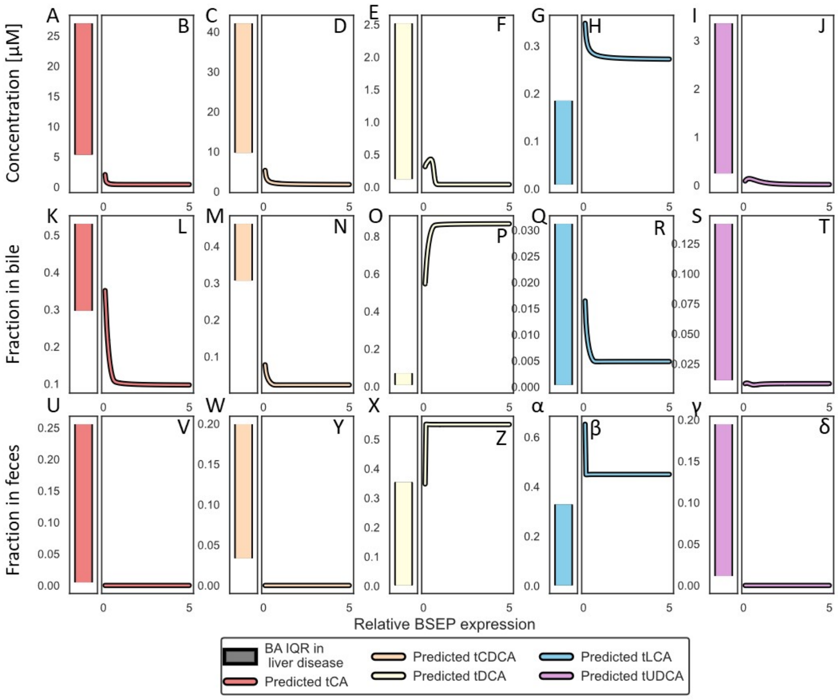

Figure B.8: Parameter scan of relative BSEP activity. Parameter scan of the relative BSEP activity to recapitulate BA levels observed in liver disease patients in blood plasma (first row), bile (second row) and feces (last row). Measurements in patients (blood: A, C, E, G, I; bile: K, M, O, Q, S; feces: U, W, X α, γ) are shown for reference against model predictions (blood: B, D, F, H, J; bile: L, N, P, R, T; feces: V, Y, Z β, δ). In each compartment tCA, tCDCA, tDCA, tLCA and tUDCA are shown from left to right.

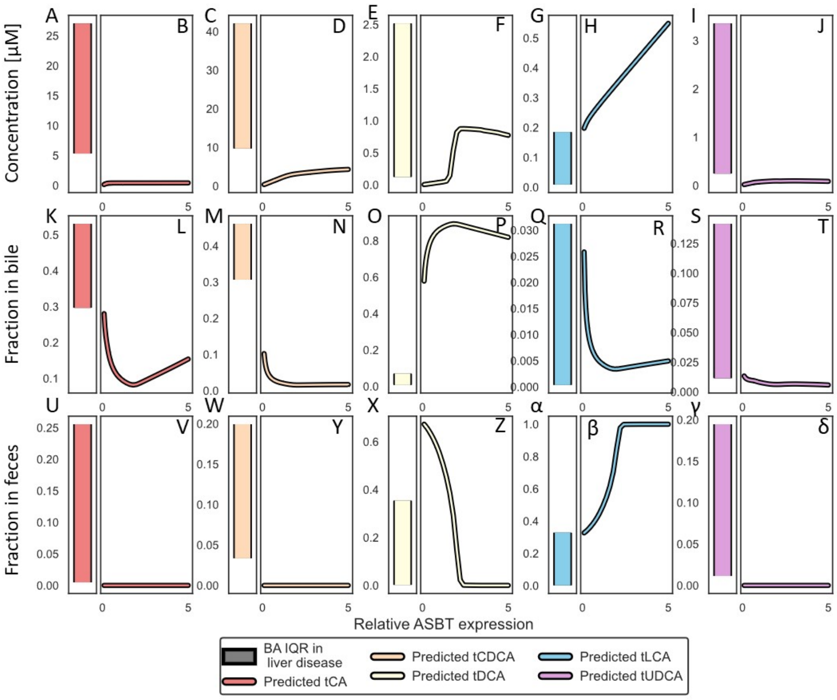

Figure B.9: Parameter scan of relative ASBT activity. Parameter scan of the relative ASBT activity to recapitulate BA levels observed in liver disease patients in blood plasma (first row), bile (second row) and feces (last row). Measurements in patients (blood: A, C, E, G, I; bile: K, M, O, Q, S; feces: U, W, X α, γ) are shown for reference against model predictions (blood: B, D, F, H, J; bile: L, N, P, R, T; feces: V, Y, Z β, δ). In each compartment tCA, tCDCA, tDCA, tLCA and tUDCA are shown from left to right.

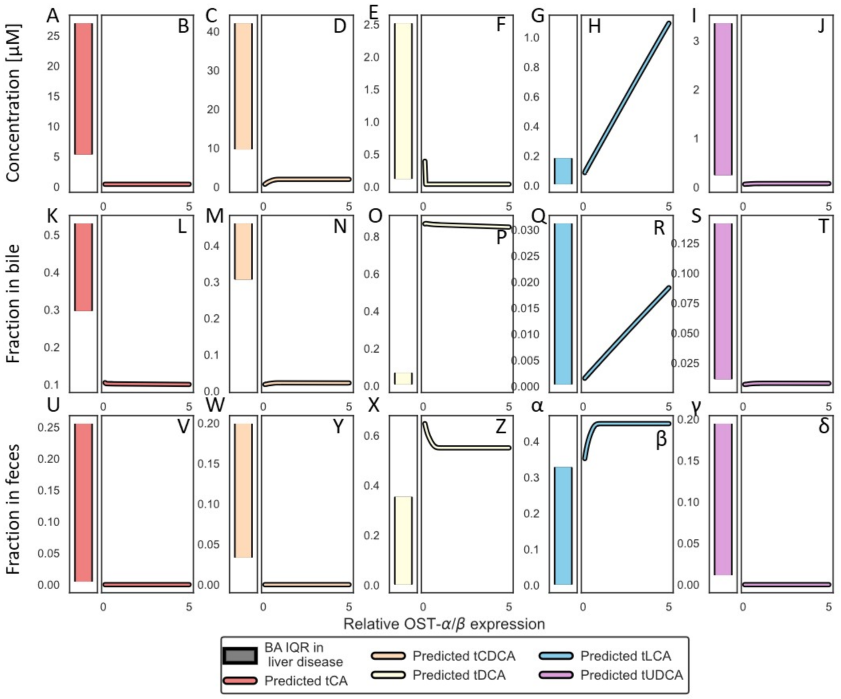

Figure B.10: Parameter scan of relative OSTα/β activity. P Parameter scan of the relative OSTα/β activity to recapitulate BA levels observed in liver disease patients in blood plasma (first row), bile (second row) and feces (last row). Measurements in patients (blood: A, C, E, G, I; bile: K, M, O, Q, S; feces: U, W, X α, γ) are shown for reference against model predictions (blood: B, D, F, H, J; bile: L, N, P, R, T; feces: V, Y, Z β, δ). In each compartment tCA, tCDCA, tDCA, tLCA and tUDCA are shown from left to right.

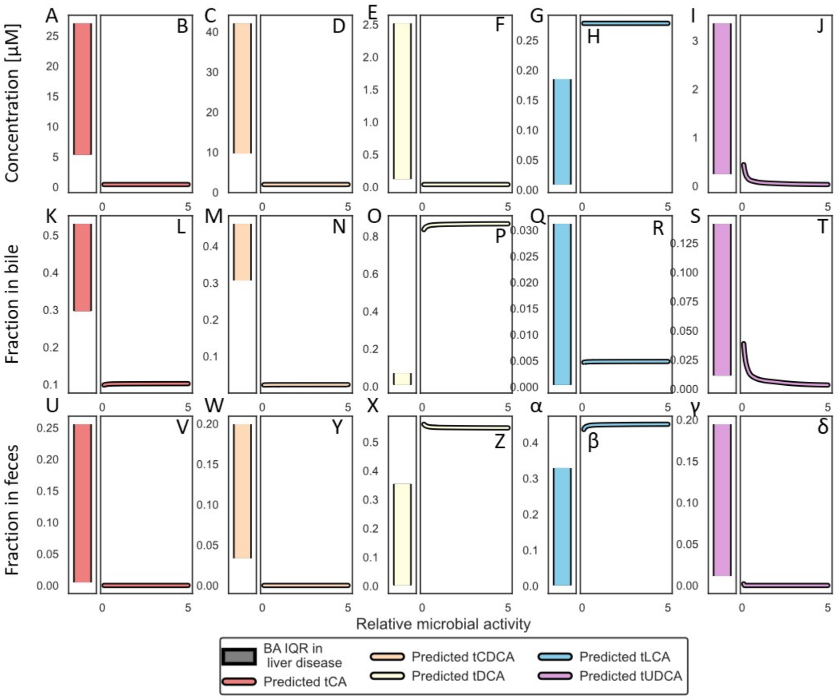

Figure B.11: Parameter scan of relative microbial activity. Parameter scan of the relative microbial activity to recapitulate BA levels observed in liver disease patients in blood plasma (first row), bile (second row) and feces (last row). Measurements in patients (blood: A, C, E, G, I; bile: K, M, O, Q, S; feces: U, W, X α, γ) are shown for reference against model predictions (blood: B, D, F, H, J; bile: L, N, P, R, T; feces: V, Y, Z β, δ). In each compartment tCA, tCDCA, tDCA, tLCA and tUDCA are shown from left to right.

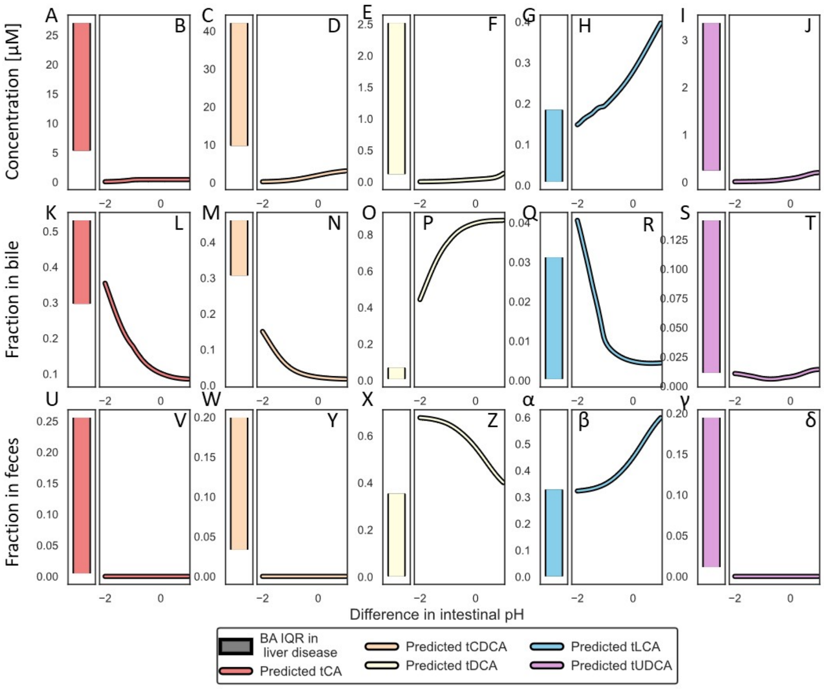

Figure B.12: Parameter scan of changes in intestinal pH. Parameter scan of changes in intestinal pH to recapitulate BA levels observed in liver disease patients in blood plasma (first row), bile (second row) and feces (last row). Measurements in patients (blood: A, C, E, G, I; bile: K, M, O, Q, S; feces: U, W, X α, γ) are shown for reference against model predictions (blood: B, D, F, H, J; bile: L, N, P, R, T; feces: V, Y, Z β, δ). In each compartment tCA, tCDCA, tDCA, tLCA and tUDCA are shown from left to right.

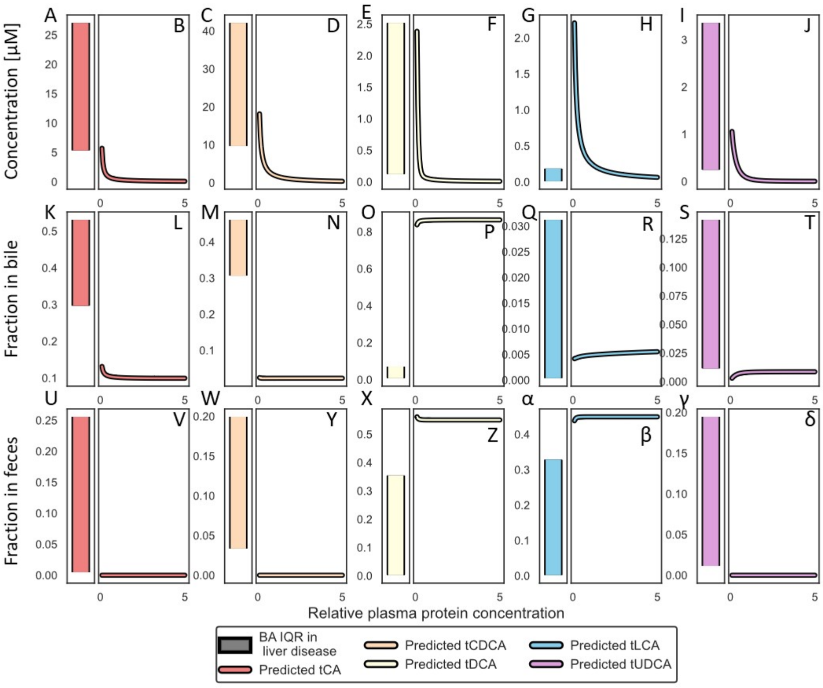

Figure B.13: Parameter scan of relative blood plasma protein concentration. Parameter scan of the relative blood plasma protein concentration to recapitulate BA levels observed in liver disease patients in blood plasma (first row), bile (second row) and feces (last row). Measurements in patients (blood: A, C, E, G, I; bile: K, M, O, Q, S; feces: U, W, X α, γ) are shown for reference against model predictions (blood: B, D, F, H, J; bile: L, N, P, R, T; feces: V, Y, Z β, δ). In each compartment tCA, tCDCA, tDCA, tLCA and tUDCA are shown from left to right.

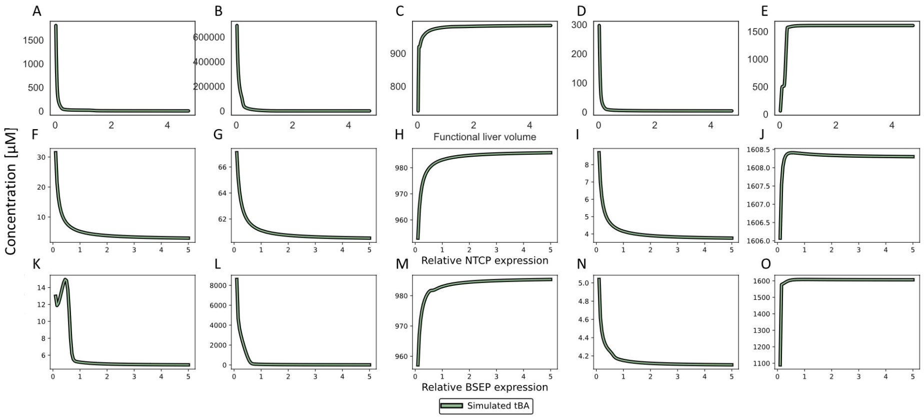

Figure B.14: Parameter scan of hepatic parameters: Concentration in EHC organs. Parameter scan of hepatic parameters with high sensitivity coefficient and corresponding concentration in portal blood (A, F, K), liver (B, G, L), small (C, H, M) and large (D, I, N) intestinal tissue and gut content (E, J, O).

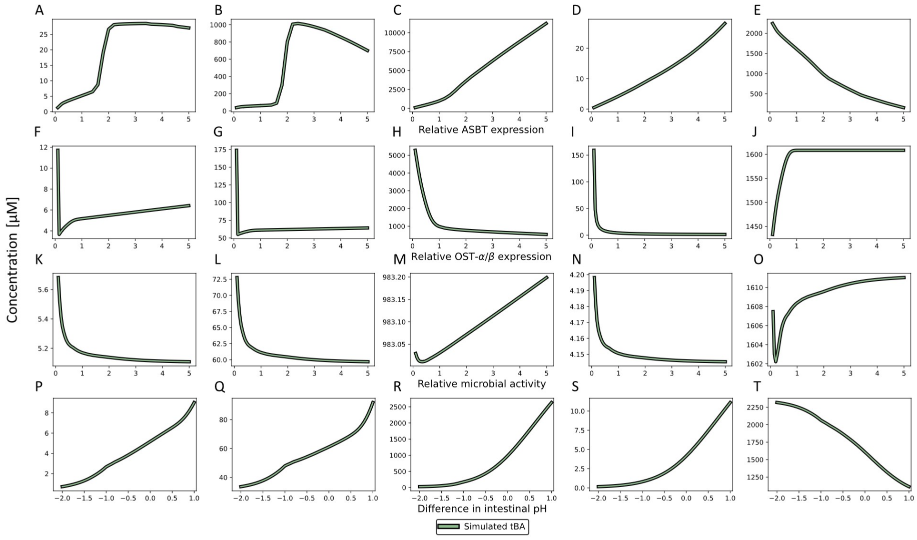

Figure B.15: Parameter scan of intestinal parameters: Concentration in EHC organs. Parameter scan of intestinal parameters with high sensitivity coefficient and corresponding concentration in portal blood (A, F, K,P), liver (B, G, L, Q), small (C, H, M, R) and large (D, I, N, S) intestinal tissue and gut content (E, J, O, T)

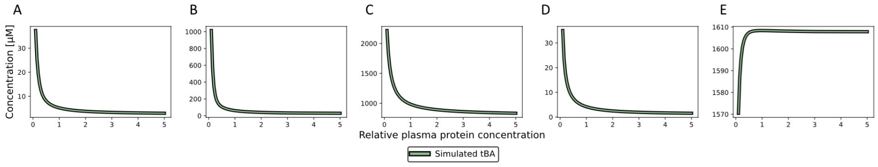

Figure B.16: Parameter scan of blood parameters: Concentration in EHC organs. Parameter scan of blood parameters with high sensitivity coefficient and corresponding concentration in portal blood (A), liver (B), small (C) and large (D) intestinal tissue and gut content (E)

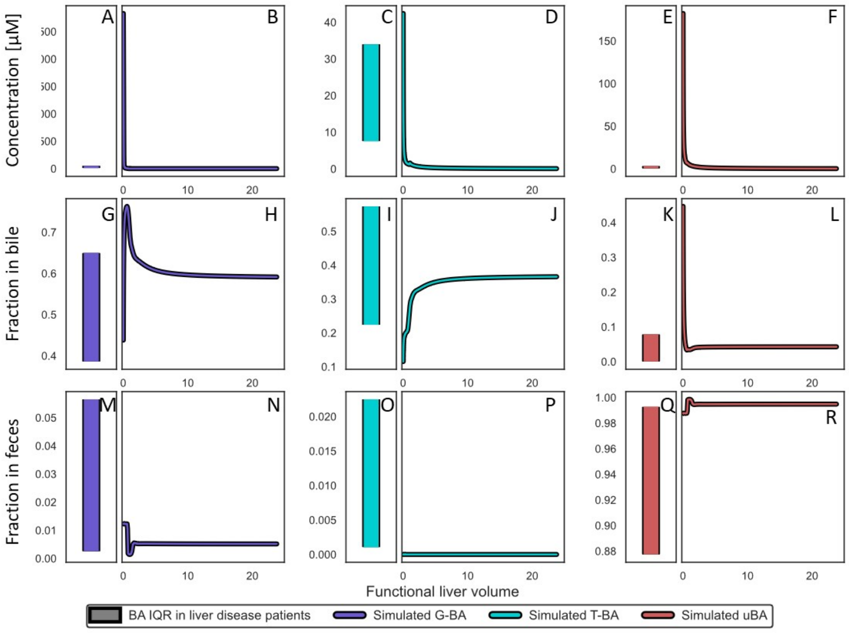

Figure B.17: Parameter scan of functional liver volume. Parameter scan of the functional liver volume to recapitulate BA levels observed in liver disease patients in blood plasma (first row), bile (second row) and feces (last row). Measurements in patients (blood: A, C, E; bile: G, I, K; feces: M, O, Q) are shown for reference against model predictions (blood: B, D, F; bile: H, J, L; feces: N, P, R). In each compartment G-BA, T-BA and uBA are shown from left to right.

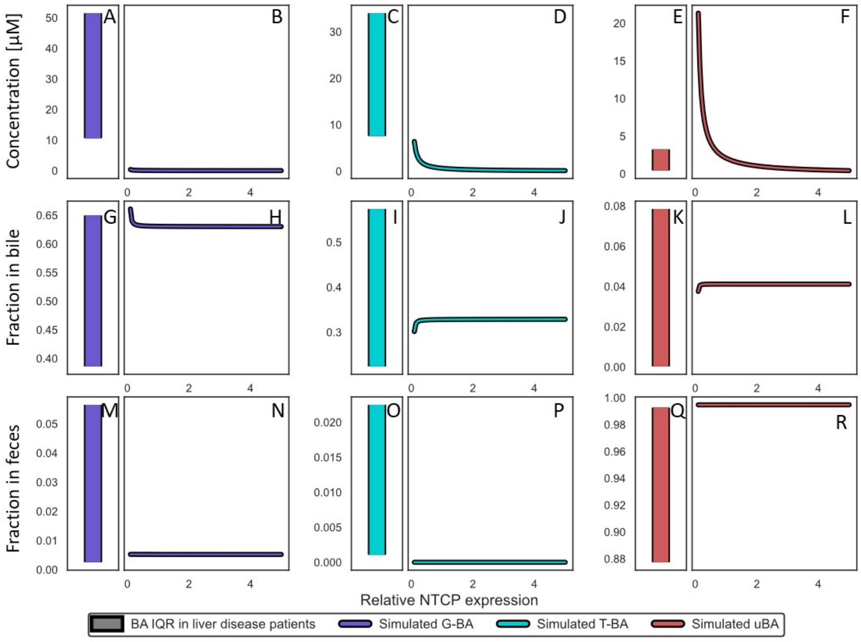

Figure B.18: Parameter scan of relative NTCP activity. Parameter scan of the relative NTCP activity to recapitulate BA levels observed in liver disease patients in blood plasma (first row), bile (second row) and feces (last row). Measurements in patients (blood: A, C, E; bile: G, I, K; feces: M, O, Q) are shown for reference against model predictions (blood: B, D, F; bile: H, J, L; feces: N, P, R). In each compartment G-BA, T-BA and uBA are shown from left to right.

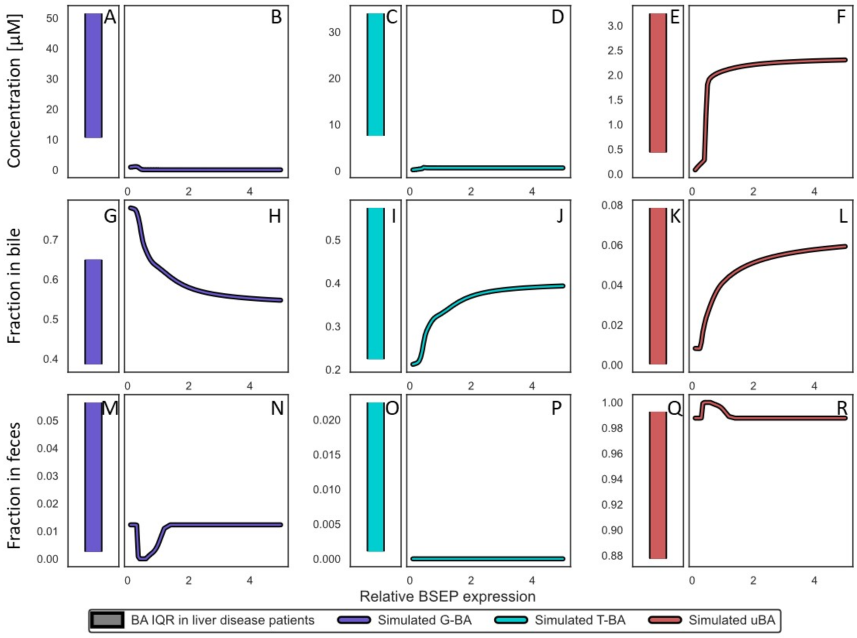

Figure B.19: Parameter scan of relative BSEP activity. Parameter scan of the relative BSEP activity to recapitulate BA levels observed in liver disease patients in blood plasma (first row), bile (second row) and feces (last row). Measurements in patients (blood: A, C, E; bile: G, I, K; feces: M, O, Q) are shown for reference against model predictions (blood: B, D, F; bile: H, J, L; feces: N, P, R). In each compartment G-BA, T-BA and uBA are shown from left to right.

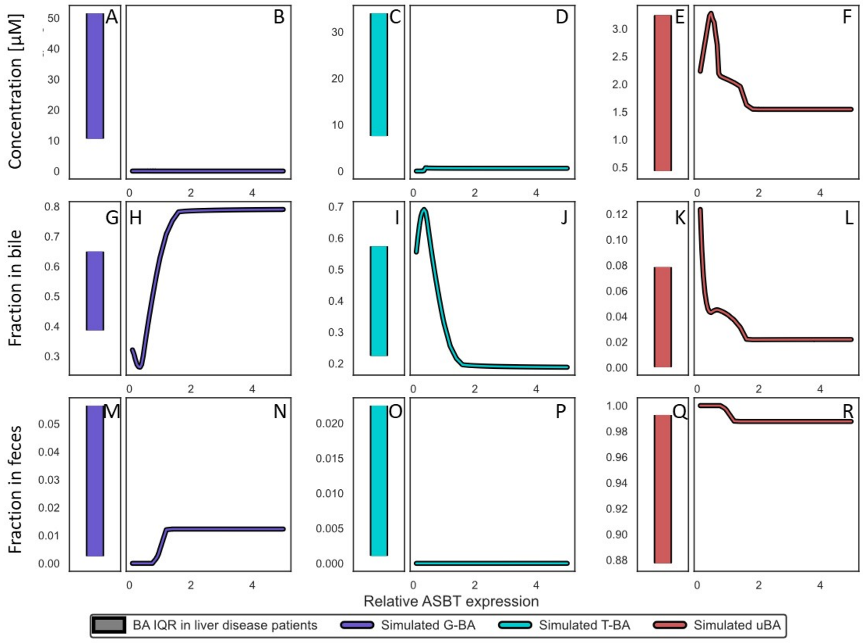

Figure B.20: Parameter scan of relative ASBT activity. Parameter scan of the relative ASBT activity to recapitulate BA levels observed in liver disease patients in blood plasma (first row), bile (second row) and feces (last row). Measurements in patients (blood: A, C, E; bile: G, I, K; feces: M, O, Q) are shown for reference against model predictions (blood: B, D, F; bile: H, J, L; feces: N, P, R). In each compartment G-BA, T-BA and uBA are shown from left to right.

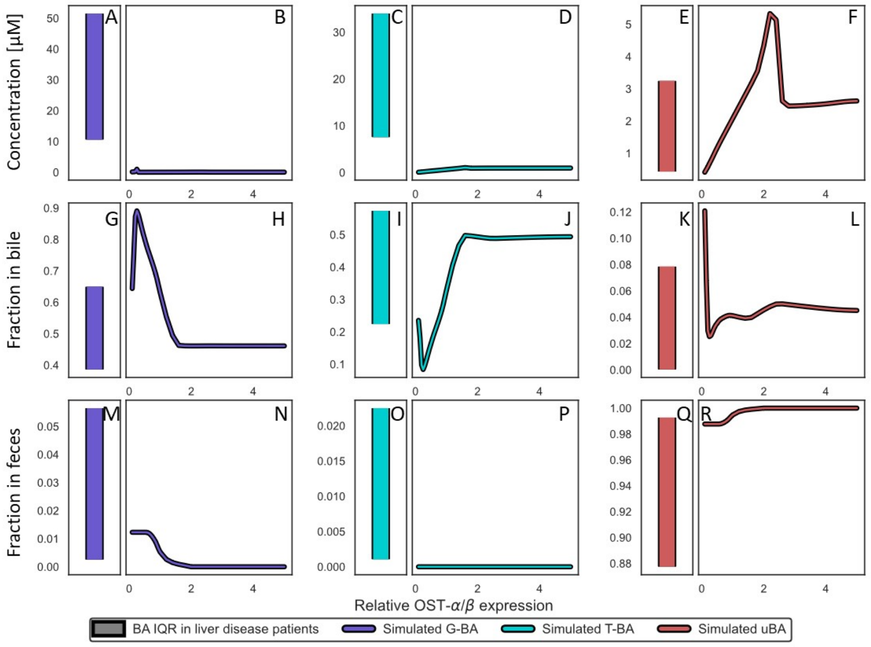

Figure B.21: Parameter scan of relative OSTα/β activity. Parameter scan of the relative OSTα/β activity to recapitulate BA levels observed in liver disease patients in blood plasma (first row), bile (second row) and feces (last row). Measurements in patients (blood: A, C, E; bile: G, I, K; feces: M, O, Q) are shown for reference against model predictions (blood: B, D, F; bile: H, J, L; feces: N, P, R). In each compartment G-BA, T-BA and uBA are shown from left to right.

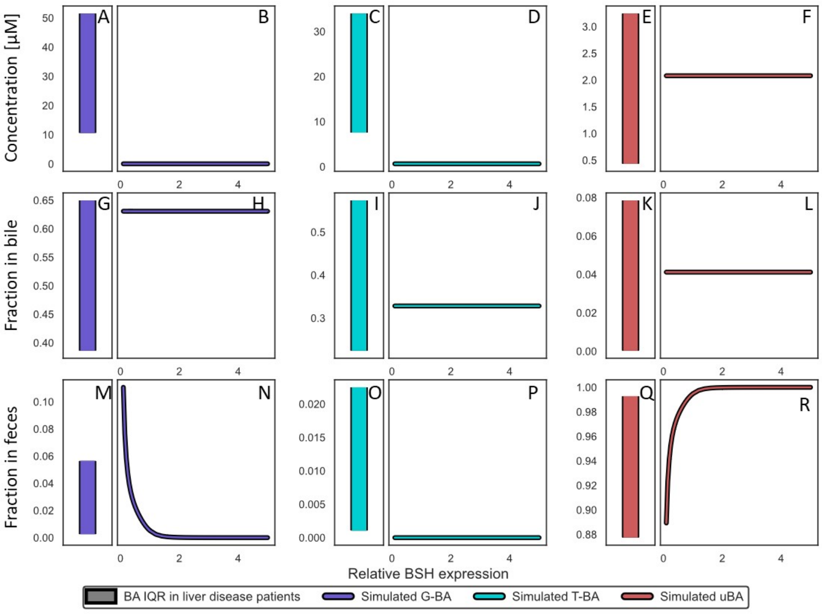

Figure B.22: Parameter scan of relative BSH activity. Parameter scan of the relative BSH activity to recapitulate BA levels observed in liver disease patients in blood plasma (first row), bile (second row) and feces (last row). Measurements in patients (blood: A, C, E; bile: G, I, K; feces: M, O, Q) are shown for reference against model predictions (blood: B, D, F; bile: H, J, L; feces: N, P, R). In each compartment G-BA, T-BA and uBA are shown from left to right.

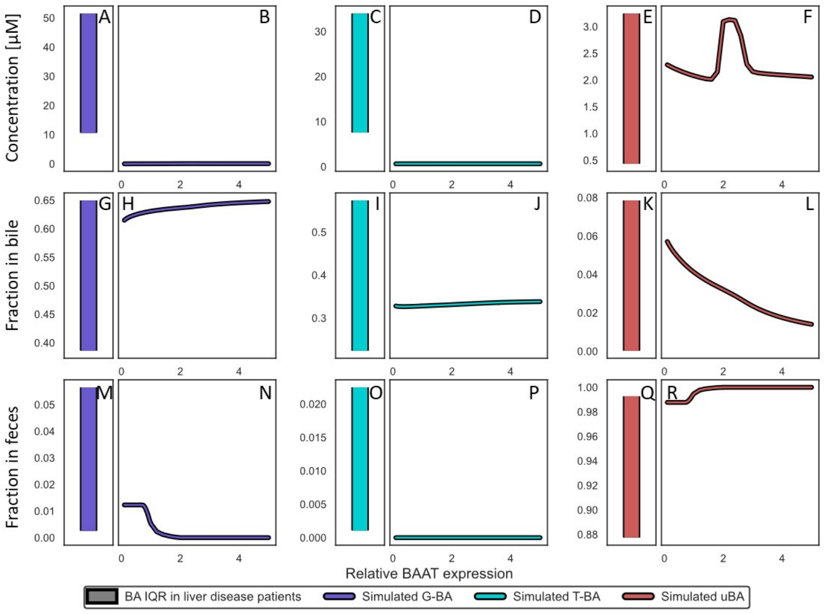

Figure B.23: Parameter scan of relative BAAT activity. Parameter scan of the relative BAAT activity to recapitulate BA levels observed in liver disease patients in blood plasma (first row), bile (second row) and feces (last row). Measurements in patients (blood: A, C, E; bile: G, I, K; feces: M, O, Q) are shown for reference against model predictions (blood: B, D, F; bile: H, J, L; feces: N, P, R). In each compartment G-BA, T-BA and uBA are shown from left to right.

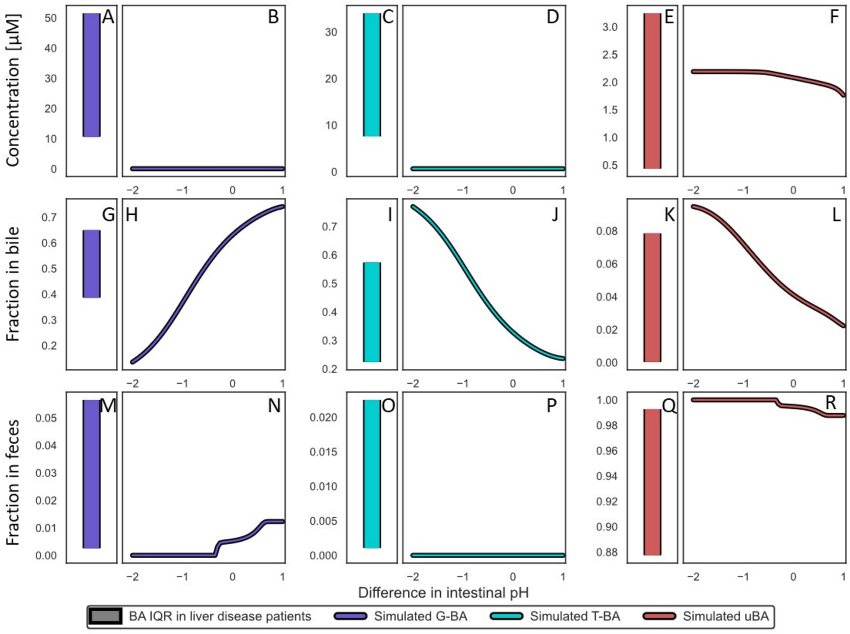

Figure B.24: Parameter scan of changes in intestinal pH. Parameter scan of changes in intestinal pH to recapitulate BA levels observed in liver disease patients in blood plasma (first row), bile (second row) and feces (last row). Measurements in patients (blood: A, C, E; bile: G, I, K; feces: M, O, Q) are shown for reference against model predictions (blood: B, D, F; bile: H, J, L; feces: N, P, R). In each compartment G-BA, T-BA and uBA are shown from left to right.

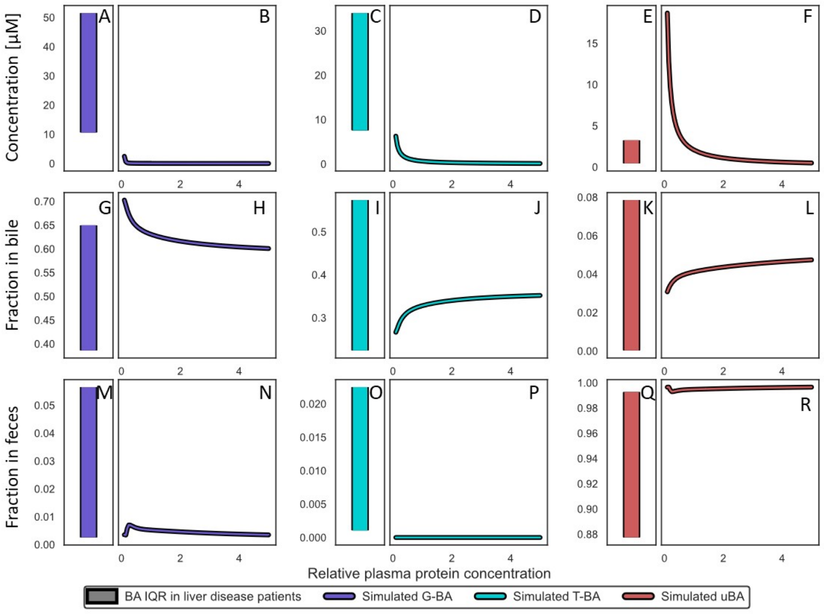

Figure B.25: Parameter scan of relative blood plasma protein concentration. Parameter scan of the relative blood plasma protein concentration to recapitulate BA levels observed in liver disease patients in blood plasma (first row), bile (second row) and feces (last row). Measurements in patients (blood: A, C, E; bile: G, I, K; feces: M, O, Q) are shown for reference against model predictions (blood: B, D, F; bile: H, J, L; feces: N, P, R). In each compartment G-BA, T-BA and uBA are shown from left to right.

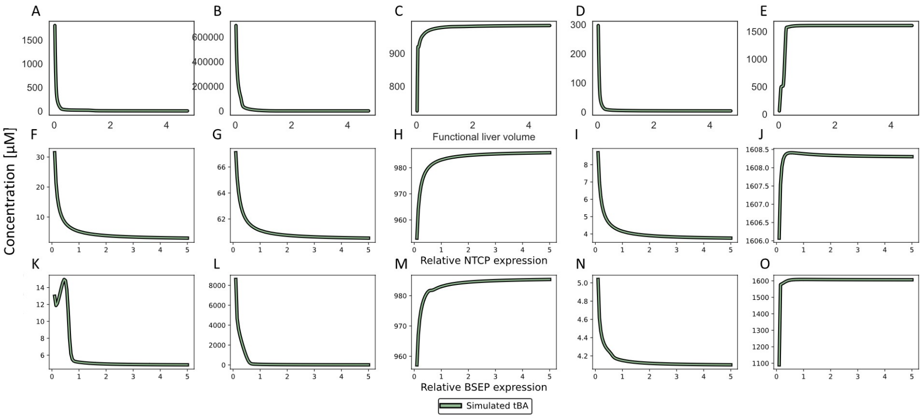

Figure B.26: Parameter scan of hepatic parameters: Concentration in EHC organs. Parameter scan of hepatic parameters with high sensitivity coefficient and corresponding concentration in portal blood (A, F, K,P), liver (B, G, L, Q), small (C, H, M, R) and large (D, I, N, S) intestinal tissue and gut content (E, J, O, T).

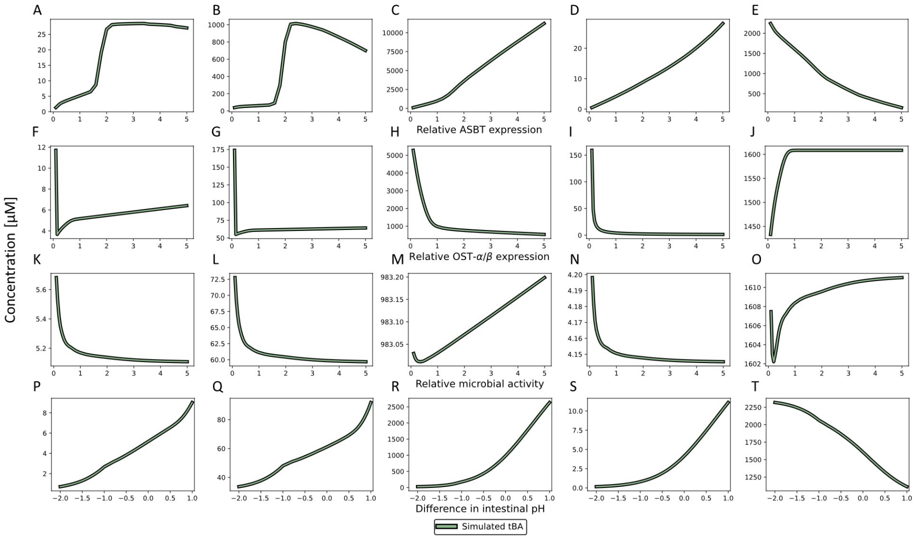

Figure B.27: Parameter scan of intestinal parameters: Concentration in EHC organs. Parameter scan of intestinal parameters with high sensitivity coefficient and corresponding concentration in portal blood (A, F, K,P), liver (B, G, L, Q), small (C, H, M, R) and large (D, I, N, S) intestinal tissue and gut content (E, J, O, T)

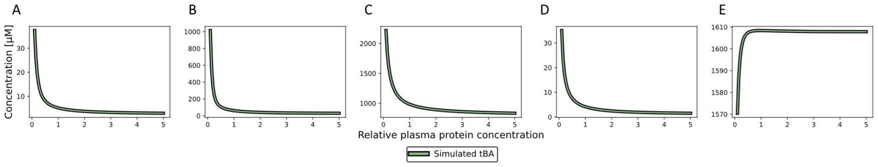

Figure B.28: Parameter scan of blood parameters: Concentration in EHC organs. Parameter scan of blood parameters with high sensitivity coefficient and corresponding concentration in portal blood (A), liver (B), small (C) and large (D) intestinal tissue and gut content (E)

Table B.1: Data of bile acid concentration in venous blood plasma derived from literature used for model development.

Bile acid	Value	SEM	Unit	Number of studies	Source
tBA	2.83	1.1	μM	18	[326; 327; 328; 330; 331; 355; 357; 358; 360; 361; 362; 363; 364; 365; 366; 367; 368; 369]
Conj-BA	1.74	0.72	μM	4	[327; 357; 363; 368]
Glyco-BA	1.52	0.66	μM	3	[357; 363; 368]
tCA	0.50	0.25	μM	5	[327; 355; 362; 363; 368]
G-CA	0.18	0.14	μM	2	[363; 368]
T-CA	0.06	0.05	μM	2	[363; 368]
CA	0.23	0.15	μM	2	[363; 368]
tCDCA	1.21	0.53	μM	5	[327; 355; 362; 363; 368]
G-CDCA	0.76	0.43	μM	2	[363; 368]
T-CDCA	0.13	0.29	μM	2	[363; 368]
CDCA	0.30	0.20	μM	2	[363; 368]
tDCA	0.82	0.39	μM	5	[327; 355; 362; 363; 368]
G-DCA	0.34	0.22	μM	2	[363; 368]
T-DCA	0.07	0.06	μM	2	[363; 368]
DCA	0.44	0.28	μM	2	[363; 368]
tLCA	0.26	0.18	μM	3	[362; 363; 368]
G-LCA	0.07	0.06	μM	2	[363; 368]
T-LCA	0.04	0.04	μM	2	[363; 368]
LCA	0.02	0.01	μM	1	[368]
tUDCA	0.20	0.11	μM	4	[327; 360; 363; 368]
G-UDCA	0.15	0.12	μM	2	[363; 368]
T-UDCA	0.01	2e-3	μM	1	[368]
UDCA	0.09	0.08	μM	2	[363; 368]

Table B.2: Data of bile acid concentration in portal blood plasma derived from literature used for model development.

Bile acid	Value	SEM	Unit	Number of studies	Source
tCA	5.16	0.71	μM	4	[328; 329; 330; 331]
tCDCA	5.32	1.48	μM	4	[328; 329; 330; 331]
tDCA	3.62	1.04	μM	4	[328; 329; 330; 331]

Table B.3: Data of bile acid pool size in liver derived from literature used for model development.

Bile acid	Value	SEM	Unit	Number of studies	Source
tCA	60.99	4.18	μmol	4	[9; 332; 333; 334]
tCDCA	62.48	3.99	μmol	4	[9; 332; 333; 334]
tDCA	14.29	8.77	μmol	4	[9; 332; 333; 334]
tLCA	2.16	1.59	μmol	4	[9; 332; 333; 334]
tUDCA	5.01	1.24	μmol	4	[9; 332; 333; 334]

Table B.4: Data of synthesis and excretion rates derived from literature used for model development.

Rates	Value	SEM	Unit	Number of studies	Source
CA synthesis	0.62	0.20	mmol/day	5	[325; 370; 371; 372; 373]
CDCA synthesis	0.37	0.10	mmol/day	4	[370; 371; 372; 373]
Renal excretion	4.29	3.1	μmol/day	4	[364; 374; 375; 376]

Table B.5: Data of bile acid composition in feces derived from literature used for model development.

Bile acid	Value	SEM	Unit	Number of studies	Source
tCA	3.5	2.8	%	2	[363; 377]
tCDCA	3.4	2.7	%	2	[363; 377]
tDCA	58.2	16.1	%	2	[363; 377]
tLCA	35.0	15.2	%	2	[363; 377]
tUDCA	1.4	1.2	%	2	[363; 377]

Table B.6: Data of bile acid composition in bile derived from literature used for model development.

Bile acid	Value	SEM	Unit	Number of studies	Source
CA	0.09	0.07	%	1	[378]
G-CA	29.77	58.26	%	1	[378]
T-CA	2.45	3.49	%	1	[378]
G-CDCA	20.51	43.56	%	1	[378]
T-CDCA	8.20	14.61	%	1	[378]
G-DCA	27.61	64.83	%	1	[378]
T-DCA	8.56	16.45	%	1	[378]
G-LCA	0.55	1.30	%	1	[378]
T-LCA	0.22	0.57	%	1	[378]
UDCA	0.00	0.00	%	1	[378]
G-UDCA	1.97	2.65	%	1	[378]
T-UDCA	0.08	0.25	%	1	[378]

Table B.7: Data of intestinal bile flows derived from literature used for model development.

Flows	Value	SEM	Unit	Number of studies	Source
Duodenal bile flow (basal)	7.44	3.5	μmol/min	1	[323]
Jejunal bile flow (basal)	5.29	2.16	μmol/min	1	[323]
Ileal bile flow (basal)	2.66	1.65	μmol/min	1	[323]
Per day	30.0	3.40	mmol/day	1	[324]
First hour postprandial	2.56	0.37	mmol/h	1	[324]
Overnight (12h)	0.90	0.11	μmol/min	1	[324]

Table B.8: Literature data of postprandial responses in small intestine used for model development. Error was calculated using all measurements within one segment as individual measurements as no measurement error was determined within the study.

Segment	Time [min]	Flux [μmol/min]	Error (calculated)	Source
Duodenum	30	59.84	17.00	[323]
Duodenum	60	64.88	17.00	[323]
Duodenum	90	63.54	17.00	[323]
Duodenum	120	48.37	17.00	[323]
Duodenum	150	41.87	17.00	[323]
Duodenum	180	43.56	17.00	[323]
Duodenum	210	26.75	17.00	[323]
Duodenum	240	18.29	17.00	[323]
Jejunum	30	33.40	32.96	[323]
Jejunum	60	117.52	32.96	[323]
Jejunum	90	54.78	32.96	[323]
Jejunum	120	26.35	32.96	[323]
Jejunum	150	31.97	32.96	[323]
Jejunum	180	26.05	32.96	[323]
Jejunum	210	22.33	32.96	[323]
Jejunum	240	15.84	32.96	[323]
Ileum	30	16.04	39.59	[323]

Continuation of table B.8

Segment	Time [min]	Flux [μmol/min]	Error (calculated)	Source
Ileum	60	105.49	39.59	[323]
Ileum	120	82.42	39.59	[323]
Ileum	180	31.86	39.59	[323]
Ileum	210	17.91	39.59	[323]
Ileum	240	12.81	39.59	[323]

Table B.9: Fitted parameter values of enzymatic reactions and postprandial responses in the 5BA model.

Parameter	Value	Unit
Parameter	Value	Unit
Synthesis rate (tCA)	9.5E-01	μmol/min
Synthesis rate (tCDCA)	4.4E-01	μmol/min
Renal Clearance (Km)	9.5E+02	μmol/l
Renal Clearance (TSmax)	6.0E-03	μmol/l/min
tCA →tDCA (Km)	2.4E+01	μmol/l
tCA →tDCA (vmax)	2.0E+02	μmol/l/min
tCDCA →tLCA (Km)	1.1E+02	μmol/l
tCDCA →tLCA (vmax)	9.5E+02	μmol/l/min
tCDCA →tUDCA (Km)	1.0E+03	μmol/l
tCDCA →tUDCA (vmax)	4.3E+03	μmol/l/min
tUDCA →tLCA (Km)	9.5E+02	μmol/l
tUDCA →tLCA (vmax)	1.8E+01	μmol/l/min
Gallbladder emptying lag time	9.00	min
Gallbladder ejection half-time	59.73	min
EHC continuous fraction	0.50	
Gallbladder ejection fraction	0.40	

Table B.10: **Fitted parameter values of hepatic transport reactions in the 5BA model.**

Parameter	Value	Unit
BSEP (tCA; Km)	9.5E+02	μmol/l
BSEP (tCDCA; Km)	9.6E+02	μmol/l
BSEP (tDCA; Km)	2.9E+02	μmol/l
BSEP (tLCA; Km)	9.1E+02	μmol/l
BSEP (tUDCA; Km)	9.9E+02	μmol/l
BSEP (tCA; vmax)	9.2E+00	μmol/l/min
BSEP (tCDCA; vmax)	6.5E+00	μmol/l/min
BSEP (tDCA; vmax)	1.4E+01	μmol/l/min
BSEP (tLCA; vmax)	4.4E+01	μmol/l/min
BSEP (tUDCA; vmax)	5.3E+00	μmol/l/min
NTCP (tCA; Km)	7.6E+02	μmol/l
NTCP (tCDCA; Km)	9.2E+02	μmol/l
NTCP (tDCA; Km)	4.5E+01	μmol/l
NTCP (tLCA; Km)	8.0E+02	μmol/l
NTCP (tUDCA; Km)	6.3E+02	μmol/l
NTCP (tCA; vmax)	2.4E+03	μmol/l/min
NTCP (tCDCA; vmax)	4.8E+02	μmol/l/min
NTCP (tDCA; vmax)	4.9E+03	μmol/l/min
NTCP (tLCA; vmax)	2.6E+03	μmol/l/min
NTCP (tUDCA; vmax)	1.1E+03	μmol/l/min

Table B.11: **Fitted parameter values of intestinal transport reactions in the 5BA model.**

Parameter	Value	Unit
ASBT (tCA; Km)	1.0E+03	μmol/l
ASBT (tCDCA; Km)	1.6E+02	μmol/l
ASBT (tDCA; Km)	1.3E+02	μmol/l
ASBT (tLCA; Km)	2.4E+01	μmol/l
ASBT (tUDCA; Km)	4.4E+01	μmol/l
ASBT (tCA; vmax)	4.1E+02	μmol/l/min
ASBT (tCDCA; vmax)	1.3E+01	μmol/l/min
ASBT (tDCA; vmax)	5.0E+03	μmol/l/min
ASBT (tLCA; vmax)	2.1E+03	μmol/l/min
ASBT (tUDCA; vmax)	3.8E+03	μmol/l/min

Continuation of table B.11

Parameter	Value	Unit
OSTα/β (tCA; Km)	9.2E-01	μmol/l
OSTα/β (tCDCA; Km)	1.0E+03	μmol/l
OSTα/β (tDCA; Km)	6.7E+01	μmol/l
OSTα/β (tLCA; Km)	9.6E+02	μmol/l
OSTα/β (tUDCA; Km)	2.2E+01	μmol/l
OSTα/β (tCA; vmax)	5.0E+03	μmol/l/min
OSTα/β (tCDCA; vmax)	1.3E+00	μmol/l/min
OSTα/β (tDCA; vmax)	5.0E+03	μmol/l/min
OSTα/β (tLCA; vmax)	2.5E+00	μmol/l/min
OSTα/β (tUDCA; vmax)	5.0E+03	μmol/l/min

Table B.12: Sensitivity analysis of fitted 5BA model parameters on BA concentration in liver tissue. Shown are only parameters with sensitivity coefficient above 1 or below -1. (LU: Lumen, nRE: normalized relative expression, ITR: intestinal transit rate)

Liver conc. [μM]	Parameter PK	Model	Sensitivity coefficient
tDCA	C_tEnd	pH (intracellular)	31.9944845
tCA	C_tEnd	pH (intracellular)	17.11378011
tUDCA	C_tEnd	pH (intracellular)	13.97256935
tCA	C_max	pH (intracellular)	12.07650294
tCDCA	C_tEnd	pH (intracellular)	5.85872439
tCDCA	C_max	pH (intracellular)	4.991866588
tUDCA	C_max	LU-ColonTransversum-pH	4.505388517
tUDCA	C_tEnd	LU-ColonTransversum-pH	4.240910746
tLCA	C_tEnd	pH (intracellular)	4.073137463
tLCA	C_max	pH (intracellular)	4.019450905
tUDCA	C_tEnd	LU-ColonAscendens-pH	3.882990266
tUDCA	C_max	LU-ColonAscendens-pH	3.65838723
tDCA	C_max	LU-ColonTransversum-pH	2.917986484
tUDCA	C_tEnd	tUDCA-BSEP-Transporter conc.	2.393989835
tUDCA	C_tEnd	tUDCA-BSEP-Km	2.367941416
tDCA	C_tEnd	LU-ColonTransversum-pH	1.958689547
tUDCA	C_max	pH (intracellular)	1.603376642
tDCA	C_max	LargeIntestine-Volume	1.599188632
tDCA	C_max	tDCA-ASBT-Vmax	1.598491523
tDCA	C_max	ASBT-Reference conc.	1.598491

Continuation of table B.12

Liver conc. [μM]	Parameter PK	Model	Sensitivity coefficient
tCA	C_max	LU-UpperJejunum-pH	1.464134251
tDCA	C_max	LU-ColonSigmoid-pH	1.375806945
tCA	C_max	LU-LowerJejunum-pH	1.326492148
tDCA	C_max	LU-ColonAscendens-pH	1.217174344
tCA	C_max	tCA-BSEP-Transporter conc.	1.149417133
tDCA	C_max	LU-ColonDescendens-pH	1.145034962
tCA	C_tEnd	tCA-BSEP-Transporter conc.	1.077890765
tDCA	C_tEnd	tDCA-BSEP-Transporter conc.	1.070917766
tCA	C_tEnd	CA Synthesis	1.061881727
tUDCA	C_tEnd	tCDCA-Reference pH	1.050403834
tCA	C_max	LU-UpperIleum-pH	1.04571481
tDCA	C_tEnd	tDCA-ASBT-Vmax	1.030887998
tDCA	C_tEnd	ASBT-Reference conc.	1.030887391
tDCA	C_tEnd	LargeIntestine-Volume	1.030677599
tCDCA	C_tEnd	tCDCA-BSEP-Transporter conc.	1.024140911
tCA	C_tEnd	tCA-BSEP-Km	1.010803635
tDCA	C_tEnd	tDCA-BSEP-Km	1.006357959
tCA	C_max	tCA-BSEP-Km	0.99562348
tDCA	C_tEnd	tDCA-Reference pH	-26.94516932
tDCA	C_tEnd	pH (plasma)	-17.04857036
tCA	C_tEnd	pH (plasma)	-14.46369982
tUDCA	C_tEnd	pH (plasma)	-13.37675652
tCA	C_max	pH (plasma)	-11.09993064
tCDCA	C_tEnd	pH (plasma)	-5.277854973
tCDCA	C_max	pH (plasma)	-4.440434037
tLCA	C_tEnd	pH (plasma)	-3.69925463
tLCA	C_max	pH (plasma)	-3.65526187
tUDCA	C_tEnd	tUDCA-BSEP-Vmax	-2.429421653
tUDCA	C_tEnd	BSEP-nRE	-2.428166255
tUDCA	C_tEnd	BSEP-Reference conc.	-2.428166255
tUDCA	C_tEnd	Plasma protein scale factor	-2.026701006
tDCA	C_max	Liver volume	-1.62739183
tUDCA	C_max	pH (plasma)	-1.626816028
tDCA	C_max	tDCA-ASBT-Transporter conc.	-1.614541824
tUDCA	C_tEnd	Liver volume	-1.232711789
tCA	C_max	Liver volume	-1.16600029
tCA	C_max	BSEP-nRE	-1.161375182
tCA	C_max	tCA-BSEP-Vmax	-1.161375182

Continuation of table B.12

Liver conc. [μM]	Parameter		Sensitivity coefficient
	PK	Model	
tCA	C_max	BSEP-Reference conc.	-1.161375182
tCA	C_tEnd	BSEP-nRE	-1.08840449
tCA	C_tEnd	tCA-BSEP-Vmax	-1.08840449
tCA	C_tEnd	BSEP-Reference conc.	-1.08840449
tDCA	C_tEnd	BSEP-nRE	-1.087745064
tDCA	C_tEnd	BSEP-Reference conc.	-1.087745064
tDCA	C_tEnd	tDCA-BSEP-Vmax	-1.087744864
tCA	C_tEnd	Liver volume	-1.077689392
tDCA	C_tEnd	Liver volume	-1.041976912
tDCA	C_tEnd	tDCA-ASBT-Transporter conc.	-1.040897522
tCDCA	C_tEnd	Liver volume	-1.038407643
tCDCA	C_tEnd	BSEP-nRE	-1.032870503
tCDCA	C_tEnd	tCDCA-BSEP-Vmax	-1.032870503
tCDCA	C_tEnd	BSEP-Reference conc.	-1.032870503
tLCA	C_tEnd	Liver volume	-1.008927428
tLCA	C_max	Liver volume	-1.008112716

Table B.13: Sensitivity analysis of fitted 5BA model parameters on BA concentration in portal blood plasma. Shown are only parameters with sensitivity coefficient above 1 or below -1. (LU: Lumen, nRE: normalized relative expression, ITR: intestinal transit rate)

PV conc. [μM]	Parameter		Sensitivity coefficient
	PK	Model	
tUDCA	C_max	LU-ColonTransversum-pH	4.3729379
tUDCA	C_tEnd	LU-ColonAscendens-pH	3.9703496
tUDCA	C_tEnd	LU-ColonTransversum-pH	3.9181622
tUDCA	C_max	LU-ColonAscendens-pH	3.5860018
tUDCA	C_tEnd	pH (intracellular)	3.1905393
tDCA	C_tEnd	pH (intracellular)	2.5552293
tDCA	C_tEnd	LU-ColonTransversum-pH	1.8712197
tCA	C_max	LU-UpperJejunum-pH	1.6335009
tCA	C_max	LU-LowerJejunum-pH	1.4993914
tCDCA	C_tEnd	LU-UpperJejunum-pH	1.4874916
tDCA	C_max	LU-ColonTransversum-pH	1.4513677
tCDCA	C_tEnd	LU-LowerJejunum-pH	1.3183371
tUDCA	C_tEnd	G-UDCA-BSEP-Transporter (conc.)	1.1901658

Continuation of table B.13

PV conc. [μM]	Parameter PK	 Model	Sensitivity coefficient
tCA	C_max	LU-UpperIleum-pH	1.1879025
tUDCA	C_tEnd	G-UDCA-BSEP-Km	1.1700289
tCDCA	C_tEnd	LU-UpperIleum-pH	1.0265776
tDCA	C_tEnd	G-DCA-ASBT-Vmax	1.0056986
tDCA	C_tEnd	ASBT-Reference (conc.)	1.0056985
tCA	C_max	G-CA-ASBT-Vmax	0.9994424
tCA	C_max	ASBT-Reference (conc.)	0.9994424
tCA	C_tEnd	CA Synthesis	0.9961191
tUDCA	C_tEnd	pH (plasma)	-3.4751055
tUDCA	C_tEnd	Plasma protein scale factor	-1.8422361
tDCA	C_tEnd	pH (plasma)	-1.6321044
tUDCA	C_tEnd	G-UDCA-BSEP-Vmax	-1.1933893
tUDCA	C_tEnd	Liver-BSEP-nRE	-1.1923093
tUDCA	C_tEnd	BSEP-Reference (conc.)	-1.1923093
tDCA	C_tEnd	G-DCA-ASBT-Transporter (conc.)	-1.0145027
tCA	C_max	G-CA-ASBT-Transporter (conc.)	-1.0074924

Table B.14: Sensitivity analysis of fitted 5BA model parameters on BA concentration in venous blood plasma. Shown are only parameters with sensitivity coefficient above 1 or below -1. (LU: Lumen, nRE: normalized relative expression, ITR: intestinal transit rate)

VB conc. [μM]	Parameter PK	 Model	Sensitivity coefficient
tUDCA	C_max	LU-ColonTransversum-pH	4.3694825
tUDCA	C_tEnd	LU-ColonAscendens-pH	3.9628173
tUDCA	C_tEnd	LU-ColonTransversum-pH	3.9365879
tUDCA	C_max	LU-ColonAscendens-pH	3.5885654
tUDCA	C_tEnd	pH (intracellular)	3.1175547
tDCA	C_tEnd	pH (intracellular)	2.6874616
tDCA	C_tEnd	LU-ColonTransversum-pH	1.886788
tCA	C_max	LU-UpperJejunum-pH	1.6322001
tDCA	C_max	LU-ColonTransversum-pH	1.50361
tCA	C_max	LU-LowerJejunum-pH	1.4979095
tCDCA	C_max	LU-UpperJejunum-pH	1.4727287
tCDCA	C_tEnd	LU-UpperJejunum-pH	1.4727287

Continuation of table B.14

VB conc. [μM]	Parameter		Sensitivity coefficient
	PK	Model	
tCDCA	C_tEnd	LU-LowerJejunum-pH	1.3052323
tUDCA	C_tEnd	NTCP-tUDCA-Transporter conc.	1.2525896
tUDCA	C_tEnd	NTCP-tUDCA-Km	1.252555
tCDCA	C_max	LU-LowerJejunum-pH	1.2074457
tBA	C_max	LU-ColonTransversum-pH	1.202544
tCA	C_max	LU-UpperIleum-pH	1.1867188
tUDCA	C_tEnd	BSEP-tUDCA-Transporter conc.	1.1765779
tUDCA	C_tEnd	BSEP-tUDCA-Km	1.1564472
tBA	C_tEnd	LU-UpperJejunum-pH	1.0345437
tCDCA	C_tEnd	LU-UpperIleum-pH	1.0163646
tDCA	C_tEnd	ASBT-tDCA-Vmax	1.0069596
tDCA	C_tEnd	ASBT-Reference conc.	1.0069593
tDCA	C_tEnd	LargeIntestine-Volume	1.0047401
tCA	C_tEnd	NTCP-tCA-Transporter conc.	1.0018435
tCA	C_tEnd	NTCP-tCA-Km	1.0016644
tCA	C_max	NTCP-tCA-Transporter conc.	1.0003698
tCA	C_max	NTCP-tCA-Km	0.9997669
tCDCA	C_tEnd	NTCP-tCDCA-Transporter conc.	0.9990476
tLCA	C_tEnd	NTCP-tLCA-Transporter conc.	0.9989371
tLCA	C_tEnd	NTCP-tLCA-Km	0.9989134
tCDCA	C_tEnd	NTCP-tCDCA-Km	0.9988419
tCA	C_max	SmallIntestine-Volume	0.9986935
tCA	C_max	ASBT-tCA-Vmax	0.9986693
tCA	C_max	ASBT-Reference conc.	0.9986693
tDCA	C_max	NTCP-tDCA-Transporter conc.	0.9983784
tLCA	C_max	NTCP-tLCA-Transporter conc.	0.9981881
tLCA	C_max	NTCP-tLCA-Km	0.9981639
tCA	C_tEnd	PARAM_CA_Synth	0.9968358
tUDCA	C_tEnd	pH (plasma)	-3.3985921
tUDCA	C_tEnd	tUDCA-Fraction unbound	-2.146039
tUDCA	C_tEnd	Plasma protein scale factor	-2.1392429
tDCA	C_tEnd	pH (plasma)	-1.7607259
tUDCA	C_tEnd	Liver-Volume	-1.2829974
tUDCA	C_tEnd	NTCP-tUDCA-Vmax	-1.2670235
tUDCA	C_tEnd	Liver-NTCP-nRE	-1.2664176
tUDCA	C_tEnd	NTCP-Reference conc.	-1.2664176
tUDCA	C_tEnd	BSEP-tUDCA-Vmax	-1.1794629
tUDCA	C_tEnd	Liver-BSEP-nRE	-1.1783772

Continuation of table B.14

VB conc. [μM]	Parameter PK	 Model	Sensitivity coefficient
tUDCA	C_tEnd	BSEP-Reference conc.	-1.1783772
tCDCA	C_tEnd	Liver-Volume	-1.0464546
tBA	C_tEnd	Liver-Volume	-1.0451438
tCDCA	C_max	Liver-Volume	-1.0333219
tBA	C_tEnd	Plasma protein scale factor	-1.0328262
tCA	C_tEnd	Liver-Volume	-1.0190721
tCA	C_tEnd	Plasma protein scale factor	-1.0169512
tCA	C_tEnd	tCA-Fraction unbound	-1.0169512
tDCA	C_tEnd	Liver-Volume	-1.0167699
tDCA	C_tEnd	ASBT-tDCA-Transporter conc.	-1.0160475
tLCA	C_tEnd	Liver-Volume	-1.0146817
tCA	C_max	Liver-Volume	-1.0144239
tBA	C_tEnd	Liver-NTCP-nRE	-1.0144121
tBA	C_tEnd	NTCP-Reference conc.	-1.0144121
tLCA	C_max	Liver-Volume	-1.0138707
tCA	C_tEnd	Liver-NTCP-nRE	-1.0099432
tCA	C_tEnd	NTCP-tCA-Vmax	-1.0099432
tCA	C_tEnd	NTCP-Reference conc.	-1.0099432
tCA	C_max	Liver-NTCP-nRE	-1.0084272
tCA	C_max	NTCP-tCA-Vmax	-1.0084272
tCA	C_max	NTCP-Reference conc.	-1.0084272
tCA	C_max	Plasma protein scale factor	-1.0080239
tCA	C_max	tCA-Fraction unbound	-1.0080239
tCDCA	C_tEnd	Plasma protein scale factor	-1.0073496
tCDCA	C_tEnd	tCDCA-Fraction unbound	-1.0073496
tCDCA	C_tEnd	Liver-NTCP-nRE	-1.0070713
tCDCA	C_tEnd	NTCP-tCDCA-Vmax	-1.0070713
tCDCA	C_tEnd	NTCP-Reference conc.	-1.0070713
tLCA	C_tEnd	Liver-NTCP-nRE	-1.0069631
tLCA	C_tEnd	NTCP-tLCA-Vmax	-1.0069631
tLCA	C_tEnd	NTCP-Reference conc.	-1.0069631
tCA	C_max	ASBT-tCA-Transporter conc.	-1.0067331
tDCA	C_max	Liver-NTCP-nRE	-1.006457
tDCA	C_max	NTCP-tDCA-Vmax	-1.006457
tDCA	C_max	NTCP-Reference conc.	-1.006457
tLCA	C_max	Liver-NTCP-nRE	-1.0061948
tLCA	C_max	NTCP-tLCA-Vmax	-1.0061948
tLCA	C_max	NTCP-Reference conc.	-1.0061948
tDCA	C_tEnd	Plasma protein scale factor	-1.0002279

Continuation of table B.14

VB conc. [μM]	Parameter PK	 Model	Sensitivity coefficient
tDCA	C_tEnd	tDCA-Fraction unbound	-1.0002279
tDCA	C_tEnd	Liver-NTCP-nRE	-0.9990662
tDCA	C_tEnd	NTCP-tDCA-Vmax	-0.9990662
tDCA	C_tEnd	NTCP-Reference conc.	-0.9990662
tCDCA	C_max	Plasma protein scale factor	-0.9977069
tCDCA	C_max	tCDCA-Fraction unbound	-0.9977069
tCDCA	C_max	Liver-NTCP-nRE	-0.997466
tCDCA	C_max	NTCP-tCDCA-Vmax	-0.997466
tCDCA	C_max	NTCP-Reference conc.	-0.997466

Table B.15: Sensitivity analysis of fitted 5BA model parameters on BA composition in feces. Shown are only parameters with sensitivity coefficient above 1 or below -1. (LU: Lumen, nRE: normalized relative expression, ITR: intestinal transit rate)

Fraction of fecal BA	Parameter PK	 Model	Sensitivity coefficient
tUDCA	C_tEnd	Height	7.9945916
tCA	C_tEnd	Height	7.7055212
tCA	C_tEnd	tCA to tDCA: Enzyme conc.	6.4314569
tCA	C_tEnd	tCA to tDCA: Km	6.4314461
tCA	C_tEnd	ASBT-tCA-Transporter conc.	4.9095078
tUDCA	C_max	Height	4.8635012
tCA	C_tEnd	ASBT-tCA-Km	4.8527381
tCDCA	C_max	tCDCA to tLCA: Enzyme conc.	4.1313135
tCDCA	C_tEnd	tCDCA to tLCA: Enzyme conc.	4.1312937
tCDCA	C_tEnd	tCDCA to tLCA: Km	4.1310864
tCDCA	C_max	tCDCA to tLCA: Km	4.1290789
tUDCA	C_tEnd	ASBT-tUDCA-Transporter conc.	3.127982
tUDCA	C_tEnd	ASBT-tUDCA-Km	3.1224815
tUDCA	C_max	tUDCA to tLCA: Enzyme conc.	2.5578622
tUDCA	C_max	tUDCA to tLCA: Km	2.5089005
tCA	C_tEnd	PARAM_CA_Synth	2.2087872
tUDCA	C_max	ASBT-tUDCA-Transporter conc.	2.1835994
tUDCA	C_max	ASBT-tUDCA-Km	2.1762542
tCA	C_tEnd	pH (intracellular)	2.0365092
tCDCA	C_max	tCDCA to tUDCA: Enzyme conc.	1.9307918
tCDCA	C_max	tCDCA to tUDCA: Km	1.9306866

Continuation of table B.15

Fraction of	Parameter		Sensitivity
fecal BA	PK	Model	coefficient
tCDCA	C_tEnd	tCDCA to tUDCA: Enzyme conc.	1.9299186
tCDCA	C_tEnd	tCDCA to tUDCA: Km	1.9299089
tUDCA	C_tEnd	tUDCA to tLCA: Enzyme conc.	1.8020316
tUDCA	C_tEnd	tUDCA to tLCA: Km	1.7972666
tUDCA	C_tEnd	PARAM_CDCA_synth	1.5330521
tCDCA	C_tEnd	PARAM_CDCA_synth	1.3042242
tCA	C_tEnd	LU-ColonTransversum-pH	1.0161884
tCDCA	C_tEnd	LU-ColonTransversum-pH	1.0161883
tUDCA	C_max	LU-ColonAscendens-ITR	1.0138497
tUDCA	C_tEnd	LU-ColonTransversum-pH	-102.01434
tCA	C_tEnd	LU-UpperJejunum-pH	-9.9057838
tUDCA	C_max	LU-ColonDescendens-pH	-9.7392697
tCA	C_tEnd	tCA to tDCA-Reference conc.	-6.7400329
tCA	C_tEnd	tCA to tDCA: Vmax	-6.7400329
tCDCA	C_tEnd	LI-Large intestinal transit time	-6.3683225
tCA	C_tEnd	LI-Large intestinal transit time	-6.3597312
tCDCA	C_max	LI-Large intestinal transit time	-6.3350181
tCA	C_tEnd	SI-Volume	-5.0423829
tCA	C_tEnd	ASBT-tCA-Vmax	-5.0418771
tUDCA	C_max	LI-Large intestinal transit time	-4.9545943
tUDCA	C_tEnd	LI-Large intestinal transit time	-4.8231005
tCA	C_tEnd	ASBT-Reference conc.	-4.4773098
tCDCA	C_max	tCDCA to tLCA: Vmax	-4.25488
tCDCA	C_max	tCDCA to tLCA-Reference conc.	-4.2548796
tCDCA	C_tEnd	tCDCA to tLCA-Reference conc.	-4.2548649
tCDCA	C_tEnd	tCDCA to tLCA: Vmax	-4.2548649
tUDCA	C_tEnd	ASBT-Reference conc.	-3.5943911
tUDCA	C_tEnd	ASBT-tUDCA-Vmax	-3.2045471
tCA	C_tEnd	SI-Small intestinal transit time	-3.1280892
tUDCA	C_tEnd	LI-Volume	-2.661764
tUDCA	C_max	tUDCA to tLCA-Reference conc.	-2.6316646
tUDCA	C_max	tUDCA to tLCA: Vmax	-2.6316646
tCA	C_tEnd	LU-Duodenum-pH	-2.5843208
tCA	C_tEnd	LU-LowerJejunum-pH	-2.2844423
tUDCA	C_max	LU-ColonTransversum-pH	-2.2769556
tUDCA	C_max	ASBT-tUDCA-Vmax	-2.2225699
tUDCA	C_max	LI-Volume	-2.0339603
tUDCA	C_max	ASBT-Reference conc.	-2.02119

Continuation of table B.15

Fraction of fecal BA	Parameter PK	 Model	Sensitivity coefficient
tCDCA	C_max	tCDCA to tUDCA: Vmax	-1.9503048
tCDCA	C_max	tCDCA to tUDCA-Reference conc.	-1.9503047
tCDCA	C_tEnd	tCDCA to tUDCA-Reference conc.	-1.9494041
tCDCA	C_tEnd	tCDCA to tUDCA: Vmax	-1.9494041
tCA	C_tEnd	pH (plasma)	-1.8845356
tUDCA	C_tEnd	tUDCA to tLCA-Reference conc.	-1.8235796
tUDCA	C_tEnd	tUDCA to tLCA: Vmax	-1.8235796
tCA	C_tEnd	UpperJejunum-ASBT-nRE	-1.8157343
tUDCA	C_tEnd	LU-ColonAscendens-pH	-1.4496658
tUDCA	C_tEnd	LU-UpperJejunum-pH	-1.4338182
tUDCA	C_tEnd	LU-LowerJejunum-pH	-1.2808166
tCDCA	C_tEnd	LU-UpperJejunum-pH	-1.2723119
tCDCA	C_tEnd	LU-LowerJejunum-pH	-1.134935
tCDCA	C_tEnd	tCA Synthesis	-1.0454137
tLCA	C_tEnd	tCA Synthesis	-1.0454137
tUDCA	C_tEnd	tCA Synthesis	-1.0454135
tCA	C_tEnd	Caecum-tCA to tDCA-nRE	-1.0071679
tCA	C_tEnd	ColonAscendens-tCA to tDCA-nRE	-1.0071162
tCA	C_tEnd	ColonTransversum-tCA to tDCA-nRE	-1.007067
tCA	C_tEnd	ColonSigmoid-tCA to tDCA-nRE	-1.0066847
tCA	C_tEnd	ColonDescendens-tCA to tDCA-nRE	-1.0066079
tUDCA	C_tEnd	UpperIleum-pH	-1.0054961

Table B.16: Sensitivity analysis of fitted 5BA model parameters on BA composition in bile. Shown are only parameters with sensitivity coefficient above 1 or below -1. (LU: Lumen, nRE: normalized relative expression, ITR: intestinal transit rate)

Fraction of biliary BA	Parameter PK	 Model	Sensitivity coefficient
tUDCA	C_max	LU-ColonTransversum-pH	3.337207
tUDCA	C_max	LU-ColonAscendens-pH	2.9916003
tUDCA	C_tEnd	LU-ColonAscendens-pH	2.7152065
tUDCA	C_tEnd	LU-ColonTransversum-pH	2.6706766
tCA	C_tEnd	LU-ColonTransversum-pH	-1.558907
tCDCA	C_tEnd	LU-ColonTransversum-pH	-1.5589069
tLCA	C_tEnd	LU-ColonTransversum-pH	-1.0595932

Table B.17: **Fitted parameter values of enzymatic reactions and postprandial responses in the human conjugation model.**

Parameter	Value	Unit
Synthesis rate (uBA)	7.92E-01	μmol/min
Renal Clearance (Km)	8.59E+02	μmol/l
Renal Clearance (TSmax)	2.39E-03	μmol/l/min
BAAT (G-BA, Km)	1.49E+02	μmol/l
BAAT (G-BA, vmax)	4.53E+03	μmol/l/min
BAAT (T-BA, Km)	1.09E+02	μmol/l
BAAT (T-BA, vmax)	2.06E+03	μmol/l/min
BSH (G-BA, Km)	6.30E+02	μmol/l
BSH (G-BA, vmax)	6.31E+03	μmol/l/min
BSH (T-BA, Km)	3.51E+02	μmol/l
BSH (T-BA, vmax)	5.59E+03	μmol/l/min
EHC continuous fraction	0.49	
Gallbladder ejection fraction	0.57	
Gallbladder ejection half-time	63.47	min
Gallbladder emptying lag time	10.66	min

Table B.18: **Fitted parameter values of transport reactions in the human conjugation model.**

Parameter	Value	Unit
ASBT (G-BA; Km)	5.56E+01	μmol/l
ASBT (T-BA; Km)	1.52E+02	μmol/l
ASBT (uBA; Km)	1.00E-03	μmol/l
ASBT (G-BA; vmax)	3754.32389	μmol/l/min
ASBT (T-BA; vmax)	3.11E+03	μmol/l/min
ASBT (uBA; vmax)	9.80E+03	μmol/l/min
BSEP (G-BA; Km)	7.86E+02	μmol/l
BSEP (T-BA; Km)	1.66E+02	μmol/l
BSEP (uBA; Km)	1.20E+02	μmol/l
BSEP (G-BA; vmax)	49.324107	μmol/l/min
BSEP (T-BA; vmax)	1.29E+01	μmol/l/min
BSEP (uBA; vmax)	8.96E+03	μmol/l/min
NTCP (G-BA; Km)	3.75E+00	μmol/l
NTCP (T-BA; Km)	7.30E+01	μmol/l

Continuation of table B.18

Parameter	Value	Unit
NTCP (uBA; Km)	2.68E+02	μmol/l
NTCP (G-BA; vmax)	412.059148	μmol/l/min
NTCP (T-BA; vmax)	9.59E+03	μmol/l/min
NTCP (uBA; vmax)	1.85E+03	μmol/l/min
OSTα/β (G-BA; Km)	1.00E+03	μmol/l
OSTα/β (T-BA; Km)	9.85E+02	μmol/l
OSTα/β (uBA; Km)	1.00E+03	μmol/l
OSTα/β (G-BA; vmax)	651.110682	μmol/l/min
OSTα/β (T-BA; vmax)	3.40E+02	μmol/l/min
OSTα/β (uBA; vmax)	4.46E+01	μmol/l/min

Table B.19: Sensitivity analysis of fitted human conjugation BA model parameters on BA concentration in liver tissue. Shown are only parameters with sensitivity coefficient above 1 or below -1. (LU: Lumen, nRE: normalized relative expression, ITR: intestinal transit rate)

Liver conc. [μM]	Parameter PK	Model	Sensitivity coefficient
G-BA	C_max	LU-UpperJejunum-pH	3.6353717
G-BA	C_tEnd	pH (intracellular)	3.4231309
tBA	C_tEnd	pH (intracellular)	2.9478903
T-BA	C_tEnd	pH (intracellular)	2.9330913
G-BA	C_max	LU-LowerJejunum-pH	2.5873231
tBA	C_max	LU-UpperJejunum-pH	2.3397513
T-BA	C_max	ASBT-T-BA-Transporter conc.	2.1771248
T-BA	C_max	OSTβ-Reference conc.	2.0534585
G-BA	C_max	SI-Volume	2.0497788
T-BA	C_max	OSTβ-T-BA-Vmax	2.0138462
G-BA	C_max	pH (intracellular)	1.9812359
G-BA	C_max	ASBT-Reference conc.	1.7277806
G-BA	C_max	ASBT-G-BA-Vmax	1.7248532
tBA	C_max	SI-Volume	1.7238621
T-BA	C_max	SI-Duodenum-OSTβ-nRE	1.6955757
G-BA	C_max	BSEP-G-BA-Transporter conc.	1.6944266
tBA	C_max	LU-LowerJejunum-pH	1.6269015
T-BA	C_max	OSTα-Reference conc.	1.5881191
T-BA	C_max	OSTα-T-BA-Vmax	1.5614959

Continuation of table B.19

Liver	Parameter		Sensitivity
conc. [μM]	PK	Model	coefficient
G-BA	C_max	LU-UpperIleum-pH	1.556468
T-BA	C_tEnd	BSEP-T-BA-Transporter conc.	1.5283556
T-BA	C_max	SI-Volume	1.5276289
T-BA	C_tEnd	SI-Volume	1.4328847
tBA	C_tEnd	BSEP-T-BA-Transporter conc.	1.4215024
tBA	C_tEnd	SI-Volume	1.3645412
tBA	C_max	pH (intracellular)	1.3565212
T-BA	C_max	SI-Duodenum-OSTα-nRE	1.3517233
tBA	C_max	ASBT-T-BA-Transporter conc.	1.1726046
tBA	C_max	OSTβ-Reference conc.	1.1236862
T-BA	C_max	ASBT-T-BA-Km	1.0989362
tBA	C_max	ASBT-G-BA-Vmax	1.0569371
T-BA	C_max	BSEP-T-BA-Transporter conc.	1.0389323
T-BA	C_tEnd	BSEP-T-BA-Km	0.9997167
tBA	C_max	BSEP-G-BA-Transporter conc.	0.9975245
G-BA	C_tEnd	BSEP-G-BA-Transporter conc.	0.9967107
G-BA	C_tEnd	BSEP-G-BA-Km	0.99573
G-BA	C_tEnd	pH (plasma)	-3.5130521
tBA	C_tEnd	pH (plasma)	-3.0255431
T-BA	C_tEnd	pH (plasma)	-3.005719
T-BA	C_max	ASBT-Reference conc.	-2.1886153
T-BA	C_max	ASBT-T-BA-Vmax	-2.1698161
T-BA	C_max	SI-Duodenum-ASBT-nRE	-2.1690524
G-BA	C_max	Liver-Volume	-2.0902338
G-BA	C_max	pH (plasma)	-2.0356951
T-BA	C_max	OSTβ-T-BA-Transporter conc.	-2.0197987
T-BA	C_max	Liver-Volume	-1.7530751
G-BA	C_max	Liver-BSEP-nRE	-1.7383457
G-BA	C_max	BSEP-Reference conc.	-1.7383457
G-BA	C_max	ASBT-G-BA-Transporter conc.	-1.7301226
G-BA	C_max	BSEP-G-BA-Vmax	-1.7024199
T-BA	C_tEnd	Liver-BSEP-nRE	-1.5674197
T-BA	C_tEnd	BSEP-Reference conc.	-1.5674197
G-BA	C_tEnd	Liver-BSEP-nRE	-1.5633473
G-BA	C_tEnd	BSEP-Reference conc.	-1.5633473
tBA	C_tEnd	Liver-BSEP-nRE	-1.5581026
tBA	C_tEnd	BSEP-Reference conc.	-1.5581026
T-BA	C_max	OSTα-T-BA-Transporter conc.	-1.5568956

Continuation of table B.19

Liver conc. [μM]	Parameter PK	Model	Sensitivity coefficient
T-BA	C_tEnd	BSEP-T-BA-Vmax	-1.5373683
T-BA	C_tEnd	Liver-Volume	-1.5370558
tBA	C_tEnd	BSEP-T-BA-Vmax	-1.4298853
tBA	C_max	Liver-BSEP-nRE	-1.4031247
tBA	C_max	BSEP-Reference conc.	-1.4031247
tBA	C_max	pH (plasma)	-1.3975984
G-BA	C_max	ASBT-G-BA-Km	-1.3679444
tBA	C_max	ASBT-T-BA-Vmax	-1.1647297
T-BA	C_max	Liver-BSEP-nRE	-1.1330459
T-BA	C_max	BSEP-Reference conc.	-1.1330459
tBA	C_max	SI-Duodenum-ASBT-nRE	-1.1060082
tBA	C_max	ASBT-G-BA-Transporter conc.	-1.0578696
T-BA	C_max	BSEP-T-BA-Vmax	-1.0382934
G-BA	C_tEnd	Liver-Volume	-1.0051559
G-BA	C_tEnd	BSEP-G-BA-Vmax	-0.9995321
tBA	C_max	BSEP-G-BA-Vmax	-0.9989048
BA	C_max	Liver-Volume	-0.9970143

Table B.20: Sensitivity analysis of fitted human conjugation model parameters on BA composition in portal vein plasma. Shown are only parameters with sensitivity coefficient above 1 or below -1. (LU: Lumen, nRE: normalized relative expression, ITR: intestinal transit rate)

Fraction of biliary BA	Parameter PK	Model	Sensitivity coefficient
G-BA	C_max	LU-UpperJejunum-pH	1.778047191
G-BA	C_max	LU-LowerJejunum-pH	1.351933359

Table B.21: **Sensitivity analysis of fitted human conjugation BA model parameters on BA concentration in venous blood plasma. Shown are only parameters with sensitivity coefficient above 1 or below -1. (LU: Lumen, nRE: normalized relative expression, ITR: intestinal transit rate)**

VB conc. [μM]	Parameter PK	Model	Sensitivity coefficient
G-BA	C_max	LU-UpperJejunum-pH	2.12803302
G-BA	C_max	LU-LowerJejunum-pH	1.576753241
G-BA	C_max	SmallIntestine-Volume	1.196755404
tBA	C_max	LU-UpperJejunum-pH	1.184911802
G-BA	C_max	NTCP-G-BA-Transporter conc.	1.173879148
uBA	C_tEnd	NTCP-BA-Transporter conc.	1.000557844
uBA	C_tEnd	NTCP-BA-Km	1.000084727
uBA	C_max	NTCP-BA-Transporter conc.	0.999572152
uBA	C_max	NTCP-BA-Km	0.998721573
T-BA	C_max	NTCP-T-BA-Transporter conc.	0.996460368
G-BA	C_max	NTCP-G-BA-Km	0.995735674
T-BA	C_tEnd	NTCP-T-BA-Transporter conc.	0.995235872
G-BA	C_max	Liver-Volume	-1.203215815
G-BA	C_max	NTCP-G-BA-Vmax	-1.178444521
G-BA	C_max	Liver-BA-NTCP-nRE	-1.178441653
G-BA	C_max	NTCP-Reference conc.	-1.178441653
tBA	C_max	Liver-BA-NTCP-nRE	-1.099073166
tBA	C_max	NTCP-Reference conc.	-1.099073166
tBA	C_max	Liver-Volume	-1.054346051
T-BA	C_tEnd	Liver-Volume	-1.005138972
uBA	C_tEnd	NTCP-BA-Vmax	-1.003434057
uBA	C_tEnd	Liver-BA-NTCP-nRE	-1.003108846
uBA	C_tEnd	NTCP-Reference conc.	-1.003108846
uBA	C_max	NTCP-BA-Vmax	-1.002437702
uBA	C_max	Liver-BA-NTCP-nRE	-1.002289385
uBA	C_max	NTCP-Reference conc.	-1.002289385
tBA	C_tEnd	Liver-BA-NTCP-nRE	-1.001829475
tBA	C_tEnd	NTCP-Reference conc.	-1.001829475
T-BA	C_tEnd	T-BA-Fraction unbound	-1.000564201
T-BA	C_tEnd	Plasma protein scale factor	-1.000337499
T-BA	C_max	NTCP-T-BA-Vmax	-0.999328678
T-BA	C_max	Liver-BA-NTCP-nRE	-0.999318169
T-BA	C_max	NTCP-Reference conc.	-0.999318169

Continuation of table B.21

VB conc. [μM]	Parameter PK	 Model	Sensitivity coefficient
T-BA	C_tEnd	NTCP-T-BA-Vmax	-0.998094013
T-BA	C_tEnd	Liver-BA-NTCP-nRE	-0.998090374
T-BA	C_tEnd	NTCP-Reference conc.	-0.998090374
G-BA	C_tEnd	Liver-Volume	-0.99695951
uBA	C_max	Liver-Volume	-0.99676741

Table B.22: Sensitivity analysis of fitted human conjugation model parameters on BA composition in feces. Shown are only parameters with sensitivity coefficient above 1 or below -1. (LU: Lumen, nRE: normalized relative expression, ITR: intestinal transit rate)

Amount in feces [μmol]	Parameter PK	 Model	Sensitivity coefficient
T-BA	C_max	Height	10.583065
T-BA	C_tEnd	Height	10.583065
T-BA	C_max	ASBT-T-BA-Transporter conc.	8.3651467
T-BA	C_tEnd	ASBT-T-BA-Transporter conc.	8.3651467
uBA	C_max	ASBT-BA-Transporter conc.	8.1279775
uBA	C_tEnd	ASBT-BA-Transporter conc.	8.1279775
uBA	C_max	BAAT: Vmax	7.7927574
uBA	C_tEnd	BAAT: Vmax	7.7927574
T-BA	C_max	ASBT-T-BA-Km	6.2330472
T-BA	C_tEnd	ASBT-T-BA-Km	6.2330472
T-BA	C_max	BSH: Enzyme conc.	6.0501466
T-BA	C_max	BSH: Km	6.0501466
T-BA	C_tEnd	BSH: Enzyme conc.	6.0501466
T-BA	C_tEnd	BSH: Km	6.0501466
uBA	C_max	BSEP-BA-Transporter conc.	5.8712037
uBA	C_tEnd	BSEP-BA-Transporter conc.	5.8712037
uBA	C_max	Liver-BAAT-nRE	5.8710698
uBA	C_max	BAAT-Reference conc.	5.8710698
uBA	C_tEnd	Liver-BAAT-nRE	5.8710698
uBA	C_tEnd	BAAT-Reference conc.	5.8710698
uBA	C_max	BSEP-BA-Km	5.87073
uBA	C_tEnd	BSEP-BA-Km	5.87073
G-BA	C_max	BSH: Enzyme conc.	5.6810792
G-BA	C_tEnd	BSH: Enzyme conc.	5.6810792

Continuation of table B.22

Amount in feces [μmol]	Parameter		Sensitivity coefficient
	PK	Model	
G-BA	C_max	BSH: Km	5.6762958
G-BA	C_tEnd	BSH: Km	5.6762958
uBA	C_max	Height	3.6582752
uBA	C_tEnd	Height	3.6582752
uBA	C_max	PARAM_BA_Synth	3.5967195
uBA	C_tEnd	PARAM_BA_Synth	3.5967195
uBA	C_max	ASBT-G-BA-Transporter conc.	2.639368
uBA	C_tEnd	ASBT-G-BA-Transporter conc.	2.639368
uBA	C_max	OSTβ-Reference conc.	2.5695675
uBA	C_tEnd	OSTβ-Reference conc.	2.5695675
uBA	C_max	OSTβ-BA-Vmax	2.5349419
uBA	C_tEnd	OSTβ-BA-Vmax	2.5349419
uBA	C_max	Duodenum-OSTβ-nRE	2.5347704
uBA	C_tEnd	Duodenum-OSTβ-nRE	2.5347704
T-BA	C_max	OSTβ-Reference conc.	2.3623013
T-BA	C_tEnd	OSTβ-Reference conc.	2.3623013
T-BA	C_max	OSTβ-T-BA-Vmax	2.3089447
T-BA	C_tEnd	OSTβ-T-BA-Vmax	2.3089447
T-BA	C_max	Duodenum-OSTβ-nRE	2.289922
T-BA	C_tEnd	Duodenum-OSTβ-nRE	2.289922
G-BA	C_max	ASBT-G-BA-Transporter conc.	2.1960783
G-BA	C_tEnd	ASBT-G-BA-Transporter conc.	2.1960783
uBA	C_max	ASBT-G-BA-Km	2.0812893
uBA	C_tEnd	ASBT-G-BA-Km	2.0812893
uBA	C_max	LU-ITR	2.0473523
uBA	C_tEnd	LU-ITR	2.0473523
uBA	C_max	OSTα-Reference conc.	1.956585
uBA	C_tEnd	OSTα-Reference conc.	1.956585
uBA	C_max	BSH: Enzyme conc.	1.9516646
uBA	C_tEnd	BSH: Enzyme conc.	1.9516646
uBA	C_max	BSH: Km	1.9496696
uBA	C_tEnd	BSH: Km	1.9496696
uBA	C_max	OSTα-BA-Vmax	1.9296766
uBA	C_tEnd	OSTα-BA-Vmax	1.9296766
uBA	C_max	Duodenum-OSTα-nRE	1.9294667
uBA	C_tEnd	Duodenum-OSTα-nRE	1.9294667
uBA	C_max	BAAT: Enzyme conc.	1.8439035
uBA	C_tEnd	BAAT: Enzyme conc.	1.8439035
uBA	C_max	BAAT: Km	1.843745

Continuation of table B.22

Amount in feces [μmol]	Parameter		Sensitivity coefficient
	PK	Model	
uBA	C_tEnd	BAAT: Km	1.843745
T-BA	C_max	OSTα-Reference conc.	1.8029483
T-BA	C_tEnd	OSTα-Reference conc.	1.8029483
G-BA	C_max	ASBT-G-BA-Km	1.7882178
G-BA	C_tEnd	ASBT-G-BA-Km	1.7882178
T-BA	C_max	OSTα-T-BA-Vmax	1.762539
T-BA	C_tEnd	OSTα-T-BA-Vmax	1.762539
T-BA	C_max	Duodenum-OSTα-nRE	1.7469398
T-BA	C_tEnd	Duodenum-OSTα-nRE	1.7469398
uBA	C_max	SI-Volume	1.7335741
uBA	C_tEnd	SI-Volume	1.7335741
uBA	C_max	LU-Caecum-ITR	1.4689352
uBA	C_tEnd	LU-Caecum-ITR	1.4689352
T-BA	C_max	LU-UpperJejunum-ITR	1.2470412
T-BA	C_tEnd	LU-UpperJejunum-ITR	1.2470412
T-BA	C_max	LU-LowerJejunum-ITR	1.1686478
T-BA	C_tEnd	LU-LowerJejunum-ITR	1.1686478
uBA	C_max	ASBT-BA-Km	1.1592525
uBA	C_tEnd	ASBT-BA-Km	1.1592525
G-BA	C_max	BAAT: Vmax	1.0622429
G-BA	C_tEnd	BAAT: Vmax	1.0622429
G-BA	C_max	Height	1.0561234
G-BA	C_tEnd	Height	1.0561234
T-BA	C_max	LU-UpperIleum-ITR	1.0517555
T-BA	C_tEnd	LU-UpperIleum-ITR	1.0517555
G-BA	C_max	LU-Caecum-ITR	1.0012465
G-BA	C_tEnd	LU-Caecum-ITR	1.0012465
G-BA	C_max	LU-ColonAscendens-ITR	1.0010454
G-BA	C_tEnd	LU-ColonAscendens-ITR	1.0010454
T-BA	C_max	LU-ColonAscendens-ITR	1.0007286
T-BA	C_tEnd	LU-ColonAscendens-ITR	1.0007286
T-BA	C_max	LU-Caecum-ITR	1.0005722
T-BA	C_tEnd	LU-Caecum-ITR	1.0005722
uBA	C_max	LU-ColonSigmoid-ITR	0.9999785
uBA	C_tEnd	LU-ColonSigmoid-ITR	0.9999785
uBA	C_max	LU-ColonDescendens-ITR	0.9999293
uBA	C_tEnd	LU-ColonDescendens-ITR	0.9999293
T-BA	C_max	LU-ColonTransversum-ITR	0.9999287
T-BA	C_tEnd	LU-ColonTransversum-ITR	0.9999287

Continuation of table B.22

Amount in feces [μmol]	Parameter PK	Model	Sensitivity coefficient
T-BA	C_max	LU-ColonSigmoid-ITR	0.9999016
T-BA	C_tEnd	LU-ColonSigmoid-ITR	0.9999016
G-BA	C_max	LU-ColonTransversum-ITR	0.9998954
G-BA	C_tEnd	LU-ColonTransversum-ITR	0.9998954
T-BA	C_max	LU-ColonDescendens-ITR	0.9998795
T-BA	C_tEnd	LU-ColonDescendens-ITR	0.9998795
G-BA	C_max	LU-ColonSigmoid-ITR	0.9998607
G-BA	C_tEnd	LU-ColonSigmoid-ITR	0.9998607
G-BA	C_max	LU-ColonDescendens-ITR	0.99983
G-BA	C_tEnd	LU-ColonDescendens-ITR	0.99983
T-BA	C_max	LU-LowerIleum-ITR	0.998399
T-BA	C_tEnd	LU-LowerIleum-ITR	0.998399
uBA	C_max	ASBT-Reference conc.	-11.438292
uBA	C_tEnd	ASBT-Reference conc.	-11.438292
T-BA	C_max	ASBT-Reference conc.	-8.6172557
T-BA	C_tEnd	ASBT-Reference conc.	-8.6172557
T-BA	C_max	ASBT-T-BA-Vmax	-8.5218648
T-BA	C_tEnd	ASBT-T-BA-Vmax	-8.5218648
uBA	C_max	LI-Volume	-8.5176656
uBA	C_tEnd	LI-Volume	-8.5176656
uBA	C_max	ASBT-BA-Vmax	-8.3388525
uBA	C_tEnd	ASBT-BA-Vmax	-8.3388525
uBA	C_max	BAAT: Enzyme conc.	-7.9583222
uBA	C_tEnd	BAAT: Enzyme conc.	-7.9583222
uBA	C_max	BAAT: Km	-7.9577771
uBA	C_tEnd	BAAT: Km	-7.9577771
uBA	C_max	LI-Large intestinal transit time	-6.4920478
uBA	C_tEnd	LI-Large intestinal transit time	-6.4920478
T-BA	C_max	BSH: Vmax	-6.1518782
T-BA	C_tEnd	BSH: Vmax	-6.1518782
T-BA	C_max	BSH-Reference conc.	-6.1518774
T-BA	C_tEnd	BSH-Reference conc.	-6.1518774
T-BA	C_max	LI-Large intestinal transit time	-6.1288216
T-BA	C_tEnd	LI-Large intestinal transit time	-6.1288216
G-BA	C_max	LI-Large intestinal transit time	-6.1247161
G-BA	C_tEnd	LI-Large intestinal transit time	-6.1247161
uBA	C_max	BSEP-BA-Vmax	-5.9594318
uBA	C_tEnd	BSEP-BA-Vmax	-5.9594318

Continuation of table B.22

Amount in feces [μmol]	Parameter		Sensitivity coefficient
	PK	Model	
G-BA	C_max	BSH-Reference conc.	-5.7703063
G-BA	C_max	BSH: Vmax	-5.7703063
G-BA	C_tEnd	BSH-Reference conc.	-5.7703063
G-BA	C_tEnd	BSH: Vmax	-5.7703063
uBA	C_max	Liver-BSEP-nRE	-5.5358196
uBA	C_max	BSEP-Reference conc.	-5.5358196
uBA	C_tEnd	Liver-BSEP-nRE	-5.5358196
uBA	C_tEnd	BSEP-Reference conc.	-5.5358196
T-BA	C_max	SI-Small intestinal transit time	-5.3013893
T-BA	C_tEnd	SI-Small intestinal transit time	-5.3013893
uBA	C_max	ColonTransversum-ASBT-nRE	-4.8568242
uBA	C_tEnd	ColonTransversum-ASBT-nRE	-4.8568242
T-BA	C_max	SI-Volume	-4.089028
T-BA	C_tEnd	SI-Volume	-4.089028
T-BA	C_max	Duodenum-ASBT-nRE	-3.8527549
T-BA	C_tEnd	Duodenum-ASBT-nRE	-3.8527549
uBA	C_max	LU-UpperJejunum-pH	-3.8472539
uBA	C_tEnd	LU-UpperJejunum-pH	-3.8472539
uBA	C_max	LU-LowerJejunum-pH	-3.3193746
uBA	C_tEnd	LU-LowerJejunum-pH	-3.3193746
uBA	C_max	ASBT-G-BA-Vmax	-2.6342134
uBA	C_tEnd	ASBT-G-BA-Vmax	-2.6342134
uBA	C_max	OSTβ-BA-Transporter conc.	-2.5567892
uBA	C_tEnd	OSTβ-BA-Transporter conc.	-2.5567892
G-BA	C_max	LU-UpperJejunum-pH	-2.5558186
G-BA	C_tEnd	LU-UpperJejunum-pH	-2.5558186
uBA	C_max	LU-UpperIleum-pH	-2.5379802
uBA	C_tEnd	LU-UpperIleum-pH	-2.5379802
G-BA	C_max	LU-LowerJejunum-pH	-2.3955171
G-BA	C_tEnd	LU-LowerJejunum-pH	-2.3955171
T-BA	C_max	OSTβ-T-BA-Transporter conc.	-2.3174613
T-BA	C_tEnd	OSTβ-T-BA-Transporter conc.	-2.3174613
G-BA	C_max	ASBT-G-BA-Vmax	-2.1939454
G-BA	C_tEnd	ASBT-G-BA-Vmax	-2.1939454
G-BA	C_max	ASBT-Reference conc.	-2.1915613
G-BA	C_tEnd	ASBT-Reference conc.	-2.1915613
uBA	C_max	BSH: Vmax	-1.9766947
uBA	C_tEnd	BSH: Vmax	-1.9766947
uBA	C_max	BSH-Reference conc.	-1.9766944

Continuation of table B.22

Amount in feces [μmol]	Parameter		Sensitivity coefficient
	PK	Model	
uBA	C_tEnd	BSH-Reference conc.	-1.9766944
uBA	C_max	OSTα-BA-Transporter conc.	-1.9438237
uBA	C_tEnd	OSTα-BA-Transporter conc.	-1.9438237
G-BA	C_max	LU-UpperIleum-pH	-1.8647071
G-BA	C_tEnd	LU-UpperIleum-pH	-1.8647071
uBA	C_max	BAAT: Vmax	-1.8488975
uBA	C_tEnd	BAAT: Vmax	-1.8488975
uBA	C_max	ColonAscendens-ASBT-nRE	-1.8414507
uBA	C_tEnd	ColonAscendens-ASBT-nRE	-1.8414507
T-BA	C_max	OSTα-T-BA-Transporter conc.	-1.7690188
T-BA	C_tEnd	OSTα-T-BA-Transporter conc.	-1.7690188
T-BA	C_max	UpperJejunum-ASBT-nRE	-1.2000989
T-BA	C_tEnd	UpperJejunum-ASBT-nRE	-1.2000989
G-BA	C_max	SI-Volume	-1.1441746
G-BA	C_tEnd	SI-Volume	-1.1441746
G-BA	C_max	Enzyme conc.	-1.0647761
G-BA	C_tEnd	Enzyme conc.	-1.0647761
G-BA	C_max	BAAT: Km	-1.0647111
G-BA	C_tEnd	BAAT: Km	-1.0647111
uBA	C_max	LU-Duodenum-pH	-1.0435492
uBA	C_tEnd	LU-Duodenum-pH	-1.0435492
T-BA	C_max	UpperIleum-ASBT-nRE	-1.0286472
T-BA	C_tEnd	UpperIleum-ASBT-nRE	-1.0286472
T-BA	C_max	LowerJejunum-ASBT-nRE	-1.0248725
T-BA	C_tEnd	LowerJejunum-ASBT-nRE	-1.0248725
T-BA	C_max	LowerIleum-ASBT-nRE	-1.0154996
T-BA	C_tEnd	LowerIleum-ASBT-nRE	-1.0154996
uBA	C_max	LU-LowerIleum-pH	-1.0098133
uBA	C_tEnd	LU-LowerIleum-pH	-1.0098133
G-BA	C_max	LU-Caecum-BSH-nRE	-1.0067195
G-BA	C_tEnd	LU-Caecum-BSH-nRE	-1.0067195
T-BA	C_max	LU-Caecum-BSH-nRE	-1.0024085
T-BA	C_tEnd	LU-Caecum-BSH-nRE	-1.0024085
T-BA	C_max	LU-Rectum-BSH-nRE	-0.9950211
T-BA	C_tEnd	LU-Rectum-BSH-nRE	-0.9950211

Table B.23: Sensitivity analysis of fitted human conjugation model parameters on BA composition in bile. Shown are only parameters with sensitivity coefficient above 1 or below -1. (LU: Lumen, nRE: normalized relative expression, ITR: intestinal transit rate)

Fraction of biliary BA	Parameter		Sensitivity coefficient
	PK	Model	
T-BA	C_tEnd	ASBT-Reference conc.	-1.3832474
uBA	C_max	LU-UpperJejunum-pH	-1.0501335
uBA	C_tEnd	LU-UpperJejunum-pH	-1.0500202
uBA	C_tEnd	LU-LowerJejunum-pH	-1.0075484
uBA	C_max	LU-LowerJejunum-pH	-1.0063512

Bibliography

[1] M. Makishima, A. Y. Okamoto, J. J. Repa, H. Tu, R. M. Learned, A. Luk, M. V. Hull, K. D. Lustig, D. J. Mangelsdorf, and B. Shan, "Identification of a nuclear receptor for bile acids," *Science*, vol. 284, no. 5418, pp. 1362–1365, 1999.

[2] D. J. Parks, S. G. Blanchard, R. K. Bledsoe, G. Chandra, T. G. Consler, S. A. Kliewer, J. B. Stimmel, T. M. Willson, A. M. Zavacki, D. D. Moore, and J. M. Lehmann, "Bile acids: Natural ligands for an orphan nuclear receptor," *Science*, vol. 284, no. 5418, pp. 1365–1368, 1999.

[3] H. Wang, J. Chen, K. Hollister, L. C. Sowers, and B. M. Forman, "Endogenous bile acids are ligands for the nuclear receptor fxr/bar," *Molecular Cell*, vol. 3, pp. 543–553, May 1999.

[4] J. L. Staudinger, B. Goodwin, S. A. Jones, D. Hawkins-Brown, K. I. MacKenzie, A. LaTour, Y. Liu, C. D. Klaassen, K. K. Brown, J. Reinhard, T. M. Willson, B. H. Koller, and S. A. Kliewer, "The nuclear receptor pxr is a lithocholic acid sensor that protects against liver toxicity.," *Proceedings of the National Academy of Sciences of the United States of America*, vol. 98, pp. 3369–74, Mar 2001.

[5] T. Inagaki, M. Choi, A. Moschetta, L. Peng, C. L. Cummins, J. G. McDonald, G. Luo, S. A. Jones, B. Goodwin, J. A. Richardson, R. D. Gerard, J. J. Repa, D. J. Mangelsdorf, and S. A. Kliewer, "Fibroblast growth factor 15 functions as an enterohepatic signal to regulate bile acid homeostasis.," *Cell metabolism*, vol. 2, pp. 217–25, Oct 2005.

[6] B. Lin, M. Wang, C. Blackmore, and L. Desnoyers, "Liver-specific activities of fgf19 require klotho beta," *Journal of Biological Chemistry*, vol. 282, pp. 27277–27284, 9 2007.

[7] M. Potthoff, J. Boney-Montoya, M. Choi, T. He, N. Sunny, S. Satapati, K. Suino-Powell, H. Xu, R. Gerard, B. Finck, S. Burgess,

D. Mangelsdorf, and S. Kliewer, “Fgf15/19 regulates hepatic glucose metabolism by inhibiting the creb-pgc-1x3b1; pathway,” *Cell Metabolism*, vol. 13, pp. 729–738, June 2011.

[8] M. Watanabe, S. M. Houten, L. Wang, A. Moschetta, D. J. Mangelsdorf, R. A. Heyman, D. D. Moore, and J. Auwerx, “Bile acids lower triglyceride levels via a pathway involving fxr, shp, and srebp-1c,” *The Journal of Clinical Investigation*, vol. 113, pp. 1408–1418, 5 2004.

[9] K. D. Setchell, C. M. Rodrigues, C. Clerici, A. Solinas, A. Morelli, C. Gartung, and J. Boyer, “Bile acid concentrations in human and rat liver tissue and in hepatocyte nuclei.,” *Gastroenterology*, vol. 112, pp. 226–35, Jan 1997.

[10] S. Sayin, A. Wahlström, J. Felin, S. Jäntti, H.-U. Marschall, K. Bamberg, B. Angelin, T. Hyötyläinen, M. Orešič, and F. Bäckhed, “Gut microbiota regulates bile acid metabolism by reducing the levels of tauro-beta-muricholic acid, a naturally occurring fxr antagonist,” *Cell Metabolism*, vol. 17, no. 2, pp. 225 – 235, 2013.

[11] J.-L. Lew, A. Zhao, J. Yu, L. Huang, N. de Pedro, F. Peláez, S. D. Wright, and J. Cui, “The farnesoid x receptor controls gene expression in a ligand- and promoter-selective fashion *,” *Journal of Biological Chemistry*, vol. 279, pp. 8856–8861, Mar. 2004.

[12] R. Thakare, J. A. Alamoudi, N. Gautam, A. D. Rodrigues, and Y. Alnouti, “Species differences in bile acids i. plasma and urine bile acid composition,” *Journal of Applied Toxicology*, vol. 38, no. 10, pp. 1323–1335, 2018.

[13] J. Fiamoncini, A. M. Yiorkas, K. Gedrich, M. Rundle, S. I. Alsters, G. Roeselers, T. J. van den Broek, T. Clavel, I. Lagkouvardos, S. Wopereis, G. Frost, B. van Ommen, A. I. Blakemore, and H. Daniel, “Determinants of postprandial plasma bile acid kinetics in human volunteers,” *American Journal of Physiology-Gastrointestinal and Liver Physiology*, vol. 313, no. 4, pp. G300–G312, 2017. PMID: 28663304.

[14] E. C. E. Meessen, F. L. P. Sips, H. M. Eggink, M. Koehorst, J. A. Romijn, A. K. Groen, N. A. W. van Riel, and M. R. Soeters, “Model-based data analysis of individual human postprandial plasma bile acid responses indicates a major role for the gallbladder and intestine,” *Physiological reports*, vol. 8, pp. e14358–e14358, Mar. 2020.

[15] C. Steiner, A. Othman, C. H. Saely, P. Rein, H. Drexel, A. von Eckardstein, and K. M. Rentsch, “Bile acid metabolites in serum:

intraindividual variation and associations with coronary heart disease, metabolic syndrome and diabetes mellitus.," *PloS one*, vol. 6, p. e25006, 2011.

[16] J. M. Ridlon, D.-J. Kang, and P. B. Hylemon, "Bile salt biotransformations by human intestinal bacteria," *Journal of Lipid Research*, vol. 47, pp. 241–259, Feb. 2006.

[17] J. Li and P. A. Dawson, "Animal models to study bile acid metabolism," *Biochimica et Biophysica Acta (BBA) - Molecular Basis of Disease*, vol. 1865, no. 5, pp. 895 – 911, 2019. Animal Models in Liver Disease.

[18] T. Inagaki, A. Moschetta, Y.-K. Lee, L. Peng, G. Zhao, M. Downes, R. T. Yu, J. M. Shelton, J. A. Richardson, J. J. Repa, D. J. Mangelsdorf, and S. A. Kliewer, "Regulation of antibacterial defense in the small intestine by the nuclear bile acid receptor.," *Proceedings of the National Academy of Sciences of the United States of America*, vol. 103, pp. 3920–5, Mar 2006.

[19] Y. Tian, W. Gui, I. Koo, P. B. Smith, E. L. Allman, R. G. Nichols, B. Rimal, J. Cai, Q. Liu, and A. D. Patterson, "The microbiome modulating activity of bile acids," *Gut Microbes*, vol. 11, no. 4, pp. 979–996, 2020. PMID: 32138583.

[20] A. Wahlström, S. Sayin, H.-U. Marschall, and F. Bäckhed, "Intestinal crosstalk between bile acids and microbiota and its impact on host metabolism," *Cell Metabolism*, vol. 24, no. 1, pp. 41 – 50, 2016.

[21] C. Staley, A. R. Weingarden, A. Khoruts, and M. J. Sadowsky, "Interaction of gut microbiota with bile acid metabolism and its influence on disease states," *Applied microbiology and biotechnology*, vol. 101, pp. 47–64, Jan. 2017.

[22] H. Duboc, S. Rajca, D. Rainteau, D. Benarous, M.-A. Maubert, E. Quervain, G. Thomas, V. Barbu, L. Humbert, G. Despras, C. Bridonneau, F. Dumetz, J.-P. Grill, J. Masliah, L. Beaugerie, J. Cosnes, O. Chazouillères, R. Poupon, C. Wolf, J.-M. Mallet, P. Langella, G. Trugnan, H. Sokol, and P. Seksik, "Connecting dysbiosis, bile-acid dysmetabolism and gut inflammation in inflammatory bowel diseases," *Gut*, vol. 62, no. 4, pp. 531–539, 2013.

[23] R. Poupon, O. Chazouillères, and R. Poupon, "Chronic cholestatic diseases," *Journal of Hepatology*, vol. 32, pp. 129–140, 2000.

[24] E. A. Rodríguez-Garay, "Cholestasis: human disease and experimental animal models," *Annals of Hepatology*, vol. 2, no. 4, pp. 150–158, 2003.

[25] M. Strazzabosco, L. Fabris, and C. Spirli, "Pathophysiology of cholangiopathies," *Journal of Clinical Gastroenterology*, vol. 39, no. 4, 2005.

[26] F. Casellas, S. Aguade, B. Soriano, A. Accarino, J. Molero, and L. Guarner, "Intestinal permeability to 99m tc–diethylenetriaminopentaacetic acid in inflammatory bowel disease.," *American Journal of Gastroenterology (Springer Nature)*, vol. 81, no. 9, 1986.

[27] R. Jenkins, J. Ramage, D. Jones, S. Collins, R. Goodacre, and R. Hunt, "Small bowel and colonic permeability to 51cr-edta in patients with active inflammatory bowel disease," *Clinical and investigative medicine. Medecine clinique et experimentale*, vol. 11, p. 151—155, April 1988.

[28] W. Jia, G. Xie, and W. Jia, "Bile acid-microbiota crosstalk in gastrointestinal inflammation and carcinogenesis," *Nature Reviews Gastroenterology Hepatology*, vol. 15, no. 2, pp. 111–128, 2018.

[29] K. J. Ho, "Circadian distribution of bile acid in the enterohepatic circulatory system in hamsters.," *Journal of lipid research*, vol. 17, pp. 600–4, Nov 1976.

[30] K. J. Ho, "Circadian distribution of bile acids in the enterohepatic circulatory system in rats.," *The American journal of physiology*, vol. 230, pp. 1331–5, May 1976.

[31] Y.-K. J. Zhang, G. L. Guo, and C. D. Klaassen, "Diurnal variations of mouse plasma and hepatic bile acid concentrations as well as expression of biosynthetic enzymes and transporters.," *PloS one*, vol. 6, p. e16683, Feb 2011.

[32] H. M. Eggink, J. E. Oosterman, P. de Goede, E. M. de Vries, E. Foppen, M. Koehorst, A. K. Groen, A. Boelen, J. A. Romijn, S. E. la Fleur, M. R. Soeters, and A. Kalsbeek, "Complex interaction between circadian rhythm and diet on bile acid homeostasis in male rats," *Chronobiology International*, vol. 34, no. 10, pp. 1339–1353, 2017. PMID: 29028359.

[33] B. Kister, A. Viehof, U. Rolle-Kampczyk, A. Schwentker, N. S. Treichel, S. A. V. Jennings, T. H. Wirtz, L. M. Blank, M. W. Hornef,

M. von Bergen, T. Clavel, and L. Kuepfer, “A physiologically based model of bile acid metabolism in mice,” *iScience*, vol. 26, Oct. 2023.

[34] J. L. Boyer, “Bile formation and secretion.,” *Comprehensive Physiology*, vol. 3, pp. 1035–78, Jul 2013.

[35] A. F. Hofmann and K. J. Mysels, “Bile salts as biological surfactants,” *Colloids and Surfaces*, vol. 30, no. 1, pp. 145–173, 1987. Symposium for the Division of Colloid and Surface Chemistry, American Chemical Society, National Meeting.

[36] M. J. Monte, J. J. Marin, A. Antelo, and J. Vazquez-Tato, “Bile acids: chemistry, physiology, and pathophysiology,” *World journal of gastroenterology: WJG*, vol. 15, no. 7, p. 804, 2009.

[37] C. Thomas, R. Pellicciari, M. Pruzanski, J. Auwerx, and K. Schoonjans, “Targeting bile-acid signalling for metabolic diseases,” *Nature Reviews Drug Discovery*, vol. 7, no. 8, pp. 678–693, 2008.

[38] G. A. Haslewood, “The biological significance of chemical differences in bile salts.,” *Biological reviews of the Cambridge Philosophical Society*, vol. 39, pp. 537–74, Nov 1964.

[39] G. A. Haslewood, “Bile salt evolution.,” *Journal of lipid research*, vol. 8, pp. 535–50, Nov 1967.

[40] A. F. Hofmann and L. R. Hagey, “Bile acids: Chemistry, pathochemistry, biology, pathobiology, and therapeutics,” *Cellular and Molecular Life Sciences*, vol. 65, no. 16, pp. 2461–2483, 2008.

[41] M. Nurunnabi, Z. Khatun, V. Revuri, M. Nafiujjaman, S. Cha, S. Cho, K. Moo Huh, and Y.-k. Lee, “Design and strategies for bile acid mediated therapy and imaging,” *RSC Adv.*, vol. 6, pp. 73986–74002, 2016.

[42] A. N. Bukiya, J. McMillan, A. L. Parrill, and A. M. Dopico, “Structural determinants of monohydroxylated bile acids to activate x3b2;¡sub¿1¡/sub¿ subunit-containing bk channels *¡sup¿sx20de;¡/sup¿,” *Journal of Lipid Research*, vol. 49, pp. 2441–2451, Nov. 2008.

[43] O. Martinez-Augustin and F. S. de Medina, “Intestinal bile acid physiology and pathophysiology,” *World journal of gastroenterology*, vol. 14, no. 37, pp. 5630–5640, 2008.

[44] J. Maldonado-Valderrama, N. C. Woodward, A. P. Gunning, M. J. Ridout, F. A. Husband, A. R. Mackie, V. J. Morris, and P. J. Wilde,

"Interfacial characterization of -lactoglobulin networks: Displacement by bile salts," *Langmuir*, vol. 24, pp. 6759–6767, July 2008.

[45] S. R. Euston, U. Bellstedt, K. Schillbach, and P. S. Hughes, "The adsorption and competitive adsorption of bile salts and whey protein at the oil–water interface," *Soft Matter*, vol. 7, pp. 8942–8951, 2011.

[46] A. Roda, A. Minutello, M. A. Angellotti, and A. Fini, "Bile acid structure-activity relationship: evaluation of bile acid lipophilicity using 1-octanol/water partition coefficient and reverse phase hplc," *Journal of lipid research*, vol. 31, pp. 1433–1443, Aug. 1990.

[47] J. Maldonado-Valderrama, P. Wilde, A. Macierzanka, and A. Mackie, "The role of bile salts in digestion," *Advances in Colloid and Interface Science*, vol. 165, no. 1, pp. 36–46, 2011. Food Colloids 2010 - On the Road from Interfaces to Consumers.

[48] N. Pavlović, S. Golocorbin-Kon, M. anić (Stojančević), B. Stanimirov, H. Al-Salami, K. Stankov, and M. Mikov, "Bile acids and their derivatives as potential modifiers of drug release and pharmacokinetic profiles," *Frontiers in Pharmacology*, vol. 9, 11 2018.

[49] D. Madenci and S. Egelhaaf, "Self-assembly in aqueous bile salt solutions," *Current Opinion in Colloid Interface Science*, vol. 15, no. 1, pp. 109–115, 2010.

[50] S. E. Lucangioli, C. N. Carducci, V. P. Tripodi, and E. Kenndler, "Retention of bile salts in micellar electrokinetic chromatography: relation of capacity factor to octanol–water partition coefficient and critical micellar concentration," *Journal of Chromatography B: Biomedical Sciences and Applications*, vol. 765, no. 2, pp. 113–120, 2001.

[51] R. Holm, A. Müllertz, and H. Mu, "Bile salts and their importance for drug absorption," *International Journal of Pharmaceutics*, vol. 453, no. 1, pp. 44–55, 2013. Poorly Soluble Drugs.

[52] C. Faustino, C. Serafim, P. Rijo, and C. P. Reis, "Bile acids and bile acid derivatives: use in drug delivery systems and as therapeutic agents," *Expert Opinion on Drug Delivery*, vol. 13, no. 8, pp. 1133–1148, 2016. PMID: 27102882.

[53] K. Matsuoka, M. Suzuki, C. Honda, K. Endo, and Y. Moroi, "Micellization of conjugated chenodeoxy- and ursodeoxycholates and solubilization of cholesterol into their micelles: comparison with other four conjugated bile salts species," *Chemistry and Physics of Lipids*, vol. 139, no. 1, pp. 1–10, 2006.

[54] M. Calabresi, P. Andreozzi, and C. La Mesa, "Supra-molecular association and polymorphic behaviour in systems containing bile acid salts," *Molecules*, vol. 12, no. 8, pp. 1731–1754, 2007.

[55] J. Twisk, M. F. Hoekman, W. H. Mager, A. F. Moorman, P. A. de Boer, L. Scheja, H. M. Princen, and R. Gebhardt, "Heterogeneous expression of cholesterol 7 alpha-hydroxylase and sterol 27-hydroxylase genes in the rat liver lobulus.," *The Journal of Clinical Investigation*, vol. 95, pp. 1235–1243, 3 1995.

[56] W. J. Insull, "Clinical utility of bile acid sequestrants in the treatment of dyslipidemia: a scientific review.," *Southern medical journal*, vol. 99, pp. 257–73, Mar 2006.

[57] D. W. Russell, "The enzymes, regulation, and genetics of bile acid synthesis," *Annual Review of Biochemistry*, vol. 72, no. 1, pp. 137–174, 2003. PMID: 12543708.

[58] L. B. Agellon, "Chapter 15 - metabolism and function of bile acids," in *Biochemistry of Lipids, Lipoproteins and Membranes (Fifth Edition)* (D. E. Vance and J. E. Vance, eds.), pp. 423–440, San Diego: Elsevier, fifth edition ed., 2008.

[59] H. C. Shea, D. D. Head, K. D. R. Setchell, and D. W. Russell, "Analysis of hsd3b7 knockout mice reveals that a 3-hydroxyl stereochemistry is required for bile acid function," *Proceedings of the National Academy of Sciences*, vol. 104, no. 28, pp. 11526–11533, 2007.

[60] L. Fan, J. F. Joseph, P. Durairaj, M. K. Parr, and M. Bureik, "Conversion of chenodeoxycholic acid to cholic acid by human cyp8b1," *Biological Chemistry*, vol. 400, no. 5, pp. 625–628, 2019.

[61] J. Li-Hawkins, E. G. Lund, S. D. Turley, and D. W. Russell, "Disruption of the oxysterol 7x3b1;-hydroxylase gene in mice *," *Journal of Biological Chemistry*, vol. 275, pp. 16536–16542, June 2000.

[62] S. Dzeletovic, O. Breuer, E. Lund, and U. Diczfalusy, "Determination of cholesterol oxidation products in human plasma by isotope dilution-mass spectrometry," *Analytical Biochemistry*, vol. 225, no. 1, pp. 73–80, 1995.

[63] W. M. Pandak and G. Kakiyama, "The acidic pathway of bile acid synthesis: Not just an alternative pathway," *Liver Research*, vol. 3, no. 2, pp. 88–98, 2019.

[64] D. W. Russell, R. W. Halford, D. M. Ramirez, R. Shah, and T. Kotti, "Cholesterol 24-hydroxylase: An enzyme of cholesterol turnover in

the brain," *Annual Review of Biochemistry*, vol. 78, no. 1, pp. 1017–1040, 2009. PMID: 19489738.

[65] M. Schwarz, D. W. Russell, J. M. Dietschy, and S. D. Turley, "Marked reduction in bile acid synthesis in cholesterol 7x3b1;-hydroxylase-deficient mice does not lead to diminished tissue cholesterol turnover or to hypercholesterolemia," *Journal of Lipid Research*, vol. 39, pp. 1833–1843, Sept. 1998.

[66] M. Schwarz, D. W. Russell, J. M. Dietschy, and S. D. Turley, "Alternate pathways of bile acid synthesis in the cholesterol 7x3b1;-hydroxylase knockout mouse are not upregulated by either cholesterol or cholestyramine feeding," *Journal of Lipid Research*, vol. 42, pp. 1594–1603, Oct. 2001.

[67] C. R. Pullinger, C. Eng, G. Salen, S. Shefer, A. K. Batta, S. K. Erickson, A. Verhagen, C. R. Rivera, S. J. Mulvihill, M. J. Malloy, and J. P. Kane, "Human cholesterol 7-hydroxylase (cyp7a1) deficiency has a hypercholesterolemic phenotype," *The Journal of Clinical Investigation*, vol. 110, pp. 109–117, 7 2002.

[68] Z. D. Fu, I. L. Csanaky, and C. D. Klaassen, "Gender-divergent profile of bile acid homeostasis during aging of mice," *PLOS ONE*, vol. 7, pp. 1–13, 03 2012.

[69] S. Takahashi, T. Fukami, Y. Masuo, C. N. Brocker, C. Xie, K. W. Krausz, C. R. Wolf, C. J. Henderson, and F. J. Gonzalez, "Cyp2c70 is responsible for the species difference in bile acid metabolism between mice and humans," *Journal of Lipid Research*, vol. 57, no. 12, pp. 2130–2137, 2016.

[70] A. Honda, T. Miyazaki, J. Iwamoto, T. Hirayama, Y. Morishita, T. Monma, H. Ueda, S. Mizuno, F. Sugiyama, S. Takahashi, and T. Ikegami, "Regulation of bile acid metabolism in mouse models with hydrophobic bile acid composition.," *Journal of lipid research*, vol. 61, pp. 54–69, Jan 2020.

[71] J. F. de Boer, M. Schonewille, M. Boesjes, H. Wolters, V. W. Bloks, T. Bos, T. H. van Dijk, A. Jurdzinski, R. Boverhof, J. C. Wolters, J. A. Kuivenhoven, J. M. van Deursen, R. P. Oude Elferink, A. Moschetta, C. Kremoser, H. J. Verkade, F. Kuipers, and A. K. Groen, "Intestinal farnesoid x receptor controls transintestinal cholesterol excretion in mice," *Gastroenterology*, vol. 152, no. 5, pp. 1126–1138.e6, 2017.

[72] G. L. Guo and J. Y. L. Chiang, "Is cyp2c70 the key to new mouse models to understand bile acids in humans?¡sup¿1¡/sup¿," *Journal of Lipid Research*, vol. 61, pp. 269–271, Mar. 2020.

[73] J. F. de Boer, E. Verkade, N. L. Mulder, H. D. de Vries, N. Huijkman, M. Koehorst, T. Boer, J. C. Wolters, V. W. Bloks, B. van de Sluis, and F. Kuipers, "A human-like bile acid pool induced by deletion of hepatic ¡em¿cyp2c70¡/em¿ modulates effects of fxr activation in mice [s]," *Journal of Lipid Research*, vol. 61, pp. 291–305, Mar. 2020.

[74] C. N. Falany, H. Fortinberry, E. H. Leiter, and S. Barnes, "Cloning, expression, and chromosomal localization of mouse liver bile acid coa:amino acid n-acyltransferase," *Journal of Lipid Research*, vol. 38, pp. 1139–1148, June 1997.

[75] M. Schwenk, A. F. Hofmann, G. L. Carlson, J. A. Carter, F. Coulston, and H. Greim, "Bile acid conjugation in the chimpanzee: effective sulfation of lithocholic acid," *Archives of Toxicology*, vol. 40, no. 2, pp. 109–118, 1978.

[76] K. Linnet, "Postprandial plasma concentrations of glycine and taurine conjugated bile acids in healthy subjects.," *Gut*, vol. 24, no. 3, pp. 249–252, 1983.

[77] Y. Alnouti, "Bile Acid Sulfation: A Pathway of Bile Acid Elimination and Detoxification," *Toxicological Sciences*, vol. 108, pp. 225–246, 01 2009.

[78] M. Rius, A. T. Nies, J. Hummel-Eisenbeiss, G. Jedlitschky, and D. Keppler, "Cotransport of reduced glutathione with bile salts by mrp4 (abcc4) localized to the basolateral hepatocyte membrane," *Hepatology*, vol. 38, no. 2, pp. 374–384, 2003.

[79] E. Halilbasic, T. Claudel, and M. Trauner, "Bile acid transporters and regulatory nuclear receptors in the liver and beyond," *Journal of Hepatology*, vol. 58, no. 1, pp. 155–168, 2013.

[80] R. H. Palmer and M. G. Bolt, "Bile acid sulfates. i. synthesis of lithocholic acid sulfates and their identification in human bile," *Journal of Lipid Research*, vol. 12, no. 6, pp. 671–679, 1971.

[81] Y. Zhang and C. D. Klaassen, "Effects of feeding bile acids and a bile acid sequestrant on hepatic bile acid composition in mice [s]," *Journal of Lipid Research*, vol. 51, pp. 3230–3242, Nov. 2010.

[82] S. N. Chaudhari, D. A. Harris, H. Aliakbarian, J. N. Luo, M. T. Henke, R. Subramaniam, A. H. Vernon, A. Tavakkoli, E. G. Sheu, and A. S. Devlin, "Bariatric surgery reveals a gut-restricted tgr5 agonist with anti-diabetic effects," *Nature Chemical Biology*, vol. 17, no. 1, pp. 20–29, 2021.

[83] A. Radominska, K. A. Comer, P. Zimniak, J. Falany, M. Iscan, and C. N. Falany, "Human liver steroid sulphotransferase sulphates bile acids," *Biochemical Journal*, vol. 272, pp. 597–604, 12 1990.

[84] L. Feng, Y.-L. Yuen, J. Xu, X. Liu, M. Y.-C. Chan, K. Wang, W.-P. Fong, W.-T. Cheung, and S. S.-T. Lee, "Identification and characterization of a novel pparx3b1;-regulated and 7x3b1;-hydroxyl bile acid-preferring cytosolic sulfotransferase ml-stl (sult2a8) [s]," *Journal of Lipid Research*, vol. 58, pp. 1114–1131, June 2017.

[85] J. Robben, G. Parmentier, and H. Eyssen, "Isolation of a rat intestinal clostridium strain producing 5 alpha- and 5 beta-bile salt 3 alpha-sulfatase activity," *Applied and Environmental Microbiology*, vol. 51, no. 1, pp. 32–38, 1986.

[86] S. Marion, N. Studer, L. Desharnais, L. Menin, S. Escrig, A. Meibom, S. Hapfelmeier, and R. Bernier-Latmani, "In vitro and in vivo characterization of clostridium scindens bile acid transformations," *Gut Microbes*, vol. 10, no. 4, pp. 481–503, 2019. PMID: 30589376.

[87] H. Eyssen, G. D. Pauw, J. Stragier, and A. Verhulst, "Cooperative formation of omega-muricholic acid by intestinal microorganisms," *Applied and Environmental Microbiology*, vol. 45, no. 1, pp. 141–147, 1983.

[88] H. Brunner, T. C. Northfield, A. F. Hofmann, V. L. Go, and W. H. Summerskill, "Gastric emptying and secretion of bile acids, cholesterol, and pancreatic enzymes during digestion. duodenal perfusion studies in healthy subjects.," *Mayo Clinic proceedings*, vol. 49, pp. 851–60, Nov 1974.

[89] H. Y. Mok, K. von Bergmann, and S. M. Grundy, "Regulation of pool size of bile acids in man," *Gastroenterology*, vol. 73, no. 4, Part 1, pp. 684–690, 1977.

[90] S. Mita, H. Suzuki, H. Akita, H. Hayashi, R. Onuki, A. F. Hofmann, and Y. Sugiyama, "Vectorial transport of unconjugated and conjugated bile salts by monolayers of llc-pk1 cells doubly transfected with human ntcp and bsep or with rat ntcp and bsep," *American Journal of Physiology-Gastrointestinal and Liver Physiology*, vol. 290, no. 3, pp. G550–G556, 2006. PMID: 16474011.

[91] S. S. Strautnieks, L. N. Bull, A. S. Knisely, S. A. Kocoshis, N. Dahl, H. Arnell, E. Sokal, K. Dahan, S. Childs, V. Ling, M. S. Tanner, A. F. Kagalwalla, A. Németh, J. Pawlowska, A. Baker, G. Mieli-Vergani,

N. B. Freimer, R. M. Gardiner, and R. J. Thompson, "A gene encoding a liver-specific abc transporter is mutated in progressive familial intrahepatic cholestasis," *Nature Genetics*, vol. 20, no. 3, pp. 233–238, 1998.

[92] B. Stieger, Y. Meier, and P. J. Meier, "The bile salt export pump," *Pflügers Archiv - European Journal of Physiology*, vol. 453, no. 5, pp. 611–620, 2007.

[93] T. Kagawa, N. Watanabe, K. Mochizuki, A. Numari, Y. Ikeno, J. Itoh, H. Tanaka, I. M. Arias, and T. Mine, "Phenotypic differences in pfic2 and bric2 correlate with protein stability of mutant bsep and impaired taurocholate secretion in mdck ii cells," *American Journal of Physiology-Gastrointestinal and Liver Physiology*, vol. 294, no. 1, pp. G58–G67, 2008. PMID: 17947449.

[94] P. Lam, C. L. Pearson, C. J. Soroka, S. Xu, A. Mennone, and J. L. Boyer, "Levels of plasma membrane expression in progressive and benign mutations of the bile salt export pump (bsep/abcb11) correlate with severity of cholestatic diseases," *American Journal of Physiology-Cell Physiology*, vol. 293, no. 5, pp. C1709–C1716, 2007. PMID: 17855769.

[95] P. Anderle, T. Sengstag, D. M. Mutch, M. Rumbo, V. Praz, R. Mansourian, M. Delorenzi, G. Williamson, and M.-A. Roberts, "Changes in the transcriptional profile of transporters in the intestine along the anterior-posterior and crypt-villus axes," *BMC Genomics*, vol. 6, no. 1, p. 69, 2005.

[96] B. Kister, A. Viehof, U. Rolle-Kampczyk, A. Schwentker, N. S. Treichel, S. Jennings, T. H. Wirtz, L. M. Blank, M. W. Hornef, M. von Bergen, T. Clavel, and L. Kuepfer, "A physiologically based model of bile acid metabolism in mice," *bioRxiv*, 2022.

[97] P. Hruz, C. Zimmermann, H. Gutmann, L. Degen, U. Beuers, L. Terracciano, J. Drewe, and C. Beglinger, "Adaptive regulation of the ileal apical sodium dependent bile acid transporter (asbt) in patients with obstructive cholestasis," *Gut*, vol. 55, no. 3, pp. 395–402, 2006.

[98] P. A. Dawson, J. Haywood, A. L. Craddock, M. Wilson, M. Tietjen, K. Kluckman, N. Maeda, and J. S. Parks, "Targeted deletion of the ileal bile acid transporter eliminates enterohepatic cycling of bile acids in mice," *The Journal of biological chemistry*, vol. 278, pp. 33920–33927, Sept. 2003.

[99] L. B. Agellon, M. J. Toth, and A. B. R. Thomson, "Intracellular lipid binding proteins of the small intestine," *Molecular and Cellular Biochemistry*, vol. 239, no. 1, pp. 79–82, 2002.

[100] R. Wang, M. Salem, I. M. Yousef, B. Tuchweber, P. Lam, S. J. Childs, C. D. Helgason, C. Ackerley, M. J. Phillips, and V. Ling, "Targeted inactivation of sister of p-glycoprotein gene (spgp) in mice results in nonprogressive but persistent intrahepatic cholestasis," *Proceedings of the National Academy of Sciences*, vol. 98, no. 4, pp. 2011–2016, 2001.

[101] D. J. Seward, A. S. Koh, J. L. Boyer, and N. Ballatori, "Functional complementation between a novel mammalian polygenic transport complex and an evolutionarily ancient organic solute transporter, ostalpha-ostbeta.," *The Journal of biological chemistry*, vol. 278, pp. 27473–82, Jul 2003.

[102] N. Ballatori, W. V. Christian, J. Y. Lee, P. A. Dawson, C. J. Soroka, J. L. Boyer, M. S. Madejczyk, and N. Li, "Ost-ost: A major basolateral bile acid and steroid transporter in human intestinal, renal, and biliary epithelia," *Hepatology*, vol. 42, no. 6, pp. 1270–1279, 2005.

[103] P. A. Dawson, M. Hubbert, J. Haywood, A. L. Craddock, N. Zerangue, W. V. Christian, and N. Ballatori, "The heteromeric organic solute transporter alpha-beta, ostalpha-ostbeta, is an ileal basolateral bile acid transporter," *The Journal of biological chemistry*, vol. 280, pp. 6960–6968, Feb. 2005.

[104] A. Rao, J. Haywood, A. L. Craddock, M. G. Belinsky, G. D. Kruh, and P. A. Dawson, "The organic solute transporter -, ost-ost, is essential for intestinal bile acid transport and homeostasis," *Proceedings of the National Academy of Sciences*, vol. 105, no. 10, pp. 3891–3896, 2008.

[105] P. J. Meier, "Molecular mechanisms of hepatic bile salt transport from sinusoidal blood into bile.," *The American journal of physiology*, vol. 269, pp. G801–12, Dec 1995.

[106] E. Jacquemin, B. Hagenbuch, B. Stieger, A. W. Wolkoff, and P. J. Meier, "Expression cloning of a rat liver na(+)-independent organic anion transporter.," *Proceedings of the National Academy of Sciences*, vol. 91, no. 1, pp. 133–137, 1994.

[107] H. Lu, S. Choudhuri, K. Ogura, I. L. Csanaky, X. Lei, X. Cheng, P.-z. Song, and C. D. Klaassen, "Characterization of Organic Anion Transporting Polypeptide 1b2-null Mice: Essential Role in Hepatic Uptake/Toxicity of Phalloidin and Microcystin-LR," *Toxicological Sciences*, vol. 103, pp. 35–45, 02 2008.

[108] X. Cheng, J. Maher, C. Chen, and C. D. Klaassen, "Tissue distribution and ontogeny of mouse organic anion transporting polypeptides (oatps)," *Drug Metabolism and Disposition*, vol. 33, no. 7, pp. 1062–1073, 2005.

[109] C. Pauli-Magnus and P. J. Meier, "Hepatobiliary transporters and drug-induced cholestasis," *Hepatology*, vol. 44, no. 4, pp. 778–787, 2006.

[110] S. Choudhuri and C. D. Klaassen, "Molecular regulation of bile acid homeostasis," *Drug Metabolism and Disposition*, vol. 50, no. 4, pp. 425–455, 2022.

[111] D. J. Peet, S. D. Turley, W. Ma, B. A. Janowski, J.-M. A. Lobaccaro, R. E. Hammer, and D. J. Mangelsdorf, "Cholesterol and bile acid metabolism are impaired in mice lacking the nuclear oxysterol receptor lxr," *Cell*, vol. 93, no. 5, pp. 693–704, 1998.

[112] B. Goodwin, M. A. Watson, H. Kim, J. Miao, J. K. Kemper, and S. A. Kliewer, "Differential Regulation of Rat and Human CYP7A1 by the Nuclear Oxysterol Receptor Liver X Receptor-," *Molecular Endocrinology*, vol. 17, pp. 386–394, 03 2003.

[113] B. Goodwin, S. A. Jones, R. R. Price, M. A. Watson, D. D. McKee, L. B. Moore, C. Galardi, J. G. Wilson, M. C. Lewis, M. E. Roth, P. R. Maloney, T. M. Willson, and S. A. Kliewer, "A regulatory cascade of the nuclear receptors fxr, shp-1, and lrh-1 represses bile acid biosynthesis," *Molecular Cell*, vol. 6, no. 3, pp. 517–526, 2000.

[114] O. Barbier, J. Trottier, J. Kaeding, P. Caron, and M. Verreault, "Lipid-activated transcription factors control bile acid glucuronidation," *Molecular and Cellular Biochemistry*, vol. 326, no. 1, pp. 3–8, 2009.

[115] S. A. Kliewer and D. J. Mangelsdorf, "Bile Acids as Hormones: The FXR-FGF15/19 Pathway," *Digestive Diseases*, vol. 33, pp. 327–331, 05 2015.

[116] B. Kong, L. Wang, J. Y. Chiang, Y. Zhang, C. D. Klaassen, and G. L. Guo, "Mechanism of tissue-specific farnesoid x receptor in suppressing the expression of genes in bile-acid synthesis in mice," *Hepatology*, vol. 56, no. 3, pp. 1034–1043, 2012.

[117] J. Y. L. Chiang, "Negative feedback regulation of bile acid metabolism: impact on liver metabolism and diseases.," *Hepatology (Baltimore, Md.)*, vol. 62, pp. 1315–7, Oct 2015.

[118] C. Brendel, K. Schoonjans, O. A. Botrugno, E. Treuter, and J. Auwerx, "The Small Heterodimer Partner Interacts with the Liver X Receptor and Represses Its Transcriptional Activity," *Molecular Endocrinology*, vol. 16, pp. 2065–2076, 09 2002.

[119] A. del Castillo-Olivares and G. Gil, "Suppression of sterol 12-hydroxylase transcription by the short heterodimer partner: insights into the repression mechanism," *Nucleic Acids Research*, vol. 29, pp. 4035–4042, 10 2001.

[120] M. Zhang and J. Y. L. Chiang, "Transcriptional regulation of the human sterol 12x3b1;-hydroxylase gene (¡em¿cyp8b1¡/em¿): Roles of hepatocyte nuclear factor 4x3b1; in mediating bile acid repression *," *Journal of Biological Chemistry*, vol. 276, pp. 41690–41699, Nov. 2001.

[121] T. de Aguiar Vallim, E. Tarling, H. Ahn, L. Hagey, C. Romanoski, R. Lee, M. Graham, H. Motohashi, M. Yamamoto, and P. Edwards, "Mafg is a transcriptional repressor of bile acid synthesis and metabolism," *Cell Metabolism*, vol. 21, pp. 298–311, Feb. 2015.

[122] A. Geier, M. Wagner, C. G. Dietrich, and M. Trauner, "Principles of hepatic organic anion transporter regulation during cholestasis, inflammation and liver regeneration," *Biochimica et Biophysica Acta (BBA) - Molecular Cell Research*, vol. 1773, no. 3, pp. 283–308, 2007.

[123] W. A. Alrefai and R. K. Gill, "Bile acid transporters: Structure, function, regulation and pathophysiological implications," *Pharmaceutical Research*, vol. 24, no. 10, pp. 1803–1823, 2007.

[124] M. S. Anwer, "Cellular regulation of hepatic bile acid transport in health and cholestasis," *Hepatology*, vol. 39, no. 3, pp. 581–590, 2004.

[125] H. Wolters, B. M. Elzinga, J. F. W. Baller, R. Boverhof, M. Schwarz, B. Stieger, H. J. Verkade, and F. Kuipers, "Effects of bile salt flux variations on the expression of hepatic bile salt transporters in vivo in mice," *Journal of Hepatology*, vol. 37, pp. 556–563, Nov. 2002.

[126] F. G. Schaap, N. A. van der Gaag, D. J. Gouma, and P. L. M. Jansen, "High expression of the bile salt-homeostatic hormone fibroblast growth factor 19 in the liver of patients with extrahepatic cholestasis.," *Hepatology (Baltimore, Md.)*, vol. 49, pp. 1228–35, Apr 2009.

[127] M. Wagner, P. Fickert, G. Zollner, A. Fuchsbichler, D. Silbert, O. Tsybrovskyy, K. Zatloukal, G. L. Guo, J. D. Schuetz, F. J. Gonzalez, H.-U. Marschall, H. Denk, and M. Trauner, "Role of farnesoid x receptor in determining hepatic abc transporter expression and liver injury in

bile duct-ligated mice," *Gastroenterology*, vol. 125, pp. 825–838, Sept. 2003.

[128] G. Zollner, P. Fickert, D. Silbert, A. Fuchsbichler, H. U. Marschall, K. Zatloukal, H. Denk, and M. Trauner, "Adaptive changes in hepatobiliary transporter expression in primary biliary cirrhosis.," *Journal of hepatology*, vol. 38, pp. 717–27, Jun 2003.

[129] A. Kassam, B. Miao, P. R. Young, and R. Mukherjee, "Retinoid x receptor (rxr) agonist-induced antagonism of farnesoid x receptor (fxr) activity due to absence of coactivator recruitment and decreased dna binding.," *The Journal of biological chemistry*, vol. 278, pp. 10028–32, Mar 2003.

[130] T. Bosse, C. M. Piaseckyj, E. Burghard, J. J. Fialkovich, S. Rajagopal, W. T. Pu, and S. D. Krasinski, "Gata4 is essential for the maintenance of jejunal-ileal identities in the adult mouse small intestine.," *Molecular and cellular biology*, vol. 26, pp. 9060–70, Dec 2006.

[131] M. A. Battle, B. J. Bondow, M. A. Iverson, S. J. Adams, R. J. Jandacek, P. Tso, and S. A. Duncan, "Gata4 is essential for jejunal function in mice.," *Gastroenterology*, vol. 135, pp. 1676–1686.e1, Nov 2008.

[132] W. A. Alrefai, Z. Sarwar, S. Tyagi, S. Saksena, P. K. Dudeja, and R. K. Gill, "Cholesterol modulates human intestinal sodium-dependent bile acid transporter.," *American journal of physiology. Gastrointestinal and liver physiology*, vol. 288, pp. G978–85, May 2005.

[133] N. Li, Z. Cui, F. Fang, J. Y. Lee, and N. Ballatori, "Heterodimerization, trafficking and membrane topology of the two proteins, ost alpha and ost beta, that constitute the organic solute and steroid transporter.," *The Biochemical journal*, vol. 407, pp. 363–72, Nov 2007.

[134] T. Frankenberg, A. Rao, F. Chen, J. Haywood, B. L. Shneider, and P. A. Dawson, "Regulation of the mouse organic solute transporter -, ost-ost, by bile acids," *American Journal of Physiology-Gastrointestinal and Liver Physiology*, vol. 290, no. 5, pp. G912–G922, 2006. PMID: 16357058.

[135] M. Okuwaki, T. Takada, Y. Iwayanagi, S. Koh, Y. Kariya, H. Fujii, and H. Suzuki, "Lxr alpha transactivates mouse organic solute transporter alpha and beta via ir-1 elements shared with fxr.," *Pharmaceutical research*, vol. 24, pp. 390–8, Feb 2007.

[136] S. P. S. Saini, J. Sonoda, L. Xu, D. Toma, H. Uppal, Y. Mu, S. Ren, D. D. Moore, R. M. Evans, and W. Xie, "A novel constitutive androstane receptor-mediated and cyp3a-independent pathway of bile

acid detoxification," *Molecular Pharmacology*, vol. 65, no. 2, pp. 292–300, 2004.

[137] J. Zhang, W. Huang, M. Qatanani, R. M. Evans, and D. D. Moore, "The constitutive androstane receptor and pregnane x receptor function coordinately to prevent bile acid-induced hepatotoxicity *," *Journal of Biological Chemistry*, vol. 279, pp. 49517–49522, Nov. 2004.

[138] C. A. M. Stedman, C. Liddle, S. A. Coulter, J. Sonoda, J. G. A. Alvarez, D. D. Moore, R. M. Evans, and M. Downes, "Nuclear receptors constitutive androstane receptor and pregnane x receptor ameliorate cholestatic liver injury," *Proceedings of the National Academy of Sciences*, vol. 102, no. 6, pp. 2063–2068, 2005.

[139] M. Makishima, T. T. Lu, W. Xie, G. K. Whitfield, H. Domoto, R. M. Evans, M. R. Haussler, and D. J. Mangelsdorf, "Vitamin d receptor as an intestinal bile acid sensor.," *Science (New York, N.Y.)*, vol. 296, pp. 1313–6, May 2002.

[140] W. Xie, A. Radominska-Pandya, Y. Shi, C. M. Simon, M. C. Nelson, E. S. Ong, D. J. Waxman, and R. M. Evans, "An essential role for nuclear receptors sxr/pxr in detoxification of cholestatic bile acids," *Proceedings of the National Academy of Sciences*, vol. 98, no. 6, pp. 3375–3380, 2001.

[141] G. L. Guo, G. Lambert, M. Negishi, J. M. Ward, J. Brewer, H.Bryan, S. A. Kliewer, F. J. Gonzalez, and C. J. Sinal, "Complementary roles of farnesoid x receptor, pregnane x receptor, and constitutive androstane receptor in protection against bile acid toxicity *," *Journal of Biological Chemistry*, vol. 278, pp. 45062–45071, Nov. 2003.

[142] W. Huang, J. Zhang, S. S. Chua, M. Qatanani, Y. Han, R. Granata, and D. D. Moore, "Induction of bilirubin clearance by the constitutive androstane receptor (car)," *Proceedings of the National Academy of Sciences*, vol. 100, no. 7, pp. 4156–4161, 2003.

[143] S. P. S. Saini, Y. Mu, H. Gong, D. Toma, H. Uppal, S. Ren, S. Li, S. M. Poloyac, and W. Xie, "Dual role of orphan nuclear receptor pregnane x receptor in bilirubin detoxification in mice," *Hepatology*, vol. 41, no. 3, pp. 497–505, 2005.

[144] A. L. Sberna, M. Assem, T. Gautier, J. Grober, B. Guiu, A. Jeannin, J.-P. Pais de Barros, A. Athias, L. Lagrost, and D. Masson, "Constitutive androstane receptor activation stimulates faecal bile acid excretion and reverse cholesterol transport in mice," *Journal of Hepatology*, vol. 55, pp. 154–161, July 2011.

[145] M. Wagner, E. Halilbasic, H.-U. Marschall, G. Zollner, P. Fickert, C. Langner, K. Zatloukal, H. Denk, and M. Trauner, "Car and pxr agonists stimulate hepatic bile acid and bilirubin detoxification and elimination pathways in mice," *Hepatology*, vol. 42, no. 2, pp. 420–430, 2005.

[146] T. W. H. Pols, T. Puchner, H. I. Korkmaz, M. Vos, M. R. Soeters, and C. J. M. de Vries, "Lithocholic acid controls adaptive immune responses by inhibition of th1 activation through the vitamin d receptor," *PLOS ONE*, vol. 12, pp. 1–16, 05 2017.

[147] J. Sun, R. Mustafi, S. Cerda, A. Chumsangsri, Y. R. Xia, Y. C. Li, and M. Bissonnette, "Lithocholic acid down-regulation of nf-b activity through vitamin d receptor in colonic cancer cells," *The Journal of Steroid Biochemistry and Molecular Biology*, vol. 111, no. 1, pp. 37–40, 2008.

[148] X. Song, X. Sun, S. F. Oh, M. Wu, Y. Zhang, W. Zheng, N. Geva-Zatorsky, R. Jupp, D. Mathis, C. Benoist, and D. L. Kasper, "Microbial bile acid metabolites modulate gut ror+ regulatory t cell homeostasis," *Nature*, vol. 577, no. 7790, pp. 410–415, 2020.

[149] J. Wang, L. B. Thingholm, J. Skiecevičienė, P. Rausch, M. Kummen, J. R. Hov, F. Degenhardt, F.-A. Heinsen, M. C. Rühlemann, S. Szymczak, K. Holm, T. Esko, J. Sun, M. Pricop-Jeckstadt, S. Al-Dury, P. Bohov, J. Bethune, F. Sommer, D. Ellinghaus, R. K. Berge, M. Hübenthal, M. Koch, K. Schwarz, G. Rimbach, P. Hübbe, W.-H. Pan, R. Sheibani-Tezerji, R. Häsler, P. Rosenstiel, M. D'Amato, K. Cloppenborg-Schmidt, S. Künzel, M. Laudes, H.-U. Marschall, W. Lieb, U. Nöthlings, T. H. Karlsen, J. F. Baines, and A. Franke, "Genome-wide association analysis identifies variation in vitamin d receptor and other host factors influencing the gut microbiota," *Nature Genetics*, vol. 48, no. 11, pp. 1396–1406, 2016.

[150] G. Vassileva, A. Golovko, L. Markowitz, S. Abbondanzo, M. Zeng, S. Yang, L. Hoos, G. Tetzloff, D. Levitan, N. Murgolo, K. Keane, J. Davis, Harry R., J. Hedrick, and E. Gustafson, "Targeted deletion of Gpbar1 protects mice from cholesterol gallstone formation," *Biochemical Journal*, vol. 398, pp. 423–430, 08 2006.

[151] Y. Kawamata, R. Fujii, M. Hosoya, M. Harada, H. Yoshida, M. Miwa, S. Fukusumi, Y. Habata, T. Itoh, Y. Shintani, S. Hinuma, Y. Fujisawa, and M. Fujino, "A g protein-coupled receptor responsive to bile acids *," *Journal of Biological Chemistry*, vol. 278, pp. 9435–9440, Mar. 2003.

[152] D. P. Kumar, A. Asgharpour, F. Mirshahi, S. H. Park, S. Liu, Y. Imai, J. L. Nadler, J. R. Grider, K. S. Murthy, and A. J. Sanyal, "Activation of transmembrane bile acid receptor tgr5 modulates pancreatic islet x3b1; cells to promote glucose homeostasis *," *Journal of Biological Chemistry*, vol. 291, pp. 6626–6640, Mar. 2016.

[153] S. Rajagopal, D. P. Kumar, S. Mahavadi, S. Bhattacharya, R. Zhou, C. U. Corvera, N. W. Bunnett, J. R. Grider, and K. S. Murthy, "Activation of g protein-coupled bile acid receptor, tgr5, induces smooth muscle relaxation via both epac- and pka-mediated inhibition of rhoa/rho kinase pathway," *American Journal of Physiology-Gastrointestinal and Liver Physiology*, vol. 304, no. 5, pp. G527–G535, 2013. PMID: 23275618.

[154] T. H. Pols, M. Nomura, T. Harach, G. Lo Sasso, M. Oosterveer, C. Thomas, G. Rizzo, A. Gioiello, L. Adorini, R. Pellicciari, J. Auwerx, and K. Schoonjans, "Tgr5 activation inhibits atherosclerosis by reducing macrophage inflammation and lipid loading," *Cell Metabolism*, vol. 14, pp. 747–757, Dec. 2011.

[155] D. D. Jensen, C. B. Godfrey, C. Niklas, M. Canals, M. Kocan, D. P. Poole, J. E. Murphy, F. Alemi, G. S. Cottrell, C. Korbmacher, N. A. Lambert, N. W. Bunnett, and C. U. Corvera, "The bile acid receptor tgr5 does not interact with x3b2;-arrestins or traffic to endosomes but transmits sustained signals from plasma membrane rafts *," *Journal of Biological Chemistry*, vol. 288, pp. 22942–22960, Aug. 2013.

[156] M. Reich, K. Deutschmann, A. Sommerfeld, C. Klindt, S. Kluge, R. Kubitz, C. Ullmer, W. T. Knoefel, D. Herebian, E. Mayatepek, D. Häussinger, and V. Keitel, "Tgr5 is essential for bile acid-dependent cholangiocyte proliferation in vivo and in vitro," *Gut*, vol. 65, no. 3, pp. 487–501, 2016.

[157] L. A. Velazquez-Villegas, A. Perino, V. Lemos, M. Zietak, M. Nomura, T. W. H. Pols, and K. Schoonjans, "Tgr5 signalling promotes mitochondrial fission and beige remodelling of white adipose tissue," *Nature Communications*, vol. 9, no. 1, p. 245, 2018.

[158] M.-M. Hu, W.-R. He, P. Gao, Q. Yang, K. He, L.-B. Cao, S. Li, Y.-Q. Feng, and H.-B. Shu, "Virus-induced accumulation of intracellular bile acids activates the tgr5--arrestin-src axis to enable innate antiviral immunity," *Cell Research*, vol. 29, no. 3, pp. 193–205, 2019.

[159] A. Perino, T. W. H. Pols, M. Nomura, S. Stein, R. Pellicciari, and K. Schoonjans, "Tgr5 reduces macrophage migration through mtor-

induced c/ebp differential translation," *The Journal of Clinical Investigation*, vol. 124, pp. 5424–5436, 12 2014.

[160] H. Zhai, Z. Li, M. Peng, Z. Huang, T. Qin, L. Chen, H. Li, H. Zhang, W. Zhang, and G. Xu, "Takeda g protein-coupled receptor 5-mechanistic target of rapamycin complex 1 signaling contributes to the increment of glucagon-like peptide-1 production after roux-en-y gastric bypass," *eBioMedicine*, vol. 32, pp. 201–214, June 2018.

[161] E. Studer, X. Zhou, R. Zhao, Y. Wang, K. Takabe, M. Nagahashi, W. M. Pandak, P. Dent, S. Spiegel, R. Shi, W. Xu, X. Liu, P. Bohdan, L. Zhang, H. Zhou, and P. B. Hylemon, "Conjugated bile acids activate the sphingosine-1-phosphate receptor 2 in primary rodent hepatocytes," *Hepatology*, vol. 55, no. 1, pp. 267–276, 2012.

[162] Y. Kageyama, H. Ikeda, N. Watanabe, M. Nagamine, Y. Kusumoto, M. Yashiro, Y. Satoh, T. Shimosawa, K. Shinozaki, T. Tomiya, Y. Inoue, T. Nishikawa, N. Ohtomo, Y. Tanoue, H. Yokota, T. Koyama, K. Ishimaru, Y. Okamoto, Y. Takuwa, K. Koike, and Y. Yatomi, "Antagonism of sphingosine 1-phosphate receptor 2 causes a selective reduction of portal vein pressure in bile duct-ligated rodents," *Hepatology*, vol. 56, no. 4, pp. 1427–1438, 2012.

[163] Y. Wang, H. Aoki, J. Yang, K. Peng, R. Liu, X. Li, X. Qiang, L. Sun, E. C. Gurley, G. Lai, L. Zhang, G. Liang, M. Nagahashi, K. Takabe, W. M. Pandak, P. B. Hylemon, and H. Zhou, "The role of sphingosine 1-phosphate receptor 2 in bile-acid-induced cholangiocyte proliferation and cholestasis-induced liver injury in mice," *Hepatology*, vol. 65, no. 6, 2017.

[164] Y. Le, P. M. Murphy, and J. M. Wang, "Formyl-peptide receptors revisited," *Trends in Immunology*, vol. 23, pp. 541–548, Nov. 2002.

[165] X. Chen, D. Yang, W. Shen, H. F. Dong, J. M. Wang, J. J. Oppenheim, and O. M. Z. Howard, "Characterization of chenodeoxycholic acid as an endogenous antagonist of the g-coupled formyl peptide receptors," *Inflammation Research*, vol. 49, no. 12, pp. 744–755, 2000.

[166] X. Chen, R. D. Mellon, L. Yang, H. Dong, J. J. Oppenheim, and O. M. Z. Howard, "Regulatory effects of deoxycholic acid, a component of the anti-inflammatory traditional chinese medicine niuhuang, on human leukocyte response to chemoattractants," *Biochemical Pharmacology*, vol. 63, no. 3, pp. 533–541, 2002.

[167] S. Amonyingcharoen, T. Suriyo, A. Thiantanawat, P. Watcharasit, and J. Satayavivad, "Taurolithocholic acid promotes intrahepatic

cholangiocarcinoma cell growth via muscarinic acetylcholine receptor and egfr/erk1/2 signaling pathway," *Int J Oncol*, vol. 46, no. 6, pp. 2317–2326, 2015.

[168] K. Cheng, Y. Chen, P. Zimniak, J.-P. Raufman, Y. Xiao, and H. Frucht, "Functional interaction of lithocholic acid conjugates with m3 muscarinic receptors on a human colon cancer cell line," *Biochimica et Biophysica Acta (BBA) - Molecular Basis of Disease*, vol. 1588, no. 1, pp. 48–55, 2002.

[169] S. Khurana, M. Yamada, J. Wess, R. H. Kennedy, and J.-P. Raufman, "Deoxycholyltaurine-induced vasodilation of rodent aorta is nitric oxide- and muscarinic m3 receptor-dependent," *European Journal of Pharmacology*, vol. 517, no. 1, pp. 103–110, 2005.

[170] E. Ibrahim, I. Diakonov, D. Arunthavarajah, T. Swift, M. Goodwin, S. McIlvride, V. Nikolova, C. Williamson, and J. Gorelik, "Bile acids and their respective conjugates elicit different responses in neonatal cardiomyocytes: role of gi protein, muscarinic receptors and tgr5," *Scientific Reports*, vol. 8, no. 1, p. 7110, 2018.

[171] S. H. Sheikh Abdul Kadir, M. Miragoli, S. Abu-Hayyeh, A. V. Moshkov, Q. Xie, V. Keitel, V. O. Nikolaev, C. Williamson, and J. Gorelik, "Bile acid-induced arrhythmia is mediated by muscarinic m2 receptors in neonatal rat cardiomyocytes," *PLOS ONE*, vol. 5, pp. 1–10, 03 2010.

[172] H. Gohlke, B. Schmitz, A. Sommerfeld, R. Reinehr, and D. Häussinger, "51-integrins are sensors for tauroursodeoxycholic acid in hepatocytes," *Hepatology*, vol. 57, no. 3, pp. 1117–1129, 2013.

[173] A. Sommerfeld, R. Reinehr, and D. Häussinger, "Tauroursodeoxycholate Protects Rat Hepatocytes from Bile Acid-Induced Apoptosis via 1-Integrin- and Protein Kinase A-Dependent Mechanisms," *Cellular Physiology and Biochemistry*, vol. 36, pp. 866–883, 05 2015.

[174] B.-H. Cha, M.-J. Jung, B.-K. Moon, J.-S. Kim, Y. Ma, Y. Arai, M. Noh, J.-Y. Shin, B.-S. Kim, and S.-H. Lee, "Administration of tauroursodeoxycholic acid enhances osteogenic differentiation of bone marrow-derived mesenchymal stem cells and bone regeneration," *Bone*, vol. 83, pp. 73–81, 2016.

[175] H. Hirokane, M. Nakahara, S. Tachibana, M. Shimizu, and R. Sato, "Bile acid reduces the secretion of very low density lipoprotein by repressing microsomal triglyceride transfer protein gene expression mediated by hepatocyte nuclear factor-4 *," *Journal of Biological Chemistry*, vol. 279, pp. 45685–45692, Oct. 2004.

[176] S. Caron, C. H. Samanez, H. Dehondt, M. Ploton, O. Briand, F. Lien, E. Dorchies, J. Dumont, C. Postic, B. Cariou, P. Lefebvre, and B. Staels, "Farnesoid x receptor inhibits the transcriptional activity of carbohydrate response element binding protein in human hepatocytes," *Molecular and Cellular Biology*, vol. 33, no. 11, pp. 2202–2211, 2013. PMID: 23530060.

[177] T. Claudel, Y. Inoue, O. Barbier, D. Duran-Sandoval, V. Kosykh, J. Fruchart, J.-C. Fruchart, F. J. Gonzalez, and B. Staels, "Farnesoid x receptor agonists suppress hepatic apolipoprotein ciii expression," *Gastroenterology*, vol. 125, pp. 544–555, Aug. 2003.

[178] H. R. Kast, C. M. Nguyen, C. J. Sinal, S. A. Jones, B. A. Laffitte, K. Reue, F. J. Gonzalez, T. M. Willson, and P. A. Edwards, "Farnesoid X-Activated Receptor Induces Apolipoprotein C-II Transcription: a Molecular Mechanism Linking Plasma Triglyceride Levels to Bile Acids," *Molecular Endocrinology*, vol. 15, pp. 1720–1728, 10 2001.

[179] T. Claudel, E. Sturm, H. Duez, I. P. Torra, A. Sirvent, V. Kosykh, J.-C. Fruchart, J. Dallongeville, D. W. Hum, F. Kuipers, and B. Staels, "Bile acid-activated nuclear receptor fxr suppresses apolipoprotein a-i transcription via a negative fxr response element," *The Journal of Clinical Investigation*, vol. 109, pp. 961–971, 4 2002.

[180] T. Gautier, W. de Haan, J. Grober, D. Ye, M. J. Bahr, T. Claudel, N. Nijstad, T. J. C. Van Berkel, L. M. Havekes, M. P. Manns, S. M. Willems, P. C. W. Hogendoorn, L. Lagrost, F. Kuipers, M. Van Eck, P. C. N. Rensen, and U. J. F. Tietge, "Farnesoid x receptor activation increases cholesteryl ester transfer protein expression in humans and transgenic mice¡sup¿¡/sup¿," *Journal of Lipid Research*, vol. 54, pp. 2195–2205, Aug. 2013.

[181] J. Schmitt, B. Kong, B. Stieger, O. Tschopp, S. M. Schultze, M. Rau, A. Weber, B. Müllhaupt, G. L. Guo, and A. Geier, "Protective effects of farnesoid x receptor (fxr) on hepatic lipid accumulation are mediated by hepatic fxr and independent of intestinal fgf15 signal," *Liver International*, vol. 35, no. 4, pp. 1133–1144, 2015.

[182] M. Miyata, Y. Sakaida, H. Matsuzawa, K. Yoshinari, and Y. Yamazoe, "Fibroblast growth factor 19 treatment ameliorates disruption of hepatic lipid metabolism in farnesoid x receptor (fxr)-null mice," *Biological and Pharmaceutical Bulletin*, vol. 34, no. 12, pp. 1885–1889, 2011.

[183] S. Bhatnagar, H. A. Damron, and F. B. Hillgartner, "Fibroblast growth factor-19, a novel factor that inhibits hepatic fatty acid

synthesis *¡sup¿ ¡/sup¿," *Journal of Biological Chemistry*, vol. 284, pp. 10023–10033, Apr. 2009.

[184] C. Jiang, C. Xie, F. Li, L. Zhang, R. G. Nichols, K. W. Krausz, J. Cai, Y. Qi, Z.-Z. Fang, S. Takahashi, N. Tanaka, D. Desai, S. G. Amin, I. Albert, A. D. Patterson, and F. J. Gonzalez, "Intestinal farnesoid x receptor signaling promotes nonalcoholic fatty liver disease.," *The Journal of clinical investigation*, vol. 125, pp. 386–402, Jan 2015.

[185] K. Ma, P. K. Saha, L. Chan, and D. D. Moore, "Farnesoid x receptor is essential for normal glucose homeostasis," *The Journal of Clinical Investigation*, vol. 116, pp. 1102–1109, 4 2006.

[186] B. Cariou, K. van Harmelen, D. Duran-Sandoval, T. H. van Dijk, A. Grefhorst, M. Abdelkarim, S. Caron, G. Torpier, J.-C. Fruchart, F. J. Gonzalez, F. Kuipers, and B. Staels, "The farnesoid x receptor modulates adiposity and peripheral insulin sensitivity in mice *¡sup¿ ¡/sup¿," *Journal of Biological Chemistry*, vol. 281, pp. 11039–11049, Apr. 2006.

[187] K. Yamagata, H. Daitoku, Y. Shimamoto, H. Matsuzaki, K. Hirota, J. Ishida, and A. Fukamizu, "Bile acids regulate gluconeogenic gene expression via small heterodimer partner-mediated repression of hepatocyte nuclear factor 4 and foxo1 *," *Journal of Biological Chemistry*, vol. 279, pp. 23158–23165, May 2004.

[188] Y. Zhang, F. Y. Lee, G. Barrera, H. Lee, C. Vales, F. J. Gonzalez, T. M. Willson, and P. A. Edwards, "Activation of the nuclear receptor fxr improves hyperglycemia and hyperlipidemia in diabetic mice," *Proceedings of the National Academy of Sciences*, vol. 103, no. 4, pp. 1006–1011, 2006.

[189] S. Kir, S. A. Beddow, V. T. Samuel, P. Miller, S. F. Previs, K. Suino-Powell, H. E. Xu, G. I. Shulman, S. A. Kliewer, and D. J. Mangelsdorf, "Fgf19 as a postprandial, insulin-independent activator of hepatic protein and glycogen synthesis," *Science*, vol. 331, no. 6024, pp. 1621–1624, 2011.

[190] M. Düfer, K. Hörth, R. Wagner, B. Schittenhelm, S. Prowald, T. F. Wagner, J. Oberwinkler, R. Lukowski, F. J. Gonzalez, P. Krippeit-Drews, and G. Drews, "Bile Acids Acutely Stimulate Insulin Secretion of Mouse -Cells via Farnesoid X Receptor Activation and KATP Channel Inhibition," *Diabetes*, vol. 61, pp. 1479–1489, 05 2012.

[191] V. Massafra, A. Milona, H. R. Vos, R. J. Ramos, J. Gerrits, E. C. Willemsen, J. M. Ramos Pittol, N. Ijssennagger, M. Houweling,

H. C. Prinsen, N. M. Verhoeven-Duif, B. M. Burgering, and S. W. van Mil, "Farnesoid x receptor activation promotes hepatic amino acid catabolism and ammonium clearance in mice," *Gastroenterology*, vol. 152, no. 6, pp. 1462–1476.e10, 2017.

[192] B. Renga, A. Mencarelli, S. Cipriani, C. D'Amore, A. Zampella, M. C. Monti, E. Distrutti, and S. Fiorucci, "The nuclear receptor fxr regulates hepatic transport and metabolism of glutamine and glutamate," *Biochimica et Biophysica Acta (BBA) - Molecular Basis of Disease*, vol. 1812, no. 11, pp. 1522–1531, 2011.

[193] C. Ma, M. Han, B. Heinrich, Q. Fu, Q. Zhang, M. Sandhu, D. Agdashian, M. Terabe, J. A. Berzofsky, V. Fako, T. Ritz, T. Longerich, C. M. Theriot, J. A. McCulloch, S. Roy, W. Yuan, V. Thovarai, S. K. Sen, M. Ruchirawat, F. Korangy, X. W. Wang, G. Trinchieri, and T. F. Greten, "Gut microbiome-mediated bile acid metabolism regulates liver cancer via nkt cells," *Science*, vol. 360, no. 6391, p. eaan5931, 2018.

[194] M. D. Thompson, A. Moghe, P. Cornuet, R. Marino, J. Tian, P. Wang, X. Ma, M. Abrams, J. Locker, S. P. Monga, and K. Nejak-Bowen, "-catenin regulation of farnesoid x receptor signaling and bile acid metabolism during murine cholestasis," *Hepatology*, vol. 67, no. 3, 2018.

[195] P. Fickert, E. Krones, M. J. Pollheimer, A. Thueringer, T. Moustafa, D. Silbert, E. Halilbasic, M. Yang, H. Jaeschke, G. Stokman, R. G. Wells, K. Eller, A. R. Rosenkranz, G. Eggertsen, C. A. Wagner, C. Langner, H. Denk, and M. Trauner, "Bile acids trigger cholemic nephropathy in common bile-duct–ligated mice," *Hepatology*, vol. 58, no. 6, pp. 2056–2069, 2013.

[196] P. S. Hench, "Effect of jaundice on rheumatoid arthritis," *BMJ*, vol. 2, no. 4050, pp. 394–398, 1938.

[197] P. P. Ho and L. Steinman, "Obeticholic acid, a synthetic bile acid agonist of the farnesoid x receptor, attenuates experimental autoimmune encephalomyelitis," *Proceedings of the National Academy of Sciences*, vol. 113, no. 6, pp. 1600–1605, 2016.

[198] N. D. Lewis, L. A. Patnaude, J. Pelletier, D. J. Souza, S. M. Lukas, F. J. King, J. D. Hill, D. E. Stefanopoulos, K. Ryan, S. Desai, D. Skow, S. G. Kauschke, A. Broermann, D. Kuzmich, C. Harcken, E. R. Hickey, and L. K. Modis, "A gpbar1 (tgr5) small molecule agonist shows

specific inhibitory effects on myeloid cell activation in vitro and reduces experimental autoimmune encephalitis (eae) in vivo," *PLOS ONE*, vol. 9, pp. 1–11, 06 2014.

[199] G. L. Guo, S. Santamarina-Fojo, T. E. Akiyama, M. J. Amar, B. J. Paigen, B. Brewer, and F. J. Gonzalez, "Effects of fxr in foam-cell formation and atherosclerosis development," *Biochimica et Biophysica Acta (BBA) - Molecular and Cell Biology of Lipids*, vol. 1761, no. 12, pp. 1401–1409, 2006.

[200] E. A. Hanniman, G. Lambert, T. C. McCarthy, and C. J. Sinal, "Loss of functional farnesoid x receptor increases atherosclerotic lesions in apolipoprotein e-deficient mice," *Journal of Lipid Research*, vol. 46, pp. 2595–2604, Dec. 2005.

[201] H. B. Hartman, S. J. Gardell, C. J. Petucci, S. Wang, J. A. Krueger, and M. J. Evans, "Activation of farnesoid x receptor prevents atherosclerotic lesion formation in ldlr¡sup¿x2212;/x2212;¡/sup¿ and apoe¡sup¿x2212;/x2212;¡/sup¿ mice," *Journal of Lipid Research*, vol. 50, pp. 1090–1100, June 2009.

[202] S. Miyazaki-Anzai, M. Masuda, S. Kohno, M. Levi, Y. Shiozaki, A. L. Keenan, and M. Miyazaki, "Simultaneous inhibition of fxr and tgr5 exacerbates atherosclerotic formation," *Journal of Lipid Research*, vol. 59, pp. 1709–1713, Sept. 2018.

[203] S. Miyazaki-Anzai, M. Masuda, M. Levi, A. L. Keenan, and M. Miyazaki, "Dual activation of the bile acid nuclear receptor fxr and g-protein-coupled receptor tgr5 protects mice against atherosclerosis," *PLOS ONE*, vol. 9, pp. 1–9, 09 2014.

[204] Y.-D. Wang, W.-D. Chen, D. Yu, B. M. Forman, and W. Huang, "The g-protein-coupled bile acid receptor, gpbar1 (tgr5), negatively regulates hepatic inflammatory response through antagonizing nuclear factor kappa light-chain enhancer of activated b cells (nf-b) in mice," *Hepatology*, vol. 54, no. 4, pp. 1421–1432, 2011.

[205] S. Zhang, J. Wang, Q. Liu, and D. C. Harnish, "Farnesoid x receptor agonist way-362450 attenuates liver inflammation and fibrosis in murine model of non-alcoholic steatohepatitis," *Journal of Hepatology*, vol. 51, pp. 380–388, Aug. 2009.

[206] R. H. McMahan, X. X. Wang, L. L. Cheng, T. Krisko, M. Smith, K. El Kasmi, M. Pruzanski, L. Adorini, L. Golden-Mason, M. Levi, and H. R. Rosen, "Bile acid receptor activation modulates hepatic monocyte activity and improves nonalcoholic fatty liver disease *," *Journal of Biological Chemistry*, vol. 288, pp. 11761–11770, Apr. 2013.

[207] J. M. Ferrell, P. Pathak, S. Boehme, T. Gilliland, and J. Y. L. Chiang, "Deficiency of both farnesoid x receptor and takeda g protein-coupled receptor 5 exacerbated liver fibrosis in mice," *Hepatology*, vol. 70, no. 3, 2019.

[208] D.-H. Kim, Z. Xiao, S. Kwon, X. Sun, D. Ryerson, D. Tkac, P. Ma, S.-Y. Wu, C.-M. Chiang, E. Zhou, H. E. Xu, J. J. Palvimo, L.-F. Chen, B. Kemper, and J. K. Kemper, "A dysregulated acetyl/sumo switch of fxr promotes hepatic inflammation in obesity," *The EMBO Journal*, vol. 34, no. 2, pp. 184–199, 2015.

[209] Y.-D. Wang, W.-D. Chen, M. Wang, D. Yu, B. M. Forman, and W. Huang, "Farnesoid x receptor antagonizes nuclear factor b in hepatic inflammatory response," *Hepatology*, vol. 48, no. 5, pp. 1632–1643, 2008.

[210] J. Yao, C.-S. Zhou, X. Ma, B.-Q. Fu, L.-S. Tao, M. Chen, and Y.-P. Xu, "Fxr agonist gw4064 alleviates endotoxin-induced hepatic inflammation by repressing macrophage activation.," *World journal of gastroenterology*, vol. 20, pp. 14430–41, Oct 2014.

[211] G. M. Hirschfield, R. W. Chapman, T. H. Karlsen, F. Lammert, K. N. Lazaridis, and A. L. Mason, "The genetics of complex cholestatic disorders," *Gastroenterology*, vol. 144, pp. 1357–1374, June 2013.

[212] J. R. Hov, V. Keitel, J. K. Laerdahl, L. Spomer, E. Ellinghaus, A. ElSharawy, E. Melum, K. M. Boberg, T. Manke, T. Balschun, C. Schramm, A. Bergquist, T. Weismüller, D. Gotthardt, C. Rust, L. Henckaerts, C. M. Onnie, R. K. Weersma, M. Sterneck, A. Teufel, H. Runz, A. Stiehl, C. Y. Ponsioen, C. Wijmenga, M. H. Vatn, for the IBSEN study group, P. C. F. Stokkers, S. Vermeire, C. G. Mathew, B. A. Lie, U. Beuers, M. P. Manns, S. Schreiber, E. Schrumpf, D. Häussinger, A. Franke, and T. H. Karlsen, "Mutational characterization of the bile acid receptor tgr5 in primary sclerosing cholangitis," *PLOS ONE*, vol. 5, pp. 1–13, 08 2010.

[213] S. W. C. van Mil, A. Milona, P. H. Dixon, R. Mullenbach, V. L. Geenes, J. Chambers, V. Shevchuk, G. E. Moore, F. Lammert, A. G. Glantz, L.- Mattsson, J. Whittaker, M. G. Parker, R. White, and C. Williamson, "Functional variants of the central bile acid sensor ¡em¿fxr¡/em¿ identified in intrahepatic cholestasis of pregnancy," *Gastroenterology*, vol. 133, pp. 507–516, Aug. 2007.

[214] N. Gomez-Ospina, C. J. Potter, R. Xiao, K. Manickam, M.-S. Kim, K. H. Kim, B. L. Shneider, J. L. Picarsic, T. A. Jacobson, J. Zhang,

W. He, P. Liu, A. S. Knisely, M. J. Finegold, D. M. Muzny, E. Boerwinkle, J. R. Lupski, S. E. Plon, R. A. Gibbs, C. M. Eng, Y. Yang, G. C. Washington, M. H. Porteus, W. E. Berquist, N. Kambham, R. J. Singh, F. Xia, G. M. Enns, and D. D. Moore, "Mutations in the nuclear bile acid receptor fxr cause progressive familial intrahepatic cholestasis," *Nature Communications*, vol. 7, no. 1, p. 10713, 2016.

[215] V. Keitel, C. Dröge, and D. Häussinger, "Targeting fxr in cholestasis," *Bile Acids and Their Receptors*, pp. 299–324, 2019.

[216] S. Modica, R. M. Gadaleta, and A. Moschetta, "Deciphering the nuclear bile acid receptor fxr paradigm," *Nuclear Receptor Signaling*, vol. 8, no. 1, p. nrs.08005, 2010. PMID: 21383957.

[217] R. Pellicciari, S. Fiorucci, E. Camaioni, C. Clerici, G. Costantino, P. R. Maloney, A. Morelli, D. J. Parks, and T. M. Willson, "6-ethylchenodeoxycholic acid (6-ecdca), a potent and selective fxr agonist endowed with anticholestatic activity," *Journal of Medicinal Chemistry*, vol. 45, no. 17, pp. 3569–3572, 2002. PMID: 12166927.

[218] Y. Liu, J. Binz, M. J. Numerick, S. Dennis, G. Luo, B. Desai, K. I. MacKenzie, T. A. Mansfield, S. A. Kliewer, B. Goodwin, and S. A. Jones, "Hepatoprotection by the farnesoid x receptor agonist gw4064 in rat models of intra- and extrahepatic cholestasis," *The Journal of Clinical Investigation*, vol. 112, pp. 1678–1687, 12 2003.

[219] S. Fiorucci, C. Clerici, E. Antonelli, S. Orlandi, B. Goodwin, B. M. Sadeghpour, G. Sabatino, G. Russo, D. Castellani, T. M. Willson, M. Pruzanski, R. Pellicciari, and A. Morelli, "Protective effects of 6-ethyl chenodeoxycholic acid, a farnesoid x receptor ligand, in estrogen-induced cholestasis," *Journal of Pharmacology and Experimental Therapeutics*, vol. 313, no. 2, pp. 604–612, 2005.

[220] C. Guo, S. Xie, Z. Chi, J. Zhang, Y. Liu, L. Zhang, M. Zheng, X. Zhang, D. Xia, Y. Ke, L. Lu, and D. Wang, "Bile acids control inflammation and metabolic disorder through inhibition of nlrp3 inflammasome," *Immunity*, vol. 45, pp. 802–816, Oct. 2016.

[221] T. Vasavan, E. Ferraro, E. Ibrahim, P. Dixon, J. Gorelik, and C. Williamson, "Heart and bile acids – clinical consequences of altered bile acid metabolism," *Biochimica et Biophysica Acta (BBA) - Molecular Basis of Disease*, vol. 1864, no. 4, Part B, pp. 1345–1355, 2018. CHOLANGIOCYTES IN HEALTH AND DISEASE: FROM BASIC SCIENCE TO NOVEL TREATMENTS.

[222] P. P. Rainer, U. Primessnig, S. Harenkamp, B. Doleschal, M. Wallner, G. Fauler, T. Stojakovic, R. Wachter, A. Yates, K. Groschner, M. Trauner, B. M. Pieske, and D. von Lewinski, "Bile acids induce arrhythmias in human atrial myocardium—implications for altered serum bile acid composition in patients with atrial fibrillation," *Heart*, vol. 99, no. 22, pp. 1685–1692, 2013.

[223] J. Pu, A. Yuan, P. Shan, E. Gao, X. Wang, Y. Wang, W. B. Lau, W. Koch, X.-L. Ma, and B. He, "Cardiomyocyte-expressed farnesoid-X-receptor is a novel apoptosis mediator and contributes to myocardial ischaemia/reperfusion injury," *European Heart Journal*, vol. 34, pp. 1834–1845, 02 2012.

[224] M. S. Desai, Z. Shabier, M. Taylor, F. Lam, S. Thevananther, A. Kosters, and S. J. Karpen, "Hypertrophic cardiomyopathy and dysregulation of cardiac energetics in a mouse model of biliary fibrosis," *Hepatology*, vol. 51, no. 6, pp. 2097–2107, 2010.

[225] R. M. Fryer, K. J. Ng, S. G. N. Mazurek, L. Patnaude, D. J. Skow, A. Muthukumarana, K. E. Gilpin, R. M. Dinallo, D. Kuzmich, J. Lord, S. Sanyal, H. Yu, C. Harcken, M. A. Cerny, E. R. Hickey, and L. K. Modis, "G protein–coupled bile acid receptor 1 stimulation mediates arterial vasodilation through a kca1.1 (bkca)–dependent mechanism," *Journal of Pharmacology and Experimental Therapeutics*, vol. 348, no. 3, pp. 421–431, 2014.

[226] Z. Eblimit, S. Thevananther, S. J. Karpen, H. Taegtmeyer, D. D. Moore, L. Adorini, D. J. Penny, and M. S. Desai, "Tgr5 activation induces cytoprotective changes in the heart and improves myocardial adaptability to physiologic, inotropic, and pressure-induced stress in mice," *Cardiovascular Therapeutics*, vol. 36, no. 5, p. e12462, 2018.

[227] F. Alemi, E. Kwon, D. P. Poole, T. Lieu, V. Lyo, F. Cattaruzza, F. Cevikbas, M. Steinhoff, R. Nassini, S. Materazzi, R. Guerrero-Alba, E. Valdez-Morales, G. S. Cottrell, K. Schoonjans, P. Geppetti, S. J. Vanner, N. W. Bunnett, and C. U. Corvera, "The tgr5 receptor mediates bile acid–induced itch and analgesia," *The Journal of Clinical Investigation*, vol. 123, pp. 1513–1530, 4 2013.

[228] B. A. Neuschwander-Tetri, R. Loomba, A. J. Sanyal, J. E. Lavine, M. L. Van Natta, M. F. Abdelmalek, N. Chalasani, S. Dasarathy, A. M. Diehl, B. Hameed, K. V. Kowdley, A. McCullough, N. Terrault, J. M. Clark, J. Tonascia, E. M. Brunt, D. E. Kleiner, and E. Doo, "Farnesoid x nuclear receptor ligand obeticholic acid for non-cirrhotic, non-alcoholic steatohepatitis (flint): a multicentre,

randomised, placebo-controlled trial," *The Lancet*, vol. 385, pp. 956–965, Mar. 2015.

[229] R. J. Hodge, J. Lin, L. S. Vasist Johnson, E. P. Gould, G. D. Bowers, D. J. Nunez, and on behalf of the SB-756050 Project Team, "Safety, pharmacokinetics, and pharmacodynamic effects of a selective tgr5 agonist, sb-756050, in type 2 diabetes," *Clinical Pharmacology in Drug Development*, vol. 2, no. 3, pp. 213–222, 2013.

[230] J. Cook, E. Kennaway, and N. Kennaway, "Production of tumours in mice by deoxycholic acid," *Nature*, vol. 145, no. 3677, pp. 627–627, 1940.

[231] S. Yoshimoto, T. M. Loo, K. Atarashi, H. Kanda, S. Sato, S. Oyadomari, Y. Iwakura, K. Oshima, H. Morita, M. Hattori, K. Honda, Y. Ishikawa, E. Hara, and N. Ohtani, "Obesity-induced gut microbial metabolite promotes liver cancer through senescence secretome," *Nature*, vol. 499, no. 7456, pp. 97–101, 2013.

[232] T. Kitamura, J. Srivastava, J. DiGiovanni, and K. Kiguchi, "Bile acid accelerates erbb2-induced pro-tumorigenic activities in biliary tract cancer," *Molecular Carcinogenesis*, vol. 54, no. 6, pp. 459–472, 2015.

[233] T. Fu, S. Coulter, E. Yoshihara, T. G. Oh, S. Fang, F. Cayabyab, Q. Zhu, T. Zhang, M. Leblanc, S. Liu, M. He, W. Waizenegger, E. Gasser, B. Schnabl, A. R. Atkins, R. T. Yu, R. Knight, C. Liddle, M. Downes, and R. M. Evans, "Fxr regulates intestinal cancer stem cell proliferation," *Cell*, vol. 176, pp. 1098–1112.e18, Feb. 2019.

[234] C. Bernstein, H. Holubec, A. K. Bhattacharyya, H. Nguyen, C. M. Payne, B. Zaitlin, and H. Bernstein, "Carcinogenicity of deoxycholate, a secondary bile acid," *Archives of Toxicology*, vol. 85, no. 8, pp. 863–871, 2011.

[235] X. Wang, L. Sun, X. Wang, H. Kang, X. Ma, M. Wang, S. Lin, M. Liu, C. Dai, and Z. Dai, "Acidified bile acids enhance tumor progression and telomerase activity of gastric cancer in mice dependent on c-myc expression," *Cancer Medicine*, vol. 6, no. 4, pp. 788–797, 2017.

[236] P. Song, Y. Zhang, and C. D. Klaassen, "Dose-Response of Five Bile Acids on Serum and Liver Bile Acid Concentrations and Hepatotoxicty in Mice," *Toxicological Sciences*, vol. 123, pp. 359–367, 07 2011.

[237] F. Yang, X. Huang, T. Yi, Y. Yen, D. D. Moore, and W. Huang, "Spontaneous Development of Liver Tumors in the Absence of the Bile Acid Receptor Farnesoid X Receptor," *Cancer Research*, vol. 67, pp. 863–867, 02 2007.

[238] M. Zhou, R. M. Learned, S. J. Rossi, A. M. DePaoli, H. Tian, and L. Ling, "Engineered fibroblast growth factor 19 reduces liver injury and resolves sclerosing cholangitis in mdr2-deficient mice," *Hepatology*, vol. 63, no. 3, 2016.

[239] W. S. Lee, J. H. Jung, R. Panchanathan, J. W. Yun, D. H. Kim, H. J. Kim, G. S. Kim, C. H. Ryu, S. C. Shin, S. C. Hong, Y. H. Choi, and J.-M. Jung, "Ursodeoxycholic acid induces death receptor-mediated apoptosis in prostate cancer cells," *Journal of Cancer Prevention*, vol. 22, pp. 16–21, Mar. 2017.

[240] S. Peng, X. Huo, D. Rezaei, Q. Zhang, X. Zhang, C. Yu, K. Asanuma, E. Cheng, T. H. Pham, D. H. Wang, M. Chen, R. F. Souza, and S. J. Spechler, "In barrett's esophagus patients and barrett's cell lines, ursodeoxycholic acid increases antioxidant expression and prevents dna damage by bile acids," *American Journal of Physiology-Gastrointestinal and Liver Physiology*, vol. 307, no. 2, pp. G129–G139, 2014. PMID: 24852569.

[241] J. P. Phelan, F. J. Reen, N. Dunphy, R. O'Connor, and F. O'Gara, "Bile acids destabilise hif-1 and promote anti-tumour phenotypes in cancer cell models," *BMC Cancer*, vol. 16, no. 1, p. 476, 2016.

[242] F. G. Schaap, M. Trauner, and P. L. M. Jansen, "Bile acid receptors as targets for drug development," *Nature Reviews Gastroenterology & Hepatology*, vol. 11, no. 1, pp. 55–67, 2014.

[243] M. Rudling, "Understanding mouse bile acid formation: Is it time to unwind why mice and rats make unique bile acids?," in *Journal of lipid research*, vol. 57, pp. 2097–2098, Dec 2016.

[244] P. Fickert and M. Wagner, "Biliary bile acids in hepatobiliary injury x2013; what is the link?," *Journal of Hepatology*, vol. 67, pp. 619–631, Sept. 2017.

[245] J. SchÖLmerich, M.-S. Becher, K. Schmidt, R. Schubert, B. Kremer, S. Feldhaus, and W. Gerok, "Influence of hydroxylation and conjugation of bile salts on their membrane-damaging properties-studies on isolated hepatocytes and lipid membrane vesicles," *Hepatology*, vol. 4, no. 4, pp. 661–666, 1984.

[246] K. Kitani, S. Kanai, Y. Sato, and M. Ohta, "Tauro -muricholate is as effective as tauro -muricholate and tauroursodeoxycholate in preventing taurochenodeoxycholate-induced liver damage in the rat," *Hepatology*, vol. 19, no. 4, pp. 1007–1012, 1994.

[247] F. Hugenholtz and W. M. de Vos, "Mouse models for human intestinal microbiota research: a critical evaluation," *Cellular and molecular life sciences : CMLS*, vol. 75, pp. 149–160, Jan. 2018.

[248] N. G. Ghoshal and H. S. Bal, "Comparative morphology of the stomach of some laboratory mammals.," *Laboratory animals*, vol. 23, pp. 21–9, Jan 1989.

[249] J. H. Cummings, E. R. Beatty, S. M. Kingman, S. A. Bingham, and H. N. Englyst, "Digestion and physiological properties of resistant starch in the human large bowel," *British Journal of Nutrition*, vol. 75, no. 5, p. 733–747, 1996.

[250] E. L. McConnell, A. W. Basit, and S. Murdan, "Measurements of rat and mouse gastrointestinal ph, fluid and lymphoid tissue, and implications for in-vivo experiments.," *The Journal of pharmacy and pharmacology*, vol. 60, pp. 63–70, Jan 2008.

[251] C. C. G. M. Booijink, E. G. Zoetendal, M. Kleerebezem, and W. M. de Vos, "Microbial communities in the human small intestine: coupling diversity to metagenomics.," *Future microbiology*, vol. 2, pp. 285–95, Jun 2007.

[252] W. G. Sheridan, R. H. Lowndes, and H. L. Young, "Intraoperative tissue oximetry in the human gastrointestinal tract.," *American journal of surgery*, vol. 159, pp. 314–9, Mar 1990.

[253] M. Kleiber, "Metabolic turnover rate: a physiological meaning of the metabolic rate per unit body weight.," *Journal of theoretical biology*, vol. 53, pp. 199–204, Sep 1975.

[254] E. Sakaguchi, "Digestive strategies of small hindgut fermenters," *Animal Science Journal*, vol. 74, no. 5, pp. 327–337, 2003.

[255] H. L. B. M. Klaasen, J. P. Koopman, P. M. Scholten, M. E. V. D. Brink, and A. G. M. Theeuwes, "Effect of preventing coprophagy on colonisation by segmented filamentous bacteria in the small bowel of mice," *Microbial Ecology in Health and Disease*, vol. 3, no. 2, pp. 99–103, 1990.

[256] V. Baier, *Physiologically-based pharmacokinetic modelling for the prediction of adverse drug reactions; 1. Auflage.* Dissertation, RWTH Aachen University, Aachen, 2023. Druckausgabe: 2023. - Auch veröffentlicht auf dem Publikationsserver der RWTH Aachen University; Dissertation, RWTH Aachen University, 2022.

[257] L. Kuepfer, C. Niederalt, T. Wendl, J.-F. Schlender, S. Willmann, J. Lippert, M. Block, T. Eissing, and D. Teutonico, "Applied concepts in pbpk modeling: How to build a pbpk/pd model," *CPT: Pharmacometrics & Systems Pharmacology*, vol. 5, no. 10, pp. 516–531, 2016.

[258] A. F. Hofmann, G. Molino, M. Milanese, and G. Belforte, "Description and simulation of a physiological pharmacokinetic model for the metabolism and enterohepatic circulation of bile acids in man. cholic acid in healthy man.," *The Journal of clinical investigation*, vol. 71, pp. 1003–22, Apr 1983.

[259] A. F. Hofmann, C. Cravetto, G. Molino, G. Belforte, and B. Bona, "Simulation of the metabolism and enterohepatic circulation of endogenous deoxycholic acid in humans using a physiologic pharmacokinetic model for bile acid metabolism.," *Gastroenterology*, vol. 93, pp. 693–709, Oct 1987.

[260] G. Molino, A. F. Hofmann, C. Cravetto, G. Belforte, and B. Bona, "Simulation of the metabolism and enterohepatic circulation of endogenous chenodeoxycholic acid in man using a physiological pharmacokinetic model.," *European journal of clinical investigation*, vol. 16, pp. 397–414, Oct 1986.

[261] J. E. Edwards, C. LaCerte, T. Peyret, N. H. Gosselin, J. F. Marier, A. F. Hofmann, and D. Shapiro, "Modeling and experimental studies of obeticholic acid exposure and the impact of cirrhosis stage.," *Clinical and translational science*, vol. 9, pp. 328–336, Dec 2016.

[262] P. Zuo, R. L. Dobbins, R. L. O'Connor-Semmes, and M. A. Young, "A systems model for ursodeoxycholic acid metabolism in healthy and patients with primary biliary cirrhosis.," *CPT: pharmacometrics systems pharmacology*, vol. 5, pp. 418–26, Aug 2016.

[263] V. Voronova, V. Sokolov, A. Al-Khaifi, S. Straniero, C. Kumar, K. Peskov, G. Helmlinger, M. Rudling, and B. Angelin, "A physiology-based model of bile acid distribution and metabolism under healthy and pathologic conditions in human beings.," *Cellular and molecular gastroenterology and hepatology*, vol. 10, pp. 149–170, 2020.

[264] B. Guiastrennec, D. P. Sonne, M. Bergstrand, T. Vilsbøll, F. K. Knop, and M. O. Karlsson, "Model-based prediction of plasma concentration and enterohepatic circulation of total bile acids in humans.," *CPT: pharmacometrics systems pharmacology*, vol. 7, pp. 603–612, Sep 2018.

[265] F. L. P. Sips, H. M. Eggink, P. A. J. Hilbers, M. R. Soeters, A. K. Groen, and N. A. W. van Riel, "In silico analysis identifies intestinal transit as a key determinant of systemic bile acid metabolism," *Frontiers in physiology*, vol. 9, pp. 631–631, June 2018.

[266] V. M. P. de Bruijn, I. M. C. M. Rietjens, and H. Bouwmeester, "Population pharmacokinetic model to generate mechanistic insights in bile acid homeostasis and drug-induced cholestasis," *Archives of Toxicology*, vol. 96, no. 10, pp. 2717–2730, 2022.

[267] V. M. P. de Bruijn, W. te Kronnie, I. M. C. M. Rietjens, and H. Bouwmeester, "Intestinal in vitro transport assay combined with physiologically based kinetic modeling as a tool to predict bile acid levels in vivo," *ALTEX - Alternatives to animal experimentation*, Jul. 2023.

[268] J. L. Woodhead, K. Yang, K. L. R. Brouwer, S. Q. Siler, S. H. Stahl, J. L. Ambroso, D. Baker, P. B. Watkins, and B. A. Howell, "Mechanistic modeling reveals the critical knowledge gaps in bile acid-mediated dili.," *CPT: pharmacometrics systems pharmacology*, vol. 3, p. e123, Jul 2014.

[269] V. Baier, H. Cordes, C. Thiel, J. V. Castell, U. P. Neumann, L. M. Blank, and L. Kuepfer, "A physiology-based model of human bile acid metabolism for predicting bile acid tissue levels after drug administration in healthy subjects and bric type 2 patients," *Frontiers in physiology*, vol. 10, pp. 1192–1192, Sept. 2019.

[270] C. Thiel, S. Schneckener, M. Krauss, A. Ghallab, U. Hofmann, T. Kanacher, S. Zellmer, R. Gebhardt, J. G. Hengstler, and L. Kuepfer, "A systematic evaluation of the use of physiologically based pharmacokinetic modeling for cross-species extrapolation.," *Journal of pharmaceutical sciences*, vol. 104, pp. 191–206, Jan 2015.

[271] A. Schenk, A. Ghallab, U. Hofmann, R. Hassan, M. Schwarz, A. Schuppert, L. O. Schwen, A. Braeuning, D. Teutonico, J. G. Hengstler, and L. Kuepfer, "Physiologically-based modelling in mice suggests an aggravated loss of clearance capacity after toxic liver damage," *Scientific Reports*, vol. 7, no. 1, p. 6224, 2017.

[272] M. Krauss, S. Schaller, S. Borchers, R. Findeisen, J. Lippert, and L. Kuepfer, "Integrating cellular metabolism into a multiscale whole-body model," *PLOS Computational Biology*, vol. 8, pp. 1–13, 10 2012.

[273] A. Wahlström, S. Al-Dury, M. Ståhlman, F. Bäckhed, and H.-U. Marschall, "Cyp3a11 is not essential for the formation of murine bile acids," *Biochemistry and Biophysics Reports*, vol. 10, pp. 70 – 75, 2017.

[274] J. Chen, K. Bittinger, E. S. Charlson, C. Hoffmann, J. Lewis, G. D. Wu, R. G. Collman, F. D. Bushman, and H. Li, "Associating microbiome composition with environmental covariates using generalized unifrac distances.," *Bioinformatics (Oxford, England)*, vol. 28, pp. 2106–13, Aug 2012.

[275] C. Lozupone and R. Knight, "Unifrac: a new phylogenetic method for comparing microbial communities.," *Applied and environmental microbiology*, vol. 71, pp. 8228–35, Dec 2005.

[276] S. O'Flaherty, A. Briner Crawley, C. M. Theriot, and R. Barrangou, "The lactobacillus bile salt hydrolase repertoire reveals niche-specific adaptation.," *mSphere*, vol. 3, Jun 2018.

[277] D. S. Wishart, A. Guo, E. Oler, F. Wang, A. Anjum, H. Peters, R. Dizon, Z. Sayeeda, S. Tian, B. Lee, M. Berjanskii, R. Mah, M. Yamamoto, J. Jovel, C. Torres-Calzada, M. Hiebert-Giesbrecht, V. Lui, D. Varshavi, D. Varshavi, D. Allen, D. Arndt, N. Khetarpal, A. Sivakumaran, K. Harford, S. Sanford, K. Yee, X. Cao, Z. Budinski, J. Liigand, L. Zhang, J. Zheng, R. Mandal, N. Karu, M. Dambrova, H. Schiöth, R. Greiner, and V. Gautam, "HMDB 5.0: the Human Metabolome Database for 2022," *Nucleic Acids Research*, vol. 50, pp. D622–D631, 11 2021.

[278] D. M. Heuman, P. B. Hylemon, and Z. R. Vlahcevic, "Regulation of bile acid synthesis. iii. correlation between biliary bile salt hydrophobicity index and the activities of enzymes regulating cholesterol and bile acid synthesis in the rat.," *Journal of lipid research*, vol. 30, pp. 1161–71, Aug 1989.

[279] M. Watanabe, Y. Horai, S. M. Houten, K. Morimoto, T. Sugizaki, E. Arita, C. Mataki, H. Sato, Y. Tanigawara, K. Schoonjans, H. Itoh, and J. Auwerx, "Lowering bile acid pool size with a synthetic farnesoid x receptor (fxr) agonist induces obesity and diabetes through reduced energy expenditure," *The Journal of biological chemistry*, vol. 286, pp. 26913–26920, July 2011.

[280] D. Jung, T. Inagaki, R. D. Gerard, P. A. Dawson, S. A. Kliewer, D. J. Mangelsdorf, and A. Moschetta, "Fxr agonists and fgf15 reduce fecal bile acid excretion in a mouse model of bile acid malabsorption," *Journal of lipid research*, vol. 48, pp. 2693–2700, Dec. 2007.

[281] L. Yu, J. Li-Hawkins, R. E. Hammer, K. E. Berge, J. D. Horton, J. C. Cohen, and H. H. Hobbs, "Overexpression of abcg5 and abcg8 promotes biliary cholesterol secretion and reduces fractional absorption of dietary cholesterol," *The Journal of Clinical Investigation*, vol. 110, pp. 671–680, 9 2002.

[282] H.-U. Marschall, M. Wagner, K. Bodin, G. Zollner, P. Fickert, J. Gumhold, D. Silbert, A. Fuchsbichler, J. Sjövall, and M. Trauner, "Fxr(-/-) mice adapt to biliary obstruction by enhanced phase i detoxification and renal elimination of bile acids," *Journal of lipid research*, vol. 47, pp. 582–592, Mar. 2006.

[283] G. W. Tannock, M. P. Dashkevicz, and S. D. Feighner, "Lactobacilli and bile salt hydrolase in the murine intestinal tract.," *Applied and Environmental Microbiology*, vol. 55, no. 7, pp. 1848–1851, 1989.

[284] J. C. Link, C. Xuqi, P. Christopher, S. Borja Mark, H. Bradley, N. Oda Michael, P. Arnold Arthur, and R. Karen, "Increased high-density lipoprotein cholesterol levels in mice with xx versus xy sex chromosomes," *Arteriosclerosis, Thrombosis, and Vascular Biology*, vol. 35, pp. 1778–1786, Aug. 2015.

[285] X. Cheng, D. Buckley, and C. D. Klaassen, "Regulation of hepatic bile acid transporters ntcp and bsep expression.," *Biochemical pharmacology*, vol. 74, pp. 1665–76, Dec 2007.

[286] A. Wahlström, P. Kovatcheva-Datchary, M. Ståhlman, M.-T. Khan, F. Bäckhed, and H.-U. Marschall, "Induction of farnesoid x receptor signaling in germ-free mice colonized with a human microbiota.," *Journal of lipid research*, vol. 58, pp. 412–419, Feb 2017.

[287] F. Li, C. Jiang, K. W. Krausz, Y. Li, I. Albert, H. Hao, K. M. Fabre, J. B. Mitchell, A. D. Patterson, and F. J. Gonzalez, "Microbiome remodelling leads to inhibition of intestinal farnesoid x receptor signalling and decreased obesity.," *Nature communications*, vol. 4, p. 2384, 2013.

[288] M. Camilleri, "Bile acid diarrhea: prevalence, pathogenesis, and therapy.," *Gut and liver*, vol. 9, pp. 332–9, May 2015.

[289] M. Wagner and M. Trauner, "Recent advances in understanding and managing cholestasis [version 1; peer review: 2 approved]," *F1000Research*, vol. 5, no. 705, 2016.

[290] J. P. Jackson, K. M. Freeman, W. W. Friley, R. L. St. Claire, C. Black, and K. R. Brouwer, "Basolateral efflux transporters: A potentially important pathway for the prevention of cholestatic hepatotoxicity," *Applied In Vitro Toxicology*, vol. 2, no. 4, pp. 207–216, 2016.

[291] E. R. Castro and M. P. C. Rodrigues, "Cell death and micrornas in cholestatic liver diseases: Update on potential therapeutic applications," 2017.

[292] J. R. Walters, A. M. Tasleem, O. S. Omer, W. G. Brydon, T. Dew, and C. W. le Roux, "A new mechanism for bile acid diarrhea: Defective feedback inhibition of bile acid biosynthesis," *Clinical Gastroenterology and Hepatology*, vol. 7, no. 11, pp. 1189–1194, 2009.

[293] L. P. Degen and S. F. Phillips, "Variability of gastrointestinal transit in healthy women and men.," *Gut*, vol. 39, no. 2, pp. 299–305, 1996.

[294] M. Guicciardi and G. Gores, "Bile acid-mediated hepatocyte apoptosis and cholestatic liver disease," *Digestive and Liver Disease*, vol. 34, no. 6, pp. 387–392, 2002.

[295] E. Smecuol, J. Bai, H. Vazquez, Z. Kogan, A. Cabanne, S. Niveloni, S. Pedreira, L. Boerr, E. Maurino, and J. Meddings, "Gastrointestinal permeability in celiac disease," *Gastroenterology*, vol. 112, no. 4, pp. 1129–1136, 1997.

[296] I. Bjarnason, T. Peters, and N. Veall, "A persistent defect in intestinal permeability in coeliac disease demonstrated by a 51cr-labelled edta absorption test," *The Lancet*, vol. 321, no. 8320, pp. 323–325, 1983. Originally published as Volume 1, Issue 8320.

[297] J. D. Schulzke, I. Schulzke, M. Fromm, and E. O. Riecken, "Epithelial barrier and ion transport in coeliac sprue: electrical measurements on intestinal aspiration biopsy specimens.," *Gut*, vol. 37, no. 6, pp. 777–782, 1995.

[298] M. Schumann, D. Günzel, N. Buergel, J. F. Richter, H. Troeger, C. May, A. Fromm, D. Sorgenfrei, S. Daum, C. Bojarski, M. Heyman, M. Zeitz, M. Fromm, and J.-D. Schulzke, "Cell polarity-determining proteins par-3 and pp-1 are involved in epithelial tight junction defects in coeliac disease," *Gut*, vol. 61, no. 2, pp. 220–228, 2012.

[299] L. Pierri, P. Saggese, S. Guercio Nuzio, J. Troisi, M. Di Stasi, M. Poeta, R. Savastano, G. Marchese, R. Tarallo, G. Massa, V. Ciccone, D. Ziegenhardt, P. Cavallo, I. Bergheim, A. Weisz, and P. Vajro, "Relations of gut liver axis components and gut microbiota in obese children with fatty liver: A pilot study.," Sep 2018.

[300] A. J. Wigg, I. C. Roberts-Thomson, R. B. Dymock, P. J. McCarthy, R. H. Grose, and A. G. Cummins, "The role of small intestinal bacterial overgrowth, intestinal permeability, endotoxaemia, and tumour

necrosis factor α in the pathogenesis of non-alcoholic steatohepatitis," *Gut*, vol. 48, no. 2, pp. 206–211, 2001.

[301] A. Farhadi, S. Gundlapalli, M. Shaikh, C. Frantzides, L. Harrell, M. M. Kwasny, and A. Keshavarzian, "Susceptibility to gut leakiness: a possible mechanism for endotoxaemia in non-alcoholic steatohepatitis," *Liver International*, vol. 28, no. 7, pp. 1026–1033, 2008.

[302] A. S. Rao, B. S. Wong, M. Camilleri, S. T. Odunsi-Shiyanbade, S. McKinzie, M. Ryks, D. Burton, P. Carlson, J. Lamsam, R. Singh, and A. R. Zinsmeister, "Chenodeoxycholate in females with irritable bowel syndrome-constipation: a pharmacodynamic and pharmacogenetic analysis.," *Gastroenterology*, vol. 139, pp. 1549–58, 1558.e1, Nov 2010.

[303] B. S. Wong, M. Camilleri, P. Carlson, S. McKinzie, I. Busciglio, O. Bondar, R. B. Dyer, J. Lamsam, and A. R. Zinsmeister, "Increased bile acid biosynthesis is associated with irritable bowel syndrome with diarrhea.," *Clinical gastroenterology and hepatology : the official clinical practice journal of the American Gastroenterological Association*, vol. 10, pp. 1009–15.e3, Sep 2012.

[304] A. Bajor, A. Kilander, A. Fae, C. Gälman, O. Jonsson, L. Öhman, M. Rudling, H. Sjövall, P.-O. Stotzer, and K.-A. Ung, "Normal or increased bile acid uptake in isolated mucosa from patients with bile acid malabsorption," *European Journal of Gastroenterology & Hepatology*, vol. 18, no. 4, 2006.

[305] A. Thomson, K. Smart, M. S. Somerville, S. N. Lauder, G. Appanna, J. Horwood, L. Sunder Raj, B. Srivastava, D. Durai, M. J. Scurr, V. Keita, A. M. Gallimore, and A. Godkin, "The ussing chamber system for measuring intestinal permeability in health and disease," *BMC Gastroenterology*, vol. 19, no. 1, p. 98, 2019.

[306] K. Thelen, K. Coboeken, S. Willmann, R. Burghaus, J. B. Dressman, and J. Lippert, "Evolution of a detailed physiological model to simulate the gastrointestinal transit and absorption process in humans, part 1: Oral solutions," *Journal of Pharmaceutical Sciences*, vol. 100, no. 12, pp. 5324–5345, 2011.

[307] K. Thelen, K. Coboeken, S. Willmann, J. B. Dressman, and J. Lippert, "Evolution of a detailed physiological model to simulate the gastrointestinal transit and absorption process in humans, part ii: Extension to describe performance of solid dosage forms," *Journal of Pharmaceutical Sciences*, vol. 101, no. 3, pp. 1267–1280, 2012.

[308] A. Baghdasaryan, C. D. Fuchs, C. H. Österreicher, U. J. Lemberger, E. Halilbasic, I. Påhlman, H. Graffner, E. Krones, P. Fickert, A. Wahlström, M. Ståhlman, G. Paumgartner, H.-U. Marschall, and M. Trauner, "Inhibition of intestinal bile acid absorption improves cholestatic liver and bile duct injury in a mouse model of sclerosing cholangitis," *Journal of Hepatology*, vol. 64, no. 3, pp. 674–681, 2016.

[309] B. L. Woolbright and H. Jaeschke, "Novel insight into mechanisms of cholestatic liver injury.," *World journal of gastroenterology*, vol. 18, pp. 4985–93, Sep 2012.

[310] P. L. Jansen, A. Ghallab, N. Vartak, R. Reif, F. G. Schaap, J. Hampe, and J. G. Hengstler, "The ascending pathophysiology of cholestatic liver disease," *Hepatology*, vol. 65, no. 2, pp. 722–738, 2017.

[311] J. Dietschy, S. Turley, and D. Spady, "Role of liver in the maintenance of cholesterol and low density lipoprotein homeostasis in different animal species, including humans," *Journal of Lipid Research*, vol. 34, no. 10, pp. 1637–1659, 1993.

[312] D. Gurantz and A. F. Hofmann, "Influence of bile acid structure on bile flow and biliary lipid secretion in the hamster," *American Journal of Physiology-Gastrointestinal and Liver Physiology*, vol. 247, no. 6, pp. G736–G748, 1984. PMID: 6507626.

[313] R. F. van Golen, P. B. Olthof, L. R. de Haan, R. J. Coelen, A. Pechlivanis, M. J. de Keijzer, R. Weijer, D. R. de Waart, A. B. van Kuilenburg, J. Roelofsen, P. W. Gilijamse, M. A. Maas, M. R. Lewis, J. K. Nicholson, J. Verheij, and M. Heger, "The pathophysiology of human obstructive cholestasis is mimicked in cholestatic gold syrian hamsters," *Biochimica et Biophysica Acta (BBA) - Molecular Basis of Disease*, vol. 1864, no. 3, pp. 942–951, 2018.

[314] N. Rosenthal and S. Brown, "The mouse ascending: perspectives for human-disease models," *Nature Cell Biology*, vol. 9, no. 9, pp. 993–999, 2007.

[315] J. T. Eppig, "Mouse Genome Informatics (MGI) Resource: Genetic, Genomic, and Biological Knowledgebase for the Laboratory Mouse," *ILAR Journal*, vol. 58, pp. 17–41, 06 2017.

[316] H. Ueda, A. Honda, T. Miyazaki, Y. Morishita, T. Hirayama, J. Iwamoto, N. Nakamoto, and T. Ikegami, "Sex-, age-, and organ-dependent improvement of bile acid hydrophobicity by ursodeoxycholic acid treatment: A study using a mouse model with human-like bile acid composition," *PLOS ONE*, vol. 17, pp. 1–18, 07 2022.

[317] W. M. S. Russell and R. L. Burch, *The principles of humane experimental technique*. Methuen, 1959.

[318] B. Yilmaz, P. Juillerat, O. Øyås, C. Ramon, F. D. Bravo, Y. Franc, N. Fournier, P. Michetti, C. Mueller, M. Geuking, V. E. H. Pittet, M. H. Maillard, G. Rogler, K. Abdelrahman, G. Ademi, P. Aepli, A. Thomas, C. Anderegg, A.-T. Antonino, E. Archanioti, E. Arrigoni, D. Bakker de Jong, B. Balsiger, P. Bastürk, P. Bauerfeind, A. Becocci, D. Belli, J. M. Bengoa, L. Biedermann, J. Binek, M. Blattmann, S. Boehm, T. Boldanova, J. Borovicka, C. P. Braegger, S. Brand, L. Brügger, S. Brunner, P. Bühr, B. Burnand, S. Burk, E. Burri, S. Buyse, D.-T. Cao, O. Carstens, D. H. Criblez, S. Cunningham, F. D'Angelo, P. de Saussure, L. Degen, J. Delarive, C. Doerig, B. Dora, S. Drerup, M. Egger, A. El-Wafa, M. Engelmann, J. Ezri, C. Felley, M. Fliegner, N. Fournier, M. Fraga, Y. Franc, P. Frei, R. Frei, M. Fried, F. Froehlich, R. I. Furlano, L. Garzoni, M. Geyer, L. Girard, M. Girardin, D. Golay, I. Good, U. Graf Bigler, B. Gysi, J. Haarer, M. Halama, J. Haldemann, P. Heer, B. Heimgartner, B. Helbling, P. Hengstler, D. Herzog, C. Hess, R. Hessler, K. Heyland, T. Hinterleitner, C. Hirschi, P. Hruz, P. Juillerat, C. Khalid-de Bakker, S. Kayser, C. Keller, C. Knellwolf (-Grieger), C. Knoblauch, H. Köhler, R. Koller, C. Krieger(-Grübel), P. Künzler, R. Kusche, F. S. Lehmann, A. J. Macpherson, M. H. Maillard, M. Manz, A. Marot, R. Meier, C. Meyenberger, P. Meyer, P. Michetti, B. Misselwitz, P. Mosler, C. Mottet, C. Müller, B. Müllhaupt, L. Musso, M. Neagu, C. Nichita, J. Niess, A. Nydegger, N. Obialo, D. Ollo, C. Oropesa, U. Peter, D. Peternac, L. M. Petit, V. Pittet, D. Pohl, M. Porzner, C. Preissler, N. Raschle, R. Rentsch, A. Restellini, S. Restellini, J.-P. Richterich, F. Ris, B. Risti, M. A. Ritz, G. Rogler, N. Röhrich, J.-B. Rossel, V. Rueger, M. Rusticeanu, M. Sagmeister, G. Saner, B. Sauter, M. Sawatzki, M. Scharl, M. Schelling, S. Schibli, H. Schlauri, D. Schluckebier, D. Schmid, S. Schmid (-Uebelhart), J.-F. Schnegg, A. Schoepfer, V. Seematter, F. Seibold, M. Seirafi, G.-M. Semadeni, A. Senning, C. Sokollik, J. Sommer, J. Spalinger, H. Spangenberger, P. Stadler, P. Staub, D. Staudenmann, V. Stenz, M. Steuerwald, A. Straumann, B. Strebel, A. Stulz, M. Sulz, A. Tatu, M. Tempia-Caliera, J. Thorens, K. Truninger, R. Tutuian, P. Urfer, S. Vavricka, F. Viani, J. Vögtlin, R. Von Känel, D. Vouillamoz, R. Vulliamy, P. Wiesel, R. Wiest, S. Wöhrle, S. Zamora, S. Zander, T. Wylie, J. Zeitz, D. Zimmermann, R. Wiest, J. Stelling, A. J. Macpherson, and S. I. B. D. C. Investigators, "Microbial network disturbances in relapsing refractory crohn's disease," *Nature Medicine*, vol. 25, no. 2, pp. 323–336, 2019.

[319] M. Harrer, P. Cuijpers, T. Furukawa, and D. D. Ebert, *dmetar: Companion R Package For The Guide 'Doing Meta-Analysis in R'*, 2019. R package version 0.0.9000.

[320] M. Harrer, P. Cuijpers, F. T. A, and D. D. Ebert, *Doing Meta-Analysis With R: A Hands-On Guide*. Boca Raton, FL and London: Chapman Hall/CRC Press, 1st ed., 2021.

[321] A. A. Veroniki, D. Jackson, W. Viechtbauer, R. Bender, J. Bowden, G. Knapp, O. Kuss, J. P. T. Higgins, D. Langan, and G. Salanti, "Methods to estimate the between-study variance and its uncertainty in meta-analysis," *Research synthesis methods*, vol. 7, pp. 55–79, Mar. 2016.

[322] G. Gorkiewicz and A. Moschen, "Gut microbiome: a new player in gastrointestinal disease," *Virchows Archiv*, vol. 472, no. 1, pp. 159–172, 2018.

[323] N. F. LaRusso, N. E. Hoffman, M. G. Korman, A. F. Hofmann, and A. E. Cowen, "Determinants of fasting and postprandial serum bile acid levels in healthy man," *The American Journal of Digestive Diseases*, vol. 23, no. 5, pp. 385–391, 1978.

[324] T. C. Northfield and A. F. Hofmann, "Biliary lipid output during three meals and an overnight fast. i. relationship to bile acid pool size and cholesterol saturation of bile in gallstone and control subjects," *Gut*, vol. 16, pp. 1–11, Jan. 1975.

[325] E. Roda, R. Aldini, G. Mazzella, A. Roda, C. Sama, D. Festi, and L. Barbara, "Enterohepatic circulation of bile acids after cholecystectomy," *Gut*, vol. 19, pp. 640–649, July 1978.

[326] C. Dirksen, N. B. Jørgensen, K. N. Bojsen-Møller, U. Kielgast, S. H. Jacobsen, T. R. Clausen, D. Worm, B. Hartmann, J. F. Rehfeld, M. Damgaard, J. L. Madsen, S. Madsbad, J. J. Holst, and D. L. Hansen, "Gut hormones, early dumping and resting energy expenditure in patients with good and poor weight loss response after roux-en-y gastric bypass," *International Journal of Obesity*, vol. 37, no. 11, pp. 1452–1459, 2013.

[327] A. Al-Khaifi, S. Straniero, V. Voronova, D. Chernikova, V. Sokolov, C. Kumar, B. Angelin, and M. Rudling, "Asynchronous rhythms of circulating conjugated and unconjugated bile acids in the modulation of human metabolism," *Journal of Internal Medicine*, vol. 284, no. 5, pp. 546–559, 2018.

[328] S. Ewerth, B. Angelin, K. Einarsson, K. Nilsell, and I. Björkhem, "Serum concentrations of ursodeoxycholic acid in portal venous and systemic venous blood of fasting humans as determined by isotope dilution-mass spectrometry.," *Gastroenterology*, vol. 88, pp. 126–33, Jan 1985.

[329] E. Reihnér, I. Björkhem, B. Angelin, S. Ewerth, and K. Einarsson, "Bile acid synthesis in humans: regulation of hepatic microsomal cholesterol 7 alpha-hydroxylase activity.," *Gastroenterology*, vol. 97, pp. 1498–505, Dec 1989.

[330] K. Einarsson, J. Ahlberg, B. Angelin, I. Björkhem, and S. Ewerth, "Portal venous bile acids in cholesterol gallstone disease: Effect of treatment with chenodeoxycholic and cholic acids," *Hepatology*, vol. 5, no. 4, pp. 661–665, 1985.

[331] J. Ahlberg, B. Angelin, I. Björkhem, and K. Einarsson, "Individual bile acids in portal venous and systemic blood serum of fasting man.," *Gastroenterology*, vol. 73, pp. 1377–82, Dec 1977.

[332] J. Yanagisawa, M. Itoh, M. Ishibashi, H. Miyazaki, and F. Nakayama, "Microanalysis of bile acid in human liver tissue by selected ion monitoring," *Analytical Biochemistry*, vol. 104, no. 1, pp. 75–86, 1980.

[333] A. Honda, T. Yoshida, N. Tanaka, Y. Matsuzaki, B. He, J. Shoda, and T. Osuga, "Increased bile acid concentration in liver tissue with cholesterol gallstone disease," *Journal of Gastroenterology*, vol. 30, no. 1, pp. 61–66, 1995.

[334] Y. Akashi, H. Miyazaki, and F. Nakayama, "Correlation of bile acid composition between liver tissue and bile," *Clinica Chimica Acta*, vol. 133, no. 2, pp. 125–132, 1983.

[335] C. H. Holland, R. O. Ramirez Flores, M. Myllys, R. Hassan, K. Edlund, U. Hofmann, R. Marchan, C. Cadenas, J. Reinders, S. Hoehme, A.-L. Seddek, S. Dooley, V. Keitel, P. Godoy, B. Begher-Tibbe, C. Trautwein, C. Rupp, S. Mueller, T. Longerich, J. G. Hengstler, J. Saez-Rodriguez, and A. Ghallab, "Transcriptomic cross-species analysis of chronic liver disease reveals consistent regulation between humans and mice.," *Hepatology communications*, vol. 6, pp. 161–177, Jan 2022.

[336] U. Beuers, M. Trauner, P. Jansen, and R. Poupon, "New paradigms in the treatment of hepatic cholestasis: From udca to fxr, pxr and beyond," *Journal of Hepatology*, vol. 62, pp. S25–S37, Apr. 2015.

[337] A. Parés, L. Caballería, and J. Rodés, "Excellent long-term survival in patients with primary biliary cirrhosis and biochemical response to ursodeoxycholic acid.," *Gastroenterology*, vol. 130, pp. 715–20, Mar 2006.

[338] S. Brugiroux, M. Beutler, C. Pfann, D. Garzetti, H.-J. Ruscheweyh, D. Ring, M. Diehl, S. Herp, Y. Lötscher, S. Hussain, B. Bunk, R. Pukall, D. H. Huson, P. C. Münch, A. C. McHardy, K. D. McCoy, A. J. Macpherson, A. Loy, T. Clavel, D. Berry, and B. Stecher, "Genome-guided design of a defined mouse microbiota that confers colonization resistance against salmonella enterica serovar typhimurium," *Nature Microbiology*, vol. 2, no. 2, p. 16215, 2016.

[339] A. Afrizal, S. A. V. Jennings, T. C. A. Hitch, T. Riedel, M. Basic, A. Panyot, N. Treichel, F. T. Hager, E. O.-Y. Wong, B. Wolter, A. Viehof, A. von Strempel, C. Eberl, E. M. Buhl, B. Abt, A. Bleich, R. Tolba, L. M. Blank, W. W. Navarre, F. Kiessling, H.-P. Horz, N. Torow, V. Cerovic, B. Stecher, T. Strowig, J. Overmann, and T. Clavel, "Enhanced cultured diversity of the mouse gut microbiota enables custom-made synthetic communities," *Cell Host Microbe*, vol. 30, pp. 1630–1645.e25, Nov. 2022.

[340] T. Streidl, I. Karkossa, R. R. S. Muñoz, C. Eberl, A. Zaufel, J. Plagge, R. Schmaltz, K. Schubert, M. Basic, K. M. Schneider, M. Afify, C. Trautwein, R. Tolba, B. Stecher, H. L. Doden, J. M. Ridlon, J. Ecker, T. Moustafa, M. von Bergen, A. E. Ramer-Tait, and T. Clavel, "The gut bacterium extibacter muris produces secondary bile acids and influences liver physiology in gnotobiotic mice," *Gut Microbes*, vol. 13, no. 1, p. 1854008, 2021. PMID: 33382950.

[341] H. T. Pham, K. Arnhard, Y. J. Asad, L. Deng, T. K. Felder, L. St John-Williams, V. Kaever, M. Leadley, N. Mitro, S. Muccio, C. Prehn, M. Rauh, U. Rolle-Kampczyk, J. W. Thompson, O. Uhl, M. Ulaszewska, M. Vogeser, D. S. Wishart, and T. Koal, "Inter-Laboratory Robustness of Next-Generation Bile Acid Study in Mice and Humans: International Ring Trial Involving 12 Laboratories," *The Journal of Applied Laboratory Medicine*, vol. 1, pp. 129–142, 09 2016.

[342] J. J. Godon, E. Zumstein, P. Dabert, F. Habouzit, and R. Moletta, "Molecular microbial diversity of an anaerobic digestor as determined by small-subunit rdna sequence analysis.," *Applied and environmental microbiology*, vol. 63, pp. 2802–13, Jul 1997.

[343] I. Lagkouvardos, K. Kläring, S. S. Heinzmann, S. Platz, B. Scholz, K.-H. Engel, P. Schmitt-Kopplin, D. Haller, S. Rohn, T. Skurk, and

T. Clavel, "Gut metabolites and bacterial community networks during a pilot intervention study with flaxseeds in healthy adult men.," *Molecular nutrition & food research*, vol. 59, pp. 1614–28, Aug 2015.

[344] D. Berry, K. Ben Mahfoudh, M. Wagner, and A. Loy, "Barcoded primers used in multiplex amplicon pyrosequencing bias amplification.," *Applied and environmental microbiology*, vol. 77, pp. 7846–9, Nov 2011.

[345] A. Klindworth, E. Pruesse, T. Schweer, J. Peplies, C. Quast, M. Horn, and F. O. Glöckner, "Evaluation of general 16s ribosomal rna gene pcr primers for classical and next-generation sequencing-based diversity studies.," *Nucleic acids research*, vol. 41, p. e1, Jan 2013.

[346] F. Charlier, M. Weber, D. Izak, E. Harkin, M. Magnus, J. Lalli, L. Fresnais, M. Chan, N. Markov, O. Amsalem, S. Proost, A. Krasoulis, getzze, and S. Repplinger, "Statannotations," Oct. 2022.

[347] P.-C. Bürkner, "brms: An r package for bayesian multilevel models using stan," *Journal of Statistical Software*, vol. 80, no. 1, p. 1–28, 2017.

[348] S. Balduzzi, G. Rücker, and G. Schwarzer, "How to perform a meta-analysis with r: a practical tutorial.," *Evidence-based mental health*, vol. 22, pp. 153–160, Nov 2019.

[349] W. Viechtbauer, "Conducting meta-analyses in r with the metafor package," *Journal of Statistical Software*, vol. 36, no. 3, p. 1–48, 2010.

[350] I. Lagkouvardos, D. Joseph, M. Kapfhammer, S. Giritli, M. Horn, D. Haller, and T. Clavel, "Imngs: A comprehensive open resource of processed 16s rrna microbial profiles for ecology and diversity studies," *Scientific Reports*, vol. 6, no. 1, p. 33721, 2016.

[351] R. C. Edgar, "Uparse: highly accurate otu sequences from microbial amplicon reads.," *Nature methods*, vol. 10, pp. 996–8, Oct 2013.

[352] R. C. Edgar, "Search and clustering orders of magnitude faster than blast.," *Bioinformatics (Oxford, England)*, vol. 26, pp. 2460–1, Oct 2010.

[353] E. Pruesse, J. Peplies, and F. O. Glöckner, "Sina: accurate high-throughput multiple sequence alignment of ribosomal rna genes.," *Bioinformatics (Oxford, England)*, vol. 28, pp. 1823–9, Jul 2012.

[354] I. Lagkouvardos, S. Fischer, N. Kumar, and T. Clavel, "Rhea: a transparent and modular r pipeline for microbial profiling based on 16s rrna gene amplicons.," *PeerJ*, vol. 5, p. e2836, 2017.

[355] B. Angelin and I. Björkhem, "Postprandial serum bile acids in healthy man. evidence for differences in absorptive pattern between individual bile acids.," *Gut*, vol. 18, no. 8, pp. 606–609, 1977.

[356] J. M. J. I. Salemans, F. M. Nagengast, A. Tangerman, A. V. Schaik, A. F. J. D. Haan, and J. B. M. J. Jansen, "Postprandial conjugated and unconjugated serum bile acid levels after proctocolectomy with ileal pouch-anal anastomosis," *Scandinavian Journal of Gastroenterology*, vol. 28, no. 9, pp. 786–790, 1993.

[357] N. N. Ahmad, A. Pfalzer, and L. M. Kaplan, "Roux-en-y gastric bypass normalizes the blunted postprandial bile acid excursion associated with obesity," *International journal of obesity (2005)*, vol. 37, pp. 1553–1559, Dec. 2013.

[358] D. P. Sonne, K. J. Hare, P. Martens, J. F. Rehfeld, J. J. Holst, T. Vilsbøll, and F. K. Knop, "Postprandial gut hormone responses and glucose metabolism in cholecystectomized patients," *American Journal of Physiology-Gastrointestinal and Liver Physiology*, vol. 304, no. 4, pp. G413–G419, 2013. PMID: 23275610.

[359] T. Suzuki, J. Aoyama, M. Hashimoto, M. Ohara, S. Futami-Suda, K. Suzuki, M. Ouchi, Y. Igari, K. Watanabe, and H. Nakano, "Correlation between postprandial bile acids and body fat mass in healthy normal-weight subjects," *Clinical Biochemistry*, vol. 47, no. 12, pp. 1128–1131, 2014.

[360] V. L. Albaugh, C. R. Flynn, S. Cai, Y. Xiao, R. A. Tamboli, and N. N. Abumrad, "Early increases in bile acids post roux-en-y gastric bypass are driven by insulin-sensitizing, secondary bile acids," *The Journal of clinical endocrinology and metabolism*, vol. 100, pp. E1225–E1233, Sept. 2015.

[361] S. P. R. Bathena, S. Mukherjee, M. Olivera, and Y. Alnouti, "The profile of bile acids and their sulfate metabolites in human urine and serum," *Journal of Chromatography B*, vol. 942-943, pp. 53–62, 2013.

[362] C. Campbell, C. McGuffie, and L. Powell, "The measurement of sulphated and non-sulphated bile acids in serum using gas-liquid chromatography," *Clinica Chimica Acta*, vol. 63, no. 3, pp. 249–262, 1975.

[363] L. Humbert, M. A. Maubert, C. Wolf, H. Duboc, M. Mahé, D. Farabos, P. Seksik, J. M. Mallet, G. Trugnan, J. Masliah, and D. Rainteau, "Bile acid profiling in human biological samples: Comparison of extraction procedures and application to normal and cholestatic patients," *Journal of Chromatography B*, vol. 899, pp. 135–145, 2012.

[364] I. Makino, H. Hashimoto, K. Shinozaki, K. Yoshino, and S. Nakagawa, "Sulfated and nonsulfated bile acids in urine, serum, and bile of patients with hepatobiliary diseases," *Gastroenterology*, vol. 68, no. 3, pp. 545–553, 1975.

[365] H. Takikawa, H. Otsuka, T. Beppu, Y. Seyama, and T. Yamakawa, "Quantitative determination of bile acid glucuronides in serum by mass fragmentography.," *Journal of biochemistry*, vol. 92, pp. 985–98, Oct 1982.

[366] H. Takikawa, T. Beppu, Y. Seyama, and T. Sugimoto, "Glucuronidated and sulfated bile acids in serum of patients with acute hepatitis," *Digestive Diseases and Sciences*, vol. 31, no. 5, pp. 487–491, 1986. cited By 13.

[367] N. Murata, T. Beppu, H. Takikawa, H. Otsuka, T. Kasama, and Y. Seyama, "Determination of sulfated and nonsulfated bile acids in serum by mass fragmentography," *Steroids*, vol. 42, no. 5, pp. 575–592, 1983.

[368] S. Matysik, J. Martin, M. Bala, M. Scherer, A. Schäffler, and G. Schmitz, "Bile acid signaling after an oral glucose tolerance test," *Chemistry and Physics of Lipids*, vol. 164, no. 6, pp. 525–529, 2011. Special issue to LipidomicNet and ENOR joint workshop: Analysis and function of oxysterols and other regulatory and lipotoxic molecular lipid species.

[369] H. Suzuki and Y. Sugiyama, "Transport of drugs across the hepatic sinusoidal membrane: sinusoidal drug influx and efflux in the liver.," *Seminars in liver disease*, vol. 20, pp. 251–63, 2000.

[370] Z. R. Vlahcevic, C. C. J. Bell, D. H. Gregory, G. Buker, P. Juttijudata, and L. Swell, "Relationship of bile acid pool size to the formation of lithogenic bile in female indians of the southwest.," *Gastroenterology*, vol. 62, pp. 73–83, Jan 1972.

[371] Z. R. Vlahcevic, P. Juttijudata, C. C. J. Bell, and L. Swell, "Bile acid metabolism in patients with cirrhosis. ii. cholic and chenodeoxycholic acid metabolism.," *Gastroenterology*, vol. 62, pp. 1174–81, Jun 1972.

[372] W. C. McCormick, C. C. Bell, L. Swell, and Z. R. Vlahcevic, "Cholic acid synthesis as an index of the severity of liver disease in man," *Gut*, vol. 14, no. 11, pp. 895–902, 1973.

[373] K. Einarsson, K. Hellström, and M. Kallner, "Bile acid kinetics in relation to sex, serum lipids, body weights, and gallbladder disease

in patients with various types of hyperlipoproteinemia," *The Journal of Clinical Investigation*, vol. 54, pp. 1301–1311, 12 1974.

[374] B. Almé, A. Bremmelgaard, J. Sjövall, and P. Thomassen, "Analysis of metabolic profiles of bile acids in urine using a lipophilic anion exchanger and computerized gas-liquid chromatorgaphy-mass spectrometry," *Journal of Lipid Research*, vol. 18, no. 3, pp. 339–362, 1977.

[375] H. Nittono, K. Obinata, N. Nakatsu, T. Watanabe, S. Niijima, H. Sasaki, O. Arisaka, H. Kato, K. Yabuta, and T. Miyano, "Sulfated and nonsulfated bile acids in urine of patients with biliary atresia: analysis of bile acids by high-performance liquid chromatography.," *Journal of pediatric gastroenterology and nutrition*, vol. 5, pp. 23–9, Jan 1986.

[376] H. Takikawa, T. Beppu, and Y. Seyama, "Urinary concentrations of bile acid glucuronides and sulfates in hepatobiliary diseases," *Gastroenterologia Japonica*, vol. 19, no. 2, pp. 104–109, 1984. cited By 43.

[377] N. Keren, F. M. Konikoff, Y. Paitan, G. Gabay, L. Reshef, T. Naftali, and U. Gophna, "Interactions between the intestinal microbiota and bile acids in gallstones patients," *Environmental Microbiology Reports*, vol. 7, no. 6, pp. 874–880, 2015.

[378] K. Dilger, S. Hohenester, U. Winkler-Budenhofer, B. A. Bastiaansen, F. G. Schaap, C. Rust, and U. Beuers, "Effect of ursodeoxycholic acid on bile acid profiles and intestinal detoxification machinery in primary biliary cirrhosis and health," *Journal of Hepatology*, vol. 57, no. 1, pp. 133–140, 2012.

CURRICULUM VITAE

Name: Bastian Karl Kister
Place of Birth: Schweinfurt, Germany

WORK EXPERIENCE

Since 01/2024 **Associate Consultant,** Pharmetheus AB, Sweden

01/2020-12/2023 **PhD Candidate**, Institute of Applied Microbiology, RWTH Aachen and Institute for Systems medicine with focus on organ interactions, UK Aachen

- CRC Gut-liver axis Project-ID 403224013 – "SFB 1382"
- Topic: “Computational modelling of bile acid metabolism in mice and human”
  Supervisor: Professor Lars Kuepfer and Professor Lars Blank

EDUCATION

10/2016 – 09/2019 **Master of Sciences**, University Heidelberg

- Molecular Biosciences, Major Systems Biology
- Master’s thesis: “Multiscale mathematical modelling of IFN-α administration and induced cellular responses in mice”
  Supervisor: Professor Ursula Kummer

Final grade: 1.3

10/2013 – 06/2016 **Bachelor of Sciences**, University Heidelberg

- Life Sciences
- Bachelor’s thesis: “Characterisation of the extracellular space of non-tumorous lung tissue and non-small cell lung cancer”
  Supervisor: Professor Ursula Klingmueller
- Final grade: 1.5

06/2013 **Germ. High School Degree**, Jack-Steinberger-Gymnasium Bad Kissingen

- Finals in German, English, Mathematics, History/Social Studies and Biology
- Final grade: 1.1
-

PUBLICATIONS

Kister B, Viehof A, Rolle-Kampczyk U, Schwentker A, Treichel NS, Jennings S, et al. A physiologically based model of bile acid metabolism in mice. bioRxiv.v2022;doi:10.1101/2022.11.10.515857

Kokh DB, Kaufmann T, **Kister B** and Wade RC (2019) Machine Learning Analysis of τRAMD Trajectories to Decipher Molecular Determinants of Drug-Target Residence Times. Front. Mol. Biosci. 6:36.
doi: 10.3389/fmolb.2019.00036

CONFERENCES/POSTER

Invited posters

UK QSP Network - 3rd Exchange Workshop, University of Reading, September 2019
Quantitative Systems Pharmacology Conference 2022 (QSPC2022), Leiden University, April 2022
The 21st International Conference on Systems Biology (ICSB 2022), Humboldt University Berlin, October 2022

WORK EXPERIENCES

10/2018 – 12/2018 **Practical Student**

- Supervisor: Dr Daria Kokh | PI: Professor Rebecca Wade | Group: Molecular and Cellular Modeling | Institute: HITS, Heidelberg
- “Machine learning based analysis of τRAMD data”

03/2018 – 05/2018 **Practical Student**

- Supervisor: Dr Melania Barile | PI: Professor Thomas Hoefer | Group: Theoretical Systems Biology | Institute: BioQuant, Heidelberg
- “Mathematical modelling of haematopoietic recovery upon sub-lethal irradiation”

06/2016 – 08/2017 **Research Assistant**

- Supervisor: Dr Martin Boehm | PI: Professor Ursula Klingmueller | Group: Systems Biology of Signal Transduction | Institute: DKFZ, Heidelberg

TEACHING ACTIVITY

04/2019 – 09/2019 **Tutor**

- Lecture: “Mathematics for Biologists” | Lecturer: Professor Ursula Kummer and Dr Sven Sahle

04/2018 – 09/2018 **Tutor**

- Lecture: “Mathematics for Biologists” | Lecturer: Professor Ursula Kummer and Dr Sven Sahle

LANGUAGES

- German (native language)
- English (IELTS overall band score 8.0)

Typeset May 23, 2024